research report

Higher Capacity Cold-Formed Steel Sheathed and Framed Shear Walls for Mid-Rise Buildings: Part 1

RESEARCH REPORT RP17-5

July 2018

American Iron and Steel Institute

DISCLAIMER

The material contained herein has been developed by researchers based on their research findings and is for general information only. The information in it should not be used without first securing competent advice with respect to its suitability for any given application. The publication of the information is not intended as a representation or warranty on the part of the American Iron and Steel Institute or of any other person named herein, that the information is suitable for any general or particular use or of freedom from infringement of any patent or patents. Anyone making use of the information assumes all liability arising from such use.

HIGHER CAPACITY COLD-FORMED STEEL SHEATHED AND FRAMED SHEAR WALLS FOR MID-RISE BUILDINGS: PART 1

By

Veronica SANTOS

Project Supervisor: Colin Rogers

Department of Civil Engineering and Applied Mechanics

McGill University, Montréal, Québec, Canada

November 2017

Research Report

ABSTRACT

The use of cold-formed steel (CFS) for seismic force-resisting systems (SFRS), including shear walls, has increased throughout the years. However, the design provisions for CFS sheathed and framed shear walls available in the North American CFS standards (AISI S400 and AISI S240) are limited by the shear walls' sheathing and framing thicknesses. Design guidelines for CFS sheathed and framed shear walls for the purpose of mid-rise construction are still absent from the standards.

The main objective of this research program was to develop a design procedure for CFS sheathed and framed shear walls to achieve higher capacity and ductility to resist the higher forces experienced in mid-rise construction. The developed design procedure is proposed to be included in the provisions of the AISI S240 Standard and AISI S400 Standard.

The design procedure was developed by determining the shear strength of full-scale shear wall specimens built and tested at McGill University under monotonic and cyclic loading protocols. A total of 31 specimens, with varying building parameters, were constructed using thicker sheathing and framing members than what is currently available for design. The specimens were built using two new shear wall configurations (double-sheathed and centre-sheathed) to address out-of-plane forces experienced by shear walls tested in previous research programs.

The centre-sheathed shear wall configuration, with a confined and concentrically placed sheathing panel, reached a shear resistance four times higher than the design values tabulated in the current standards. The ductility of these CFS shear walls was also significantly improved.

A preliminary *equation-based* nominal shear strength prediction method has been developed for the centre-sheathed shear walls; the method reflects the shear wall's different configuration and superior behaviour. Following the test data analysis, preliminary design parameters for Limit States Design (LSD) used in Canada and for Load and Resistance Factor Design (LRFD) used in the USA and Mexico were determined, including the load resistance factor, ϕ, and the factor of safety. In addition, capacity based design parameters were determined for

seismic design in Canada. These parameters included the “test-based” seismic performance factors, R_d and R_o, which were found to be 2.8 and 1.5, respectively.

The superior performance of the centre-sheathed configuration showed its promising potential as a new design option for higher capacity CFS shear walls. However, before a potential implementation into mid-rise construction, further research is needed in order for a complete design procedure to be developed.

RÉSUMÉ

L'utilisation de l'acier formé à froid pour les systèmes résistants aux efforts sismiques, desquels font partie les murs de refend, a augmenté au fur et à mesure des années. Cependant, les mesures de conceptions pour les murs de refend utilisant un cadre et un parement en acier formé à froid disponibles dans les normes Nord-Américaines pour l'acier formé à froid (AISI S400 et AISI S240) sont limitées par les épaisseurs du parement et du cadre de ces murs. Les recommandations de conception pour une utilisation dans les constructions de mi-hauteur (jusque 5 étages) de ce type de mur de refend en acier formé à froid ne sont toujours pas proposées dans les normes actuelles.

L'objectif principal de ce programme de recherche était de développer une procédure de dimensionnement pour les murs de refend présentant un cadre et un parement en acier formé à froid afin d'obtenir une résistance et une ductilité augmentées leur permettant de résister aux efforts plus importants présents dans les constructions de mi-hauteur. La procédure de dimensionnement sera proposée à l'inclusion dans les normes AISI S400 et AISI S240.

La procédure de dimensionnement a été développée en déterminant la résistance au cisaillement de murs de refend construits à l'échelle 1:1 et testés dans le Laboratoire de Structures Jamieson à l'université McGill, en utilisant des protocoles de chargement monotoniques et cycliques. Au total, 31 spécimens ont été construits en utilisant des matériaux plus épais que ceux proposés pour leur dimensionnement dans les normes actuelles. Ils ont été construits selon deux nouvelles configurations (parement double et parement central) pour éliminer les efforts s'exerçant hors plan subis par les murs de refend testés lors des programmes de recherche précédents.

La configuration utilisant un parement central confiné au sein même des membres du cadre du mur de refend a atteint une résistance au cisaillement quatre fois plus élevée que les valeurs de conception tabulées dans les normes actuelles. La ductilité de ces murs de refend en acier formé à froid fut aussi améliorée de manière significative.

Une méthode préliminaire de prédiction de la résistance nominale à l'effort tranchant a été développée pour la configuration utilisant un parement central ; cette méthode prend en compte la

nouvelle configuration de construction du mur de refend ainsi que son meilleur comportement. A la suite de l'analyse des résultats, les paramètres de conception préliminaires pour le calcul aux états limites utilisé au Canada (LSD) et aux Etats-Unis et au Mexique (LRFD) ont été déterminés, notamment le facteur de résistance, ϕ, et le facteur de sécurité. De plus, les facteurs de performance sismique pour le Canada, R_d et R_o, ont été déterminés en se basant sur les résultats expérimentaux, obtenant les valeurs de 2.8 et 1.5 respectivement.

Le niveau de performance supérieur de la configuration utilisant un parement central a mis en lumière le potentiel que celle-ci présente en tant que nouvelle option pour la conception de murs de refend en acier formé à froid de plus haute résistance. Cependant, une recherche plus approfondie est nécessaire avant de pouvoir envisager une utilisation de ce type de mur de refend au sein de constructions de mi-hauteur ; cela permettra de développer une procédure de conception complète et plus spécifique à cette nouvelle configuration.

ACKNOWLEDGEMENTS

This research was made possible thanks to the financial support from the American Iron and Steel Institute (AISI), the Canadian Sheet Steel Building Institute (CSSBI) and the Natural Sciences and Engineering Research Council of Canada (NSERC). A special thank you is also extended to Bailey Metal Products Ltd., Simpson Strong-Tie Company Inc., Ontario Tools & Fasteners Ltd., UCAN Fastening Products and Arcelor Mittal for the materials and tools that were provided.

.

TABLE OF CONTENTS

LIST OF FIGURES

LIST OF TABLES

CHAPTER 1 – INTRODUCTION

1.1 General Overview

The use of cold-formed steel (CFS) as a building material has gained popularity in recent years as it is a sustainable alternative to some of the other, more commonly used, materials in the low- and mid-rise construction industry. Cold-formed steel has a high strength-to-weight ratio making it easy to handle and more economical. In addition, cold-formed steel is a non-combustible and termite-resistant material, which gives it an advantage over wood-framed construction, especially in locations where structures are prone to termite damage and rotting, Hawaii being a common example due to its climate (Hawaii Steel Alliance *(2017)*). Aside from its increase in residential construction, it has been reported by the Steel Framing Industry Association *(2017)* that 30%-35% of all non-residential buildings in the USA are built with structural and non-structural CFS framing. Figure 1.1 shows the use of cold-formed steel in mid-rise construction as part of an assisted living building in Pearl City, Hawaii.

Figure 1.1: Cold-formed steel framing used in the construction of a mid-rise building in Pearl City Hawaii, (Hawaii Steel Alliance, *(2017))*.

Although it is becoming more commonly used, in Canada the use of CFS has been restricted by the limited amount of design guidelines provided in the design standards, especially towards mid-rise construction. In CFS construction, lateral force-resisting systems (LFRSs) more commonly include gypsum-sheathed and wood-sheathed shear walls. In recent years, cold-formed steel-framed and steel-sheathed shear walls for low-rise buildings have been made available for design in the American Iron and Steel Institute, AISI S400 Standard *(2015)*, North American Standard for Seismic Design of Cold-Formed Steel Structural Systems. The implementation of these design guidelines were made possible as a result of research done by Serrette et al. *(1997)*, Yu et al. *(2007)*, Yu and Chen *(2009)*, DaBreo et al. *(2014)*, Balh et al. *(2014)*, and Shamim and Rogers *(2015)*, among others, which has provided valuable information on the behaviour of CFS sheathed and framed shear walls. Figure 1.2 shows a typical residential construction using CFS framed and sheathed shear walls. Although progress has been made in this field, design guidelines for stronger cold-formed steel framed and sheathed shear walls to be implemented in mid-rise construction are still missing from the standards. The continuing efforts in advancing the use of CFS in construction will provide designers with more options and confidence in their design, leading to an increase in its use.

Figure 1.2: Typical residential cold-formed steel framing using cold-formed steel sheathed shear walls *(photo courtesy of Jeff Ellis, Simpson Strong-Tie Co. Inc.).*

1.2 Statement of Problem

Currently, in Canada, the USA, and Mexico, the AISI S400 Standard *(2015)* includes design guidelines for cold-formed steel framed shear walls sheathed with gypsum board panels, wood structural panels, and steel sheets. Design guidelines for steel-sheathed shear walls in the USA had previously been included in the AISI S213 Standard (now the AISI S400) in 2004 and 2007, however design guidelines for steel-sheathed shear walls in Canada were only added to the latest version of the standard, as it is still a relatively new topic of research. The design values (nominal shear resistances) and building parameters (i.e. material thickness, fastener spacing, screw sizes, and aspect ratio), derived from tested specimens, are presented in the standard in tabulated form. The CFS framed and sheathed shear walls available for design, however, have nominal shear resistances only suitable for low-rise structures, with the strongest shear wall having a nominal shear strength of 23.3 kN/m (1597 lb/ft). In addition, the tabulated values are specific to one type of shear wall configuration only; steel sheathing on one side of the wall.

A method to evaluate the nominal shear resistance of CFS framed and sheathed shear walls, the Effective Strip Method developed by Yanagi and Yu *(2014)*, was also included in the AISI S400 Standard *(2015)*, but its use is only permitted in the USA and Mexico, limiting Canadians' ability to design CFS shear walls even more. Since the Effective Strip Method was developed based on test specimens built with a specific configuration (steel sheathing on one side only) and with limited building parameters, the method is also restrictive; Section E2.3.1.1.1.1 of the AISI S400 Standard *(2015)* outlines the range of the parameters within which the Effective Strip Method can be used.

The available design guidelines for lower-capacity CFS framed and sheathed shear walls limit their use in mid-rise construction. Additionally, the absence of a general, *equation-based* analytical method to determine the nominal shear strength of these walls and the lack of design guidelines for other types of shear wall configurations greatly restricts the engineer's freedom and ability to design steel-sheathed shear walls with a larger variety of building parameters to best suit the needs of specific projects.

1.3 Objectives

The purpose of this research project is to develop a design procedure for CFS sheathed and framed shear walls to achieve higher strength and ductility in order to resist the larger forces expected in mid-rise construction.

The development of this design procedure will involve determining the shear strength values for shear walls constructed with thicker framing and sheathing members not currently available for design. The design procedure will be proposed to the AISI to be included in the North American cold-formed steel standards; AISI S400 and S240. In addition, design parameters to be used in Canada, in the USA and Mexico will be determined. The detailed objectives of this research are as follow:

- Determine new CFS sheathed and framed shear wall configurations able to achieve higher shear strength and ductility than those currently available for design in the AISI S400 Standard *(2015)*;

- Determine the shear strength of the new shear wall configurations by testing full-scale single-storey specimens built with thicker framing and sheathing than what is currently available in the AISI S400 Standard *(2015)*;

- Determine the necessary design parameters from the test data in order to calculate the load resistance factor, ϕ, and factor of safety for limit states design (LSD) and load and resistance factor design (LRFD), as well as the seismic force modification factors, R_d and R_o for design in Canada.

- Propose to the AISI a design method to determine the nominal shear resistance of the new CFS sheathed and framed shear wall configurations.

1.4 Scope of Study

Full-scale 1220 mm × 2440 mm (4’ × 8’) shear wall specimens of two different configurations, the double-sheathed configuration and the centre-sheathed configuration, were

tested. The main difference between the configurations was the placement of the sheathing; the double-sheathed configuration was built with two sheathing panels, one on each side of the wall, while the centre-sheathed configuration was built with a single sheathing panel between the back-to-back chord studs. The centre-sheathed configuration deviated from the standard CFS sheathed and framed shear wall configuration available for design in the AISI S400 Standard *(2015)*, therefore it went through a design evolution throughout the testing program, where adjustments were made to the framing members to avoid failure.

The specimens were constructed with varying building parameters such as fastener spacing, material thickness, and fastener size. The fastener spacing varied between 50 mm (2”), 100 mm (4”), and 150 mm (6”) while two sizes of screws were used; No. 10 and No. 12. The material thicknesses used were 2 × 0.36 mm (0.014”), 2 × 0.47 mm (0.019”), 0.84 mm (0.033”), and 1.09 mm (0.043”) for the sheathing and 1.73 mm (0068”) and 2.46 mm (0.097”) for the framing members. A total of 31 shear wall were tested, 16 were of the double-sheathed configuration and 15 were of the centre-sheathed configuration. The author was responsible for 16 specimens (8 double-sheathed specimens and 8 centre-sheathed specimens); the remaining specimens are reported in Brière *(2017)*. The specimens were tested monotonically and cyclically using the CUREE reversed cyclic protocol or an asymmetric cyclic protocol.

The analysis of the test data of the double-sheathed shear walls was done using the Equivalent Energy Elastic Plastic (EEEP) method (Park *(1989)* and Foliente *(1996)*). A new, preliminary, design procedure was developed to evaluate the nominal shear strength of the centre-sheathed shear walls. This new procedure was based on modifications made to the Effective Strip Method by Yanagi and Yu *(2014)* to better represent the behaviour of the centre-sheathed configuration observed during the tests.

The results of the data analysis were used to determine the load resistance factor, ϕ, for the LSD and LRFD procedures used for design in Canada and in the USA and Mexico respectively. Moreover, the capacity-based design factors for seismic design in Canada; the ductility-related, R_d, and overstrength-related, R_o, factors were determined.

Coupon tests were conducted for the framing and sheathing materials to determine their nominal thickness and mechanical properties such as yield and ultimate tensile strengths.

1.5 Literature Review

Extensive research has been done with regards to CFS shear walls. Although various types of sheathing can be used, more recently CFS shear walls with steel sheet sheathing have been adopted by the current version of the CFS standards. The present research program comprises and investigation of higher capacity CFS sheathed and framed shear walls; therefore, information on past research done with this type of CFS shear walls is presented herein. The information summarized outlines major findings, testing procedures, and analysis methods used in this field of research.

1.5.1 Past Research on Cold-Formed Steel Sheathed and Framed Shear Walls

Testing of cold-formed steel framed shear walls with steel sheet sheathing was first conducted by Serrette *et al*. *(1997)* in the USA, at Santa Clara University. The research program was carried out as a follow up to the results obtained during previous testing completed in 1996 on CFS shear walls sheathed with plywood, OSB, and gypsum (Serrette *et al. (1996)*). In addition to clarifying previous research results, CFS framed shear walls with flat strap X-braces and steel sheathing were included in the 1997 program to provide a wider range of design options. The steel sheathed specimens tested included 610 mm × 2440 mm (2’ × 8’) and 1220 mm × 2440 mm (4’ × 8’) shear walls with steel sheathing thicknesses of 0.46 mm (0.018”) and 0.68 mm (0.027”), and 0.84 mm (0.033”) thick framing members. The specimens were built using the conventional configuration, adopted by the AISI S400 Standard *(2015)*; a frame consisting of back-to-back chord studs, a single interior stud, bottom and top tracks, and sheathing fastened to the frame on one side only with evenly spaced self-drilling sheet metal screws. To resist overturning, holdowns were used at each end of the wall. During the tests, the walls were loaded using displacement control (load applied at the top of the wall), where a static loading protocol and a cyclic sequential phase displacement loading protocol were followed. Serrette’s test setup is shown in Figure 1.3.

Serrette *et al. (1997)* reported that the CFS shear walls with steel sheathing failed from a combination of screw fasteners pulling out of the framing and unzipping of the sheathing due to

significant bearing deformation leading to rupture of the edges. Local buckling of the chord studs occurred in the cases where the fastener spacing was reduced from 150 mm (6”) to 100 mm (4”) and when thicker sheathing was used, resulting in higher shear forces. Overall, it was concluded that steel sheathed shear walls behaved well and that using thicker sheathing results in higher design capacities. These promising results led to further investigations by other research groups with the goal of expanding the design data available for CFS framed and sheathed shear walls.

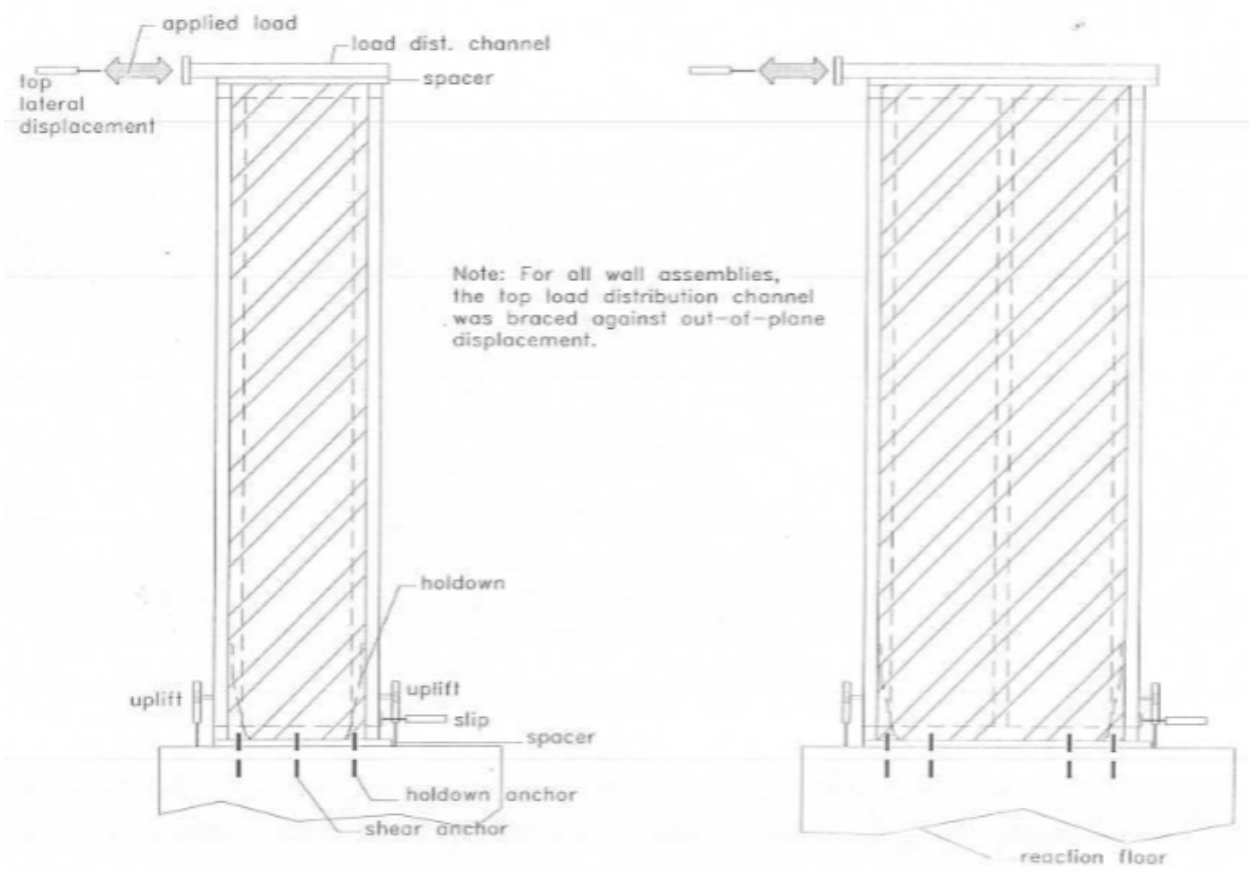

Figure 1.3: Overall test set up (Serrette *et al. (1997)*).

At the time, the design provisions for CFS framed shear walls with steel sheathing of the North American Standard for Cold-Formed Steel Framing – Lateral Design, AISI S213 Standard *(2004)*, were limited to 0.46 mm (0.018”) and 0.68 mm (0.027”) sheathing thicknesses, based on the results obtained by Serrette *et al. (1997)*. In order to address this limitation, a research program

conducted at the University of North Texas, described in the research report by Yu *et al*. *(2007)*, comprised steel sheet shear walls with 0.68 mm (0.027”), 0.76 mm (0.030”), and 0.84 mm (0.033”) sheathing thicknesses. The specimens were built using No. 8 self-drilling screws with panel edge fastener spacings of 50 mm (2”), 100 mm (4”), and 150 mm (6”). Some of the shear walls with 0.68 mm (0.027”) sheathing previously tested by Serrette *et al. (1997)* were re-tested by Yu *et al*. *(2007)*. A total of 66 test specimens were tested; 33 were tested monotonically following the ASTM E564-06 methodology, and 33 were tested cyclically following the Consortium of Universities for Research in Earthquake Engineering (CUREE) reversed cyclic protocol in accordance with the Acceptance Criteria for Prefabricated Wood Shear Panels (ICC-ES AC 130).

In terms of assembly, the walls were built at different aspect ratios (2:1 and 4:1), and with sheathing installed on one side of the wall, screwed on the outer flange of the chord stud. Back-to-back C-shaped studs were used as chord studs framed into bottom and top tracks, and one Simpson Strong-Tie ® holdown was attached to the inside of the tension chord stud to resist uplift forces during monotonic tests, while one holdown was attached to the chord studs at each end of the wall to resist uplift forces during cyclic tests. In addition, this research program also investigated the influence of fastener size (No. 8 vs. No. 10 screws), screw installation pattern (on inner chord stud, on outer chord stud, or staggered), and framing thickness.

Yu *et al. (2007)* reported that using a larger screw size did not improve the shear resistance of the shear walls; however, using a staggered screw pattern slightly improved their shear strength while reducing the flange distortion of the chord studs. The results also showed consistency with the strength reduction factor provided by the AISI S213 Standard *(2004)* for high aspect ratio shear walls (exceeding 2:1). One of the major results from this research program was the significant increase in shear strength when thicker framing members were used. The results showed to be inconsistent with the results obtained by Serrette *et al. (1997)* for shear walls with 0.68 mm (0.027”) sheathing. In a later investigation by Yu and Chen *(2009)*, it was shown that shear walls built with 0.46 mm (0.018”) were also inconsistent with Serrette’s results.

As a continuation of the program by Yu et al. *(2007)*, Yu and Chen *(2009)* further investigated the published nominal shear strengths for shear walls with 0.46 mm (0.018") and 0.68 mm (0.027") steel sheet thicknesses provided by AISI S213 *(2007)* based on results from Serrette *et al. (1997)*. Shear walls 2440 mm × 1830 mm (8' × 6') were also tested.

The discrepancy in the published shear strength for walls with 0.68 mm (0.027") sheets found in Yu *et al*. *(2007)* was confirmed. Furthermore, discrepancies were revealed on the published nominal strength of shear walls with 0.46 mm (0.018") steel sheets for seismic design.

The purpose for testing 2440 mm × 1830 mm (8' × 6') specimens was to determine seismic detailing to prevent chord stud damage (as it was observed in previous research) while improving the behaviour of the walls in terms of shear strength and ductility. The seismic details included using No. 10 screws staggered at the sheathing-to-stud connections, and a frame strapping with blocking at the mid height of the walls. The framing thickness ranged from 1.09 mm (0.043") to 1.37 mm (0.054") and the sheathing thickness ranged from 0.68 mm (0.027") to 0.84 mm (0.033"). All 2440 mm × 1830 mm (8' × 6') specimens had a fastener spacing of 50 mm (2"). Yu and Chen *(2009)* reported that the seismic detailing increased the shear strength and ductility of the shear walls. However, seismic detailing was not needed to achieve the desired behaviour in 2440 mm × 1830 mm (8' × 6') shear walls built with 0.84mm (0.033") sheathing and 1.37 mm (0.054") framing.

Following the research by Yu and Chen *(2009)*, an extensive research program was conducted in Canada at McGill University by Ong-Tone *(2009)* and Balh *(2010)*. Their test specimens were built using a similar shear wall configuration (CFS framed and sheathed with sheathing on one side only) as in the programs completed by Yu et al. *(2007)* and Yu and Chen *(2009)*. The specimens were built with combinations of various building parameters (18 different sets of parameters) such as wall aspect ratios (1:1, 2:1, and 4:1), sheathing thickness, framing thickness, detailing, and fastener spacing. The framing thicknesses were 0.84 mm (0.033") and 1.09 mm (0.043"), while the sheathing thicknesses were 0.46 mm (0.018") and 0.76 mm (0.030"). In terms of detailing, in some specimens bridging was installed horizontally at the quarter points

over the height of the wall to minimize twisting of the chord stud due to the development of a tension field in the eccentrically placed sheathing (i.e. sheathing on one side of the wall).

Overall, 54 specimens were tested; 23 by Ong-Tone *(2009)* and 31 by Balh *(2010)*. Monotonic and reversed cyclic tests followed the CUREE protocol, consistent with the protocol used by Yu et al. *(2007)* and Yu and Chen *(2009)*. For the analysis of the test data, the Equivalent Energy Elastic Plastic (EEEP) approach was used. The observed shear wall failure modes were consistent with previous research, where the main failure mode occurred at the sheathing-to-frame connections with pull-through of fasteners and tearing of the edge of the sheathing from extensive bearing. The shear strength of the shear walls was influenced by the thickness of framing and sheathing, as well as the fastener spacing. An increase in shear strength was achieved when the fastener spacing was reduced and thicker framing and sheathing were used. Although it was observed that the addition of bridging reduced chord stud damage and improved the shear strength of the shear walls, it was concluded to be inadequate as the bridging members were too slender, making them unable to provide full support to the chord studs and compromising the ductility of the shear walls. (Figure 1.4). When compared to the results obtained by Serrette *et al. (1997)* and Yu *et al. (2007)*, the shear resistances obtained by Ong-Tone *(2009)* and Balh *(2010)* were shown to be consistent.

It was proposed that a resistance factor of $\phi = 0.7$ (for Limit States Design, LSD) to be included in the CFS design standards. In addition, for seismic design, a drift limit of 2% was proposed for steel sheathed shear walls. Initially, the seismic force modification factors calculated based on test data, R_d = 2.5 and R_o = 1.7, were recommended, however these values did not meet some of the minimum requirements of the FEMA P695 *(2009)* methodology after the dynamic analysis of model buildings under representative ground motions. New R-values were recommended after the design buildings were modified. Finally, R_d = 2.0 and R_o = 1.3 were recommended.

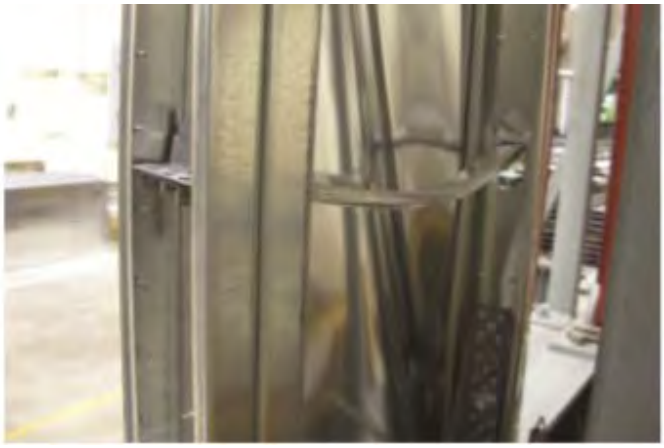

Figure 1.4: Buckling of bridging in CFS framed and sheathed shear wall (Balh *(2010)*).

A subsequent research program was conducted at McGill University to investigate CFS framed shear walls with steel sheathing under combined lateral and gravity loading with special blocking details to avoid chord stud damage. The combination of lateral and gravity loading on CFS framed shear walls with wood sheathing had been previously investigated by Hikita *(2006)*, and it served as a basis for this research program by DaBreo *(2012)*. Adjustments were made to the gravity loading system used by Hikita *(2006)* to avoid the additional lateral load experienced by the specimen from the horizontal component of the tension force in the anchors as the specimen was laterally displaced. The gravity load test system is shown in Figure 1.5 (A).

As the use of bridging to avoid twisting of the chord studs had already been investigated by Balh *(2010)* and Ong-Tone *(2009)*, DaBreo *(2012)* addressed this issue by replacing the slender bridging members with more rigid members; blocking. Additionally, DaBreo *(2012)* designed the chord studs as beam-columns to include the moments due to the eccentric loading from having sheathing on one side of the wall only.

The research by DaBreo *(2012)* involved testing 14 specimens, all 2440 mm × 1220 mm (8’ × 4’) shear walls, with varying framing and sheathing thickness and fastener spacing. Blocking was also incorporated into the shear wall configurations (Figure 1.5 (B)). The framing thicknesses were 1.09 mm (0.043”) and 1.37 mm (0.054”) and the sheathing thicknesses were 0.46 mm (0.018”) and 0.76 mm (0.030”). Fastener spacing of 50 mm (2”), 75 mm (3”), 100 mm (4”), and

150 mm (6”) were used to build the walls. As in previous research, the specimens were tested monotonically and cyclically using the CUREE reversed cyclic protocol.

The characteristic failure modes were observed; bearing at the sheathing-to-frame connections leading to sheathing tear-out and screw fastener pull-through. The shear resistance of the walls was again linked to the building parameters, DaBreo concluded that, like Balh *(2010)* and Ong-Tone *(2009)*, the shear strength of the specimens increased with smaller fastener spacing and thicker steel sheathing. When looking at the effects of blocking, the results showed that specimens with blocking were 1.37 to 1.80 stronger than identical specimens without blocking. Although their shear resistance was higher and larger energy dissipation was achieved, the blocked walls’ ductility generally decreased, similar to the specimens with bridging tested by Balh *(2010)*.

After the data was analysed using the EEEP approach, DaBreo *(2012)* recommended the same LSD resistance factor and *test-based* seismic force modification factors as Ong-Tone *(2009)* and Balh *(2010)*; $\phi = 0.7$, R_d = 2.0 and R_o = 1.3 respectively. Nonlinear time-history dynamic analysis was performed to evaluate the seismic performance of a sample building in order to validate the *test-based* R-values. The resulting adjusted collapse margin ratio (ACMR) failed to meet the FEMA P695 *(2009)* minimum requirement and therefore the *test-based* R-values were not validated.

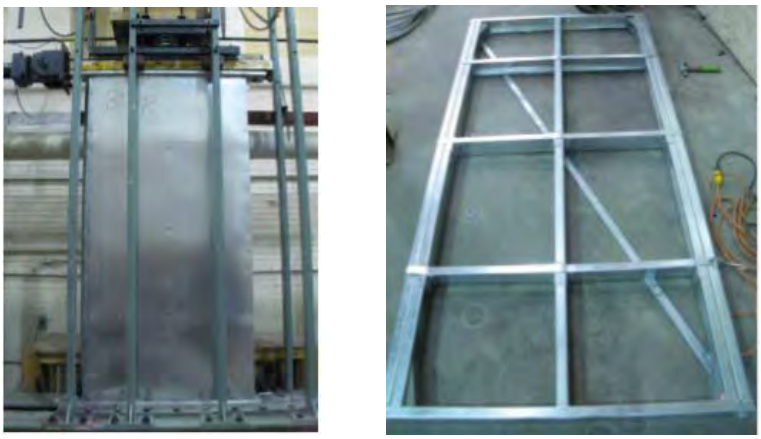

A B

Figure 1.5: A) Specimen installed in test frame with gravity load system. B) Frame assembly with blocking members (DaBreo *(2012)*).

These types of CFS shear walls were later tested dynamically by Shamim *(2012)* where test information from Balh *(2010)*, Ong-Tone *(2009)*, Yu *et al. (2007)*, and Serrette *et al*. *(1997)* were used in the design of the specimens. With the lack of design guidelines for CFS shear walls with steel sheathing in Canada, Shamim's main research objective was to develop seismic design provisions to be included in the National Building Code of Canada (NBCC) and in the AISI S213 Standard (now the AISI S400 Standard *(2015)*).

The testing of full-scale single- and double-storey CFS framed and sheathed shear walls (10 in total) was conducted on the shake table at Ecole Polytechnique de Montreal (Figure 1.6). The 1220 mm × 2440 mm (4' × 8') specimens were built with sheathing of 0.46 mm (0.018") or 0.76 mm (0.030") thickness. The single-storey walls were built with 1.09 mm (0.043") framing members while the double-storey walls were either built with 1.09 mm (0.043"), 1.37 mm (0.054"), or 1.73 mm (0.068") framing members. The sheathing was attached to the frame with No. 8 screws with a varying spacing schedule. The specimens were also constructed using frame blocking members matching the thickness of the tracks, previously investigated by DaBreo *(2012)*, to reduce twisting damage of the chord studs and improve the shear resistance of the walls.

Figure 1.6: Steel sheathed wall specimen on the shake table (Shamim *(2012)*).

The specimens were subjected to impact tests, harmonic forced vibration tests, and ground motion tests representing seismic hazards in Quebec and Vancouver, Canada. The results of the dynamic tests, failure modes and seismic performance, showed to be consistent with the statically tested (monotonically and cyclically) shear walls from previous research. The main failure modes occurred in the sheathing-to-frame connections where screw pull-out and sheathing tear-out were observed. Although damages to the studs were reported due to the compressive and in-plane lateral forces from the tension field, they were not detrimental to the overall performance of the shear walls. The use of blocking showed to increase the shear strength of the shear walls by almost 50% in specimens with a fastener spacing of 50 mm (2").

After the testing phase of the research, numerical modeling of the shear walls calibrated using the data from the dynamically tested specimens was completed. The OpenSees software was used to create the numerical models and run nonlinear time-history dynamic analyses under different ground motions to assess the prediction of the tested shear walls' seismic performance. The results of the numerical analyses; hysteresis response, strength response, and displacement response, of all steel-sheathed shear walls were consistent with the test results. The details of the numerical modelling and calibration are reported in Shamim and Rogers *(2013)*.

The calibrated numerical models of the shear walls were used in the numerical modelling of representative buildings. The seismic performance factors, R_d = 2.0 and R_o = 1.3 were recommended after the R-values were validated according to the FEMA P695 *(2009)* methodology.

Finally, the seismic design provisions for CFS shear walls with steel sheet sheathing for design in Canada were presented by Shamim and Rogers *(2015)* and were implemented, for the first time, into the replacement of the AISI S213 Standard *(2007)*, the AISI S400 Standard *(2015)*. The design guidelines were developed based on a compilation of results gathered throughout the years from different research programs, which included static testing, dynamic testing, and dynamic numerical modeling subjected to response-history analyses.

1.5.2 Cold-Formed Steel Design Standards

The North American cold-formed steel standards provide combined provisions for design in Canada, the USA, and Mexico; although variations are found depending on the provisions of the respective national (model) building code. For example, the seismic force modification factors, referred to as *R* in the USA and Mexico, are obtained from the standard for Minimum Design Loads and Associated Criteria for Buildings and Other Structures (ASCE/SEI-7 *(2016)*), while in Canada these factors are referred to as R_d and R_o, and are obtained from the National Building Code of Canada (NRC *(2015)*).

The North American Standard for Seismic Design of Cold-Formed Steel Structural Systems, AISI S400 *(2015)*, is used for LFRS design, including shear walls with strap bracing, with wood panel sheathing, with gypsum board sheathing, and with steel sheet sheathing. The AISI S400 Standard *(2015)* is the first version to include design provisions for steel-sheathed shear walls in Canada. Its previous version, the AISI S213 Standard *(2007)*, only provided guidelines for design of this type of shear wall in the USA and Mexico.

The design values, nominal shear strengths, for shear walls with steel sheet sheathing on one side of the wall are found in Table E2.3-1 of the AISI S400 Standard *(2015)* (shown in Table 1.1). The steel sheathing thicknesses available for design range from 0.46 mm (0.018") to 0.84 mm (0.033") with frame thicknesses ranging from 0.84 mm (0.033") to 1.37 mm (0.054"). Although the tabulated design values were derived from a combination of the test data from the numerous research programs, described in this chapter, they vary between the USA (and Mexico) and Canada. This is because the design values for the USA and Mexico were calculated based on analysis using the ultimate shear strength obtained during the tests, while the design values for Canada were calculated based on analyses using the yield shear strength, obtained from the Equivalent Energy Elastic Plastic (EEEP) analysis of the test data, as was done by Balh *et al. (2014)*.

Table 1.1: Nominal Shear Strength [Resistance] per Unit Length for Seismic and Other In-Plane Loads for Shear Walls With Steel Sheet Sheathing on One Side of Wall (AISI S400 *(2015)*)

U.S. and Mexico (lb/ft)								
Assembly Description	Max. Aspect Ratio (h:w)	Fastener Spacing at Panel Edges[2] (in.)				Stud Blocking Required	Designation Thickness[5] of Stud, Track and Stud Blocking (mils)	Minimum Sheathing Screw Size
		6	4	3	2			
0.018" steel sheet	2:1	390	-	-	-	No	33 (min.)	8
0.027" steel sheet	2:1[3]	-	1000	1085	1170	No	43 (min.)	8
	2:1[3]	647	710	778	845	No	33 (min.)	8
0.030" steel sheet	2:1[3]	910	1015	1040	1070	No	43 (min.)	8
	2:1[3]	-	-	-	1355	Yes	43 (min.)	10
0.033" steel sheet	2:1[3]	1055	1170	1235	1305	No	43 (min.)	8
	2:1[3]	-	-	-	1505	Yes	43 (min.)	10
	2:1[3]	-	-	-	1870	No	54 (min.)	8
	2:1[3]	-	-	-	2085	Yes	54 (min.)	10
Canada **(kN/m)**								
Assembly Description	Max. Aspect Ratio (h:w)	Fastener Spacing at Panel Edges[2] (mm)				Stud Blocking Required	Designation Thickness[5] of Stud, Track and Stud Blocking (mils)	Required Sheathing Screw Size
		150	100	75	50			
0.46 mm steel sheet	2:1	4.1	—	—	—	No	33 (min)	8
0.46 mm steel sheet	2:1	4.5	6.0	6.8	7.5	No	43 (min)	8
0.68 mm steel sheet	2:1	6.5	7.2	7.9	8.7	No	33 (min)	8
0.76 mm steel sheet	4:1	8.9	10.6	11.6	12.5	No	43 (min)	8
0.84 mm steel sheet	4:1	10.7	12.0	13.0	14.0	No	43 (min)	8
0.46 mm steel sheet	2:1	7.4	9.7	11.6	13.5	Yes	43 (min)	8
0.76 mm steel sheet	2:1	11.7	14.3	—	—	Yes	43 (min)	8
0.76 mm steel sheet	2:1	—	—	19.9	23.3	Yes	54 (min)	8

This tabulated design approach limits the shear wall design options, as a restricted number of building parameter combinations are possible with the few listed sheathing thicknesses, frame thicknesses, fastener spacing, and screw sizes. An *equation-based* approach, the Effective Strip Method, is available in Section E2.3.1.1.1 of the AISI S400 Standard *(2015)* to compute the nominal shear resistance of steel-sheathed shear walls; however, it can only be used for design in the USA and Mexico. The Effective Strip Method is based on research by Yanagi and Yu *(2014)* and it is described in Section 2.3 and Appendix B of this report. The method incorporates the

influence of key building parameters, such as frame and sheathing thickness, screw size, wall aspect ratio, and fastener spacing, on the shear resistance of the wall. The method was developed and calibrated using test data from previous research done on CFS steel-sheathed shear walls, including tests performed by Yu *(2010),* Yu and Chen *(2011),* and Balh *(2010).* Although the Effective Strip Method provides a certain freedom for the designer in terms of building parameter combinations, it is still limited by the type of wall configuration (i.e.: how the frame is assembled and placement of the sheathing) and the building parameters used to build the test specimens used in the calibration of the method.

1.6 Summary

In the past decade, significant research has been carried out on cold-formed steel framed shear walls with steel sheet sheathing. Most of this research has been focused on shear walls built with a limited range of steel sheathing thickness and frame thickness. Furthermore, virtually all shear walls were built using the same general configuration; that is, sheathing on one side of the wall, back-to-back chord studs, and a field stud in the centre. This resulted in shear walls with limited shear resistances and ductility, only adequate to resist forces experienced by low-rise structures.

The failure modes observed for this type of shear wall were consistent throughout the various research programs; mainly, failure of the sheathing-to-frame connections in the form of bearing and tear-out of the sheathing as well as pull-out of the fasteners. An undesirable and reoccurring observation also seen throughout the research programs was the twisting damage of the chord studs from out-of-plane forces. This type of damage negatively affected the shear resistance of the specimens. The issue was addressed by installing frame blocking members, however this solution showed to improve the shear resistance of the walls but reduce their ductility.

The success of the research lead, for the first time, to the implementation of design provisions into the AISI S400 Standard *(2015)* for shear walls with steel sheathing in Canada.
The information from past research has expanded the knowledge in this field and has served as a guideline in terms of loading protocols and data analysis procedures for subsequent research programs, including the one presented herein. The research presented in this report is based on

addressing the shortcoming and limitations of past research in order to achieve higher capacity steel framed and sheathed shear walls, built with new configurations, adequate for mid-rise construction.

CHAPTER 2 – DESCRIPTION OF SHEAR WALL TEST PROGRAM

2.1 Test Frame Setup and Background Information

The single-storey cold-formed steel (CFS) sheathed and framed shear wall (double-sheathed and centre-sheathed walls) research program consisted of 31 walls, which were tested during the summer and fall of 2016 in the Department of Civil Engineering and Applied Mechanics' Jamieson Structures Laboratory at McGill University. The author was responsible for 16 of the tested walls, while the remaining specimens were tested by Brière *(2017)*. Platform framing was used to construct the walls; they were assembled horizontally on the ground or tables and then erected vertically and installed into the testing frame. The testing frame was built in 2002 (Figures 2.1 and 2.2); it is equipped with a 250 kN (56.2 kips) MTS dynamic loading actuator with a ±125 mm (±5") stroke which displaces the top of the wall in-plane allowing for monotonic and cyclic tests to be performed. The out-of-plane movement of the walls is prevented by lateral supports with HSS braces installed perpendicular to the wall at the top. The specifications, design, and construction of the test frame is detailed by Zhao *(2002)*.

The actuator was attached to a loading beam through 4 bolts; the loading beam was used to attach the top of the wall to the frame and to transfer the load from the actuator to the wall. The loading beam was built by welding a 304.8 mm × 304.8 mm × 25.4 mm (12" × 12" × 1") steel plate with 4 bolt holes to one side of the HSS beam. The bolt hole patterns were pre-drilled on the HSS member before the welding of the plate. To allow smooth lateral movement of the loading beam greased Teflon strips were glue to both sides of the loading beam

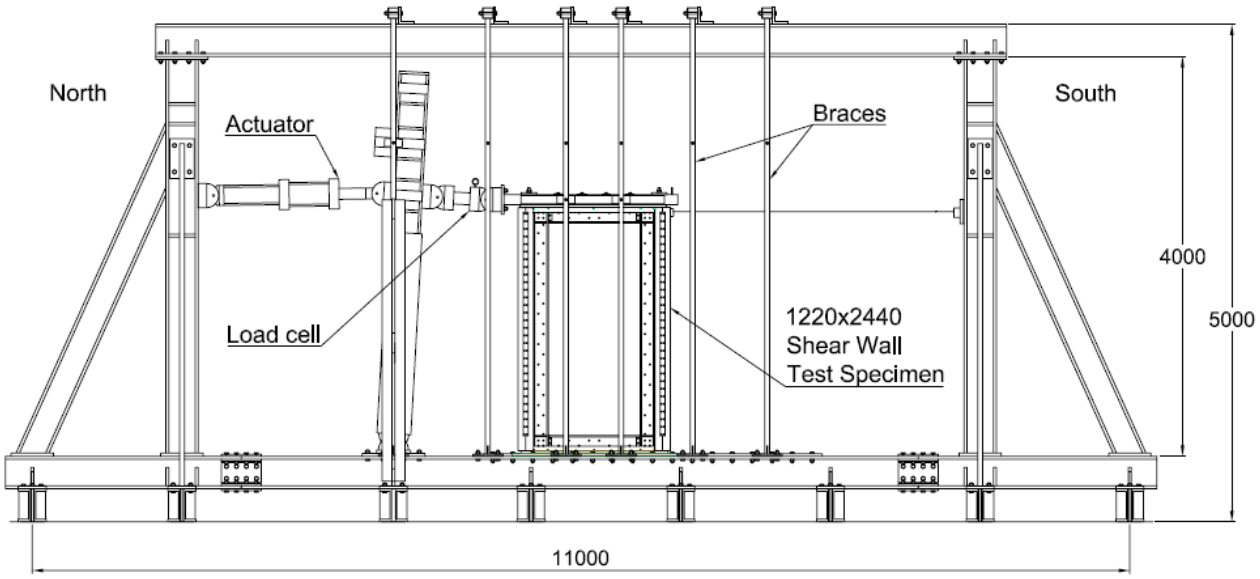

Figure 2.1: Shear wall test frame (dimensions in mm).

Figure 2.2: Shear wall specimen installed in test frame.

2.2 Steel-Sheathed and Framed Shear Wall Test Program

The wall test specimens were composed of a cold-formed steel sheathing panel screw connected to a cold-formed steel frame. The test program included different wall configurations with varying frame thickness, sheathing thickness, fastener size, fastener spacing, and type of

frame reinforcement. In addition, the test program comprised of two main sheathing placement designs, and therefore was separated into two testing categories: double-sheathed tests and centre-sheathed tests. A summary of the test program is outlined in Tables 2.1a and 2.1b. Initially the test program included 27 walls, however based on the test results 4 additional walls were tested to obtain a more complete set of data. All 31 walls were 1220 mm × 2440 mm (4' × 8'), 16 of the walls had a double-sheathed design, and 15 walls had a centre-sheathed design. The walls tested by the author are documented in this thesis; the remaining 15 walls are documented by Brière *(2017).* Schematic drawings and details of each wall configuration are found in Appendix A.

Table 2.1a: Double-Sheathed Shear Wall Test Matrix

Test	Sheathing thickness mm (in)	Framing thickness mm (in)	Sheathing screw size (#)	Fastener spacing mm (in)	Type of test[1]
Double-Sheathed Configuration					
W19[2]	2 x 0.36 (0.014)	1.73 (0.068)	10	50 (2)	M & C
W20[2]	2 x 0.36 (0.014)	1.73 (0.068)	10	100 (4)	M & C
W21[2]	2 x 0.36 (0.014)	2.46 (0.097)	10	50 (2)	M & C
W22[2]	2 x 0.36 (0.014)	2.46 (0.097)	10	100 (4)	M & C
W28[3]	2 x 0.47 (0.019)	2.46 (0.097)	10	50 (2)	M & C
W29[3]	2 x 0.47 (0.019)	2.46 (0.097)	10	100 (4)	M & C
W30[3]	2 x 0.47 (0.019)	2.46 (0.097)	12	50 (2)	M & C
W31[3]	2 x 0.47 (0.019)	2.46 (0.097)	12	100 (4)	M & C

[1] M: Monotonic; C: Cyclic
[2] Wall specimen tested by author
[3] Wall specimen tested by Brière *(2017)*

Table 2.1b: Centre-Sheathed Shear Wall Test Matrix

Test	Sheathing thickness mm (in)	Framing thickness mm (in)	Sheathing screw size (#)	Fastener spacing mm (in)	Type of test[1]
Centre-Sheathed Configuration					
W15[2]	0.84 (0.033)	2.46 (0.097)	10	50 (2)	MR3 & CR3
W15B[2,4]	0.84 (0.033)	2.46 (0.097)	10	50 (2)	CR3
W16[2]	0.84 (0.033)	2.46 (0.097)	10	50 (2)	MR & MR2
W17[2]	0.84 (0.033)	2.46 (0.097)	10	150 (6)	M & C
W18[3]	0.84 (0.033)	2.46 (0.097)	10	100 (4)	M, MR & CR
W23[3]	1.09 (0.043)	2.46 (0.097)	12	100 (4)	CR3
W23B[3,4]	1.09 (0.043)	2.46 (0.097)	12	100 (4)	CR3
W24[3]	1.09 (0.043)	2.46 (0.097)	12	150 (6)	CR3
W25[2,4]	0.84 (0.033)	2.46 (0.097)	10	100 (4)	CR3
W26[3,4]	1.09 (0.043)	2.46 (0.097)	10	100 (4)	CR3

[1] M: Monotonic; C: Cyclic; _R, _R2 and _R3: Different chord stud reinforcements tested
[2] Wall specimen tested by author
[3] Wall specimen tested by Brière *(2017)*
[4] Asymmetric cyclic test to reach a higher maximum chord rotation
Note: In all reinforced specimens double holdowns were installed at the bottom corners to carry the anticipated uplift forces.

2.2.1 Double-Sheathed Configuration

The shear wall tests performed by Rizk *(2017)* showed that walls of certain fastener configurations and with an asymmetric sheathing placement (sheathing on one side only) caused eccentric tension field forces high enough to result in the out-of-plane twisting of the wall and unwanted damage to the chord studs, thus lowering the capacity of the shear walls. Damage to the chord studs is also undesirable because they provide resistance to gravity loads applied to the wall from storeys above. To address these shortcomings a double-sheathed shear wall design was developed with the sheathing installed on both sides of the wall (Figure 2.3) to eliminate the tension field force eccentricity and to avoid out-of-plane twisting of the wall, in turn increasing the shear capacity of the wall. It was expected that by eliminating force eccentricity the frame blocking used by Rizk would not be needed, and therefore was not used to build the test specimens.

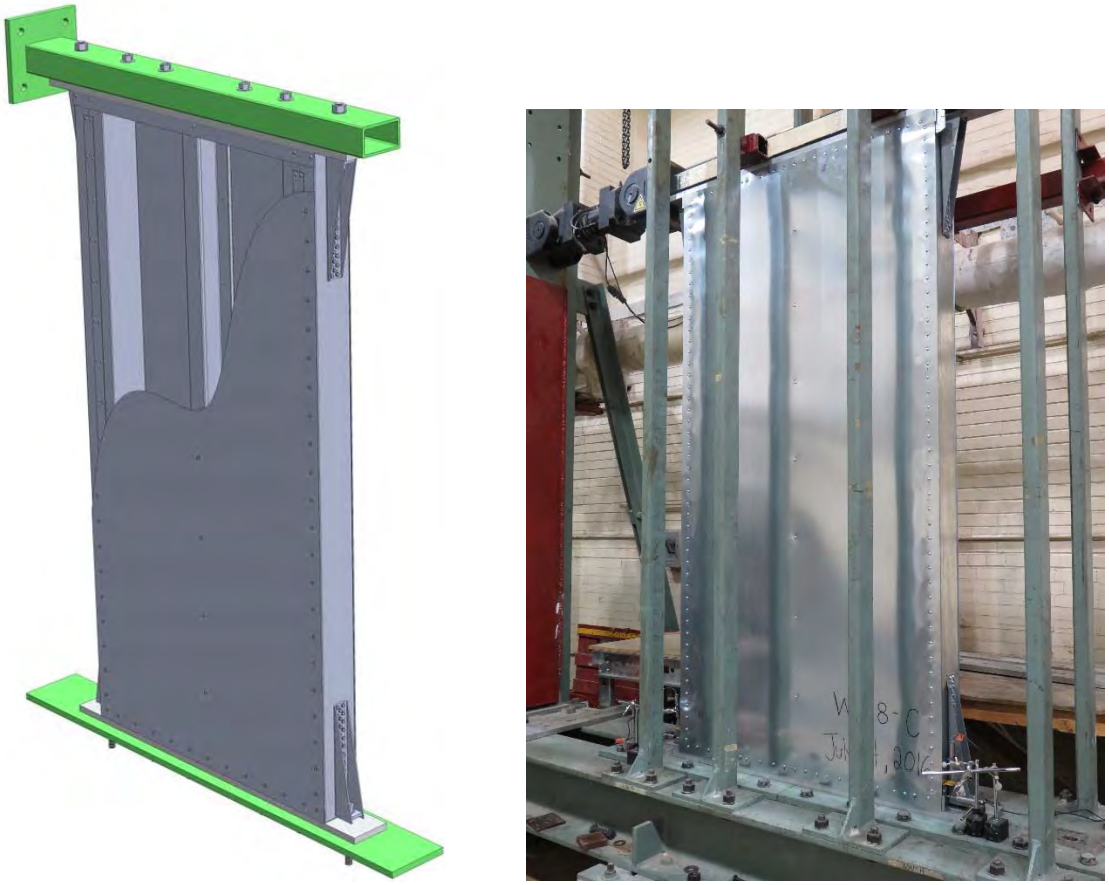

Figure 2.3: Double-sheathed shear wall configuration.

2.2.2 Centre-Sheathed Configuration

To further improve the wall's resistance and ductility under shear loading a centre-sheathed design was included in the test program. Rizk *(2017)* observed that as the in-plane rotation of the walls increased the sheathing was subjected to higher shear stresses resulting in a compression field, which caused shear bucking of the sheathing; this was also observed for the tested double-sheathed specimens. Due to this shear buckling and the force developed normal to the plane of the wall, virtually the entire sheathing panel pulled over the heads of the screw and detached from the wall (Figure 2.4) no longer contributing to the lateral resistance of the wall.

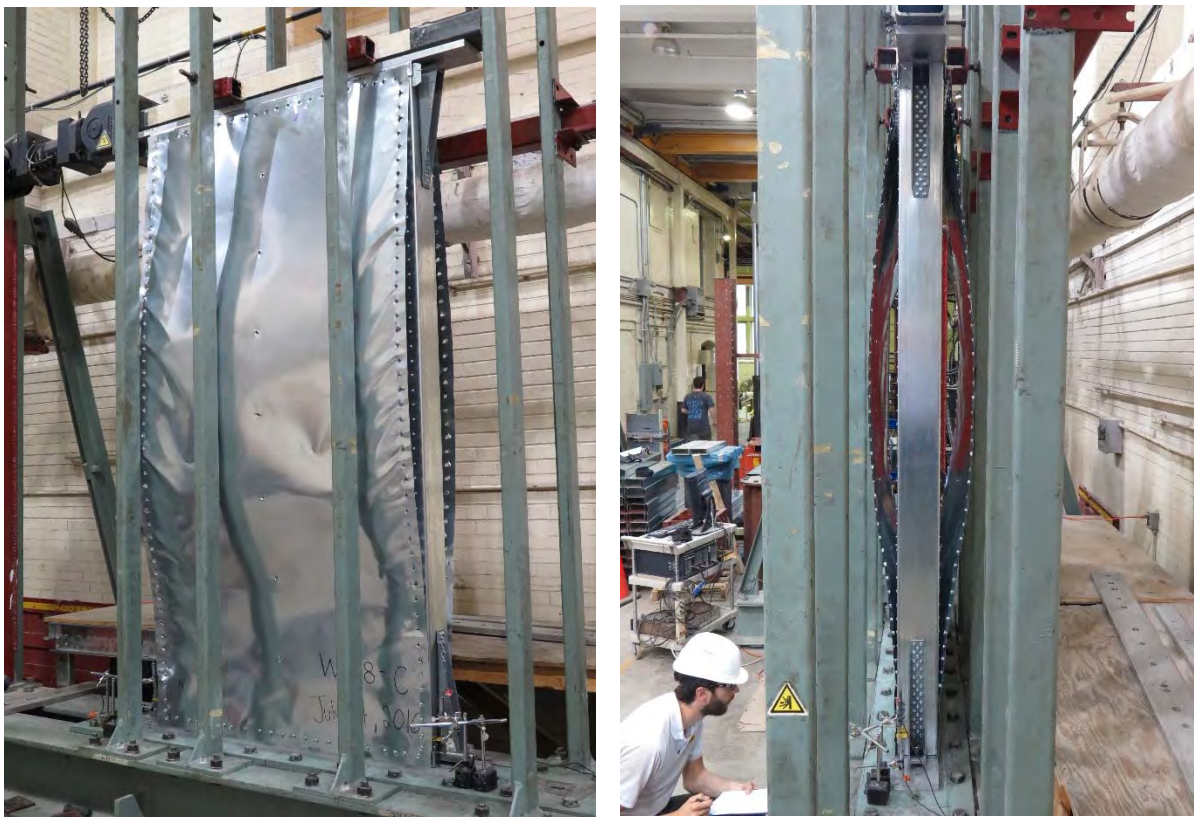

Figure 2.4: Sheathing detached from double-sheathed shear wall subjected to reversed cyclic loading.

The centre-sheathed wall design was developed with the goal of obtaining a higher shear resistance by avoiding sheathing pull-through, while having a concentric sheathing placement to stop the wall's and chord studs' out-of-plane twisting. In addition, by confining the sheathing between the framing it was anticipated that the ductility would be improved because the sheathing would not become detached from the framing, allowing for extended bearing deformations. Figure 2.5 shows the centre-sheathed design where the sheathing was installed between the webs of the wall's built-up chord stud members. In order to avoid frame failure due to the increased wall resistance, chord stud reinforcements and extra bottom holdowns had to be installed in selected wall configurations (indicated by MR, MR2, MR3, CR, and CR3 in Table 2.1b).

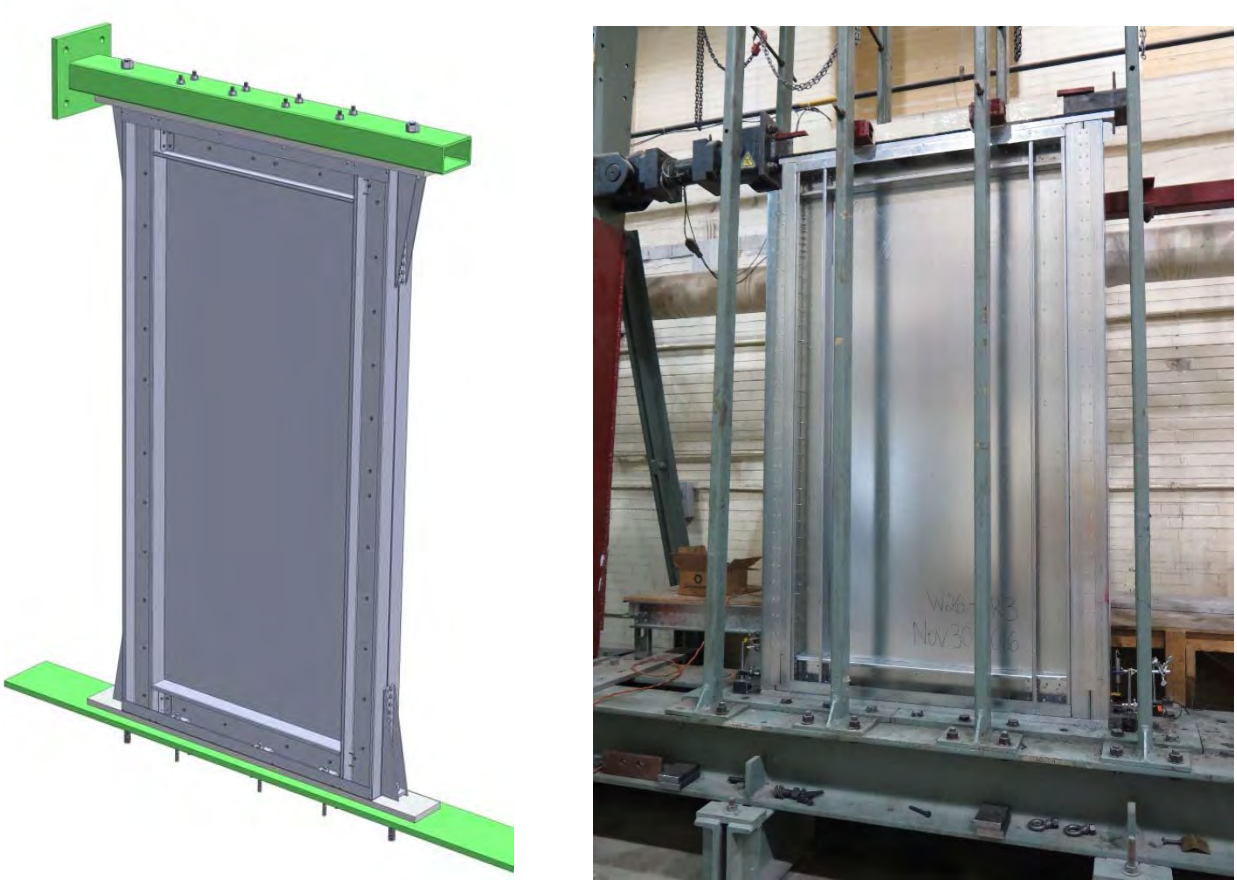

A B

Figure 2.5: Centre-sheathed wall design. A) Original wall configuration. B) Final wall configuration with chord stud reinforcement.

Furthermore, during the reversed cyclic tests of configurations W15-CR3 and W23-CR3 the wall top displacement reached the actuator's stroke limit of 125 mm (5") before degradation in the shear resistance was observed. To overcome this limitation and to observe shear force degradation, the same configurations were tested using an asymmetric cyclic protocol where the walls were installed 100 mm (4") from their initial position, allowing the actuator origin to be off-set by 100 mm (4"). During these tests, the displacement cycles were performed asymmetrically; this change allowed the walls to displace an extra 100 mm (4"), giving the walls a total displacement limit of 225 mm (9"). A comparison between wall resistance vs. displacement of the symmetric and the asymmetric cyclic tests is shown in Figure 2.6. Wall configurations W25-CR3 and W26-CR3 were expected to reach similar high levels of ductility; therefore, they were also tested asymmetrically in order to record their pre-peak and post-peak behaviour.

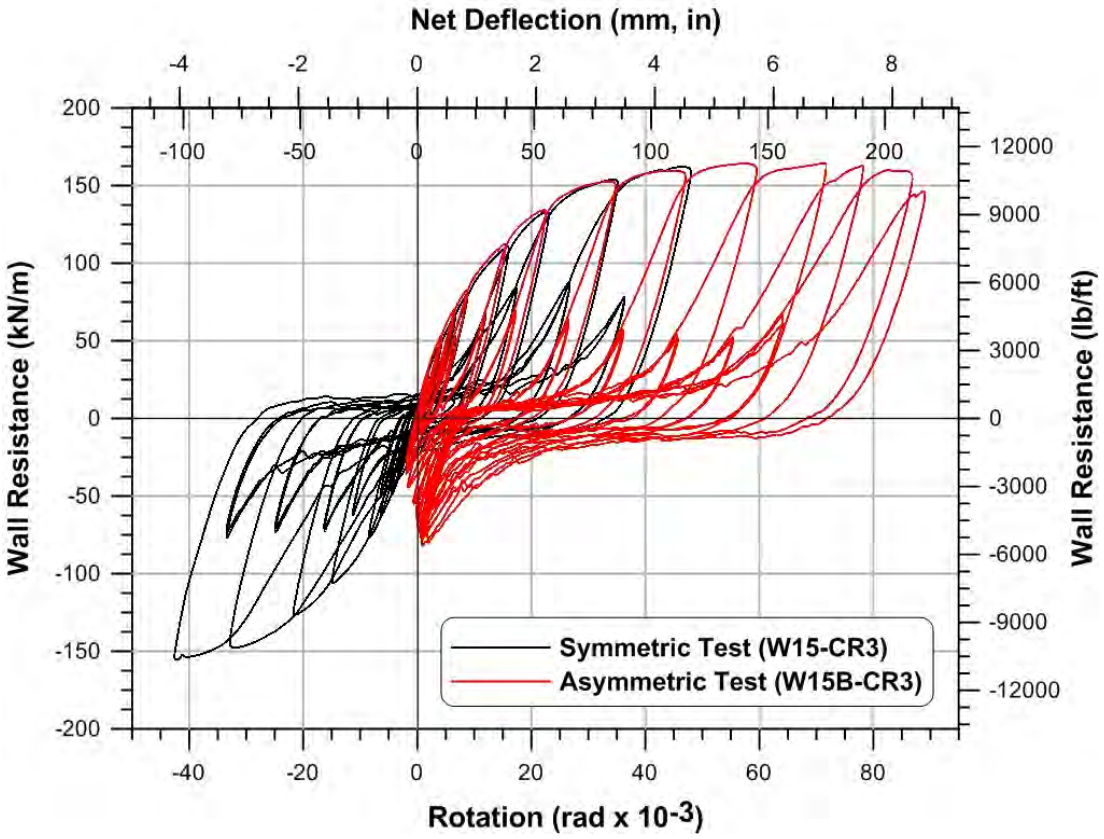

Figure 2.6: Symmetric vs. asymmetric cyclic centre-sheathed shear wall tests.

2.3 Shear Force Predictions and Selection of Member Sizes

Prior to ordering the members from the manufacturer the size of the chord stud sections were chosen according to the predicted shear force experienced by the wall. The predicted shear force was calculated as the nominal shear strength of the wall, V_n, using the Effective Strip Method described by Yanagi and Yu *(2014)*, which is also available in the AISI S400 Standard *(2015)*. The method accounts for an effective strip width of the sheathing (Figure 2.7) and Equation (2-1), W_e, that carries the diagonal tension force in the system resulting from an applied lateral load. This width is dependent on the factor λ (Equation (2-2)), which relates the tensile strength of the sheathing and the frame (represented by α_1 and α_2), the thickness of the sheathing and the frame (represented by β_1 and β_2), the fastener spacing, s (represented by β_3), and the wall's aspect ratio, a.

The method also takes into account the shear capacity of the individual fasteners (Equation (2-3)), P_{ns}, since this is the main force transfer path and the dominant failure mode within the tension field. P_{ns} becomes the minimum of the connection's tilting and bearing capacity, $P_{ns,a}$, the connection's end distance shear capacity, $P_{ns,b}$, or the manufacturer's fastener shear capacity, $P_{ns,c}$.

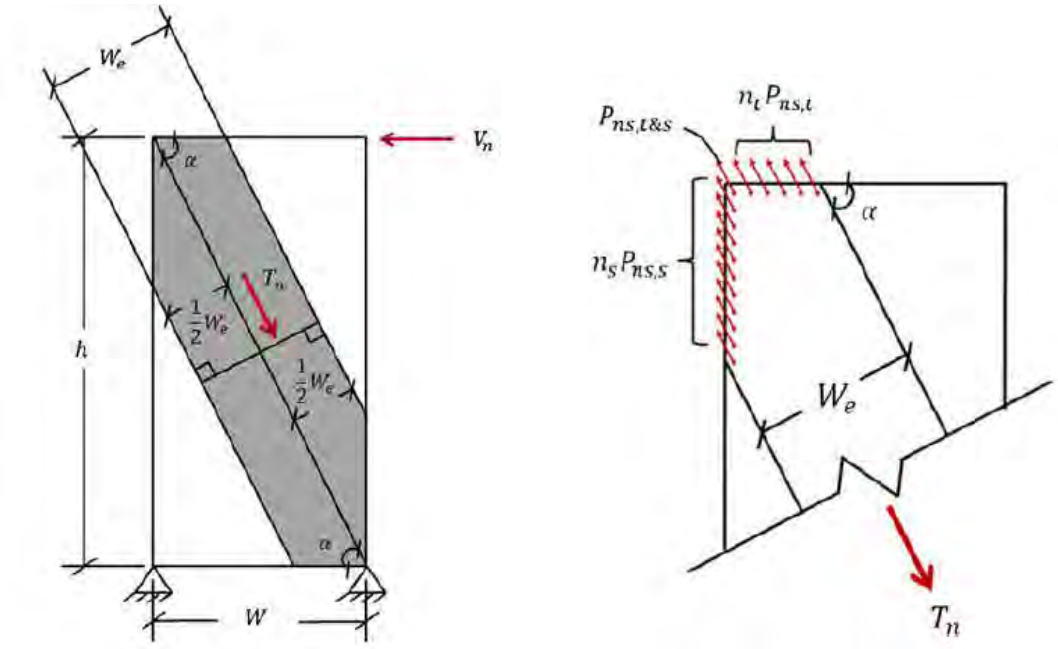

Figure 2.7: Effective Width Method tension field representation by Yanagi and Yu *(2014)*.

$$W_e = \begin{cases} W_{max,} & if\ \lambda \leq 0.0819 \\ \rho W_{max,} & if\ \lambda > 0.0819 \end{cases} \tag{2-1}$$

where,

W_{max} = maximum width of effective strip;

ρ = empirically determined strip width reduction factor based on λ.

$$\lambda = 1.736 \frac{\alpha_1 \alpha_2}{\beta_1 \beta_2 \beta_3^2 a} \tag{2-2}$$

$$P_{ns} = \min(P_{ns,a}, P_{ns,b}, P_{ns,c}) \tag{2-3}$$

Once V_n was obtained using Equation (2-4), the walls were modelled and analysed in SAP2000© in order to obtain the compression chord stud's member forces.

$$V_n = min\left\{\left(\frac{W_e}{2s\ sin\alpha}P_{ns,t} + \frac{W_e}{2s\ cos\alpha}\ P_{ns,s} + P_{ns,s\&t}\right)cos\alpha, W_e t_{sh} F_{ysh}\ cos\alpha\right\} \qquad (2\text{-}4)$$

The Strip Method was developed based on experimental research done by Yu *(2010)*, Yu and Chen *(2011)*, and Balh *(2010)* on cold-formed steel shear walls designed using the conventional single-sided sheathing placement. The test configurations included using sheathing thicknesses of 0.84 mm (0.033"), 0.76 mm (0.030"), and 0.68 mm (0.027"), a frame thickness of 1.09 mm (0.043"), and No. 8 or No. 10 sheathing screws.

2.3.1 Analysis of Chord Stud Forces

To obtain the member forces of the compression chord stud under an applied shear flow along the top of the wall, SAP2000© models of the shear wall configurations were created. The shear walls were modelled based on the Effective Strip Method where the effective width, W_e, was represented by strip elements pin-connected to the studs and tracks at the appropriate fastener spacing to simulate the sheathing screw connections. Similar to the tracks and studs, the strip elements were defined as frame sections in SAP2000©, the strip elements' dimensions and section properties were calculated based on the geometry of the wall and of the diagonal tension field.

First, the number of screws along the chord studs and tracks, n, within the sheathing effective width, W_e, were calculated using Equation (2-5), where s is the fasteners spacing along the chord studs and α is the angle between the track and the sheathing effective width (Figure 2.7). All wall configurations had an aspect ratio, a, of 2:1 therefore a theoretical track fastener spacing, s_t, was calculated (Equation (2-6)) in order connect the same number of strip elements along the tracks and chord studs in the model. In reality, the number of screws along the tracks within the effective width were less than n because the tracks were shorter than the chord stud members.

$$n = \frac{W_e}{2s\,cos\alpha} \tag{2-5}$$

$$s_t = \frac{s}{a} \tag{2-6}$$

The width, w_s, of each strip (Equation (2-7)) was determined by dividing W_e by the number of strip elements, $2n+1$, since the sum of the width of all strip elements is equivalent to the effective width of the sheathing. Taking the thickness of the strip elements as the thickness of the sheathing, t_{sh}, the cross-sectional area, A_s, of each strip element was calculated (Equation (2-8)). These section properties as well as the moment of inertias, I_x and I_y, and elastic section moduli, S_x and S_y, were input into SAP2000© when defining the strip elements as frame sections. The plastic section moduli, Z_x and Z_y, were assumed to be the same as the elastic section moduli because local buckling and overall buckling of the section were expected to occur before any plastic deformation.

$$w_s = \frac{W_e}{2n+1} \tag{2-7}$$

$$A_s = w_s t_{sh} \tag{2-8}$$

The calculated nominal shear strength of the wall, V_n, was assigned as a uniformly distributed shear load (kN/m) in the global x-direction along the top frame member. To ensure that the orientation of all members was correct, the model was viewed in Extruded mode prior to the analysis. Finally, the analysis was run and the deflected shape was obtained (Figure 2.8). The maximum axial force, bending moment, and shear force of the compression chord stud were also obtained as seen in Figure 2.9. The member forces were then used to check the design of the chord stud.

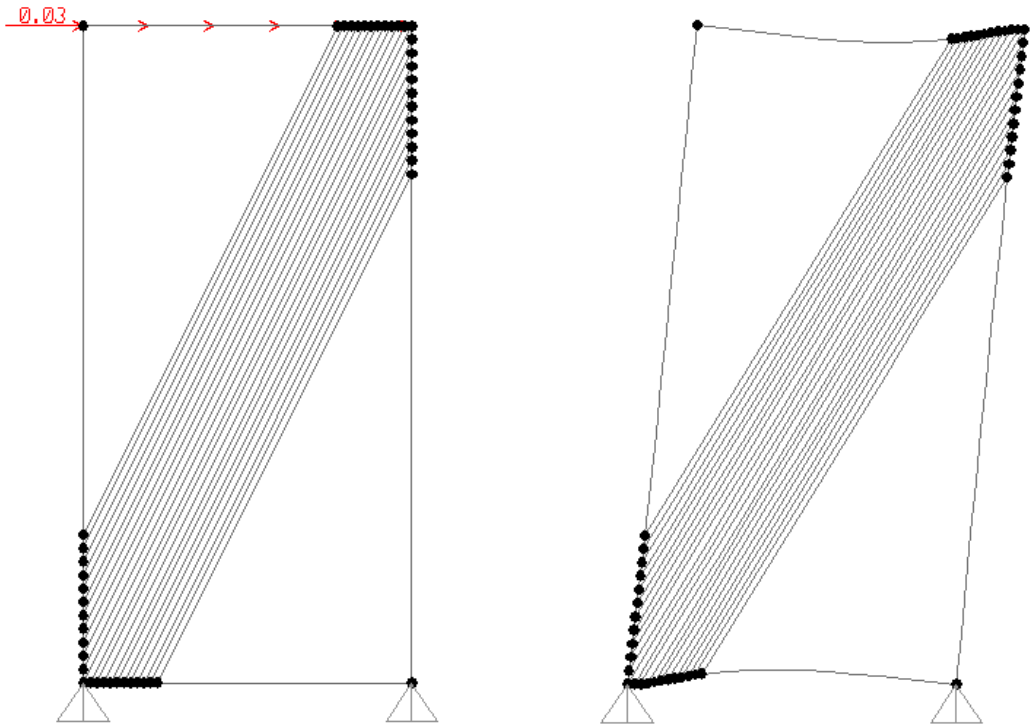

A B

Figure 2.8: SAP2000© shear wall model analysis. A) Top of the wall subjected to V_n in kN/m. B) Shear wall deflected shape.

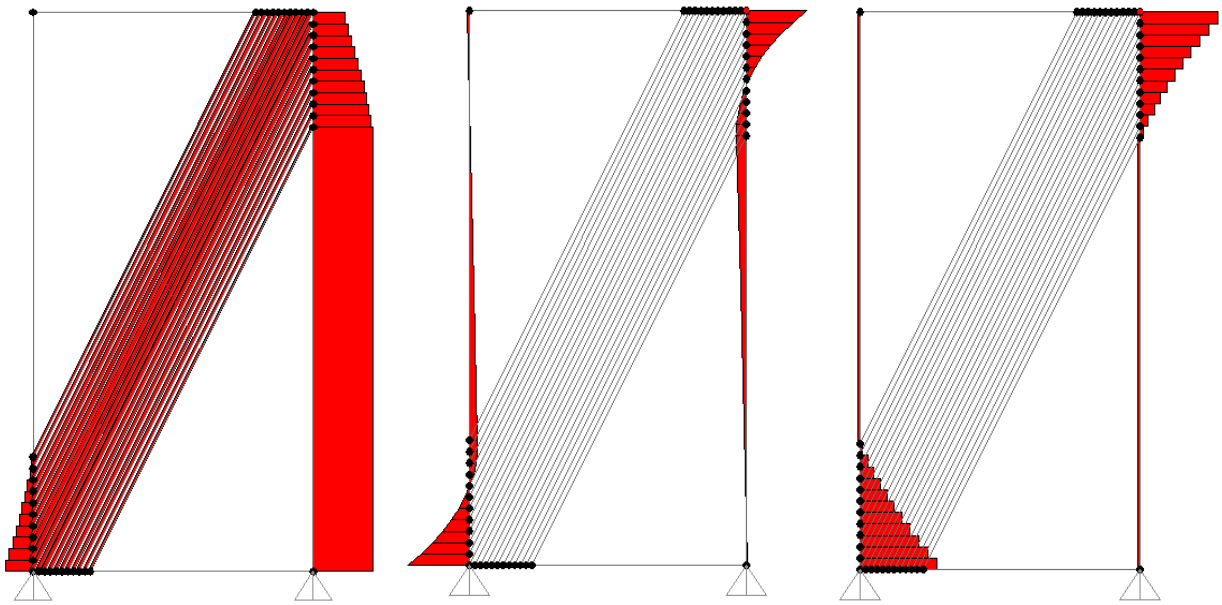

A B C

Figure 2.9: SAP2000© shear wall model force diagrams. A) Chord stud axial force diagram. B) Chord stud bending moment diagram. C) Chord stud shear force diagram.

2.3.2 Chord Stud Design Check

The design of the compression chord studs subjected to the member forces obtained from the analysis in SAP2000© was checked using the AISI S100 *(2012)* / CSA S136 *(2012)* standards to match the selected CFS 9.0 Software© specification 2012 NAS – Canada (LSD). As the chord stud was subjected to axial compression, bending moment, and shear forces simultaneously, it was designed to resist the combined bending and shear as well as the combined compressive axial load and bending (beam-column) effects. The CSA S136 Standard *(2012)* Limits States Design interaction Equations (2-9), (2-10), and (2-11) from provisions C3.3.2 and C5.2.2, were checked.

$$\sqrt{\left(\frac{M_f}{\phi_b M_{nxo}}\right)^2 + \left(\frac{V_f}{\phi_v V_n}\right)^2} \leq 1.0 \tag{2-9}$$

$$\frac{P_f}{\phi_c P_n} + \frac{C_{mx} M_{fx}}{\phi_b M_{nx} \propto_x} \leq 1.0 \tag{2-10}$$

$$\frac{P_f}{\phi_c P_{no}} + \frac{M_{fx}}{\phi_b M_{nx}} \leq 1.0 \tag{2-11}$$

where,

M_f = required flexural strength;

V_f = required shear strength;

P_f = required compressive axial strength;

M_{nxo} = nominal flexural strength about centroidal x-axis;

V_n = nominal shear strength when shear alone is considered;

P_{no} = nominal axial strength;

P_n = nominal axial strength when $F_n = F_y$;

ϕ_b = resistance factor for bending, 0.90;

ϕ_v = resistance factor for shear, 0.80;

ϕ_c = resistance factor for compressive load, 0.80;

C_{mx} = end moment coefficient, 1.0;

α_x = magnification factor, Eq. C5.2.2-4 in CSA S136 Standard *(2012)*.

To verify the chord stud design, the CFS 9.0 Software© was used. The appropriate chord stud cross-section was created and its material properties entered in the Section Inputs window of the software (Figure 2.10). A Member Check was performed where the interaction equations were computed. In the Member Parameters window the height of the wall was chosen as the unbraced lengths (L_x, L_y, and L_t) and the applied member forces P, M_x, and V_x were entered.

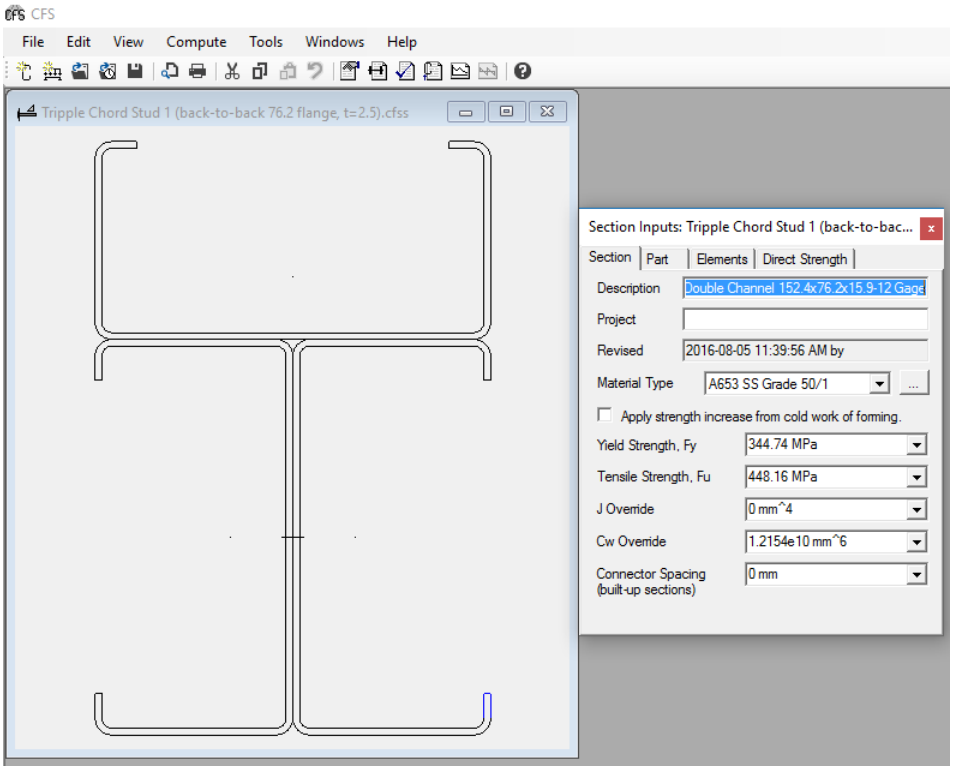

Figure 2.10: CFS 9.0 Software© member cross-section and material properties input.

In cases were the chord stud had a reinforcing member, the axial force acting on the chord stud, P, was applied through the centroid of the back-to-back chord stud member (e_x = 0 mm) as shown in Figure 2.11. This was due to the fact that the axial force on the chord stud member was a result of the shear forces from the sheathing screw connections. Applying the axial force along the longitudinal axis of the back-to-back chord stud aligned with the sheathing screws centroid. The reinforced chord stud was considered adequate if the interaction equations were satisfied.

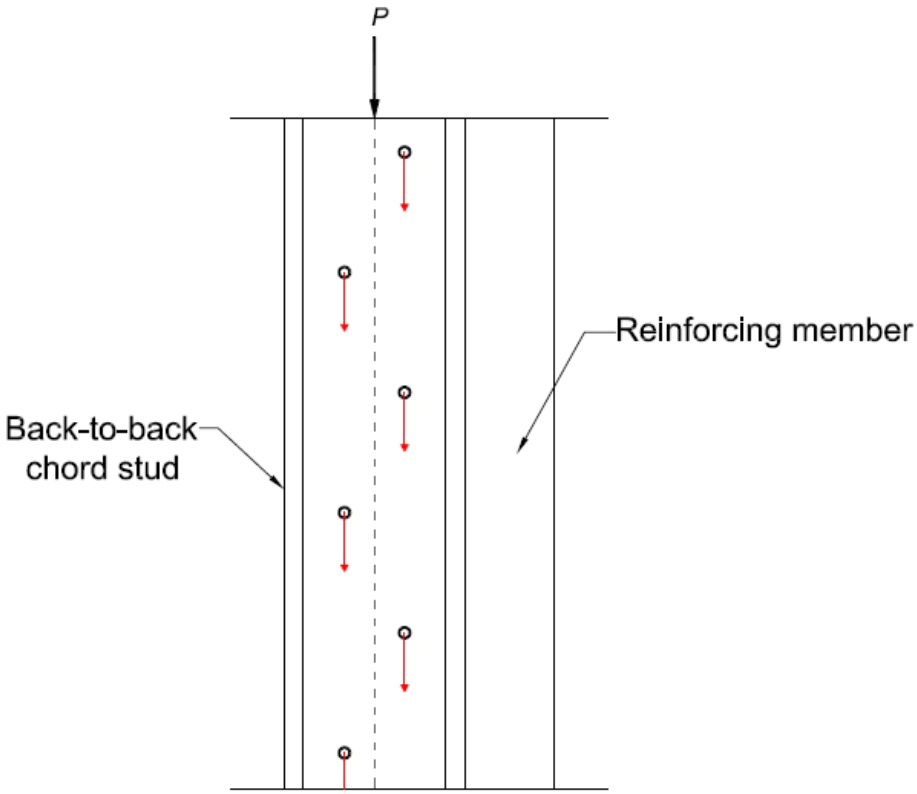

Figure 2.11: Applied axial force, *P*, at centroid of back-to-back chord stud.

2.3.3 Strip Method Limitations and Modifications

After completion of the initial shear wall tests it was observed that the predicted shear forces using the Effective Strip Method were lower than the forces reached during the tests and the observed tension field width was wider than that calculated using the method by Yanagi and Yu. This under prediction was attributed to the fact that the Effective Strip Method was developed based on tests of lower-strength shear walls with sheathing on one side only, and having framing of smaller dimension and thickness. In addition, the Effective Strip Method connection resistance was based on a 2-ply single shear connection as found in the AISI S100 Standard *(2016)* and the CSA S136 Standard *(2016)*, while the centre-sheathed walls had a 3-ply sheathing connection. Further, the test walls used for calibration of the Effective Strip method had more flexible framing members, which did not attract the same level of force as seen for the shear walls described herein. To improve the shear force prediction, and hence to select the chord stud sections for the subsequent wall specimens, the effective tension field width was not calculated using Equation (2-1) but instead was determined based on observations from the previous tests carried out for this

research project. These observations were made by looking at the damaged sheathing after the tests, the new wider tension field was determined by counting the screw connections where bearing damage had taken place.

Using a wider effective width predicted a higher V_n, which led to the need of stronger chord studs. Reinforcement members were attached to each chord stud to increase their strength. After some of the reinforced specimens were tested, it was observed that the shear forces reached higher levels, as the chord studs had a higher stiffness, and that the entire height of the wall contributed to the tension field. This resulted in using the height of the wall as W_e (Figure 2.12).

As a final modification to Yanagi's and Yu's Effective Strip Method, the cold-formed steel bolt bearing strength for an inside sheet of double shear connection (Equation (2-12)) from the AISI S100 *(2016)* / CSA S136 *(2016)* standards was used to calculate the screw fastener's nominal bearing capacity, $P_{ns,a}$. Although screws were used to fasten the sheathing to the frame, using the bolt bearing strength equation better represents the 3-ply connection of the centre-sheathed specimens. A bearing factor, *C*, of 3.0 was used for a connection of $d/t_{sh} < 10$ where d is the diameter of the fastener and t_{sh} is the thickness of the sheathing. The modification factor, $m_f = 1.33$, for an inside sheet of double shear connection using standard holes without washers was selected because it best represented the type of connection found in the tested walls.

$$P_{ns,a} = C m_f d t_{sh} F_{ush} \tag{2-12}$$

Figure 2.12 shows the progressive changes made to the Effective Strip Model to improve the shear force predictions. A detailed explanation and example of the specimens' shear capacity prediction using the Effective Strip Method, SAP2000© modelling, and CFS 9.0 software© design check is presented in Appendix B.

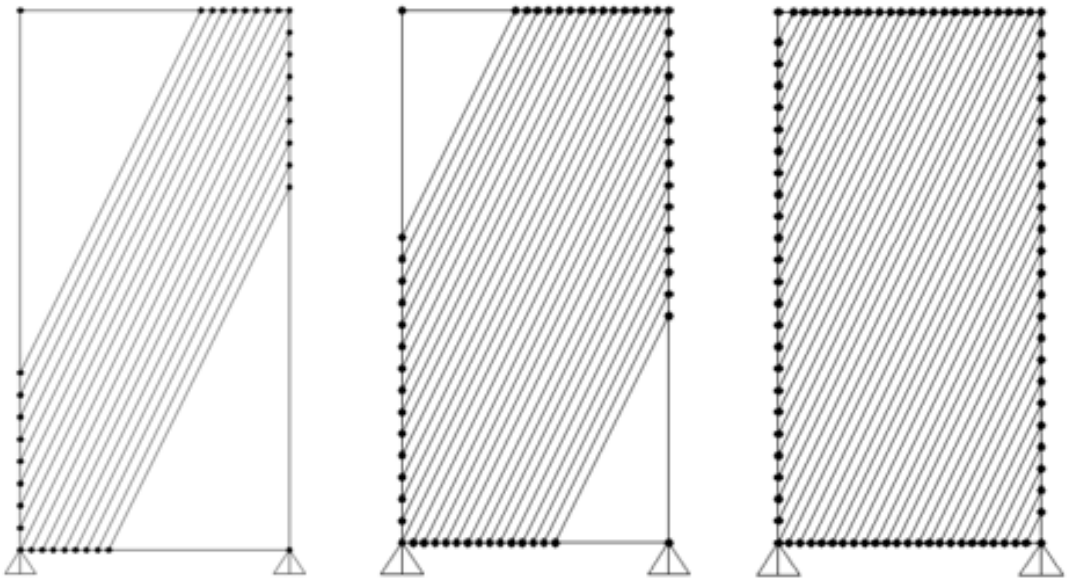

A B C

Figure 2.12: Effective tension field width, W_e, used in SAP2000© models at different stages of the test program. A) W_e calculated using the Effective Strip Method, B) W_e determined from observations of previous tests, C) W_e taken as height of the wall.

2.4 Materials, Specimen Fabrication, Test Setup, and Instrumentation

A list and description of the materials used to build both wall designs, the fabrication processes, and the test set-up and instrumentation are provided herein. Schematic drawings of each wall configuration showing the materials used are presented in Appendix A.

2.4.1 Materials

The walls were built using a combination of the following materials:

- 0.36 mm (0.014”), 0.47 mm (0.019”), 0.84 mm (0.033”), and 1.09 mm (0.043”) nominal thickness, 230 MPa (33 ksi) strength cold-formed steel sheet. Grade ASTM A653 *(2015).*

- 1.73 mm (0.068”) and 2.46 mm (0.097”), nominal thickness, 345 MPa (50 ksi) strength cold-formed steel studs. Nominal dimensions: 152.4 mm (6”) web, 76.2 mm (3”) flange, and 15.9 mm (0.625”) lip. Grade ASTM A653 *(2015).*

- 1.73 mm (0.068”) nominal thickness, 345 MPa (50 ksi) strength cold-formed steel top and bottom tracks. Nominal dimensions: 155 mm (6.107”) web and 51 mm (2”) flange. Grade ASTM A653 *(2015).*

- 2.46 mm (0.097”) and nominal thickness, 345 MPa (50 ksi) strength cold-formed steel top and bottom tracks. Nominal dimensions: 156 mm (6.153”) web and 51 mm (2”) flange. Grade ASTM A653 *(2015).*

- Simpson Strong-Tie S/HD 15S holdown connectors. Attached to the specimens using 33-No. 14 gauge 25.4 mm (1”) self-drilling Hex head screws and attached to the test frame by a 25.4 mm (1”) ASTM A193 *(2016)* grade B7 threaded anchor rod.

- No. 10 gauge 19.1 mm (3/4”) self-drilling wafer head Phillips drive screws.

- No. 10 and 12 gauge 25.4 mm (1”) self-drilling pan head Robertson drive screws.

- No. 10, 12, and 14 gauge 25.4 mm (1”) self-drilling Hex head screws.

- 1.72 mm (0.068”) nominal thickness, 345 MPa (50 ksi) strength cold-formed steel chord stud web stiffeners. Nominal dimensions: 152.4 mm (6”) web, 50.8 mm (2”) flange, 15.9 mm (0.625”) lip, and 146 mm (5 ¾”) in length.

- 19.1 mm (3/4”) and 12.7 mm (1/2”) shear bolts, ASTM F3125 *(2015)* Grade A325.

2.4.2 Specimen Fabrication and Test Set-Up

The fabrication process and test set-up of each wall design, double-sheathed and centre-sheathed, were different and are therefore explained separately in the following sections. In both cases, all frame components were prepared prior to assembly.

2.4.2.1 Fabrication of Double-Sheathed Walls and Test Set-Up

Before assembly of the walls the built-up box chord studs were built by attaching two single stud members with a 1.09 mm (0.043”) thick cold-formed steel strap on each side with 2 rows of No. 10 gauge 19.1 mm (3/4”) wafer head screws 150 mm (6”) apart along the length of the strap. The holdowns were installed 10 mm (3/8”) from the base of the box chord studs with 33-No. 14 gauge 25.4 mm (1”) Hex head screws (Figure 2.13).

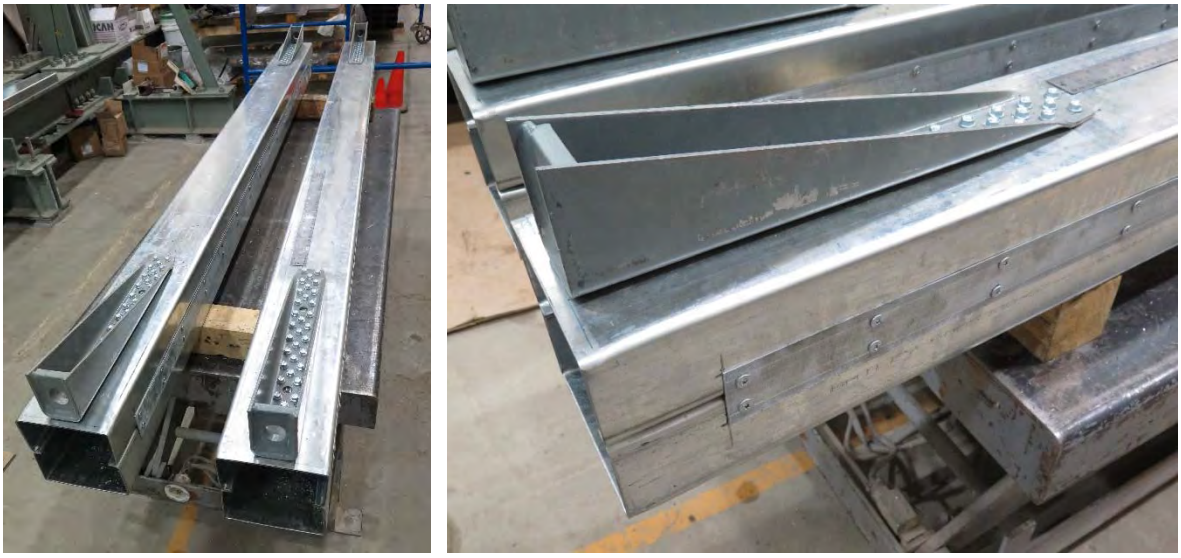

A B

Figure 2.13: A) Assembled box chord stud for double-sheathed walls. B) Steel strap used to attach the box chord stud members.

The web of the top and bottom tracks was pre-drilled to fit 19.1 mm (3/4”) A325 bolts and 25.4 mm (1”) threaded anchor rods for the holdowns. The frame components were assembled horizontally using a platform framing technique and No. 10 gauge wafer head screws. A field stud was installed at 610 mm (2”) at the centre of the 1200 mm (4”) wide walls. The holdowns were installed facing outward. As seen in Figure 2.14, 152.4 mm × 100 mm × 25.4 mm (6” × 4” × 1”) steel plates were pre-drilled and placed inside the tracks aligned with the bolt holes prior to the placement of the sheathing to prevent damage to the tracks from the high forces reached during the tests as observed by Rizk *(2017)*. The 1220 mm × 2440 mm (4’ × 8’) sheathing panels were marked following the fastener spacing listed in Table 2.1a. The first sheathing panel was fastened on one side of the wall around the perimeter using No. 10 or No. 12 gauge 25.4 mm (1”) pan head

screws 38.1 mm (1 ½”) from the edge of the chord studs and 31.8 mm (1 ¼”) from the edge of the tracks and at a spacing of 305 mm (12”) along the field stud.

A B

Figure 2.14: Assembly of a double-sheathed wall. A) Installation of field stud and track steel plates. B) Installed sheathing panel.

The frame was placed into the testing frame; the specimen was then anchored to the testing frame with 19.1 mm (3/4”) A325 bolts at the base of the frame and at the top to the loading beam through an aluminium spacer plate. Washers were placed between the steel plates inside the tracks and the nuts. Threaded rods were placed through each holdown, anchoring it to the testing frame and to the loading beam. At the top holdowns a steel plate was placed through the threaded rod between the loading beam and the washer and nut of the threaded rod to avoid bearing damage to the loading beam. Throughout the installation the load on the wall was monitored and adjusted if necessary to avoid damage. Finally, the second sheathing panel was installed (Figure 2.15) and the test instrumentation was put in place. Any minor damage to the specimen caused during assembly and installation was noted.

A B

Figure 2.15: A) Installation of specimen into the testing frame. B) Installation of second sheathing panel.

2.4.2.2 Fabrication of Centre-Sheathed Walls and Test Set-Up

The centre-sheathed specimens were assembled in full, except for the last chord stud reinforcing member which was attached once the specimens had been anchored to the testing frame. Before the assembly of the walls, the studs were marked according to the fastener spacing listed in Table 2.1b and 50 mm (2”) away from the inside of the flanges. A staggered fastener pattern was used in the centre-sheathed design to ensure the security of the sheathing sandwiched between the two stud members of the back-to-back chord stud and to ensure that the two studs acted as a built-up unit. First, the sheathing was placed on top of two 2440 mm (8’) long single studs (one on each side) and the next two studs were placed on top of the sheathing forming a back-to-back chord stud. This assembly was clamped together prior to fastening the studs and sheathing using No. 10 or No. 12 gauge 25.4 mm (1”) Hex head screws as seen in Figure 2.16. All fastener holes were pre-drilled to avoid shearing of the fasteners during installation since the screws had to penetrate through three layers of steel, as a minimum. The flanges of the top and bottom horizontal framing members, as well as the web of the top and bottom tracks were pre-

drilled to fit 12.7 mm (½") A325 bolts. Once marked, the top and bottom horizontal framing members were fastened to the sheathing using No. 10 or No. 12 gauge 25.4 mm (1") Hex head screws and to the flanges of the chord studs through a 140 mm (5 ½") long clip angle. The 146 mm (5 ¾") long stiffeners were then installed at each corner of the specimens (front and back) inside the chord studs' web (Figure 2.16).

In the case of the first centre-sheathed configurations, "M" and "C", (refer to Table 2.1b and Appendix A) no chord stud reinforcement was installed; hence, 9 extra screw holes were drilled on the holdowns to accommodate for the holes that could not be used in the centre (Figure 2.17). The holdowns were directly installed 10 mm (3/8") from the base of the chord studs (one at each corner) using 33-No. 14 gauge 25.4 mm (1") Hex head screws. After the installation of the holdowns, the wall was raised into the testing frame and anchored to it using 16-12.7 mm (1/2") A325 bolts through pre-drilled 81 mm × 63.5 mm × 19 mm (3 3/16" × 2 ½" × ¾") steel plates placed inside the flanges of the top and bottom horizontal framing members (Figure 2.18). The bolts were tightened to 110 lb·ft torque (maximum allowed for the bolts used) using a manual torque wrench to avoid stripping and elongation of the bolts. The same method as in the double-sheathed design was used to anchor the holdowns.

In the centre-sheathed configurations, "MR" and "CR", (Figures 2.19 and 2.22) a single reinforcement stud was installed back-to-back directly to the chord studs with 2 rows of fasteners spaced at 76.2 mm (3") along the height of the wall, a total of 6 holdowns were then directly installed to the reinforcement at the bottom and top corners of the specimens. The last step was the installation of the specimens into the testing frame following the same procedure that was used for the "M" and "C" configurations.

In the centre-sheathed configurations, "MR2" and "CR2", (Figures 2.20 and 2.23) once the holdowns were directly installed to the chord studs, the specimen was raised into the testing frame and anchored to the frame as it was done for the "M" and "C" configurations. After the shear bolts and holdown anchor rods were tightened, a single reinforcement stud was installed face-to-face (completely covering the holdowns) to the chord studs using a 1.37 mm (0.054") thick steel strap and 2 rows of No. 10 gauge 25.4 mm (1") Hex head screws spaced at 150 mm (6").

The last reinforced centre-sheathed configurations, “MR3” and “CR3”, (Figures 2.21 and 2.24) involved installing 2 reinforcing members. The first member and holdowns were installed similarly to the “MR” and “CR” configuration. After the holdowns were attached, the specimen was anchored to the testing frame by tightening the shear bolts and anchor rods, the second reinforcing member was installed face-to-face with the first reinforcement, forming a “box” built-up reinforcement member covering the holdowns. The second reinforcement was attached using a 1.37 mm (0.054”) thick steel strap and 2 rows of No. 10 gauge 25.4 mm (1”) Hex head screws spaced at 76.2 mm (3”) spacing.

During the anchoring process the load on the wall was monitored, and the actuator position was adjusted to maintain near zero force. Further, any minor damage to the specimens caused before testing was noted.

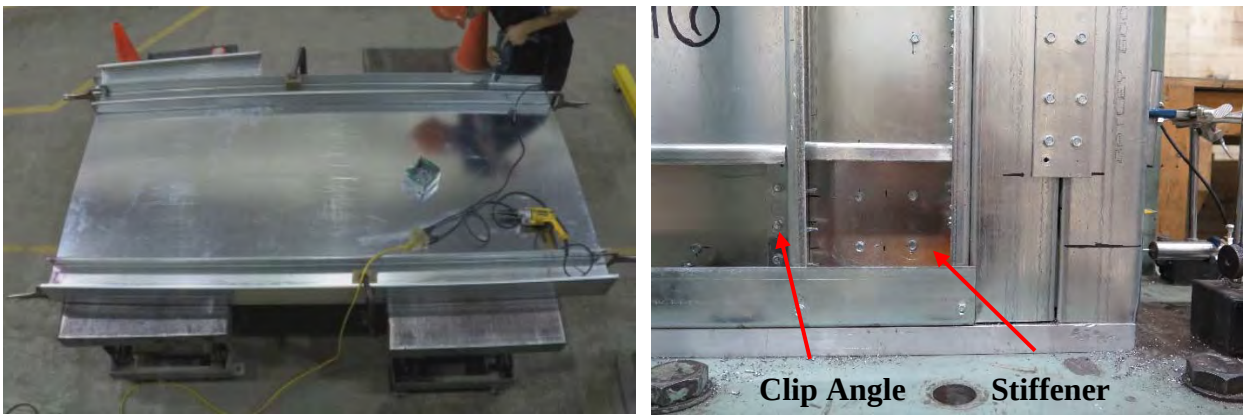

A B

Figure 2.16: A) Chord stud assembly of a centre-sheathed specimen. B) Stiffener installed at the bottom right corner of the wall.

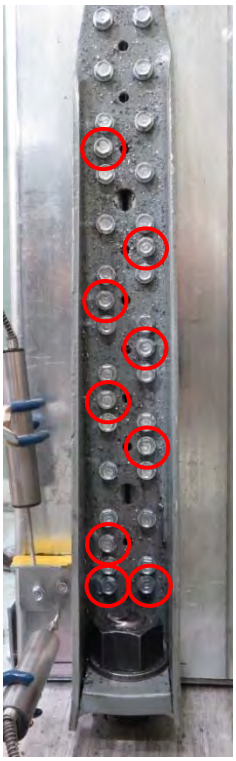

Figure 2.17: Extra holdown screws holes (circled in red) drilled to accommodate for the sheathing in the centre.

Figure 2.18: Placement of steel plates inside the flanges of the bottom horizontal framing member.

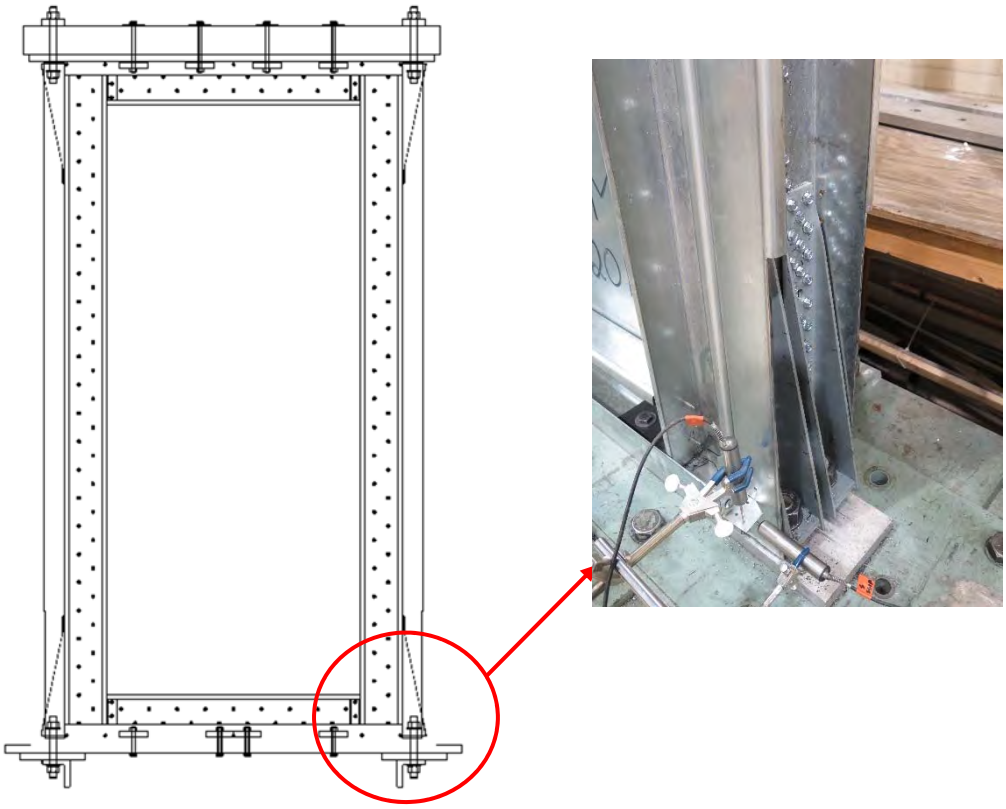

Figure 2.19: MR chord stud reinforcement.

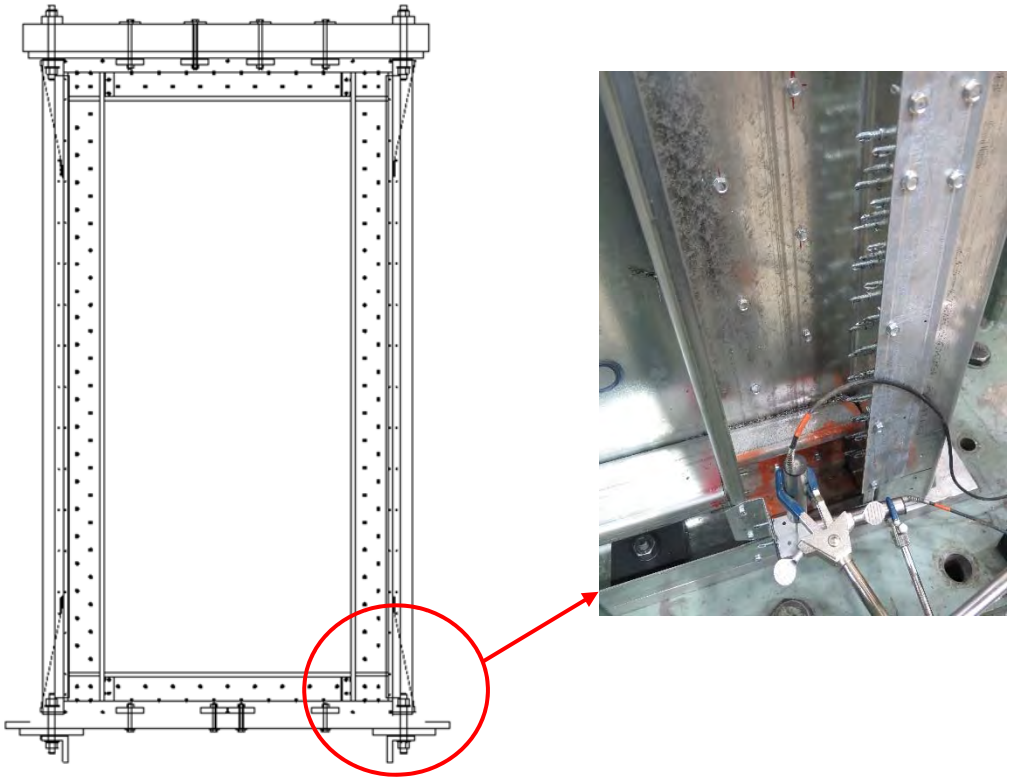

Figure 2.20: MR2 chord stud reinforcement.

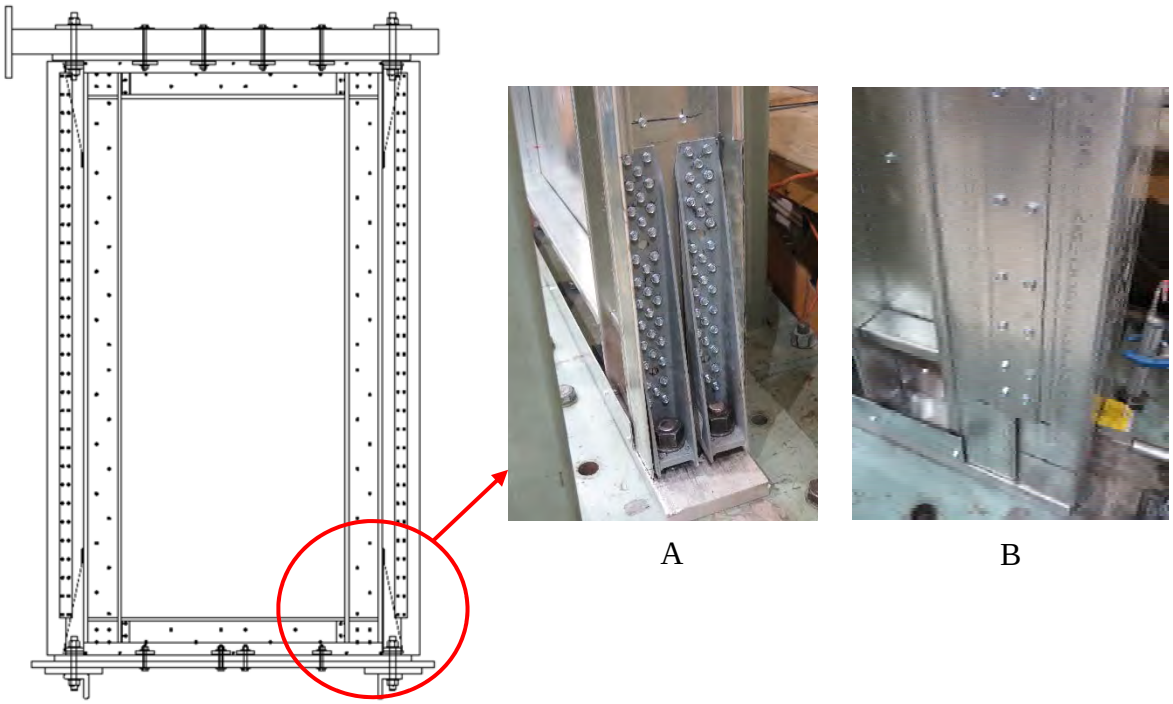

Figure 2.21: MR3 chord stud reinforcement. A) First reinforcement installed. B) Second reinforcement installed.

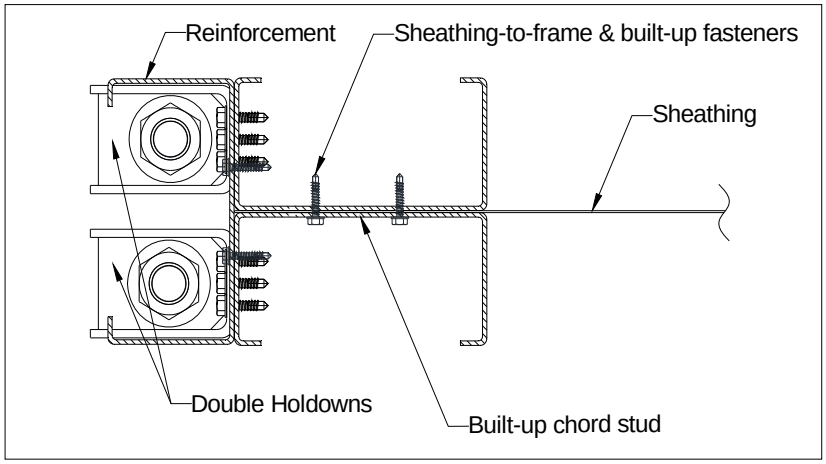

Figure 2.22: Cross-section of reinforced chord stud MR.

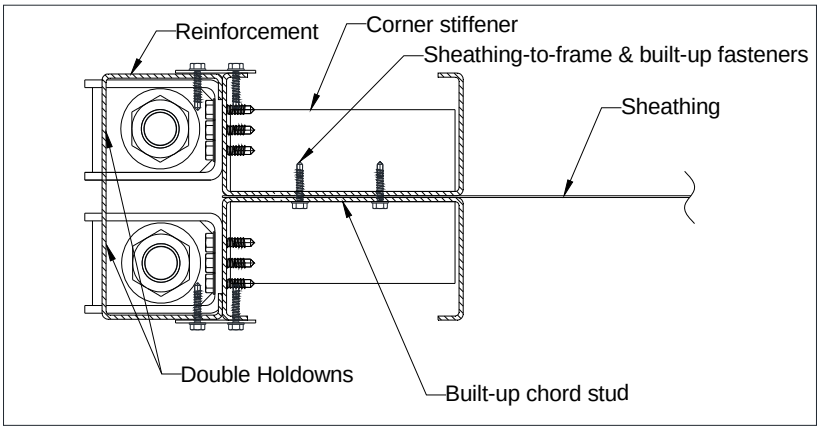

Figure 2.23: Cross-section of reinforced chord stud MR2.

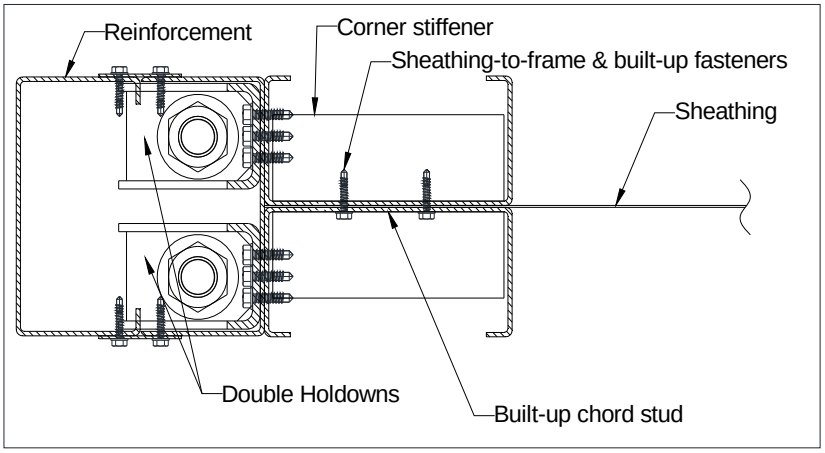

Figure 2.24: Cross-section of reinforced chord stud MR3.

2.4.3 Instrumentation and Data Acquisition

The performance of each test specimen was monitored and recorded by placing linear variable differential transformers (LVDTs) on the specimen, a load cell, and a string potentiometer. In total four LVDTs recorded the uplift movement and slip at the base of the chord studs or reinforcement while the specimen was subjected to lateral forces. The string potentiometer was attached to the top corner of the specimen to record the lateral displacement of the top of the wall. The potentiometer string was tied to a clip angle fastened to the chord stud or reinforcement. An internal LVDT in the actuator also recorded the displacement of the specimen. The locations of the instrumentation are indicated in Figure 2.25. The measurement instruments were connected to Vishay Model 5100B scanners that were used to record data using the Vishay System 5000

StrainSmart software at 2 scans/s and 100 scans/s for monotonic and symmetric cyclic tests respectively. The asymmetric cyclic test data was recorded at a rate of 25 scans/s.

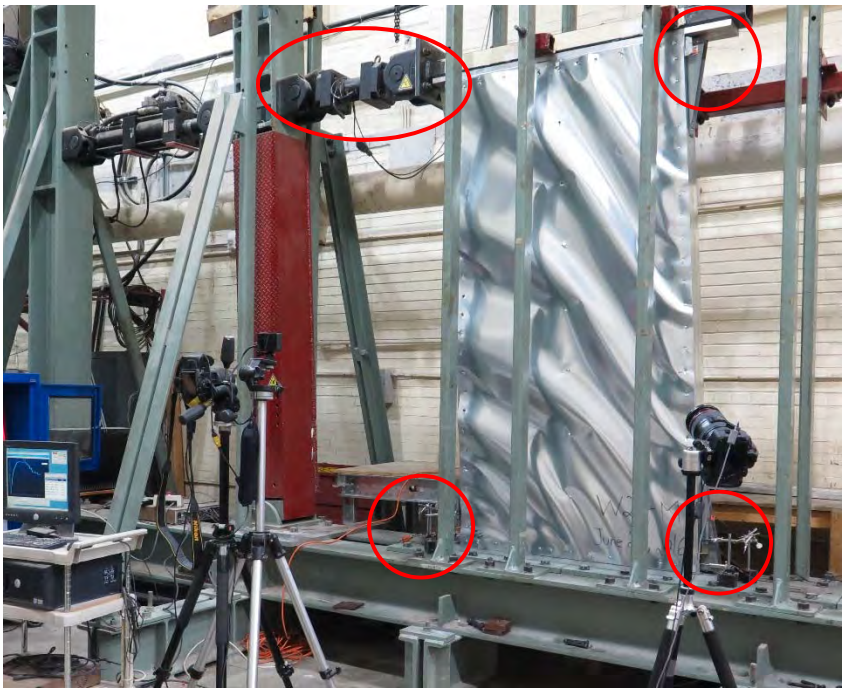

Figure 2.25: Placement of test instrumentation. Loadcell shown at the top left, string potentiometer at the top right, and LVDTs at the bottom.

2.5 Testing Protocols

All of the double-sheathed specimens were tested monotonically and then cyclically following the Consortium of Universities for Research in Earthquake Engineering (CUREE) reversed cyclic protocol (Krawinkler *et al. (2001)*, ASTM E2126 *(2011)*). A wall configuration's monotonic performance and data were used to create the reversed cyclic test protocol. In the case of the centre-sheathed walls, the monotonically tested specimens did not typically experience the resistance degradation associated with common shear walls. Hence, the post-peak deformation at 0.8 of the ultimate resistance was not always available. Instead, a standard reversed cyclic protocol was created which was used in all centre-sheathed cyclic tests; most centre-sheathed walls were only tested cyclically for this reason.

2.5.1 Monotonic Testing

During the monotonic tests a controlled lateral displacement was applied to the specimen in one direction at a constant rate of 5 mm/min, this represented shear walls under static loading conditions. A similar protocol was used by Balh *et al. (2014)* and DaBreo *et al. (2014)*, where CFS sheathed and framed shear walls for low-rise buildings and CFS shear walls under lateral and gravity loading were investigated, respectively. The protocol started at zero displacement; that is, the displacement at which the specimen was not subjected to any lateral load. Loading and displacement of the specimen stopped when approximately 50% force degradation was observed or when the actuator stroke limit was reached (125 mm or 5”). Monotonic tests of the centre-sheathed design stopped at the displacement limit of the actuator. Typically, no significant force degradation occurred due to the high ductility and shear resistance of these specimens. For this reason certain configurations (refer to Table 2.1b) were not tested monotonically. Figure 2.26 shows the typical shear resistance versus displacement behaviour during a monotonic test of a double-sheathed wall.

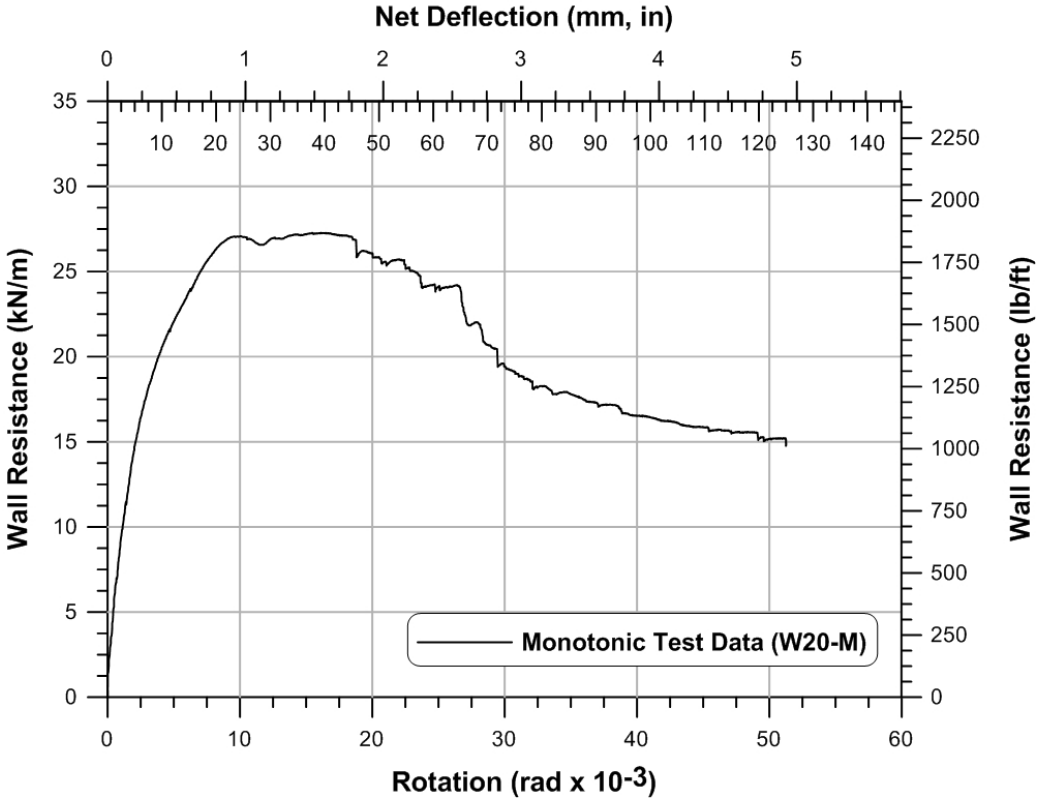

Figure 2.26: Typical monotonic test curve.

2.5.2 Reversed Cyclic Testing

All double-sheathed wall configurations were cyclically tested after the corresponding monotonic test data was obtained. The reversed cyclic tests were performed according to the CUREE ordinary ground motions protocol. The choice to use this type of cyclic protocol for CFS sheathed shear walls was based on the description by Krawinkler *et al. (2001)* and ASTM E2126 *(2011)*, as well as for consistency with previous research at McGill University on CFS framing with steel and wood sheathing walls (e.g. Balh *et al. (2014)* and Branston *et al. (2006)*).

For each specimen, the displacement of each cycle was dependent on delta, Δ, defined as 60% of the average displacement reached at 80% of the post ultimate load during the monotonic test. In the cyclic protocol, a cycle is defined as the displacement of equal amplitude to the positive side and to the negative side starting and ending at the origin. All double-sheathed specimens were tested at 0.25 Hz, the tests started with 6 initiation cycles at 0.050Δ in order for the specimens to reach their elastic range. The purpose of the initiation cycles was to verify the loading equipment, instrumentation, and the force-deformation behaviour of the specimens under small loads. Following the initiation cycles the first primary cycle, which allows the specimens to reach their inelastic range, started at a displacement of 0.075Δ followed by a set of trailing cycles which were defined as 75% of the primary displacement. The following primary cycle displacements, 0.1Δ, 0.2Δ, 0.3Δ, 0.4Δ, 0.7Δ, and 1.0Δ, were incrementally applied, additional primary cycles were included in the sequence at an increment of 0.5Δ in order to make full use of the actuator's stroke.

The cyclic test frequency was reduced to 0.05 Hz for the centre-sheathed specimens as a safety precaution after it was observed that high shear loads were reached during the W17 and W18 tests. The monotonic tests of W15, W16, W17, and W18 did not reach 80% post ultimate load degradation and therefore Δ was directly taken as 60 mm (2.36"), due to this pattern no monotonic tests were needed for the remaining centre-sheathed walls since the reversed cyclic protocol did not vary. This Δ value represents the 2.5% seismic storey drift limit of the National Building Code of Canada (NRC (*2015*)). Table 2.2 shows an example of a cyclic loading protocol. As described in Section 2.2.2, modifications to the cyclic test set-up were made in order to run asymmetric tests of specimens that reached the actuator's displacement limit before any load degradation was observed during the symmetric cyclic test. The asymmetric cyclic protocol

displacements remained the same as the symmetric protocol, however the cycles ran on the positive side of the origin only (Figure 2.6).

All cyclic protocols are found in Appendix C. Figure 2.27 illustrates a typical test displacement time-history and Figure 2.28 illustrates the shear resistance versus displacement behaviour during the reversed cyclic test.

Table 2.2: W19-C CUREE Reversed Cyclic Protocol

F_u = 48.262 kN (10850 lb)	Frame: 1.72 mm (0.068”)
$\Delta_{0.8Fu}$ = 57.048 mm (2.25”)	Sheathing: 2 x 0.36 mm (0.014”)
Δ = 0.60 $\Delta_{0.8Fu}$ = 34.229 mm (1.35”)	Screw Pattern: 50 mm (2”)

Displacement	Actuator Input (mm)	Number of Cycles	Cycle Type
0.050 Δ	1.729	6	Initiation
0.075 Δ	2.593	1	Primary
0.056 Δ	1.936	6	Trailing
0.10 Δ	3.458	1	Primary
0.075 Δ	2.593	6	Trailing
0.20 Δ	6.916	1	Primary
0.15 Δ	5.187	3	Trailing
0.30 Δ	10.373	1	Primary
0.225 Δ	7.780	3	Trailing
0.40 Δ	13.831	1	Primary
0.30 Δ	10.373	2	Trailing
0.70 Δ	24.205	1	Primary
0.525 Δ	18.153	2	Trailing
1.00 Δ	34.578	1	Primary
0.75 Δ	25.933	2	Trailing
1.5 Δ	51.867	1	Primary
1.125 Δ	38.900	2	Trailing
2.00 Δ	69.156	1	Primary
1.5 Δ	51.867	2	Trailing
2.5 Δ	86.445	1	Primary
1.875 Δ	64.834	2	Trailing
3.00 Δ	103.734	1	Primary
2.25 Δ	77.800	2	Trailing
3.50 Δ	121.023	1	Primary
2.625 Δ	90.767	2	Trailing

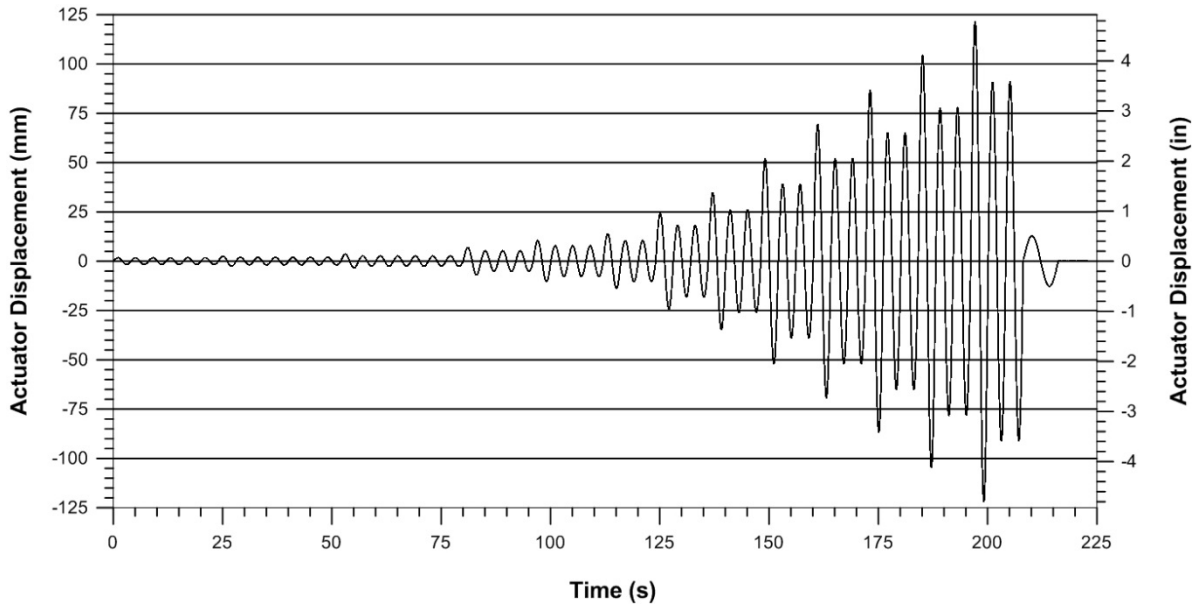

Figure 2.27: W19-C CUREE Displacement Time-History plot.

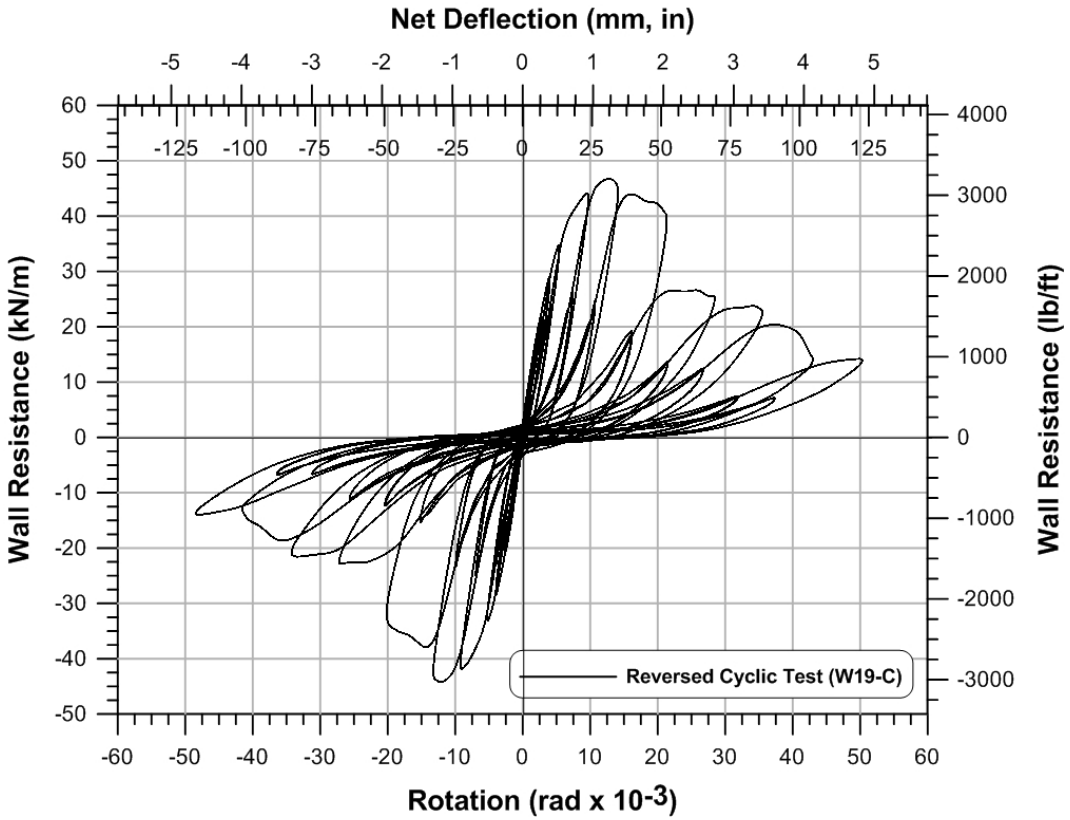

Figure 2.28: Typical reversed cyclic test curve for double-sheathed wall.

CHAPTER 3 – SHEAR WALL TEST OBSERVATIONS AND RESULTS

3.1 Observed Failure Modes

The shear forces developed from the lateral displacement applied at the top of the wall during the tests created a compression field in the sheathing, leading to the elastic shear buckling of the sheathing in all specimens. This behaviour was expected due to the thin cold-formed steel panel used as sheathing. A tension field in the sheathing was developed simultaneously in the other direction, perpendicular to the compression field. As the specimens' lateral displacement increased, damage at the sheathing connections was observed in the form of bearing and sometimes in the form of screw failure as well. In some wall configurations the steel frame was damaged from the bending moment and axial forces applied to these framing members at large displacements. To avoid undesirable frame damage, chord stud reinforcements were installed in later configurations as part of the centre-sheathed configuration. The frame-to-sheathing screw connection failure was the most common type of failure in both wall designs, while damage to the holdowns from up-lift forces and damage to the side chord stud flanges from contact with the horizontal framing were also observed in the centre-sheathed walls. Certain failure modes, such as holdown and frame damage which occurred in early tests, were addressed and design improvements were made in later tests, and thus no longer observed. Although this section describes each failure mode separately, these failure modes occurred collectively during some of the shear wall tests; detailed observations of the failures of each test are found in the test observation sheets in Appendix D.

3.1.1 Connection Failure

Failure of the individual fasteners and of the sheathing around the fasteners were observed. In most cases, a combination of the different types of connection failures described in the following sections took place.

3.1.1.1 Tilting of Chord Stud Strap Screw

Tilting of the strap screws, shown in Figure 3.1, connecting the built-up chord studs in the double-sheathed specimens was observed. This failure resulted from the large strap fastener spacing allowing movement and consequentially the development of shear action between the

individual members of the build-up stud as it was subjected to a bending moment. The strap fastener spacing was decreased to address this failure mode in subsequent tests.

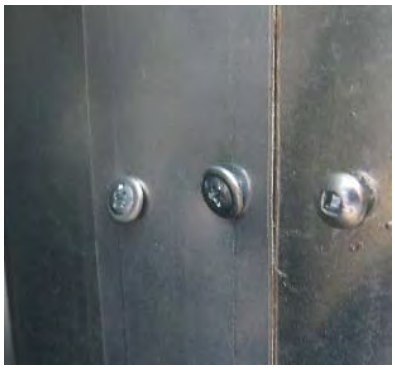

Figure 3.1: Tilting of built-up chord stud strap screws in a double-sheathed specimen.

3.1.1.2 Track, Sheathing, and Holdown Screw Shear Failure

Screw shear failure was only observed in the centre-sheathed specimens. This failure mode, where the shank of the screw fractured (Figure 3.2), occurred in some of the holdown, sheathing, and track connections. Typically, screw shear failure occurred at the sheathing connection where the screws were driven through three or more layers of steel. Overall, screw shear failure is attributed to the higher shear wall resistance reached by the centre-sheathed specimens; the fasteners' shear resistance was reached due to the resulting tension field and up-lift forces. Even though the head of the screw sheared off, the shank of the screw continued to hold the steel layers together, allowing for some force transfer to continue.

A B

Figure 3.2: A) Shear failure of holdown screws. B) Shear failure of sheathing and track screws.

3.1.1.3 Pull-Through Sheathing Failure

In pull-through sheathing failure the screw pulled through the sheathing while remaining attached to the frame. This failure mode was observed in double-sheathed specimens only along the chord stud and field stud connections. This failure was not observed in the centre-sheathed configuration because the sheathing was confined between the two members of the built-up chord studs. In the case of pull-through failure along the double-sheathed walls' chord studs, the failure happened progressively once the sheathing sustained enough bearing damage from the repeated tension and compression cycles during the cyclic tests. Although the extensive bearing damage in the sheathing around the screws was the main contributor to the pull-through failure along the chord studs, the out-of-plane forces on the connection from the shear buckling of the sheathing also contributed to the sheathing going over the screw head through the enlarged connection holes. This phenomenon led to the unzipping of the sheathing, illustrated in Figure 3.3.

A B

Figure 3.3: A) Pull-though sheathing failure. B) Sheathing unzipping.

Pull-through failure along the field stud of the walls was observed near the beginning of the test. At this point in the test, minimal bearing damage was observed and the main contributor to the pull-through failure were the out-of-plane forces from shear buckling of the sheathing. This was a result of the large fastener spacing along the field stud, 305 mm (12"), and the fasteners being located in the centre of the compression field. Figure 3.4 shows the pull-through failure of a field stud connection with almost no bearing damage.

Figure 3.4: Pull-through failure of a field stud connection from out-of-plane forces.

3.1.1.4 Bearing Sheathing Failure

Bearing failure of the sheathing was observed in both shear wall designs (Figure 3.5). During the lateral displacement of the specimen the energy was mainly dissipated via bearing damage of the sheathing material around the fasteners, which was thinner than the framing steel, resulting in shear load degradation in some cases. The levels of sheathing bearing failure varied from enlarged holes around the fasteners to tearing of the sheathing. Severe bearing damage was more often seen in the centre-sheathed walls where the screws were not able to pull-through since they were confined between the back-to-back chord studs.

A B

Figure 3.5: Sheathing bearing failure. A) Double-sheathed specimen. B) Centre-sheathed specimen.

3.1.1.5 Tear-Out Sheathing Failure

Sheathing tear-out was observed as an extreme form of bearing damage around the fasteners. Sheathing tear-out failure happened at the corners of the sheathing where the tension field forces were concentrated. Although this failure mode was seen in a few double-sheathed specimens at large displacements, extreme cases occurred in centre-sheathed specimens, shown in Figure 3.6, where the screws could not pull-through.

Figure 3.6: Bottom corner tear-out sheathing failure of centre-sheathed specimen W25-CR3.

3.1.2 Sheathing Failure

In addition to sheathing failure at the connections, which resulted from the tension field forces, sheathing shear buckling was also observed in every specimen.

3.1.2.1 Sheathing Shear Buckling and Tension Field Action

Elastic shear buckling of the sheathing was observed, in every specimen, immediately after the lateral displacement was applied at the top of the wall. The unidirectional lateral displacement caused the rectangular walls to deform, where one diagonal increased in length while the other decreased in length. Naturally, the sheathing along the diagonal with the increased length experienced tension forces, and the sheathing along the diagonal with the decreased length experienced compression forces (Figure 3.7). As a result of the compression forces, the thin cold-formed steel sheathing buckled about its weak axis creating waves in the sheathing. Because of

the nature of the waves formed, out-of-plane forces developed in the direction perpendicular to the plane of the sheathing.

Once the monotonic tests ended, the fully developed unidirectional tension field width was visible. In cyclic tests, shear buckling and tension field action developed in both directions upon reversal of the loading direction. Sheathing shear buckling and tension field action are shown for a monotonic and a cyclic test in Figure 3.8.

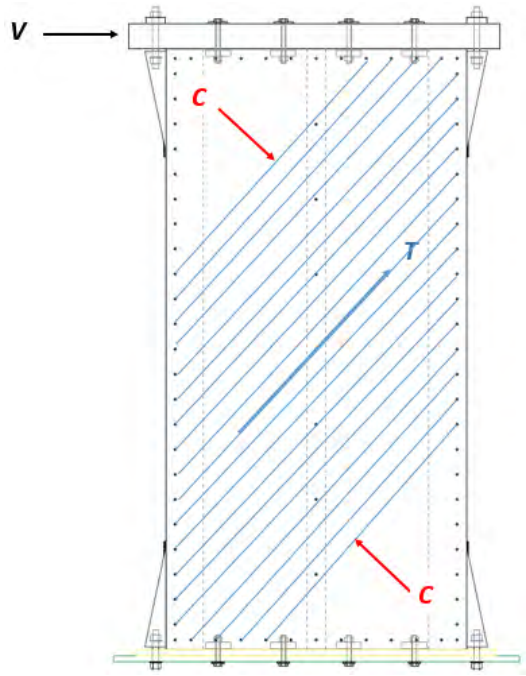

Figure 3.7: Development of compression field, C, and tension field, T, from shear force, V, created due to applied lateral displacement at the top of the wall.

A B C

Figure 3.8: Sheathing shear buckling failure and tension field action. A) Specimen prior to testing. B) Specimen after monotonic test. C) Specimen after reversed cyclic test.

3.1.3 Framing Failure

In some instances failure of the framing chord studs was observed. This failure mode was undesirable because the main purpose of the framing members in buildings is to resist gravity loads; further, failure of these members reduced the lateral resistance and stiffness of the walls. Local buckling of chord studs in compression and bending was the most commonly observed type of frame failure. In order to achieve the full shear capacity of the walls, framing failure was addressed by increasing the sheathing fastener spacing and installing chord stud reinforcements to increase their beam-column resistance.

3.1.3.1 Local Buckling of Chord Studs

In the double-sheathed specimens the web of the compression chord stud locally buckled elastically in some instances (Figure 3.9) from weak-axis bending. Similarly, local bulking of the compression chord stud flanges and lips occurred in the centre-sheathed specimens from strong-axis bending (Figure 3.10). The walls were subjected to a diagonal tension field force, its vertical component was transferred as axial compression or tension through the chord studs to the testing

frame through the holdowns. The horizontal component of the tension field force was transferred as a lateral force on the chord studs through the sheathing fasteners resulting in the bending of the member.

Figure 3.9: Chord stud web elastic local buckling of a double-sheathed specimen.

Figure 3.10: Chord stud flange local buckling of a centre-sheathed specimen.

Separation of the chord stud members also contributed to the local buckling frame failure in the centre-sheathed walls (Figure 3.11). Shear buckling of the sheathing confined between the chord studs forced the chord studs to separate, lowering the built-up member resistance.

Figure 3.11: Centre-sheathed chord stud separation from sheathing shear buckling.

3.1.4 Other Damages

Throughout testing, the wall specimens suffered other minor damage in the framing members, sheathing, and holdowns.

3.1.4.1 Framing Damage

The framing members suffered other less significant damage during testing. In the double-sheathed walls the holdowns were anchored to the test frame and screw fastened to the web of the chord studs; with increasing lateral displacement and up-lift forces the web of the tension chord stud was damaged as it was pulled from the holdown (Figure 3.12).

Figure 3.12: Double-sheathed chord stud web damage at holdown location.

In most centre-sheathed specimens the flanges of the chord studs at the corners were damaged where contact with the horizontal framing members occurred during lateral displacement. This problem was minimized by installing stiffeners at each end of the chord studs, as illustrated in Figure 3.13.

A B

Figure 3.13: Chord stud flange damage at corners. A) Before installing stiffeners. B) After installing stiffeners.

3.1.4.2 Sheathing Damage

It was observed that holes formed in the centre of the sheathing of specimen W23B-CR3, shown in Figure 3.14, late into the cyclic test at high lateral displacements (8% storey drift). The formation of the holes was due to the accumulation of plastic strain from the repeated back and forth lateral movement of the wall during each cycle. The holes formed at specific locations where inelastic shear buckling waves alternated directions from positive to negative.

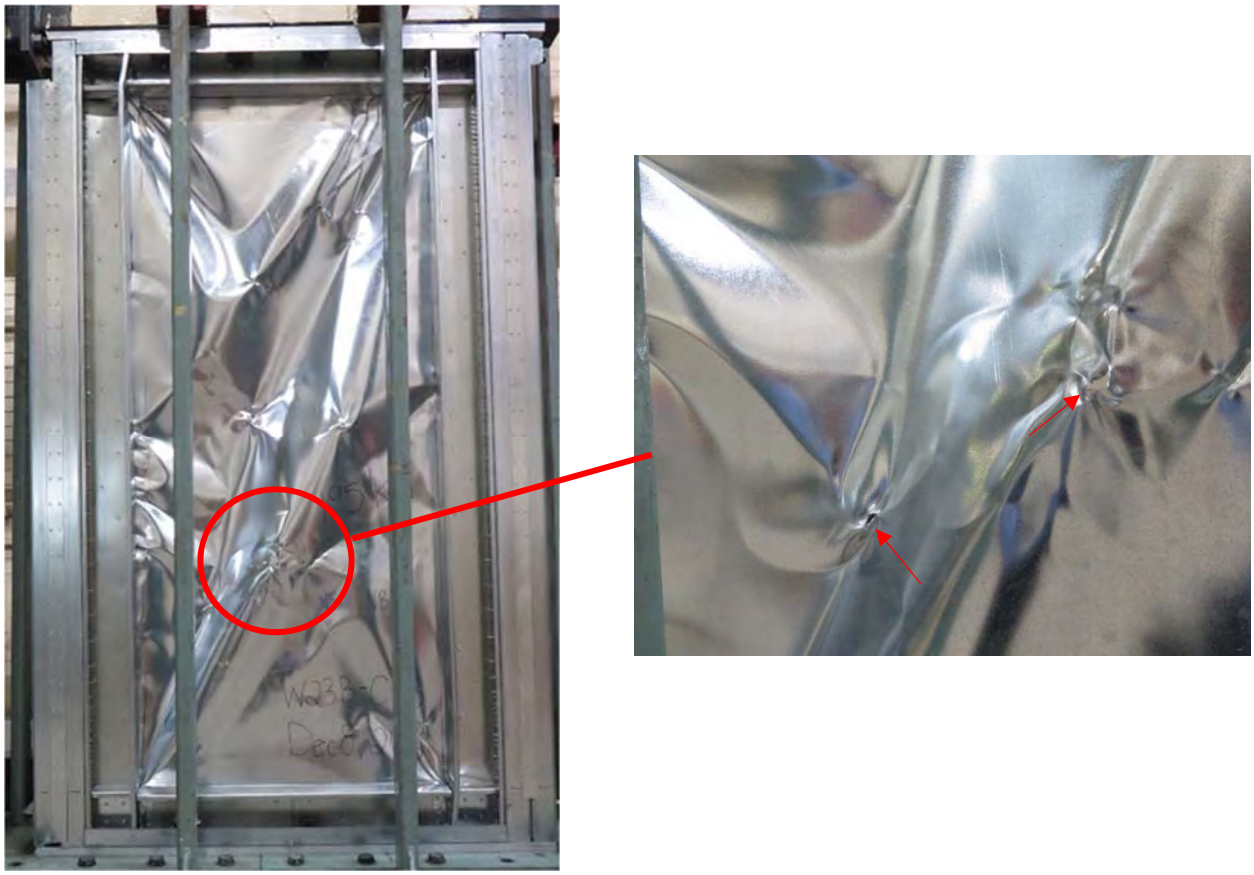

Figure 3.14: Holes formed in the centre of the sheathing of specimen W23B-CR3.

3.1.4.3 Holdown Damage

In some instances the high up-lift forces reached during the centre-sheathed tests caused damage to the holdowns as seen in Figure 3.15; the holdown plate deformed. To address this issue, a second holdown was added at the bottom of the specimens. Even with the addition of a second holdown, damage to the plates was observed in walls where the highest shear forces were reached.

A B

Figure 3.15: A) Single holdown plate damage. B) Double holdown plate damage.

3.2 Data Reduction

Processing of the raw data collected during testing was done in order to present comprehensive results in this report.

3.2.1 Lateral Displacement

The net lateral displacement of the wall, Δ_{net}, was taken as the measured wall top displacement, Δ_{top}. The net lateral displacement was also calculated in terms of wall rotation, θ_{net} (Equation (3-1)).

$$\theta_{net} = \frac{\Delta_{net}}{H} \tag{3-1}$$

where,

θ_{net} = Net chord rotation of the wall (rads);

Δ_{net} = Net lateral displacement of the wall (mm or in);

H = Height of the wall (2440 mm or 8’ for all specimens).

3.2.2 Lateral Load

The lateral load applied to the specimens throughout each test was obtained as a force in kN, it is however common practice to express the applied force as shear flow, *S*, defined in Equation (3-2).

$$S = \frac{F}{W} \tag{3-2}$$

where,

S = Shear flow along width of wall (kN/m or lb/ft);

F = Applied lateral force at the top of the wall (kN or lb);

W = Width of the wall (1220 mm or 4’ for all specimens).

For the monotonic tests, the data analysis was done using the force and deformation values obtained directly from the monotonic curve. For the cyclic tests however, a backbone curve encompassing the primary positive and negative force vs. deformation cycles was computed. The backbone curve for all cyclic tests was created by detecting the maximum force reached during each primary cycle, connecting them, and fitting a polynomial curve that best represented the relationship. Separate backbone curves were created for the positive and for the negative cycles of the reversed cyclic tests, similarly, for the asymmetric cyclic tests only a positive backbone curve was created. Once the backbone curves were computed, using a MATLAB code for efficiency, the analysis parameters could be calculated, as was done for the monotonic tests using the monotonic curves.

3.2.3 Energy Dissipation

An analysis parameter used to assess each wall’s ductility is the energy dissipated, *E*, during the monotonic and cyclic tests. The total energy dissipated during a monotonic tests is simply the area under the shear resistance-displacement monotonic curve, represented graphically in Figure 3.16.

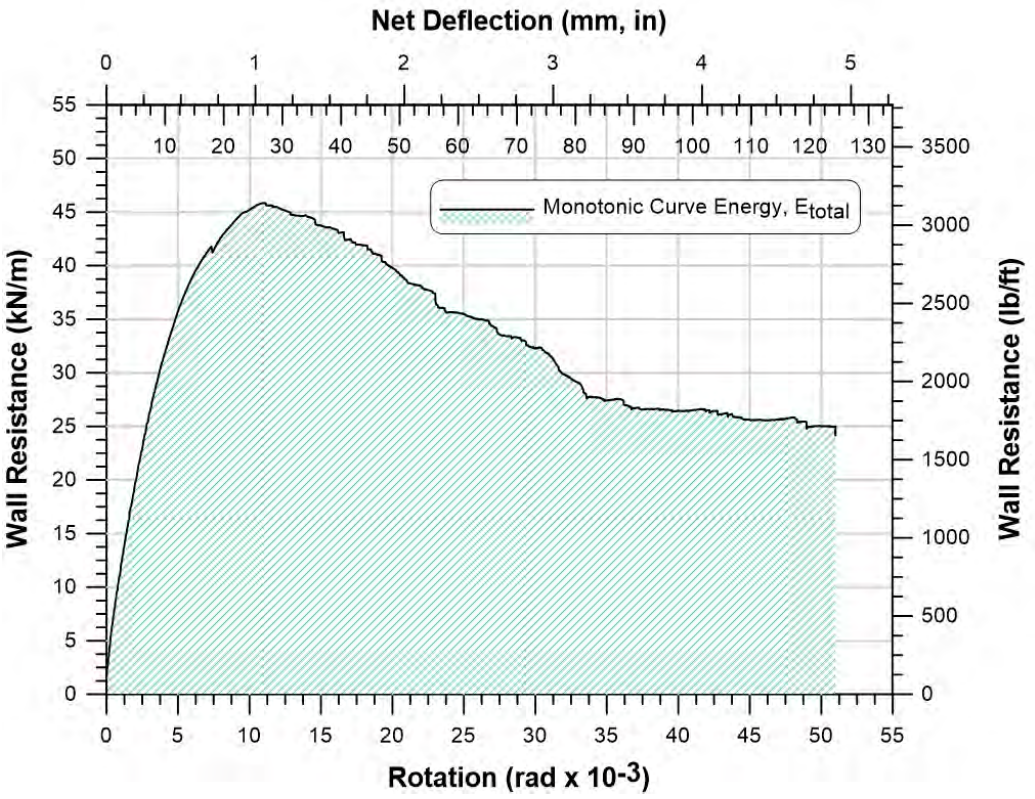

Figure 3.16: Graphical representation of energy dissipated, E_{total}, in a monotonic test as the area under the curve.

Mathematically, the total energy dissipated by a shear wall was calculated using an integral approach, where the energy dissipation at each interval was calculated separately following Equation (3-3) and then summed (Equation (3-4)).

$$E_i = \frac{F_i + F_{i-1}}{2}(\Delta_{top,i} - \Delta_{top,i-1}) \tag{3-3}$$

$$E_{total} = \sum E_i \tag{3-4}$$

where,

E_i = Energy dissipated between two consecutive points (J);

F_i = Shear force between two consecutive points (kN);

$\Delta_{top,i}$ = Measured wall top displacement (mm);

E_{total} = Total energy dissipated by specimen (J).

For efficiency, the area under the curve of each specimen was obtained using the trapezoidal numerical integration (*trapz*) function in MATLAB which uses each value in the monotonic curve as an increment *i*.

The best representation of the total energy dissipated, E_{total}, during the cyclic tests was the cumulative energy dissipation because of the multiple positive and negative cycles. The cumulative energy was calculated as the sum of the energy dissipated (area under the shear resistance-displacement curve) within each full cycle. Adding the energy within each cycle made use of all of the force and deformation data values from the cyclic test, where the energy was calculated continuously between the positive and negative displacements of each cycle. Figure 3.17 shows the graphical representation of the energy dissipated within one full cycle.

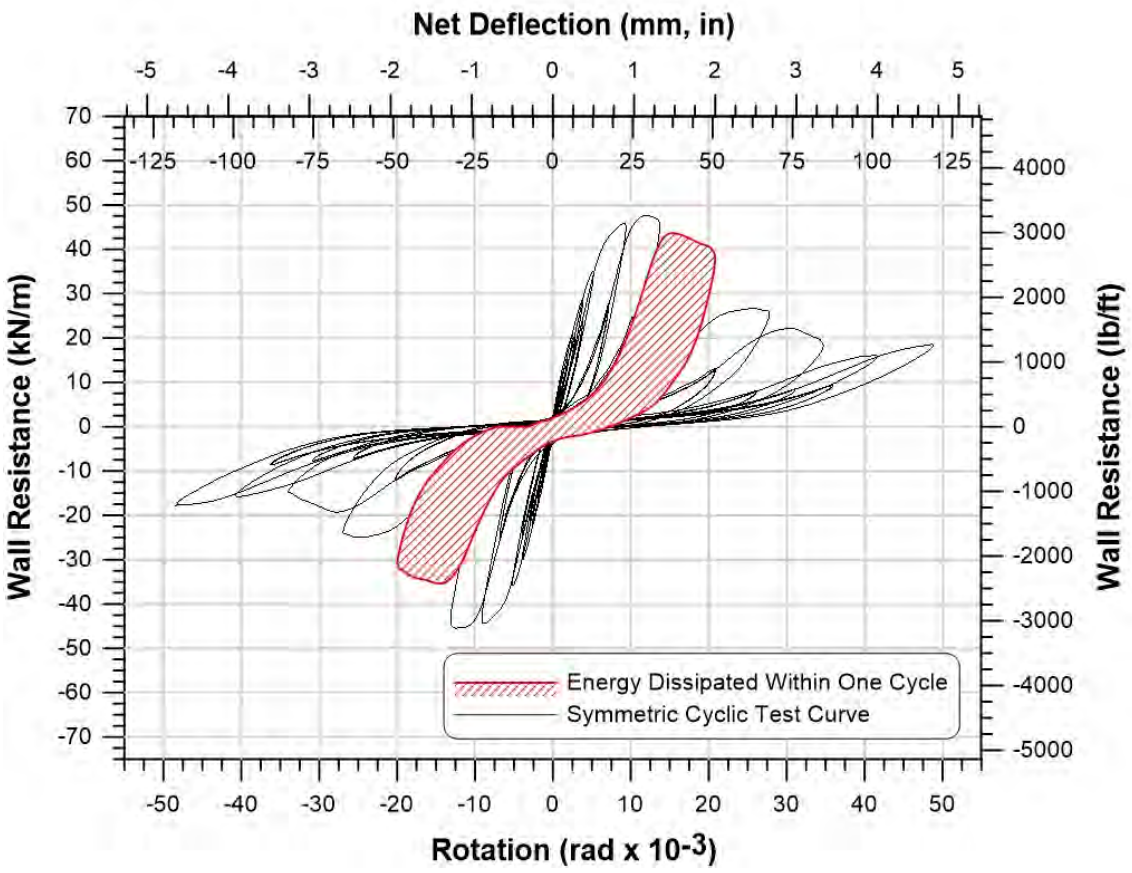

Figure 3.17: Energy dissipated within one full cycle of a cyclic test as the area under the curve.

The energy dissipated was also calculated as the area under the cyclic tests' positive and negative backbone curves separately, E_{BB+} and E_{BB-} (Figure 3.18). This procedure resulted in two different energy values, one for the area under the positive backbone curve and one for the area under the negative backbone curve, because they are not identical in nature. Similar to the monotonic energy procedure, Equations (3-3) and (3-4) were used to calculate the energy dissipation of the cyclic tests.

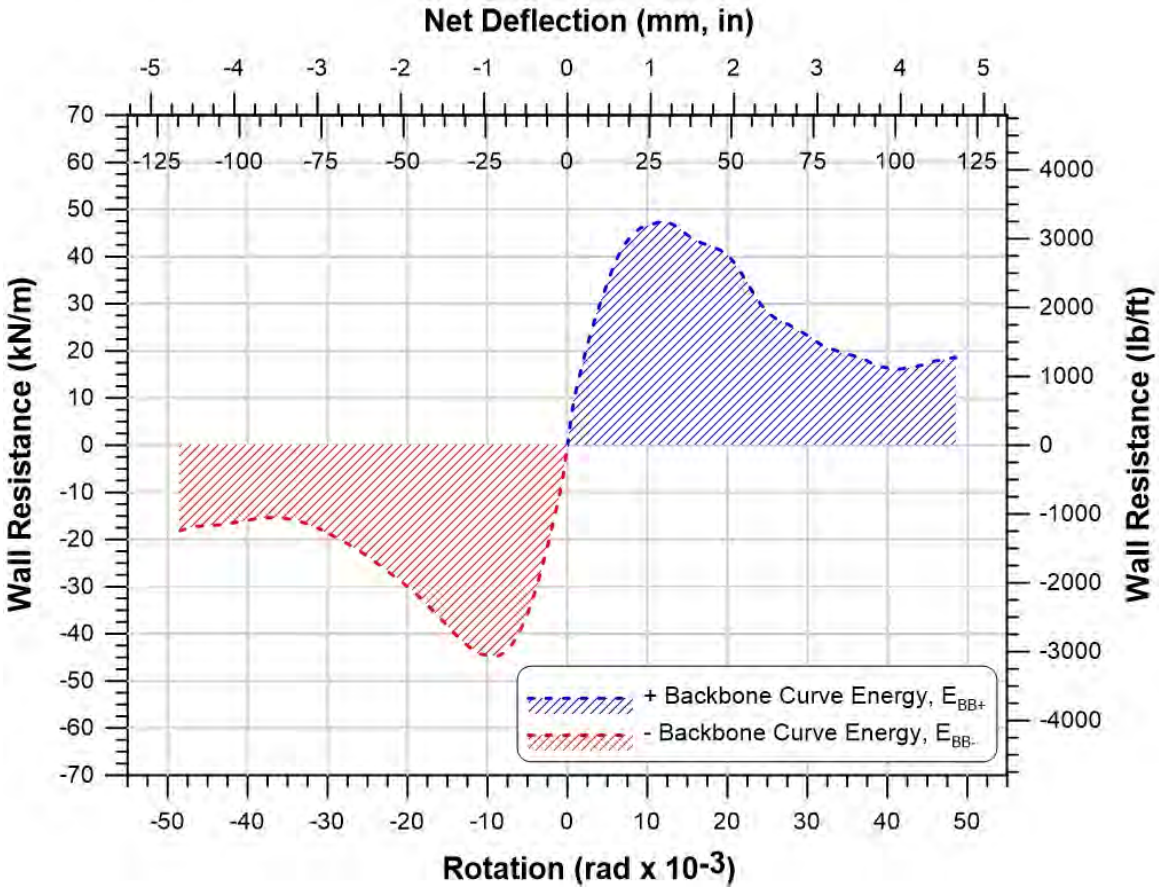

Figure 3.18: Total energy dissipation under the positive and negative backbone curves of a symmetric cyclic test.

3.3 Test Results

Various key parameters were obtained from the monotonic and cyclic test data: maximum wall resistance, S_u, wall resistance at 80% of S_u (post-peak), $S_{0.8u}$, wall resistance at 40% of S_u, $S_{0.4u}$, and the corresponding wall displacements and rotations (Δ_u, θ_u, $\Delta_{0.8u}$, $\theta_{0.8u}$, $\Delta_{0.4u}$, and $\theta_{0.4u}$). The total energy dissipated, E, was also calculated for each specimen. The parameters were

obtained for the positive and negative cycles separately for cyclic tests, all measured results and graphs of the test data are presented in Appendix E. The graphical representations of the parameters are shown in Figures 3.19 and 3.20, while Tables 3.1, 3.2, and 3.3 contain a summary of the monotonic, positive cyclic, and negative cyclic results. The 40% of the peak load, $S_{0.4u}$, was computed in order to obtain the elastic properties of the walls. The displacement corresponding to $S_{0.4u}$ also represents the NBCC's (NRC *(2015)*) serviceability limit of *1/500* of the storey height (4.89 mm, 0.192"), that allows non-structural members of a building to remain functional. Most of the double-sheathed specimens satisfied this limit, but all centre-sheathed specimens exceeded it. When determining the wall displacement corresponding to 80% of the ultimate load, it was taken as the 4% drift value (approximately 100 mm or 4") if it exceeded this value. This limit was set for the purpose of results interpretation, which is discussed in Chapter 4.

The cycles of the asymmetric cyclic tests remained in the positive range of the graph; therefore, only the positive parameters were obtained, similar to the monotonic parameters in Figure 3.19.

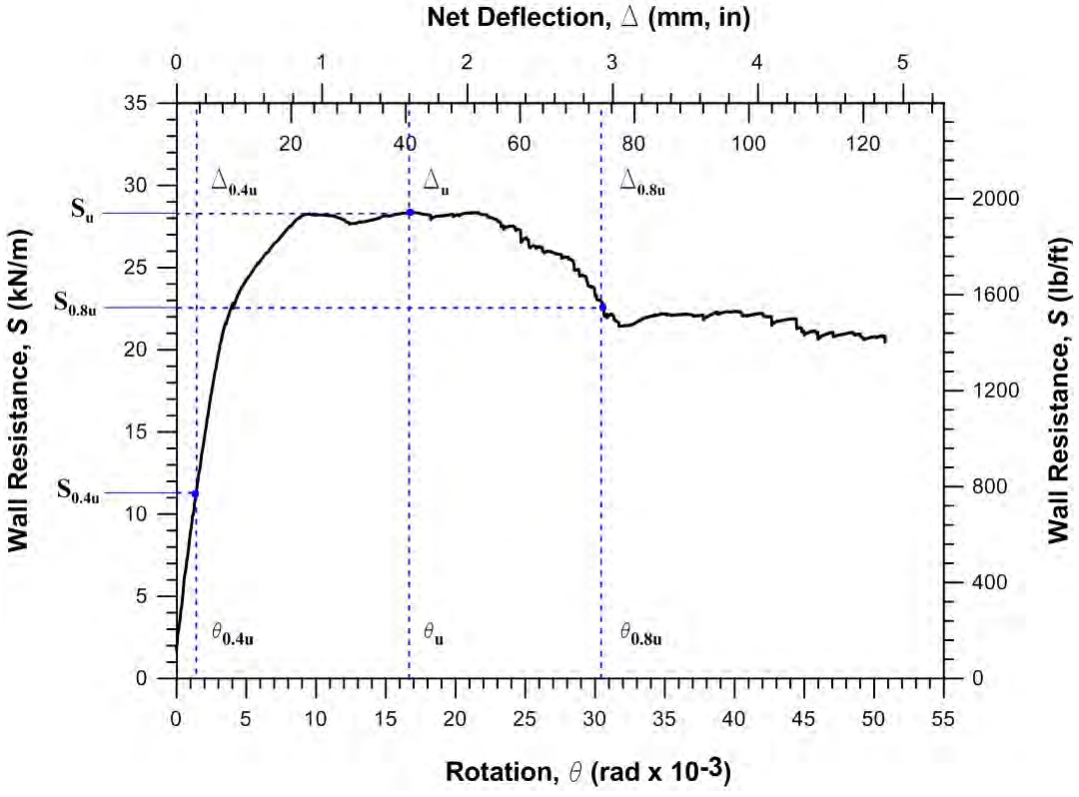

Figure 3.19: Representation of parameters from monotonic tests.

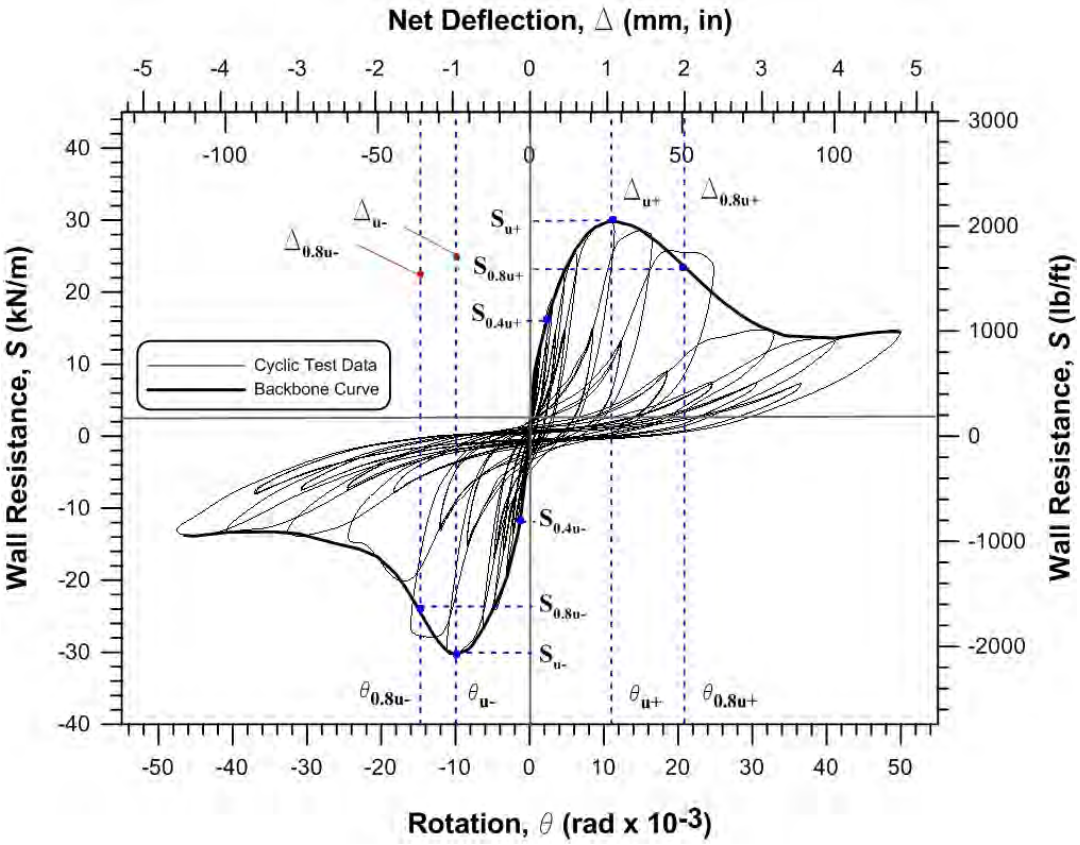

Figure 3:20: Representation of positive and negative parameters from symmetric cyclic tests.

Table 3.1: Summary of Monotonic Shear Wall Test Results – Metric

Test	S_u (kN/m)	Δ_u (mm)	$\Delta_{0.4u}$ (mm)	$\Delta_{0.8u}$[1] (mm)	θ_u (radx10^{-3})	$\theta_{0.4u}$ (radx10^{-3})	$\theta_{0.8u}$[1] (radx10^{-3})	E_{total} (J)
Double-Sheathed Configuration								
W19-M	39.6	28.1	4.65	57.1	11.5	1.91	23.4	4230
W20-M	27.3	39.3	3.18	66.7	16.1	1.31	27.4	3158
W21-M	45.9	27.0	4.47	56.1	11.1	1.83	23.0	4980
W22-M	28.4	41.2	3.45	74.5	16.9	1.41	30.5	3606
W28-M[2]	61.0	31.7	5.41	61.8	13.0	2.22	25.4	6463
W29-M[2]	38.2	34.3	3.51	85.0	14.1	1.44	34.9	4674
W30-M[2]	65.4	39.0	7.16	68.7	16.0	2.94	28.2	7248
W31-M[2]	39.3	29.9	3.21	76.2	12.3	1.32	31.2	4783
Centre-Sheathed Configuration								
W15-MR3	150	120	14.7	100	49.2	6.03	41.0	16788
W16-MR	125	67.5	12.3	100	27.7	5.06	41.0	14479
W16-MR2	130	106	15.1	100	43.3	6.21	41.0	15207
W17-M	75.7	99.4	10.9	100	40.8	4.45	41.0	9221
W18-M[2]	87.2	68.2	10.8	100	28.0	4.43	41.0	10481
W18-MR[2]	92.6	87.3	10.8	100	35.8	4.44	41.0	11211

[1] Calculated based on the 4% lateral drift (approximately 100 mm) value.
[2] Test results computed by Brière *(2017)*.

Note: Appendix E contains Tables 3.1 to 3.3 with results in imperial units.

Table 3.2: Summary of Positive Cyclic Shear Wall Test Results – Metric

Test	S_u^+ (kN/m)	Δ_u^+ (mm)	$\Delta_{0.4u}^+$ (mm)	$\Delta_{0.8u}^{+1}$ (mm)	θ_u^+ (radx10^{-3})	$\theta_{0.4u}^+$ (radx10^{-3})	$\theta_{0.8u}^{+1}$ (radx10^{-3})	E_{BB}^+ (J)	E_{total} (J)
Double-Sheathed Configuration									
W19-C	46.5	34.0	6.36	52.0	13.9	2.61	21.3	4224	15062
W20-C	29.9	28.0	3.51	50.5	11.5	1.44	20.7	2892	10508
W21-C	47.6	29.1	6.04	50.6	11.9	2.48	20.7	4158	13970
W22-C	29.8	26.2	3.17	43.4	10.7	1.30	17.8	2770	9493
W28-C[3]	61.4	29.5	5.48	50.5	12.1	2.25	20.7	5415	18482
W29-C[3]	40.8	25.7	3.48	40.4	10.6	1.43	16.6	3569	12611
W30-C[3]	71.0	38.2	6.84	59.8	15.7	2.81	24.5	7109	24628
W31-C[3]	45.7	31.9	3.86	48.4	13.1	1.58	19.9	3987	14282
Centre-Sheathed Configuration									
W15-CR3	162	112	15.0	100	45.9	6.15	41.0	16695	75743
W15B-CR3[2]	166	160	13.3	100	65.6	5.46	41.2	37285	109013
W17-C	81.8	74.3	12.4	101	30.5	5.09	41.3	7908	56432
W18-CR[3]	94.8	89.0	13.0	100	36.5	5.34	41.0	11079	64012
W23-CR3[3]	163	121	15.1	100	49.4	6.21	41.0	18288	48419
W23B-CR3[2,3]	159	122	14.0	100	49.9	5.74	41.0	30306	98377
W24-CR3[3]	135	81.2	13.5	100	33.3	5.54	41.0	14510	76112
W25-CR3[2]	117	86.0	12.7	100	35.3	5.20	41.0	20117	70483
W26-CR3[2,3]	145	65.7	12.9	83.5	27.0	5.28	34.3	19176	61059

[1] Calculated based on the 4% lateral drift (approximately 100 mm) value.
[2] Asymmetric cyclic test, only positive parameters obtained.
[3] Test results computed by Brière *(2017)*.

Note: Appendix E contains Tables 3.1 to 3.3 with results in imperial units.

Table 3.3: Summary of Negative Cyclic Shear Wall Test Results – Metric

Test	S_u^- (kN/m)	Δ_u^- (mm)	$\Delta_{0.4u}^-$ (mm)	$\Delta_{0.8u}^{-1}$ (mm)	θ_u^- (radx10^{-3})	$\theta_{0.4u}^-$ (radx10^{-3})	$\theta_{0.8u}^{-1}$ (radx10^{-3})	E_{BB}^- (J)	E_{total} (J)
Double-Sheathed Configuration									
W19-C	-42.9	-25.0	-6.43	-45.5	-10.3	-2.64	-18.7	3771	15062
W20-C	-30.3	-24.5	-3.69	-36.0	-10.0	-1.51	-14.8	2476	10508
W21-C	-44.8	-21.5	-4.80	-41.0	-8.83	-1.97	-16.8	3675	13970
W22-C	-29.8	-24.0	-3.41	-39.3	-9.83	-1.40	-16.1	2644	9493
W28-C[3]	-62.1	-26.4	-6.03	-38.1	-10.8	-2.47	-15.6	4833	18482
W29-C[3]	-39.9	-24.3	-4.90	-37.2	-9.97	-2.01	-15.3	3239	12611
W30-C[3]	-68.6	-31.2	-6.45	-44.0	-12.8	-2.65	-18.0	6204	24628
W31-C[3]	-44.4	-26.5	-3.86	-44.2	-10.9	-1.58	-18.1	3750	14282
Centre-Sheathed Configuration									
W15-CR3	-156	-103	-15.5	-100	-42.3	-6.35	-41.0	14219	75743
W15B-CR3[2]	-	-	-	-	-	-	-	-	-
W17-C	-79.8	-78.89	-10.9	-99.6	-32.4	-4.47	-40.9	7831	56432
W18-CR[3]	-89.9	-70.7	-12.7	-100	-29.0	-5.22	-41.0	9775	9775
W23-CR3[3]	-132	-50.3	-11.1	-50.3	-20.6	-4.56	-20.6	5074	5074
W23B-CR3[2,3]	-	-	-	-	-	-	-	-	-
W24-CR3[3]	-128	-78.0	-11.9	-100	-32.0	-4.88	-41.0	13367	13367
W25-CR3[2]	-	-	-	-	-	-	-	-	-
W26-CR3[2,3]	-	-	-	-	-	-	-	-	-

[1] Calculated based on the 4% lateral drift (approximately 100 mm) value.
[2] Asymmetric cyclic test, only positive parameters obtained.
[3] Test results computed by Brière *(2017)*.

Note: Appendix E contains Tables 3.1 to 3.3 with results in imperial units.

3.4 Comparison of Shear Walls

Different wall choices of parameter values (construction details) were tested under each shear wall configuration. The parameters that were varied included the thickness of the sheathing, the thickness of the framing, the screw diameter (gauge), the sheathing fastener spacing, and the type of chord stud reinforcement. A comparison between the specimens in this test program was done to show how these parameters and the overall shear wall configurations affected the shear resistance and ductility of the walls. Brière *(2017)* has provided comparisons of some of the shear wall tests for both the double-sheathed and centre-sheathed configurations. The sheathing connection screw diameter was kept constant for the specimens tested by the author. For a comparison of test results for walls with different sheathing screw size, see Brière *(2017)*. Further, a comparison is made, at the end of this section, between the shear walls tested during this research program and the walls tested by Risk *(2017)* and Balh *(2010)*.

3.4.1 Double-Sheathed Configuration

The monotonic and cyclic behaviour of the double-sheathed walls was observed to be similar, however some differences were recorded (Section 3.4.1.4). Within the cyclic tests, the walls showed a higher capacity during the positive cycles when compared to the negative cycles because the test started with displacement in the positive direction. As a wall reached its inelastic range and plastic deformation started, its shear capacity was decreased when it was displaced in the negative direction. The varying wall construction parameters affected the performance of the specimens resulting in some walls behaving better than others in terms of shear capacity. Out of all the double-sheathed shear walls that were tested, W30 reached the highest ultimate shear resistance; 65.4 kN/m (4483 lb/ft) during the monotonic test and 71.0 kN/m (4862 lb/ft) during the cyclic test. This shear resistance was achieved through the combination of small fastener spacing, 50 mm (2”), thicker framing members, 2.46 mm (0.097”), thicker sheathing, 0.47 mm (0.019”), and larger screw size, No. 12.

3.4.1.1 Effect of Fastener Spacing

The double-sheathed specimens were tested with 50 mm (2”) or 100 mm (4”) sheathing fastener spacing. The walls with smaller fastener spacing developed a higher shear resistance than those with larger fastener spacing. This behaviour is shown in Figure 3.21; comparison of W19-

M with W20-M and W21-M with W22-M. When the sheathing (0.36 mm, 0.014”) and framing (1.72 mm, 0.068”) thicknesses were constant, the wall with the smaller fastener spacing, W19-M, reached a maximum shear force of 39.56 kN/m (2711 lb/ft), whereas the wall with the larger fastener spacing, W20-M, reached 27.28 kN/m (1869 lb/ft). The shear resistance in this case was increased by 45%. When comparing configurations W21-M and W22-M, which had the same sheathing thickness but thicker framing (2.46 mm, 0.097”), the same pattern was observed, as expected. However, it was also observed that the walls with a 100 mm (4”) fastener spacing behaved slightly better in terms of ductility; that is, the force degradation occurred more gradually compared to the 50 mm (2”) walls. These results indicate that fastener spacing in the double-sheathed walls affects the shear resistance of the wall. Smaller fastener spacing allows more fasteners to dissipate energy and provide a higher lateral resistance.

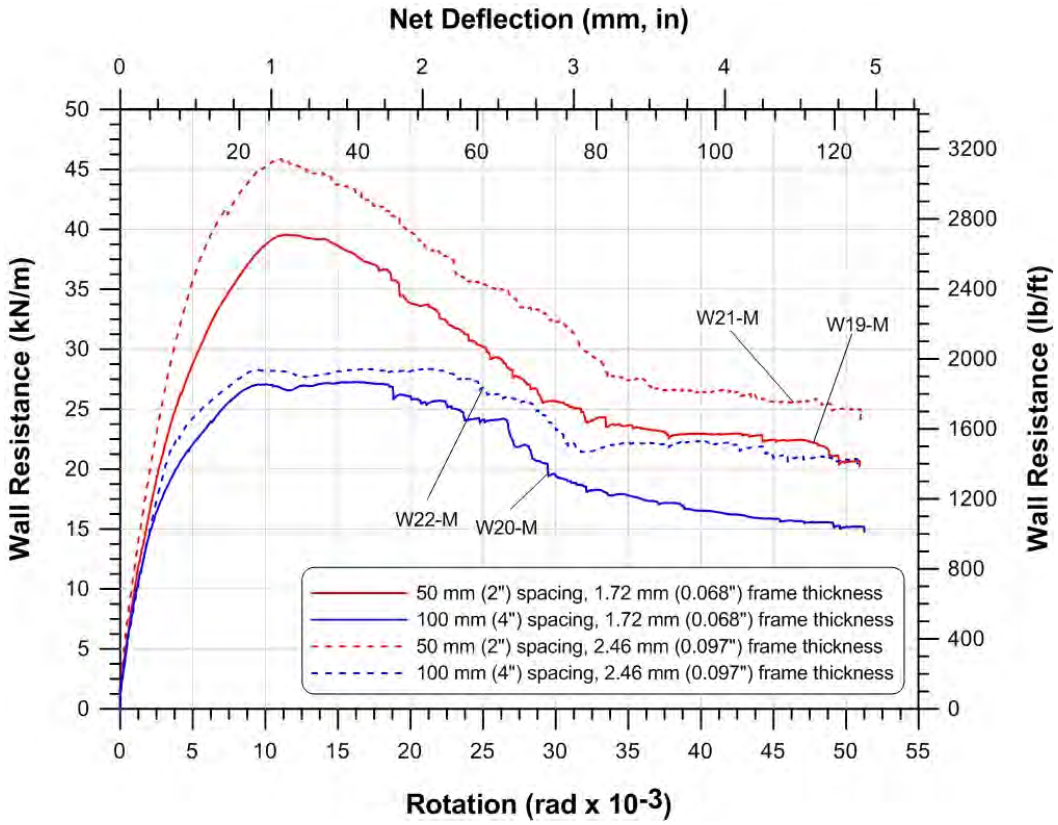

Figure 3.21: Comparison of sheathing fastener spacing and frame thickness between double-sheathed specimens W19-M, W20-M, W21-M, and W22-M. Constant sheathing thickness of 0.36 mm (0.014”).

3.4.1.2 Effect of Framing Thickness

The behaviour of the walls was investigated in terms of framing thickness. Two different stud and track thicknesses were used in the construction of the double-sheathed configurations; 1.72 mm (0.0.68”) and 2.46 mm (0.097”). Overall, the shear resistance of walls with thicker framing were higher than that of the walls with thinner framing. The effect of framing thickness is shown by the results in Figure 3.21, where the sheathing thickness (0.36 mm, 0.014”) and the fastener spacing (50 mm and 100 mm, 2” and 4”) are kept constant. When comparing W19-M and W21-M, thinner and thicker framing respectively, the maximum shear force reached by W21-M was 16% higher than that reached by W19-M, while ductility was not affected. Similar behaviour, although to a lesser extent (4% shear resistance increase), was observed between W20-M and W22-M, which were built using a constant fastener spacing of 100 mm (4”), but had varying framing thickness. Framing member thickness affected the shear capacity of the walls, however fastener spacing seemed to have a greater impact.

3.4.1.3 Effect of Sheathing Thickness

The double-sheathed configurations were built using two sheets of 0.36 mm (0.014”) or 0.47 mm (0.019”) thick sheathing; with these shear wall specimens, the effect of sheathing thickness was evaluated. Figure 3.22 illustrates the increase in shear resistance when thicker sheathing was used. Specimens W21-M and W28-M were built using 2.46 mm (0.097”) framing and 50 mm (2”) fastener spacing. Using thicker sheathing to build W28-M resulted in an increase in shear capacity; 33% higher than what was reached by W21-M, which was constructed with thinner sheathing. Similarly, this behaviour was observed for specimens W22-M and W29-M, which used a fastener spacing of 100 mm (4”) instead of 50 mm (2”). A higher shear capacity was achieved when a thicker sheathing was used because of the increased resistance of the connections.

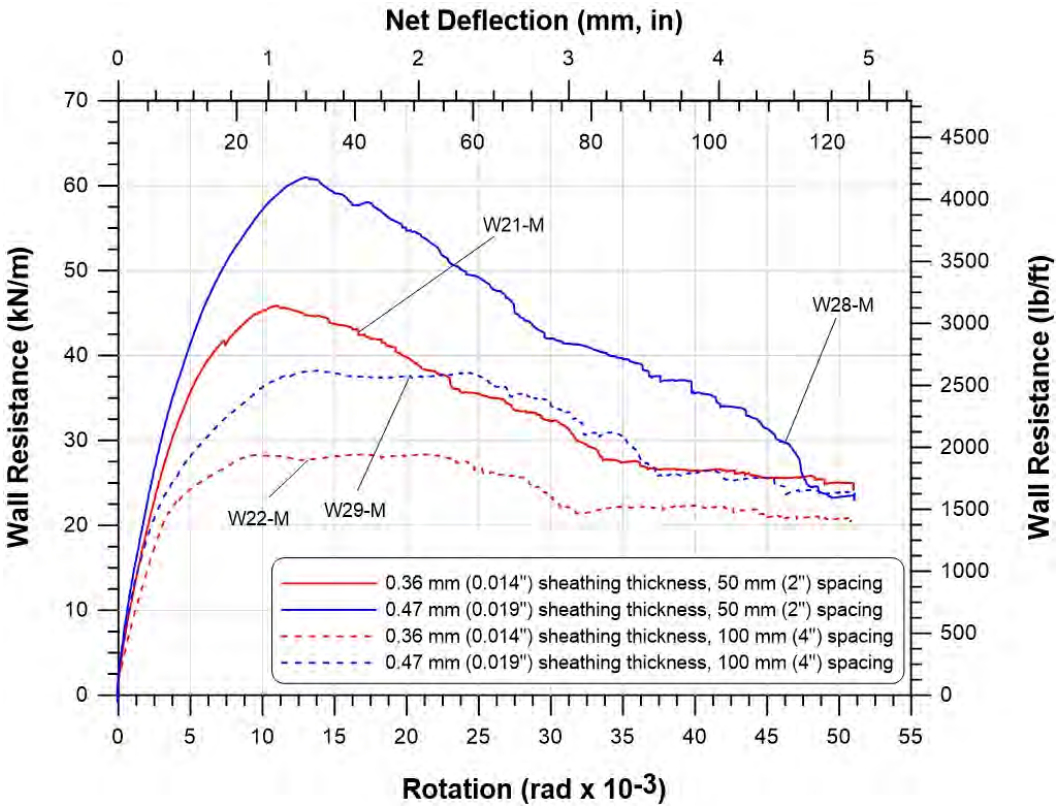

Figure 3.22: Comparison of sheathing thickness between double-sheathed specimens W22-M, W29-M, W21-M, and W28-M.

3.4.1.4 Comparison of Monotonic and Cyclic Test Results

All double-sheathed wall configurations were tested monotonically and cyclically. The behaviour of the walls during the cyclic tests differed slightly from their behaviour during the monotonic tests, shown in Figure 3.23. During the cyclic tests the specimens reached larger ultimate shear strength compared to the strength reached during the monotonic tests of the same wall construction. Additionally, the specimens experienced strength degradation earlier (at smaller lateral displacement) than during the monotonic tests. This faster loss of strength was a result of the repeated back and forth cycles, which caused bearing deformation around the sheathing connections in both directions (creating a slotted hole). This larger slot around a screw allowed the sheathing to pull over the fastener head more easily, thus detaching from the frame. This was not the case during the monotonic tests since the lateral displacement was unidirectional, making it more difficult for the sheathing to pull over the screw head.

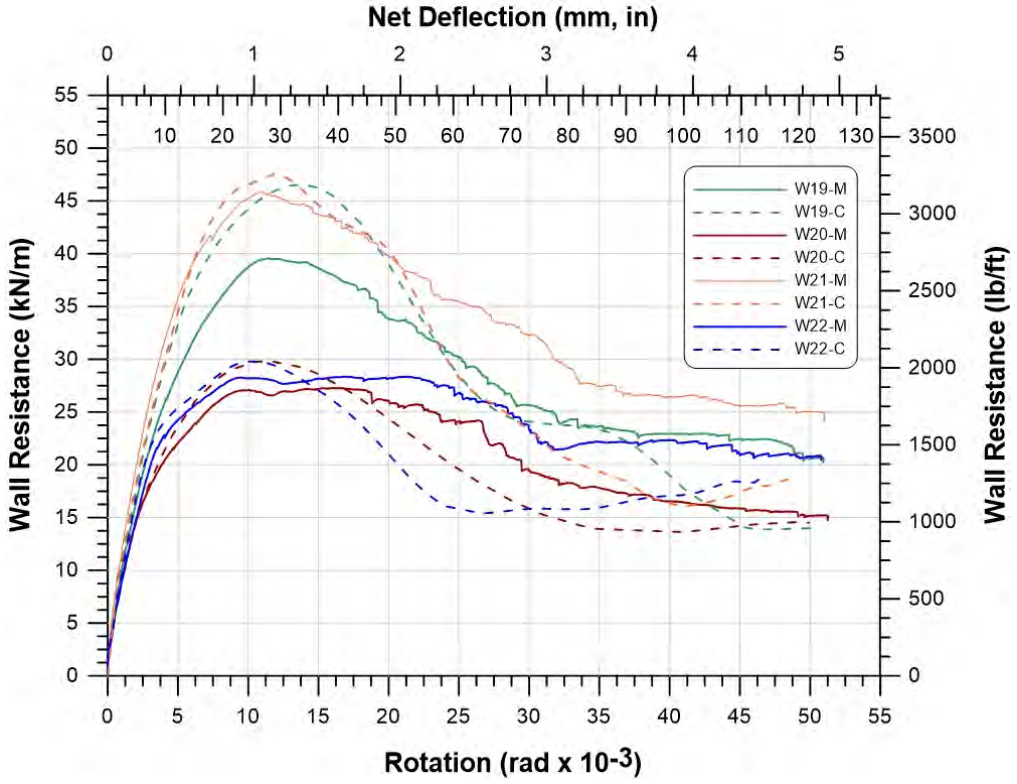

Figure 3.23: Comparison between monotonic and cyclic behaviour of double-sheathed specimens (only positive backbone data shown for cyclic tests).

3.4.2 Centre-Sheathed Configuration

In addition to the typical wall configuration parameters discussed in Section 3.4, centre-sheathed configurations varied based on the type of chord stud reinforcement used. The addition of chord stud reinforcement was a result of the local buckling failure of the compression chord studs due to the larger than anticipated shear forces experienced during the centre-sheathed tests. When the appropriate chord stud reinforcement was installed (discussed in Section 3.4.2.4) the frame did not fail, allowing the walls to reach their shear resistance potential from extensive bearing deformation at the connections. Similar to the double-sheathed walls, the varying construction parameters affected the behaviour of the wall. Lastly, testing certain specimens using an asymmetric cyclic protocol vs. a symmetric cyclic protocol did not impact the behaviour of the walls.

The centre-sheathed wall with the highest shear capacity was W15B-CR3, which reached 166 kN/m (11354 lb/ft) with force degradation observed at approximately 8% lateral drift. The

high shear capacity and ductility while avoiding frame failure resulted from the combination of thinner sheathing (2.46 mm, 0.097”), small fastener spacing (50 mm, 2”), and larger chord stud reinforcement (R3).

3.4.2.1 Symmetric vs. Asymmetric Cyclic Protocols

Certain centre-sheathed shear wall configurations were tested using an asymmetric cyclic protocol (Table 2.1b). The results from these asymmetric tests were used in the subsequent sections in order to compare the parameters that were varied in the construction of the centre-sheathed walls. It is important to note that the use of the asymmetric protocol had no effect on the behaviour of the walls. In Figure 3.24, the force vs. deformation results of an asymmetric cyclic test (W15B-CR3) are superimposed onto those of a symmetric cyclic test (W15-CR3); these walls were of nominally identical construction. Both showed identical behaviour up to the end of the symmetric test (at approximately 120 mm or 4.72”). This indicates that the type of cyclic protocol did not affect the test results. Hence, the results obtained from walls tested with this protocol can be used for comparison with other walls that have been tested using the symmetric cyclic protocol.

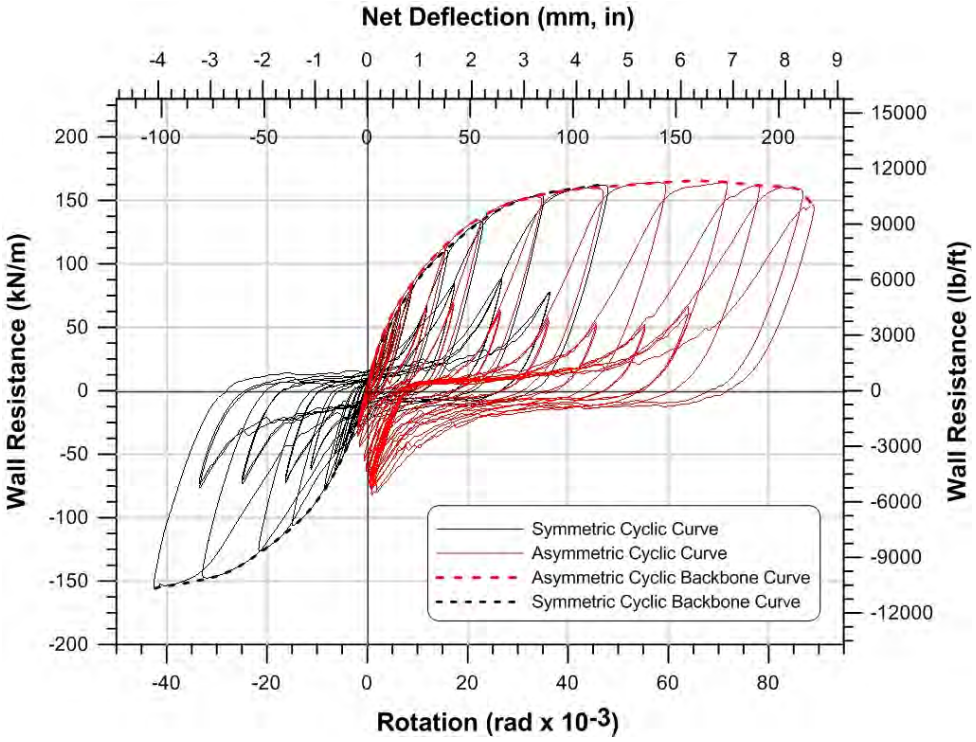

Figure 3.24: Symmetric vs. asymmetric cyclic protocols of centre-sheathed configuration W15.

3.4.2.2 Effect of Fastener Spacing

Similar to the double-sheathed configuration, the centre-sheathed configurations with smaller fastener spacing reached a higher shear resistance than configurations with larger fastener spacing. Figure 3.25 shows the comparison between specimens W15B-CR3 and W25-CR3, built with 50 mm and 100 mm screw spacing respectively. These walls had the same type of chord stud reinforcement (R3), frame and sheathing thicknesses, and sheathing screw size. The specimen with a 50 mm (2") fastener spacing reached a significantly higher shear capacity (29%) than the specimen with a 100 mm (4") fastener spacing. The bearing deformation of the sheathing screws is the main mechanism through the shear force is transferred to the sheathing, thus providing the shear resistance of the wall. The increase in number of sheathing screws (smaller spacing) therefore allowed for an increase in the wall's shear resistance. The confinement of the sheathing between the chord studs of the centre-sheathed walls, for the closely spaced screw construction, led to extensive bearing deformation at each connection, significantly improving the ductility. Brière *(2017)* further explains that having even larger sheathing screw spacing, i.e. 150 mm (6"), for the centre-sheathed configuration leads to the separation of the individual members in the built-up chord studs, which results in a loss in shear resistance of the wall and lower ductility.

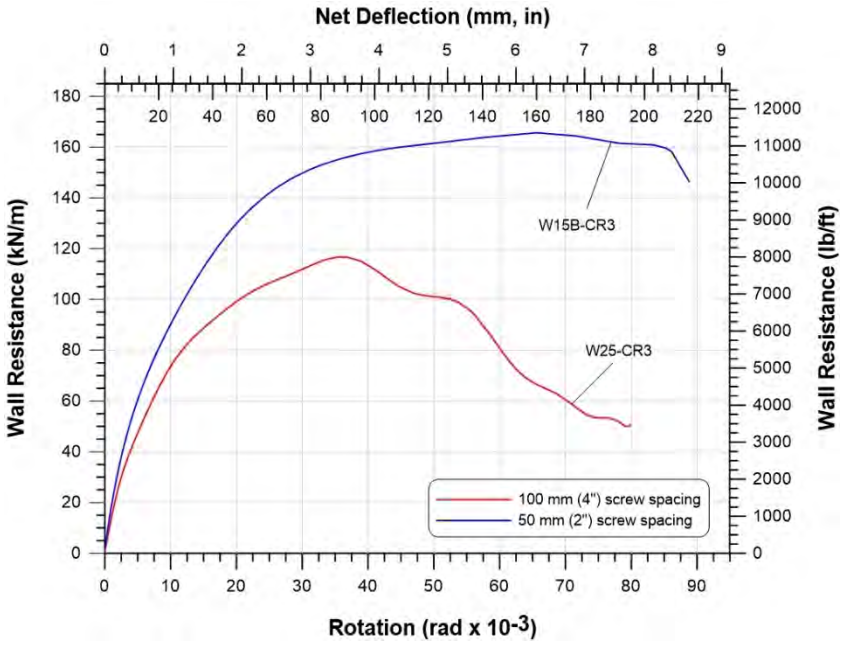

Figure 3.25: Comparison of sheathing fastener spacing between centre-sheathed specimens W15B-CR3 and W25-CR3.

3.4.2.3 Effect of Sheathing Thickness

Varying the sheathing thickness of the centre-sheathed walls resulted in the same response as found for the double-sheathed shear wall configuration. Figure 3.26 shows that the specimen with thinner sheathing (W25-CR3) had a lower shear capacity, 117 kN/m (7997 lb/ft), than the specimen with thicker sheathing (W26-CR3), which reached a shear capacity of 145 kN/m (9956 lb/ft). Both specimens had a framing thickness of 2.46 mm (0.097") and fastener spacing of 100 mm (4"). Having a thicker sheathing improves the nominal capacity of the screw connections (as explained by the Effective Strip Method) through which the force transfer occurs, resulting in a higher shear resistance. The comparison in Figure 3.21 also shows that although the thicker sheathing specimen reached a higher shear resistance, its strength degraded more quickly. The shear buckling of the thicker sheathing created higher out-of-plane forces, which pushed the members of the built-up chord studs apart causing them to become less effective in terms of their ability to carry load. This behaviour lead to the more sudden loss in shear resistance of the wall because the bearing deformation in the sheathing at the connections was not able to develop to its full potential.

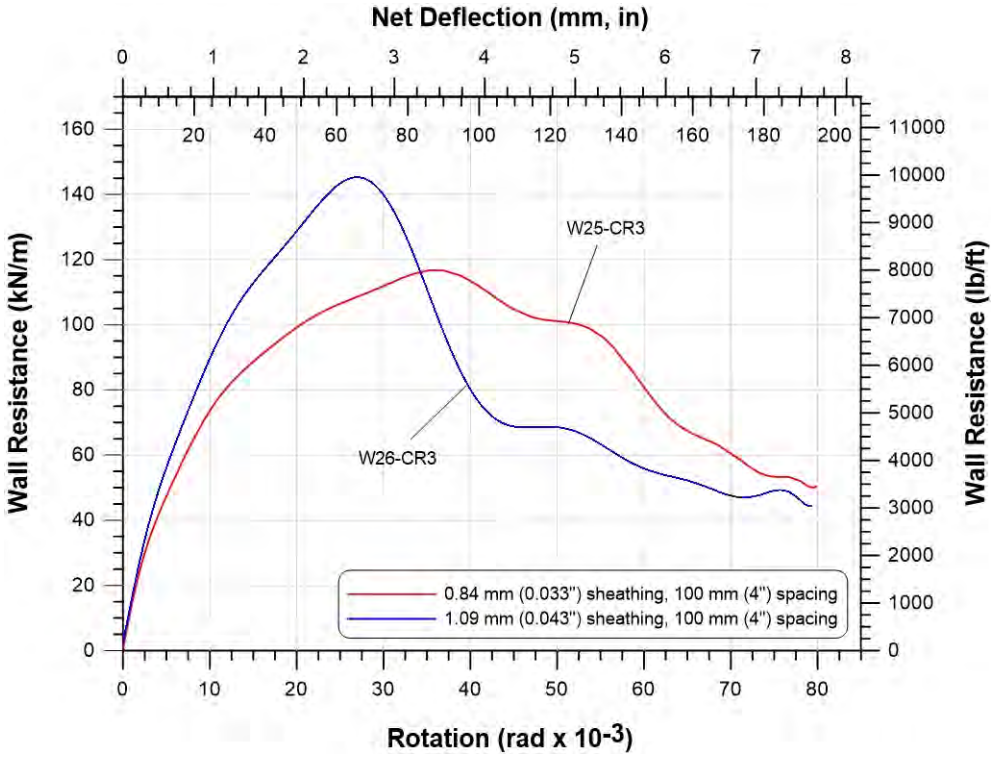

Figure 3.26: Comparison of sheathing thickness between centre-sheathed specimens W25-CR3 and W26-CR3.

3.4.2.4 Effect of Type of Reinforcement

Various types of chord stud reinforcement (Appendix A) were tested with the centre-sheathed configuration to improve the axial and bending resistance of the compression chord studs and to avoid frame failure. Initially, the centre-sheathed configuration with no chord stud reinforcement and a 100 mm (4") fastener spacing (W18-M) was tested. When a wall was built having the same parameters and with the first type of chord stud reinforcement (W18-MR), the frame did not fail and strength degradation occurred at a larger displacement compared to the specimen without reinforcement (Figure 3.27).

Next, a wall configuration with 50 mm (2") fastener spacing (W16-MR) was built using the first type of chord stud reinforcement since it was expected to experience larger forces resulting from the smaller fastener spacing. Due to the combination of bending and axial compression from the higher shear forces, the chord stud failed, showing a drop in shear strength at 70 mm (2.75") lateral displacement. In order to maximize the shear resistance of the specimen the same wall was then built, however, this time using the second type of chord stud reinforcement (W16-MR2). Although W16-MR2 reached a slightly higher ultimate shear resistance than W16-MR, the shear resistance was limited by the failure of the chord stud, causing a drop in shear strength at 105 mm (4.13") lateral displacement. Finally, the same wall was built using the third type of chord stud reinforcement (W15-CR3). The reinforcement, R3, provided the chord stud with enough resistance to avoid frame failure due to bending and axial compression, and it allowed the wall to make full use of the bearing deformations at the sheathing connections confined between the built-up chord studs. W15-CR3 reached significantly higher shear resistance (150 kN/m, 10278 lb/ft) and ductility compared to W16-MR (125 kN/m, 8565 lb/ft) and W16-MR2 (130 kN/m, 8908 lb/ft), with no strength degradation at the end of the test at 120 mm (4.75") lateral displacement. The comparison between the three types of reinforcement is shown in Figure 3.28 for the 50 mm (2") fastener spacing wall configurations W16-MR, W16-MR2, and W15-MR3.

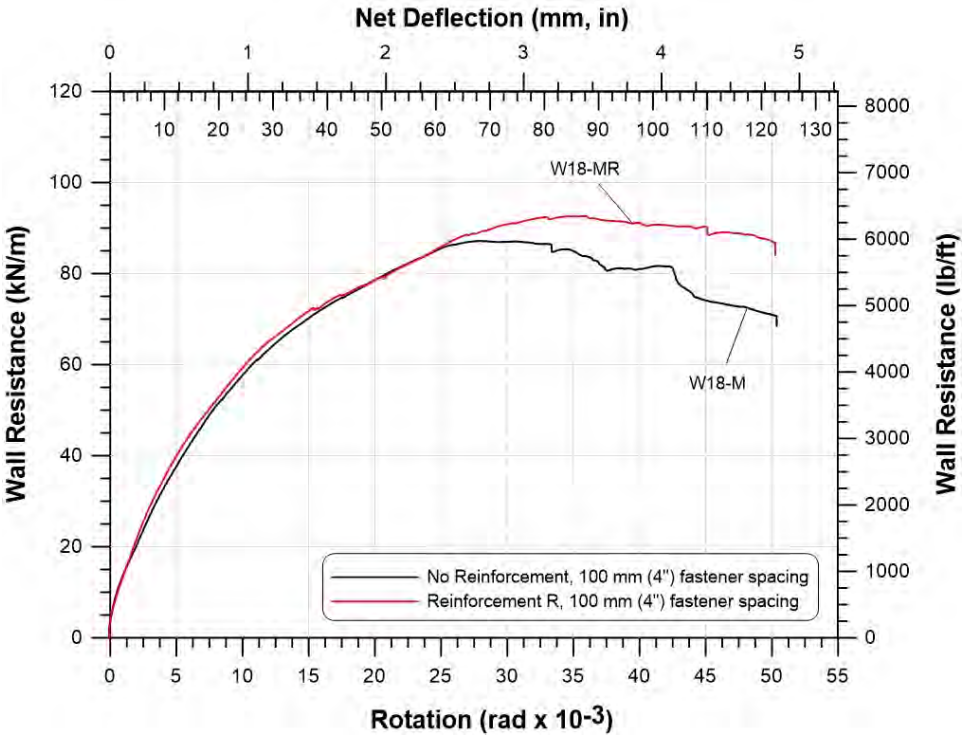

Figure 3.27: Comparison between no chord stud reinforcement with chord stud reinforcement R for 100 mm (4") fastener spacing specimens.

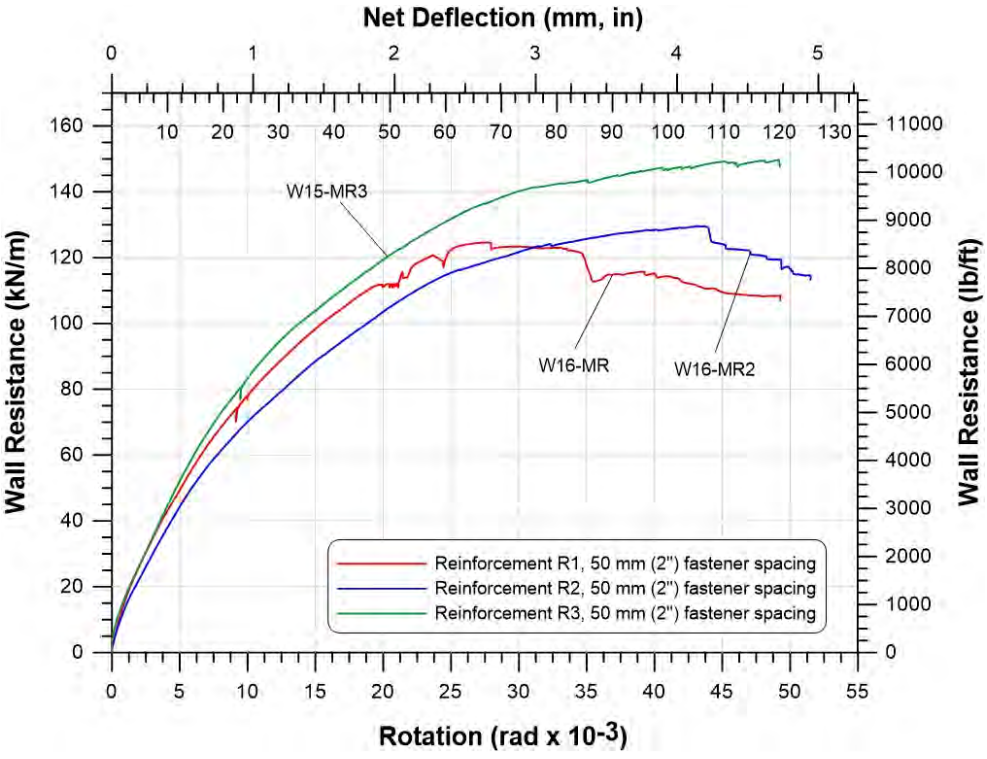

Figure 3.28: Comparison of chord stud reinforcement schemes between centre-sheathed specimens W16-MR and W16-MR2, and W15-MR3.

3.4.3 Double-Sheathed Configuration vs. Centre-Sheathed Configuration

The choice of configuration for the shear walls resulted in a significant difference in behaviour in terms of shear strength and ductility. Figure 3.29 compares the backbone curves of the strongest centre-sheathed specimen W15B-CR3 (asymmetric cyclic test), with its equivalent double-sheathed specimen, W21-C. The two wall configurations were built using the same parameters: frame thickness of 2.46 mm (0.097”), No. 10 sheathing fasteners and fastener spacing of 50 mm (2”). The sheathing thickness of the centre-sheathed wall was 0.84 mm (0.033”), whereas the combined sheathing thickness of the double-sheathed wall was 0.72 mm (0.028”). Even though the sheathing thicknesses are not identical, the walls are comparable in terms of thinner sheathing within their configuration group. The centre-sheathed wall W15B-CR3 had also been tested using a symmetric cyclic protocol; the backbone curve is also shown in Figure 3.29 for comparison.

The shear capacity of the centre-sheathed wall increased by 248% compared to the double-sheathed specimen. The ductility was also improved; W21-C experienced strength degradation at 30 mm (1.18”) immediately after it had reached its ultimate resistance (47.6 kN/m, 3262lb/ft), whereas the shear resistance of W15B-CR3, at the same lateral displacement, was still increasing beyond 100 kN/m (6852 lb/ft). The ultimate shear resistance of the centre-sheathed specimen (166 kN/m, 11375 lb/ft) was reached at 160 mm (6.30”) lateral displacement and the force degradation was only significant after the wall had displaced 180 mm (7.09”).

The superior behaviour of the centre-sheathed configuration in terms of shear strength and ductility was attributed to the confinement of the sheathing around the perimeter of the wall within the built-up chord studs. This confinement allowed full bearing deformation at the connections to develop and dissipate more energy, instead of the sheathing detaching from the frame, as was observed for the double-sheathed configuration. As the fasteners pulled through the sheathing, the sheathing unzipped from the frame in the double-sheathed configuration, inhibiting the screws from further contributing to the shear resistance of the wall.

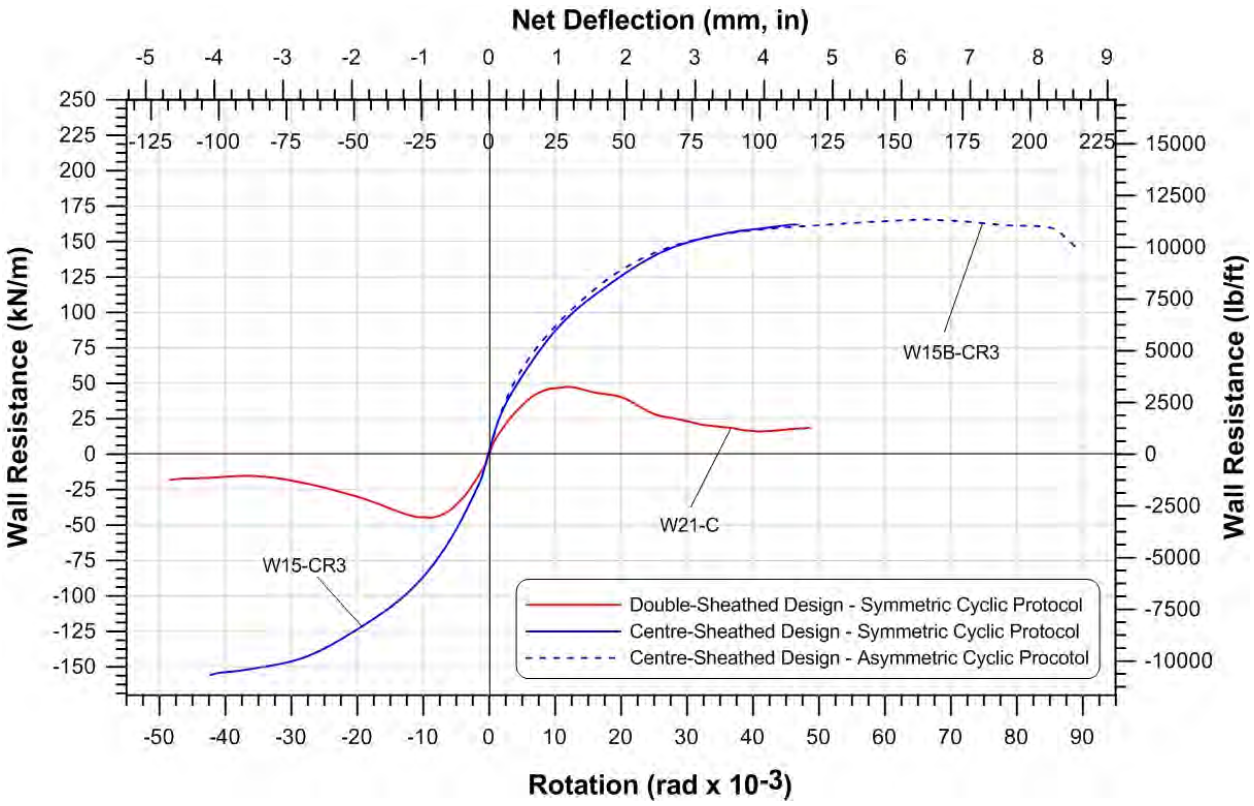

Figure 3.29: Comparison between double-sheathed and centred-sheathed configurations. Construction parameters: 2.46 mm (0.097") frame thickness, 50 mm (2") fastener spacing, #10 fasteners, 2 × 0.36 mm (0.014") sheathing (double-sheathed specimen), and 0.84 mm (0.033") sheathing (centre-sheathed specimen).

3.4.4 Comparison with Previously Tested CFS Shear Walls

The shear walls tested in this research program, using new configurations, showed significant improvement in shear resistance and ductility in comparison to what is available for design in the cold-formed steel standard AISI S400 *(2015)*. This improvement in performance was a result of changing the way the walls were built to address issues reported in previous research as well as using thicker framing and sheathing members. The strongest double-sheathed wall and centre-sheathed wall (see Sections 3.4.1 and 3.4.2) reached, respectively, shear strengths approximately two times and four times higher than what is currently tabulated for the design of steel-sheathed shear walls in the AISI S400 Standard *(2015)*.

Risk *(2017)* and Balh *(2010)* tested CFS framed and sheathed shear walls. Their test programs included specimens with the same dimensions (1.22 m × 2.44 m, 4' × 8') as those tested

for this research. The walls tested in both previous programs were built using the traditional construction detail with a single sheathing placed on one side of the wall. The use of this construction detail combined with smaller and thinner framing members resulted in shear strengths much lower than those achieved by the specimens in the current program. Balh's *(2010)* strongest wall, with the same aspect ratio, was 11.1 kN/m (761 lb/ft). The most comparable specimen with similar configuration parameters (frame thickness and fastener spacing for example), tested by Risk *(2017)* reached 39.6 kN/m (2528 lb/ft). Balh's and Rizk's specimens experienced force degradation at low lateral drifts, 1.13% and 2.05%, respectively, which showed they were significantly less ductile than the centre-sheathed walls (force degradation at up to 8% drift). In both of the previous test programs the shear resistance was reported to have been compromised due to the asymmetry of the walls, which caused twisting of the chord studs. This was not the case for the centre-sheathed walls since the wall design was symmetric (sheathing centred between the chord studs), resulting in improved shear strength and ductility. Figure 3.30 compares Rizk's *(2017)* specimen (W2-C) with the strongest wall tested in the current research program (W15B-CR3).

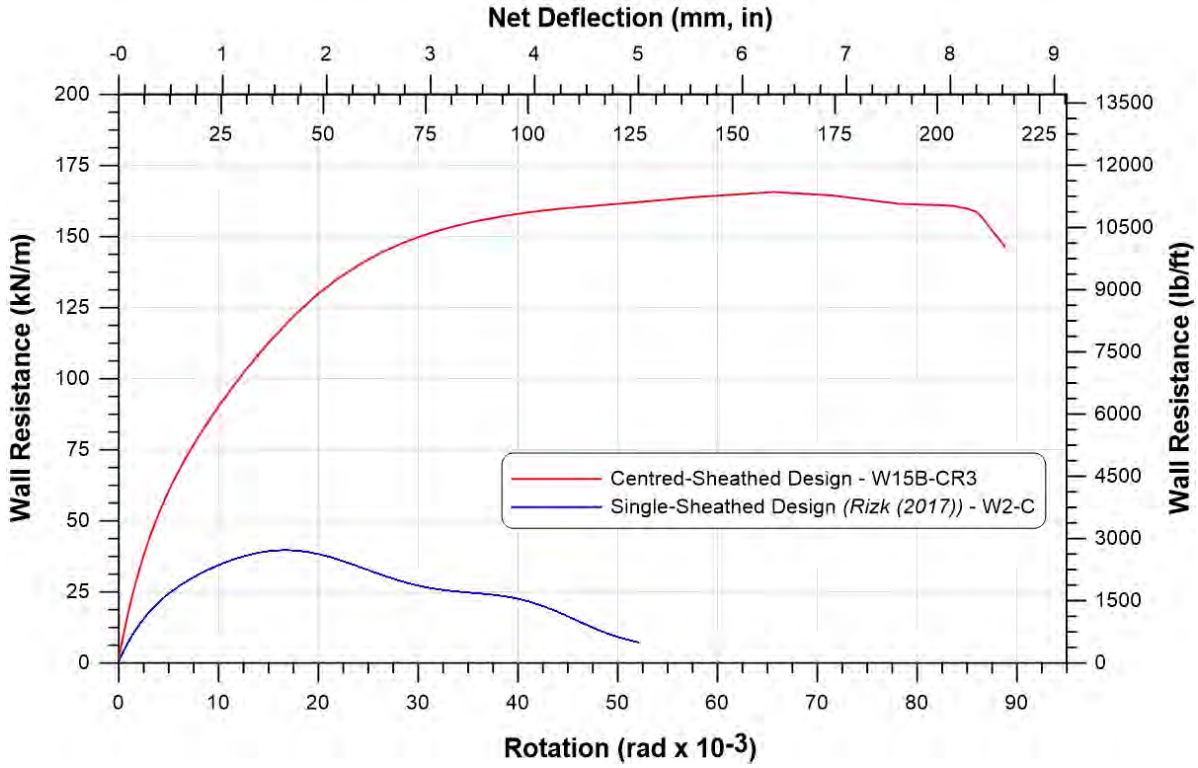

Figure 3.30: Centre-sheathed shear wall compared to Risk's *(2017)* single-sheathed shear wall.

3.5 Ancillary Testing of Materials

The material and mechanical properties of the framing and sheathing materials were determined by performing tensile coupon tests. The tests were done for each sheathing thickness; 0.36 mm (0.014”), 0.47 mm (0.019”), 0.84 mm (0.033”), and 1.09 mm (0.043”), in the transverse and longitudinal directions. The 1.72 mm (0.068”) and 2.46 mm (0.097”) framing members (studs and tracks) were also tested. In addition, coupons of the steel straps used to attach the chord stud reinforcements were tested. For each thickness of sheathing, framing and strap, either two or three coupon samples were tested following the ASTM A370 *(2017)* procedure. The coupons were subjected to tension loading at a cross-head movement of 0.002 mm/s within the elastic range, the rate was increased to 0.01 mm/s once yielding was reached, and finally to 0.1 mm/s after strain hardening. A 50 mm (2”) extensometer and two strain gauges (one on each side) were attached to each coupon to measure elongation and strain respectively.

After the tensile coupon tests were performed, in order to calculate the material properties, the zinc coating of each coupon was removed using a 25% hydrochloric acid solution to measure the base metal thickness. The mechanical and material properties resulting from the tensile coupon tests are summarized in Table 3.4. All coupon test measurements and results are found in Appendix F.

All coupons showed the typical steel stress-strain behaviour, where a linear relationship developed within the elastic range until the yielding plateau and strain hardening were reached before failure. The measured base metal thicknesses were larger than that specified by the manufacturer except for the thinner sheathing samples B and C. The measured yield strengths, F_y, were higher than the minimum specified values of 230 MPa (33 ksi) and 345 MPa (50 ksi) for the sheathing and framing members respectively. The same observation was made with respect to the measured tensile strengths, F_u, for which the minimum specified values are 310 MPa (45 ksi) and 450 MPa (65 ksi) for the sheathing and framing respectively. As per Section A3 of the AISI S400 Commentary *(2015)*, the minimum elongation over a gauge length of 50 mm (2”) is 12% and the minimum ultimate strength to yield strength ratio, F_u/F_y, is 1.15 for materials of 230 MPa (33 ksi) and 345 MPa (50 ksi) ASTM A653. All materials had a measured elongation above the minimum, however coupon samples B and C did not reach the minimum required F_u/F_y.

Table 3.4: Summary of Material Properties from Tensile Coupon Tests

Coupon	Member	*Nominal Thickness* (mm)	*Base Metal Thickness* (mm)	F_y (MPa)	F_u (MPa)	$\frac{F_u}{F_y}$	*Elongation* (%)
A Transversal dir.	Sheathing	0.84 (0.033")	0.88 (0.035")	302 (43.8 ksi)	352 (51.1 ksi)	1.17	40
A Longitudinal dir.	Sheathing	0.84 (0.033")	0.87 (0.034")	276 (40.1 ksi)	358 (51.9 ksi)	1.30	39
B Transverse dir.	Sheathing	0.48[1] (0.019")	0.48 (0.019")	318 (46.1 ksi)	361 (52.3 ksi)	1.14	37.5
B Longitudinal dir.	Sheathing	0.47[1] (0.019")	0.47 (0.019")	340 (49.3 ksi)	368 (53.3 ksi)	1.08	39
C Transverse dir.	Sheathing	0.36[1] (0.014")	0.36 (0.014")	344 (50.0 ksi)	370 (53.7 ksi)	1.07	29
C Longitudinal dir.	Sheathing	0.36[1] (0.014")	0.36 (0.014")	305 (44.2 ksi)	358 (52.0 ksi)	1.18	26
D	Sheathing	1.09 (0.043")	1.12 (0.044")	316 (45.9 ksi)	380 (55.1 ksi)	1.20	-
Strap	Steel Strap	1.09 (0.043")	1.11 (0.044")	366 (53.1 ksi)	447 (64.8 ksi)	1.22	30
Stud A / Track A	Stud/Track	1.73 (0.068")	1.77 (0.070")	386 (56.0 ksi)	466 (67.6 ksi)	1.21	34
Track B	Track	2.46 (0.097")	2.54 (0.100")	380 (55.1 ksi)	451 (65.4 ksi)	1.19	35
Stud B	Stud	2.46 (0.097")	2.54 (0.100")	389 (56.4 ksi)	461 (66.9 ksi)	1.19	34

[1]Non-standard thicknesses, no nominal value.

The measured ratio of expected yield strength and specified minimum yield strength, R_y, and the ratio of expected tensile strength and specified minimum tensile strength, R_t, are summarized in Table 3.5. In Table A3.2-1 of AISI S400 Standard *(2015)*, the R_y and R_t listed for the sheathing materials of 230 MPa (33 ksi) are 1.5 and 1.2 respectively. For the strap, studs, and tracks of 345 MPa (50 ksi), the R_y and R_t values are 1.1. The measured sheathing R_t values were the same as those in the AISI S400 Standard *(2015)*, except for the transverse 0.84 mm (0.033") sheathing, which was lower than 1.2. Only coupon samples B and C had R_y values similar to that listed in the AISI S400 Standard *(2015)*; the other sheathing materials had a lower measured R_y than 1.5. The measured R_t of the strap, tracks, and studs were lower than the listed value, while their measured R_y matched 1.1.

Table 3.5: Measured R_t and R_y Values

Coupon	**Member**	***Thickness* (mm)**	R_t	R_y
A Transversal dir.	Sheathing	0.84 (0.033”)	1.1	1.3
A Longitudinal dir.	Sheathing	0.84 (0.033”)	1.2	1.2
B Transverse dir.	Sheathing	0.48 (0.019”)	1.2	1.4
B Longitudinal dir.	Sheathing	0.47 (0.019”)	1.2	1.5
C Transverse dir.	Sheathing	0.36 (0.014”)	1.2	1.5
C Longitudinal dir.	Sheathing	0.36 (0.014”)	1.2	1.3
D	Sheathing	1.09 (0.043”)	1.2	1.4
Strap	Steel Strap	1.09 (0.043”)	1.0	1.1
Stud A / Track A	Stud/Track	1.73 (0.068”)	1.0	1.1
Track B	Track	2.46 (0.097”)	1.0	1.1
Stud B	Stud	2.46 (0.097”)	1.0	1.1

CHAPTER 4 – INTERPRETATION OF SHEAR WALL TEST RESULTS

4.1 Introduction

Using the data obtained from the shear wall tests presented in Chapter 3, design parameters for the purpose of developing a Limit States Design (LSD) approach and a Load and Resistance Factor Design (LRFD) approach were computed and discussed. The establishment of these design approaches provides key design information for the future use of cold-formed steel-sheathed and framed shear walls in mid-rise construction.

The test data for double-sheathed shear walls was evaluated using the same approaches previously used to obtain the tabulated shear strengths found in the AISI S400 Standard *(2015)*. In Canada, the Equivalent Elastic Plastic (EEEP) method was used, while in the USA and Mexico, the design parameter were taken as the ultimate shear force, S_u, reached during the tests.

It has been shown that the Equivalent Energy Elastic Plastic (EEEP) method (Park, *(1989)* and Foliente, *(1996)*) is appropriate for the simplified analysis of shear wall data, specifically for walls that behave nonlinearly under in-plane loading. Previously, Balh *et al. (2014)* and Branston *et al. (2006)* used this method to analyse steel and wood sheathed shear walls, respectively, the results of which were then included for use in design in the AISI S400 Standard *(2015)*. For the development of a LSD approach, used in Canada, the double-sheathed shear walls were also analysed using the EEEP method. A summary of the EEEP method and results are presented in Section 4.2, while the complete results are outlined in Appendix G.

In past research by Yu *(2010)* in the USA, the test peak load (ultimate force reached) was taken as the wall's nominal shear strength. Therefore, for consistency, the ultimate shear force reached by the double-sheathed specimens during the tests was taken as the design parameter used in the development of a LRFD approach, used in the USA and Mexico. The value needed, S_u, to calculate the LRFD parameters is tabulated in Chapter 3 (Tables 3.1 to 3.3) and in Appendix E.

A new approach was adopted in the evaluation of the data for the centre-sheathed shear walls since significantly higher shear forces and larger lateral displacements were reached during the tests. The design parameters, in Canada and in the USA and Mexico, were obtained from a newly developed prediction method; the Modified Effective Strip Method (MESM).

The MESM was developed as an *equation-based* approach to obtain the nominal shear strength of the centre-sheathed shear walls. This method was initially based on the Effective Strip Method by Yanagi and Yu *(2014)*, however it is still in its preliminary stages. Because the design and behaviour of the centre-sheathed configuration was significantly different than the shear wall configuration used in the development of the Effective Strip Method (discussed in Chapter 2), modifications had to be made to better represent this new and promising configuration. A thorough discussion on the MESM is presented in Section 4.3.

4.2 EEEP Method and Results (Canada)

In the EEEP method, the test data is characterized by a bilinear elastic-plastic force-deformation curve, where the curve represents the model behaviour of steel; elastic deformation and yielding. The EEEP curve is based on the energy dissipation of the test specimen up to 80% of the ultimate load post-peak. Theoretically, the 80% post-peak load represents the ultimate failure of the specimen. Figures 4.1 and 4.2 show the representation of the EEEP curve for two possible outcomes. Graphically, the area under the EEEP curve is the dissipated energy, which is equal to the area under the test curve (monotonic or cyclic backbone), up to the 80% post-peak displacement, $\Delta_{0.8u}$. Similarly, one can set areas A_1 and A_2 equal to one another to obtain the EEEP curve.

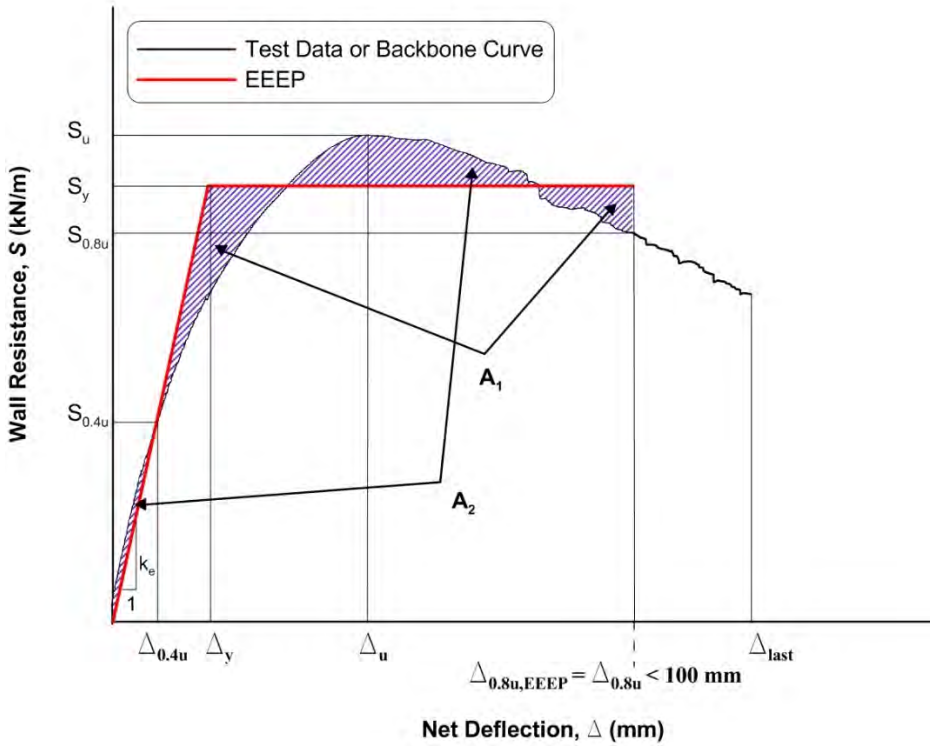

Figure 4.1: Graphical representation of the EEEP method, Case I.

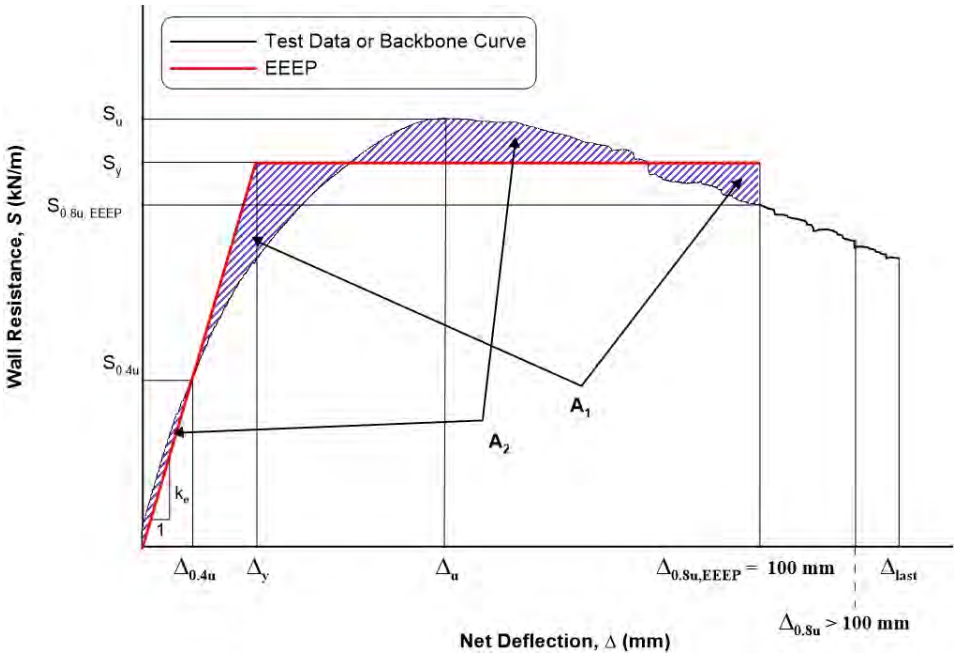

Figure 4.2: Graphical representation of the EEEP method, Case II.

The two outcomes of the EEEP method are considered because of the stronger and more ductile specimens tested during the program. Depending on the shear wall specimen, the force corresponding to 80% post-peak, $S_{0.8u}$, was not reached or it was reached at a large displacement not ideal for design. For this reason, $\Delta_{0.8u,\,EEEP}$ is used to represent the ultimate displacement of the EEEP curve and to differentiate it from the original $\Delta_{0.8u}$ if it was reached. The two EEEP cases used were the following:

CASE I) $S_{0.8u}$ reached, $\Delta_{0.8u} < 100$ mm (4"), $\Delta_{0.8u,\,EEEP} = \Delta_{0.8u}$;

CASE II) $S_{0.8u}$ not reached or $\Delta_{0.8u} > 100$ mm (4"), $\Delta_{0.8u,\,EEEP} = 100$ mm (4");

The limit of 100 mm (4") was chosen as an approximation of the 4% lateral drift of the wall. Using the 2.5% inelastic seismic lateral drift limit from the NBCC (NRC *(2015)*) would have been too conservative, since typically the wall specimens had not reached their ultimate resistance at that point, i.e. they could still dissipate energy beyond this drift limit. Even though in some cases the test specimens were displaced up to 8% lateral drift in order to observe their full behaviour, this level of lateral drift is too large and it would not usually be used in design. Therefore, the 4% lateral drift limit was chosen to represent the walls' behaviour while being considerate of real life conditions.

To create the EEEP curve, key values were obtained from the test data (monotonic) or backbone (cyclic) curves. The wall's yield resistance, S_y (Equation (4-1)), is the point where the curve transitions from elastic to plastic, and its corresponding wall displacement, Δ_y, represents the wall's elastic deflection. The wall's yield resistance was determined based on the elastic stiffness, k_e, the EEEP end displacement corresponding to the 80% post-peak load, $\Delta_{0.8u,\,EEEP}$ (see Figures 4.1 and 4.2), and the dissipated energy, A, up to 80% post-peak load. The 40% of ultimate load, $S_{0.4u}$, and the corresponding displacement, $\Delta_{0.4u}$, fall within the elastic range of the walls, and therefore were used to calculate the wall's elastic stiffness (Equation (4-2)). The yielding displacement, Δ_y, was then determined using the yielding load and the wall's stiffness as shown by Equation (4-3).

$$S_y = \frac{-\Delta_{0.8u,EEEP} \pm \sqrt{\Delta_{0.8u,EEEP}{}^2 - \frac{2A}{k_e}}}{\left(-\frac{1}{k_e}\right)} \quad (4\text{-}1)$$

$$k_e = \frac{S_{0.4u}}{\Delta_{0.4u}} \quad (4\text{-}2)$$

$$\Delta_y = \frac{S_y}{k_e} \quad (4\text{-}3)$$

where,

S_y = Wall's yield resistance (kN/m or lb/ft);

$S_{0.4u}$ = Shear load 40% of ultimate load (kN/m or lb/ft);

$\Delta_{0.8u,EEEP}$ = Wall displacement at 80% post-peak load based on EEEP case (mm or in);

$\Delta_{0.4u}$ = EEEP wall displacement at 40% of ultimate load (mm or in);

Δ_y = Wall's yield displacement at S_y (mm or in);

A = Area under test data or backbone curve up to 80% post-peak load (kN·mm or ft·lb);

k_e = Unit elastic stiffness ((kN/m)/mm or (lb/ft)/in).

The ductile behaviour of shear walls is an important characteristic when a building is subjected to seismic forces. This behaviour was measured by calculating the wall's ductility, μ, which was based on the displacement at 80% post-peak load or the maximum displacement reached during the test (Equation (4-4)).

$$\mu = \frac{\Delta_{ductility}}{\Delta_y} \quad (4\text{-}4)$$

where,

$$\Delta_{ductility} = \begin{cases} \Delta_{0.8u} & if\ S_{0.8u}\ was\ reached\ during\ the\ test \\ \Delta_{last} & if\ S_{0.8u}\ was\ not\ reached\ during\ the\ test \end{cases}$$

$\Delta_{0.8u}$ = Wall displacement at 80% post-peak load not considering EEEP case (mm or in);

Δ_y = Wall's yield displacement at S_y (mm or in);

Δ_{last} = Maximum wall displacement reached during testing (mm or in).

The EEEP curves for the monotonic tests were determined using the measured force-deformation data curve. The data of the cyclic tests (symmetric and asymmetric) were recorded as hysteric loops; in order to simplify the analysis a backbone curve was first created before completing the EEEP analysis. The cyclic backbone curve encompasses the hysteretic curves; it was created by connecting the points at which the maximum load was reached at each primary cycle. Using a MATLAB code, the backbone curves were created separately in the positive and negative direction for symmetric cyclic tests as the walls behaved slightly different in each direction; or just in the positive direction for asymmetric cyclic tests. Once the backbone curves were created, they were treated as a monotonic curve to compute the EEEP values using a second MATLAB code. Examples of the EEEP results of a monotonic, a symmetric cyclic, and an asymmetric cyclic test are graphically shown in Figures 4.3, 4.4, and 4.5, respectively. The EEEP results for all specimens are presented in Tables 4.1, 4.2, and 4.3. All of the metric and imperial EEEP results are presented in Appendix G, as well as the time-history plots for lateral displacement, wall resistance, and cumulative energy dissipated.

The cyclic protocols of specimens W18-CR and W23-CR3 were not completed due to technical problems with the actuator and out-of-plane twisting of the wall at large displacements. A full in-depth explanation of these tests is given by Brière *(2017)*.

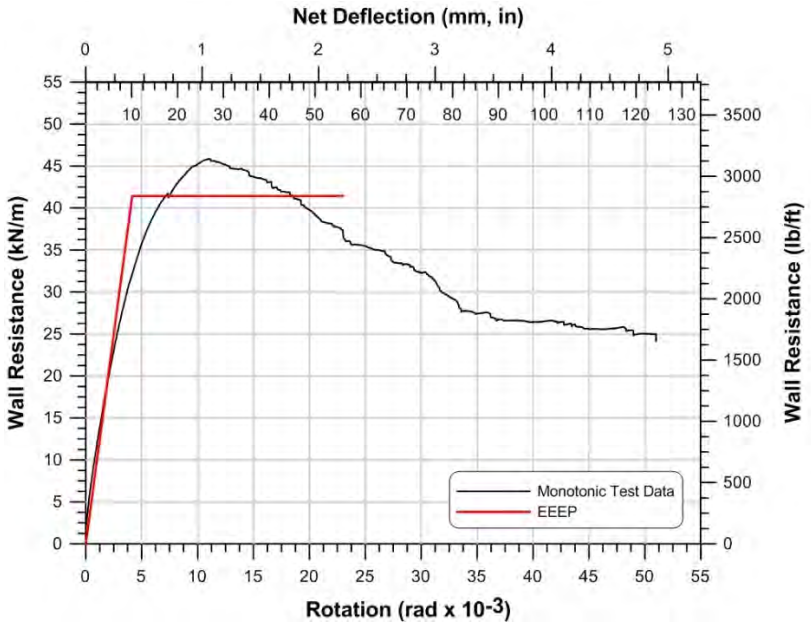

Figure 4.3: EEEP curve of monotonic test W21-M.

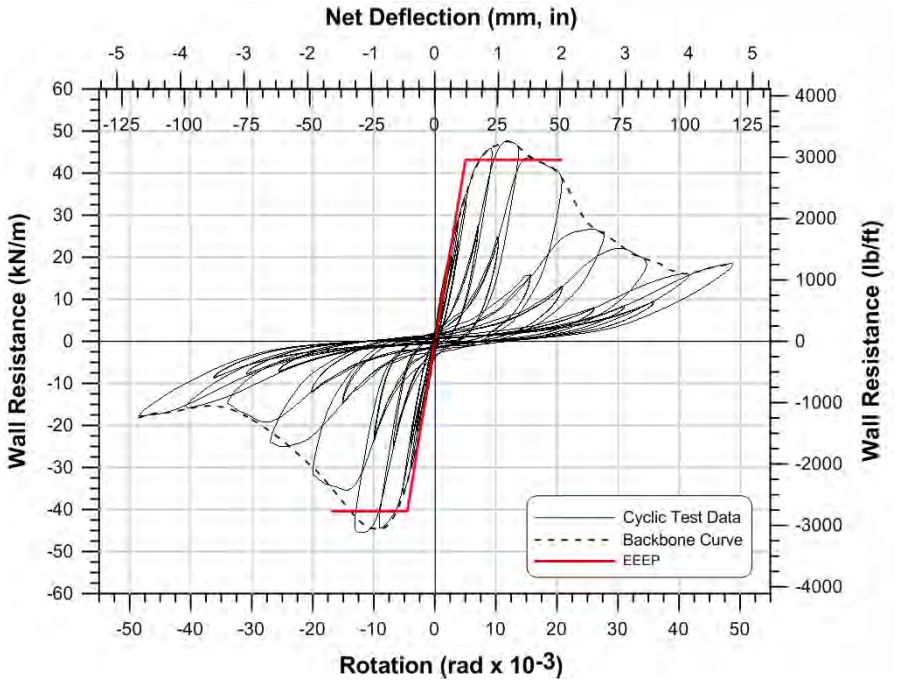

Figure 4.4: EEEP curve of reverse symmetric cyclic test W21-C.

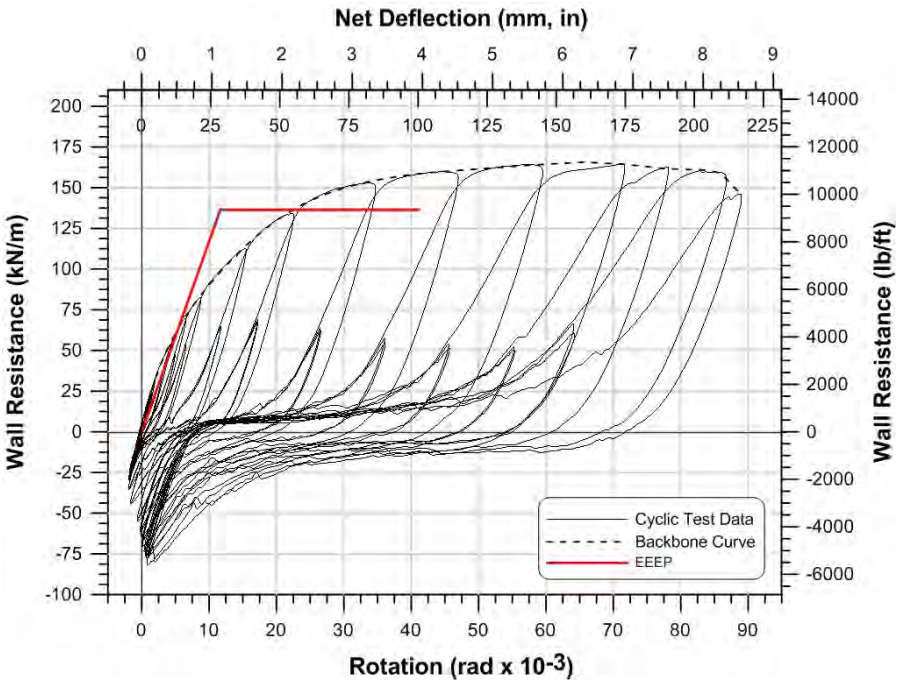

Figure 4.5: EEEP curve of asymmetric cyclic test W15B-CR3.

Table 4.1 Monotonic Shear Wall EEEP Design Values – Metric

Test	S_y (kN/m)	Δ_y (mm)	$\Delta_{0.4u}$ (mm)	θ_y (radx10^{-3})	$\theta_{0.4u}$ (radx10^{-3})	k_e ((kN/m)/mm)	μ	E_{EEEP} [2] (J)
Double-Sheathed Configuration								
W19-M	35.5	10.5	4.65	4.29	1.91	3.39	5.46	2242
W20-M	25.2	7.36	3.18	3.02	1.31	3.42	9.07	1937
W21-M	41.4	10.1	4.47	4.15	1.83	4.10	5.55	2581
W22-M	26.8	8.15	3.45	3.34	1.41	3.29	9.13	2301
W28-M[1]	54.2	12.0	5.41	4.93	2.22	4.52	5.15	3692
W29-M[1]	34.8	7.97	3.51	3.27	1.44	4.37	10.7	3440
W30-M[1]	58.8	16.1	7.16	6.61	2.94	3.65	4.26	4349
W31-M[1]	36.3	7.43	3.21	3.05	1.32	4.88	10.3	3207
Centre-Sheathed Configuration								
W15-MR3	128	31.0	14.3	12.7	5.85	4.12	3.87	13158
W16-MR	112	27.7	12.3	11.4	5.06	4.05	4.34	11774
W16-MR2	111	32.3	15.0	13.3	6.13	3.44	3.88	11377
W17-M	66.6	23.9	10.9	9.80	4.45	2.79	5.16	7154
W18-M[1]	78.3	24.3	10.8	9.96	4.43	3.23	5.06	8397
W18-MR[1]	81.5	23.8	10.8	9.75	4.44	3.43	5.15	8754

[1] Test results computed by Brière *(2017)*.
[2] Total energy dissipated under the monotonic EEEP curve.
Note: 1 in = 25.4 mm, 1 ft = 0.305 m, 1 lb = 4.45 kN

Table 4.2: Positive Cyclic Shear Wall EEEP Design Values – Metric

Test	S_y^+ (kN/m)	Δ_y^+ (mm)	$\Delta_{0.4u}^+$ (mm)	θ_y^+ (radx10^{-3})	$\theta_{0.4u}^+$ (radx10^{-3})	k_e^+ ((kN/m)/mm)	μ^+	E_{EEEP}^{+3} (J)
Double-Sheathed Configuration								
W19-C	42.1	12.4	6.36	5.07	2.61	3.40	4.20	2352
W20-C	26.5	7.41	3.51	3.04	1.44	3.58	6.82	1515
W21-C	43.2	12.3	6.04	5.03	2.48	3.52	4.12	2339
W22-C	26.9	7.18	3.17	2.95	1.30	3.75	6.05	1307
W28-C[2]	53.5	11.9	5.48	4.90	2.25	4.48	4.23	2909
W29-C[2]	36.5	7.79	3.48	3.19	1.43	4.69	5.19	1627
W30-C[2]	63.9	15.4	6.84	6.32	2.81	4.15	3.88	4063
W31-C[2]	40.3	8.52	3.86	3.50	1.58	4.73	5.68	2173
Centre-Sheathed Configuration								
W15-CR3	137	32.4	15.0	13.3	6.15	4.22	3.52	13970
W15B-CR3[1]	136	28.4	13.3	11.7	5.46	4.80	7.62	14347
W17-C	74.0	28.2	12.4	11.6	5.09	2.62	3.61	7812
W18-CR[2]	86.0	29.6	13.0	12.1	5.34	2.91	4.02	8943
W23-CR3[2]	139	32.3	15.1	13.3	6.21	4.29	3.88	14203
W23B-CR3[1,2]	138	30.4	14.0	12.5	5.74	4.54	5.00	14281
W24-CR3[2]	118	29.5	13.5	12.1	5.54	4.01	3.89	12295
W25-CR3[1]	103	26.8	12.7	11.0	5.20	3.84	5.12	10866
W26-CR3[1,2]	126	27.9	12.9	11.4	5.28	4.52	2.99	10693

[1] Asymmetric cyclic test, only positive parameters obtained.
[2] Test results computed by Brière *(2017)*.
[3] Total energy dissipated under the positive EEEP curve.
Note: 1 in = 25.4 mm, 1 ft = 0.305 m, 1 lb = 4.45 kN

Table 4.3: Negative Cyclic Shear Wall EEEP Design Values – Metric

Test	S_y^- (kN/m)	Δ_y^- (mm)	$\Delta_{0.4u}^-$ (mm)	θ_y^- (radx10^{-3})	$\theta_{0.4u}^-$ (radx10^{-3})	k_e^- ((kN/m)/mm)	μ^-	E_{EEEP}^{-3} (J)
Double-Sheathed Configuration								
W19-C	-39.1	-12.0	-6.43	-4.92	-2.64	3.26	3.79	1882
W20-C	-26.5	-7.43	-3.69	-3.05	-1.52	3.56	4.84	1043
W21-C	-40.4	-11.0	-4.80	-4.52	-1.97	3.67	3.72	1748
W22-C	-26.9	-8.17	-3.41	-3.35	-1.40	3.29	4.80	1154
W28-C[2]	-54.5	-13.2	-6.03	-5.42	-2.47	4.12	2.88	2091
W29-C[2]	-35.7	-11.0	-4.90	-4.50	-2.01	3.25	3.39	1381
W30-C[2]	-60.4	-14.2	-6.45	-5.83	-2.65	4.25	3.09	2717
W31-C[2]	-38.6	-8.40	-3.86	-3.44	-1.58	4.60	5.26	1885
Centre-Sheathed Configuration								
W15-CR3	-133	-31.9	-14.5	-13.1	-5.95	4.17	3.23	13629
W15B-CR3[1]	-	-	-	-	-	-	-	-
W17-C	-71.3	-23.6	-10.9	-9.68	-4.47	3.02	4.31	7638
W18-CR[2]	-79.0	-28.0	-12.7	-11.5	-5.22	2.83	3.58	8300
W23-CR3[2]	-106	-22.4	-11.1	-9.20	-4.56	4.74	2.11	5074
W23B-CR3[1,2]	-	-	-	-	-	-	-	-
W24-CR3[2]	-113	-26.5	-11.9	-10.9	-4.88	4.28	4.12	12006
W25-CR3[1]	-	-	-	-	-	-	-	-
W26-CR3[1,2]	-	-	-	-	-	-	-	-

[1] Asymmetric cyclic test, only positive parameters obtained.
[2] Test results computed by Brière *(2017)*.
[3] Total energy dissipated under the negative EEEP curve.
Note: 1 in = 25.4 mm, 1 ft = 0.305 m, 1 lb = 4.45 kN

4.3 Preliminary Modified Effective Strip Method for the Centre-Sheathed Configuration

It had been observed (Section 2.3.3) that the shear strength prediction method initially used, the Effective Strip Method from the AISI S400 Standard *(2015)*, underestimated the in-plane forces reached during the tests. The Effective Strip Method by Yanagi and Yu *(2014)* was based on a different shear wall configuration (single-sided sheathing and 2-ply connections) than the centre-sheathed configuration. To improve the accuracy of the prediction and to better represent the design of the centre-sheathed walls, this prediction method had to be modified based on the observations made during the tests. The initial version of the Modified Effective Strip Method (MESM), represented by Equation (4-5) and as illustrated in Figure 4.6, addressed two main differences between the centre-sheathed configuration and the traditional shear wall configuration:

1) Bearing strength of the sheathing connections;
2) Number of fasteners contributing to the shear resistance of the wall.

$$S_{n\,(MESM)} = \left[\left({}^{n}/_{2}\right) P_{nb}\, cos\alpha\right]/_{W} \tag{4-5}$$

where,

$S_{n\,(MESM)}$ = Modified Effective Strip Method nominal shear resistance (kN/m or lb/ft);

n = Total number of sheathing-to-frame fasteners;

P_{nb} = Nominal bearing strength of a single connection using the bolt bearing strength for an inside sheet of double shear connection (3-ply) from AISI S100 *(2016)* / CSA S136 *(2016)* (kN or lb);

α = Tension force projection angle;

W = Width of the wall (m or ft).

Figure 4.6: Illustration of the assumed force distribution for the Modified Effective Strip Method.

In the MESM there is no calculated effective sheathing width (W_e); instead, all of the sheathing screws around the perimeter of the wall are considered to participate in the shear resistance of the wall through bearing deformations. This conclusion was made once the walls were tested and taken apart. It was seen that there was bearing damage in the sheathing, to different extent, at every connection (Figure 4.6). Half of the screws (*n/2*) resist the shear force applied at the top of the wall through bearing and the other half of the screws transfer the tension field force as a reaction at the bottom of the wall.

To calculate the bearing resistance of each connection, P_{nb}, the bearing strength equation for bolts in a double shear connection (Equation (2-12)) was used since currently no such equation is available for screw connections in the AISI S100 and CSA S136 standards. Using this equation allows for an increase in connection strength, resulting in a better prediction of a wall's overall

shear resistance. In addition, P_{nb} was calculated using the material properties based on the results of the coupon tests summarized in Table 3.4 and Appendix F.

4.4 Limit States Design (LSD) and Load and Resistance Factor Design (LRFD)

The development of a Limit State Design (LSD) procedure and a Load and Resistance Factor Design (LRFD) procedure are required by the AISI S100 *(2016)* / CSA S136 *(2016)* standards as evaluation procedures of structural performances established by tests. Note, the CSA S136 and AISI S100 standards are the same document. A LSD procedure, used in Canada, and a LRFD procedure, used in the US and Mexico, were developed using the data obtained from the shear wall specimens tested in this program. These procedures have been adopted for previously researched CFS steel framed and sheathed shear walls in the development of the design methods found in the AISI S400 Standard *(2015)*; e.g. specifically for Canada, specimens tested by Ong-Tone *(2009)*, Balh *(2010)* and DaBreo *(2012)*. Values such as the resistance factor, factor of safety, overstrength factor, and seismic force modification factors were computed. The LSD and LRFD design parameters were obtained separately for each shear wall configuration; double-sheathed and centre-sheathed. For the double-sheathed configuration, the EEEP method was used for LSD (Canada) and the test ultimate shear load, S_u, was used as the design parameter for LRFD (USA and Mexico). In the case of the centre-sheathed configuration, the MESM was used as the nominal shear strength prediction method for both LSD and LRFD. Lastly, for the centre-sheathed configuration, only data from specimens whose chord studs did not fail (all specimens with reinforcement type R3) were used in the development of the design procedures.

4.4.1 Calibration of Resistance Factor

Limit States Design and Load and Resistance Factor Design, as described by the NBCC (NRC *(2015)*), CSA S136 Standard *(2016)*, and AISI S100 Standard *(2016)*, are represented by Equation (4-6). As a general definition of these design procedures, the factored resistance of structural elements must be larger than the combination of the loads applied to them. The applied loads are a result of the governing load combinations provided by the NBCC (NRC *(2015)*) or the ASCE/SEI-7 *(2016)*.

$$\phi R_n \geq \sum \gamma_i Q_i \tag{4-6}$$

where,

ϕ = Resistance factor for structural element;

R = Nominal resistance;

$\sum \gamma_i Q_i$ = Required strength based on the most critical load combination.

γ_i = load factors, Q_i = load effects.

A method for calculating the resistance factor, ϕ, of cold-formed steel materials following the LSD and LRFD procedures is defined by the CSA S136 *(2016)* / AISI S100 *(2016*) standards; Equation (4-7).

$$\phi = C_\phi (M_m F_m P_m) e^{-\beta_o \sqrt{V_M^2 + V_F^2 + C_P V_P^2 + V_Q^2}} \quad (4\text{-}7)$$

where,

C_ϕ = Calibration factor, 1.42 (LSD), 1.52 (LRFD);

M_m = Mean value of material factor depending on type of component involved;

F_m = Mean value of fabrication factor depending on type of component involved;

P_m = Mean value of professional factor for tested component;

e = Natural log;

β_o = Target reliability factor, 3.0 (LSD) and 2.5 (LRFD) for structural members;

V_M = Coefficient of variation of material factor for type of component involved;

V_F = Coefficient of variation of fabrication factor for type of component involved;

C_P = Sample size correction factor, *(1+1/n) m/ (m-2)* for $n \geq 4$;

where,

n = Number of tests;

m = Degrees of freedom, n-1.

V_P = Coefficient of variation of test results;

V_Q = Coefficient of variation of load effect, 0.21.

The mean values for the material and fabrication factors, M_m and F_m, as well as their corresponding coefficients of variation, V_m and V_f, are listed in Table K2.1.1-1 of the AISI S100 *(2016)* / CSA S136 *(2016)* standards. These values come from statistical analysis of the components used in the tests and their failure modes. For this analysis, two components were chosen based on observations during the tests as described in Chapter 3; 1) the chord studs, which were under axial compression and bending, and 2) the screw connections, which failed due to bearing deformations. Table 4.4 shows the statistical data for the chosen components.

Table 4.4: Statistical Data for the Determination of Resistance Factor
From AISI S100 *(2016)* / CSA S136 *(2016)*

Type of Component	M_m	V_M	F_m	V_F
1 – Wall Stud: Under Combined Forces	1.05	0.10	1.00	0.05
2 – Connections: Screw Connections	1.10	0.10	1.00	0.10

4.4.1.1 Computation of P_m and V_p

The mean value of professional factor, P_m, is the average of the ratio between the tested shear strength over the predicted shear strength of each specimen (Equation (4-8)). V_p is the coefficient of variation of P_m (Equation (4-9)).

$$P_m = \frac{\Sigma\left(\frac{R_t}{R_n}\right)}{n} \tag{4-8}$$

$$V_P = {}^{\sigma}/_{P_m} \geq 0.065 \tag{4-9}$$

$$\sigma = \sqrt{\left[\left(\frac{1}{n-1}\right)\Sigma\left(\frac{R_t}{R_n} - P_m\right)^2\right]} \tag{4-10}$$

where,

R_t = Tested wall resistance (kN/m or lb/ft);

R_n = Predicted or nominal wall resistance (kN/m or lb/ft);

n = Total number of specimens tested (sample size);

σ = Standard deviation of test/predicted ratios.

Depending on the shear wall configuration; double-sheathed or centre-sheathed, the values chosen as R_t and R_n were different because different design methods are associated with each configuration. The double-sheathed configuration follows the tabulated design approach currently found in the AISI S400 Standard *(2015)*, where the shear strengths were computed by using the EEEP method (in Canada) to analyse the test data, or using the ultimate test shear strength (in the USA and Mexico). The tabulated approach limits the type of shear walls available for design, with strengths listed for walls with specific wall parameters and aspect ratios. The centre-sheathed configuration is designed using an *equation-based* design, i.e. the prediction method described in Section 4.3. This design approach gives the freedom of designing shear walls with different parameter combinations to suit the structure being built.

4.4.1.1.1 Double-Sheathed Configuration

For the double-sheathed configuration, all specimens reached an ultimate shear strength and were able to attain 80% of the ultimate strength post-peak before the end of the tests. For these reasons, when following the LSD procedure, R_t for the double-sheathed configuration was taken as the average ultimate shear resistance, $S_{u,avg}$, reached during the tests, and R_n was taken as the specimens' average yield resistance, $S_{y,avg\ (EEEP)}$, computed from the EEEP data analysis (Tables 4.1 to 4.3). When following the LRFD procedure, R_t and R_n were both taken as $S_{u,avg}$, based directly on the values reached during testing.

Average values were used because the negative cycle resulted in slightly lower resistances as strength degradation occurred in the previous positive cycle. The average values were calculated using Equation (4-11) as an average of the monotonic and symmetric reverse cyclic test results.

$$S_{avg} = \frac{\left[S_{mono} + \left(\frac{S^{+}_{cyclic} + S^{-}_{cyclic}}{2}\right)\right]}{2} \tag{4-11}$$

Table 4.5: Test-to-Predicted Ratios for Double-Sheathed Shear Wall Configuration

Test	Test Shear Strength $S_{u,avg}$ (kN/m)	Predicted Shear Strength for LSD $S_{y,avg\ (EEEP)}$ (kN/m)	Test/Predicted Ratio LSD $S_{u,avg}/S_{y,avg\ (EEEP)}$	Test/Predicted Ratio LRFD $S_{u,avg}/S_{u,avg}$
W19	42.2	38.1	1.11	1.00
W20	28.7	25.9	1.11	1.00
W21	46.1	41.6	1.11	1.00
W22	29.1	26.9	1.08	1.00
W28	61.4	54.1	1.13	1.00
W29	39.3	35.5	1.11	1.00
W30	67.6	60.5	1.12	1.00
W31	42.2	37.9	1.11	1.00
		Average	1.11	1.00
		STD. DEV.	0.014	0.00
		C.V.	1.26%	0.00

The test-to-predicted strength ratios for the double-sheathed configuration are shown in Table 4.5. The average (P_m) obtained for LSD was 1.11 with a coefficient of variation, C.V. (V_p), of 1.26% and a standard deviation of 0.014. These low values show that the tested values are consistent with the predicted EEEP values. The average (P_m) obtained for LRFD was 1.0 since R_t and R_n were equal, and therefore the standard deviation and C.V. (V_p) was zero. As defined by Section K2.1.1 (c) of the CSA S136 *(2016)* / AISI S100 *(2016)* standards, V_p cannot be less than 6.5%; therefore, V_p was taken as 0.065 for LSD and LRFD. The professional factor, P_m, was taken as 1.0 for LRFD, and the same value was considered for LSD since a value larger than 1.0 was obtained from the ratio of the ultimate-to-yield strength. Additionally, a C_p of 1.23 was computed for a double-sheathed sample size n = 16 (8 monotonic and 8 cyclic).

4.4.1.1.2 Centre-Sheathed Configuration

For the centre-sheathed configuration, the same design parameters were used in the establishment of the LSD and LRFD procedures. This new shear wall configuration behaved differently from previously tested CFS shear walls and a new *equation-based* approach was used to predict the nominal shear strength of the centre-sheathed walls.

To compute P_m and V_p, it was concluded that S_u was not an adequate value to use as the test shear strength, R_t. During the centre-sheathed tests, S_u was reached at very large lateral

displacements (7% storey drift in some cases) which is not realistic for shear wall design for mid-rise buildings. Instead, the test shear strength was chosen as the force corresponding to the NBCC's (NRC *(2015)*) 2.5% seismic inelastic storey drift limit (61 mm or 2.4" for a 2440 mm tall wall), $S_{2.5\%,avg}$.

The predicted shear strength, R_n, was calculated using the Modified Effective Strip Method, $S_{n\,(MESM)}$, discussed in Section 4.3. For comparison, the test-to-predicted ratios using $S_{u,avg}$ and $S_{2.5\%,avg}$ as test resistances, and $S_{n\,(MESM)}$ and $S_{y,avg\,(EEEP)}$ as the predicted resistances are shown in Table 4.6.

The average value used for specimen W15 was calculated using Equation (4-11), since it was tested monotonically and cyclically with a symmetric protocol. The average value used for the specimens only tested cyclically with a symmetric cyclic protocol was taken as the average of the positive and negative values. Finally, the specimens tested cyclically with an asymmetric protocol produced a positive value only, and therefore it was taken as the average.

When looking at the ratio of the 2.5% lateral drift resistance to the yield resistance from the EEEP analysis, it shows that using $S_{2.5\%}$ as the test value, R_t, is acceptable. This ratio resulted in an average of 1.04 with a standard deviation of 0.043 and a coefficient of variation of 4.10%. Although the ratios using S_u are not used for the reasons outlined earlier in this section, an average of 1.07 for the $S_u/S_{n\,(MESM)}$ ratio with a standard deviation of 0.092 supports the assumptions made in the development of the Modified Effective Strip Method as a prediction method.

The $S_{2.5\%}/S_{n\,(MESM)}$ ratio was chosen for the computation of the professional factor, it produced an average (P_m) of 0.98, however the high standard deviation, 0.107 and coefficient of variation (V_p), 10.9% show that the prediction method needs refinement considering all of the parameters possibly affecting the behaviour of the centre-sheathed configuration. The C_p was found to be 1.58, with a small sample size (n = 8, 1 monotonic and 7 cyclic) since only the specimens with chord stud reinforcement R3 were considered.

Table 4.6: Test-to-Predicted Ratios for Centre-Sheathed Configuration

Test	Test Shear Strength (kN/m)		Predicted Shear Strength (kN/m)		Test/Predicted Ratio			
	$S_{u,avg}$	$S_{2.5\%,avg}$	$S_{y,avg\ (EEEP)}$	$S_{n\ (MESM)}$	S_u/S_y	$S_u/S_{n\ (MESM)}$	$S_{2.5\%}/S_y$	$S_{2.5\%}/S_{n\ (MESM)}$
W15	154	135	131	162	1.18	0.95	1.03	0.84
W15B-CR3[2]	166	141	136	162	1.22	1.03	1.04	0.87
W23-CR3[1,3]	147	140	139	150	1.06	0.98	1.01	0.94
W23B-CR3[2]	159	141	138	150	1.15	1.06	1.02	0.94
W24-CR3[1]	131	122	116	116	1.13	1.13	1.05	1.05
W25-CR3[2]	117	106	103	96	1.14	1.22	1.03	1.11
W26-CR3[2]	145	143	126	132	1.15	1.10	1.14	1.09
[1] Average from symmetric reverse cyclic tests				Average	1.15	1.07	1.04	0.98
[2] Positive asymmetric cyclic test values				STD.DEV	0.047	0.092	0.043	0.107
[3] Negative cycles incomplete, only positive values				C.V.	4.12%	8.65%	4.10%	10.9%

4.4.1.2 Summary of LSD and LRFD Resistance Factors

Table 4.7 summarizes all of the factors used in the calibration of the resistance factors for both shear wall configurations and design procedures (LSD and LRFD), as well as for the two types of wall components.

Table 4.7: Variables to Compute LSD and LRFD Resistance Factors

Design Procedure	C_ϕ	M_m	F_m	P_m	β_o	V_M	V_F	V_Q	n	C_p	V_p
Double-Sheathed Configuration											
LSD: Wall Studs Under Combined Forces	1.42	1.05	1.0	1.0	3.0	0.1	0.05	0.21	16	1.23	0.065
LSD: Screw Connections	1.42	1.1	1.0	1.0	3.0	0.1	0.1	0.21	16	1.23	0.065
LRFD: Wall Studs Under Combined Forces	1.52	1.05	1.0	1.0	2.5	0.1	0.05	0.21	16	1.23	0.065
LRFD: Screw Connections	1.52	1.1	1.0	1.0	2.5	0.1	0.1	0.21	16	1.23	0.065
Centre-Sheathed Configuration											
LSD: Wall Studs Under Combined Forces	1.42	1.05	1.0	0.98	3.0	0.1	0.05	0.21	8	1.58	0.109
LSD: Screw Connections	1.42	1.1	1.0	0.98	3.0	0.1	0.1	0.21	8	1.58	0.109
LRFD: Wall Studs Under Combined Forces	1.52	1.05	1.0	0.98	2.5	0.1	0.05	0.21	8	1.58	0.109
LRFD: Screw Connections	1.52	1.1	1.0	0.98	2.5	0.1	0.1	0.21	8	1.58	0.109

Following Equation (4-7), the resistance factors, ϕ, for each shear wall configuration and type of component were obtained (Table 4.8).

Table 4.8: Resistance Factors for Double-Sheathed and Centre-Sheathed Shear Walls

Design Procedure	Type of Component	ϕ	ϕ_{avg}
Double-Sheathed Configuration			
LSD	Wall Studs Under Combined Forces	0.71	0.71
	Screw Connections	0.71	
LRFD	Wall Studs Under Combined Forces	0.86	0.86
	Screw Connections	0.87	
Centre-Sheathed Configuration			
LSD	Wall Studs Under Combined Forces	0.64	0.64
	Screw Connections	0.64	
LRFD	Wall Studs Under Combined Forces	0.78	0.79
	Screw Connections	0.79	

The average resistance factors corresponding to the double-sheathed configuration were 0.71 for LSD and 0.86 for LRFD. The LSD and LRFD values computed for the centre-sheathed configuration were 0.64 and 0.79 respectively. This centre-sheathed LSD resistance factor was lower than the LSD value of 0.70 for CFS sheathed and framed shear walls previously recommended by Balh *et al. (2014)* for limit states design. A reason for this difference was the C_ϕ used, in the latest version of the CSA S136 *(2016)*/AISI S100 *(2016)* standards, new values of C_ϕ are provided, 1.42 for LSD and 1.52 for LRFD, whereas previously, a larger value of C_ϕ was used, 1.842, calculated based on documented wind load statistics by Branston *(2004).*

Another reason for the lower resistance factor of the centre-sheathed configuration was the small sample size; with plans for more specimens to be tested in the future, it is expected that the mean of the professional factor, P_m, will increase and its coefficient of variation, V_p, will be smaller, resulting in a higher resistance factor. Finally, refinement and optimization of the new

shear resistance prediction method, the Modified Effective Strip Method, is needed as it is still in its initial development stages. With a more accurate prediction, P_m will increase and the coefficient of variation will be reduced, resulting in a higher resistance factor.

Based on the results of both shear wall configurations in Table 4.8, the recommended range (lower and upper bounds) of the resistance factors for LSD and LRFD calculated using the factors provided by CSA S136 *(2016)* / AISI S100 *(2016)* are listed below.

LSD → $\phi_{\text{lower}} = 0.7$; $\phi_{\text{upper}} = 0.75$;
LRFD → $\phi_{\text{lower}} = 0.8$; $\phi_{\text{upper}} = 0.9$.

4.4.2 Factor of Safety

The factor of safety, *F.S.*, is the ratio of the shear wall's ultimate shear resistance, S_u, over the factored shear resistance, S_r; it is calculated using Equation (4.12) for monotonic and cyclic tests separately. The factor of safety is graphically represented in Figures 4.7 and 4.8. The factored shear resistance is the product of the nominal shear resistance, S_n, and the lower bound of the resistance factor given in Section 4.4.1.2; $\phi_{(LSD)} = 0.7$ and $\phi_{(LRFD)} = 0.8$. The nominal shear resistance was taken as $S_{y\,(EEEP)}$ for LSD and S_u for LRDF for the double-sheathed walls and taken as $S_{n\,(MESM)}$ for centre-sheathed walls.

For the cyclic tests, the difference in the ultimate shear force in the positive and negative directions were considered to be negligible since the negative value was only slightly smaller due to the strength degradation from the previous positive cycle. Therefore, an average of the positive and negative values was taken to calculate the factor of safety.

$$F.S. = {S_u}/{S_r} \tag{4.12}$$

where,

$F.S.$ = Factor of safety;
S_u = Ultimate shear resistance observed during the test (kN/m or lb/ft);
S_r = Factored shear resistance of the wall (kN/m or lb/ft);

$S_r = \phi S_n$;

$\phi_{(LSD)} = 0.7$ and $\phi_{(LRFD)} = 0.8$;

$S_{n,\ double\text{-}sheathed\ (LSD)} = S_{y\ (EEEP)}$;

$S_{n,\ double\text{-}sheathed\ (LRFD)} = S_u$;

$S_{n,\ centre\text{-}sheathed} = S_{n\ (MESM)}$.

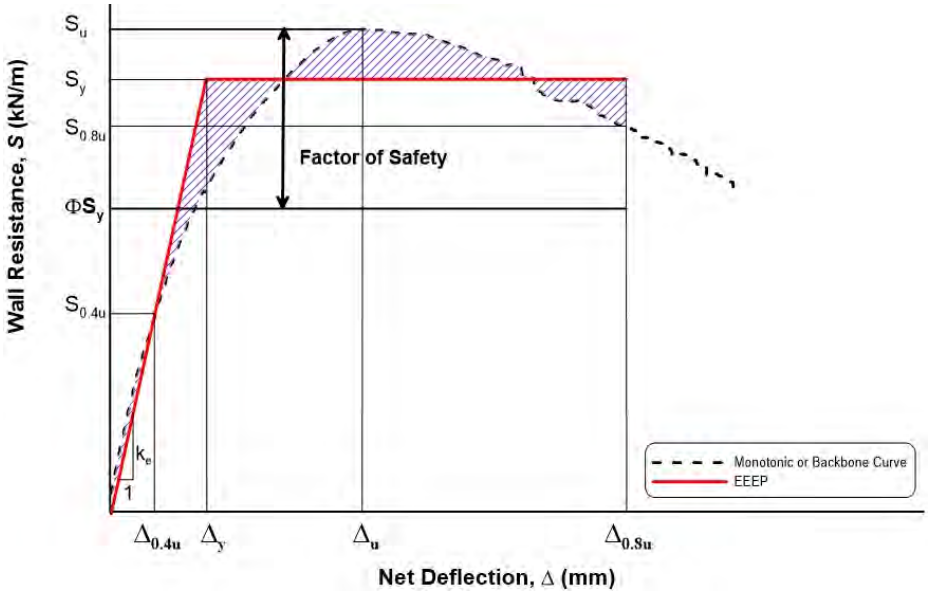

A

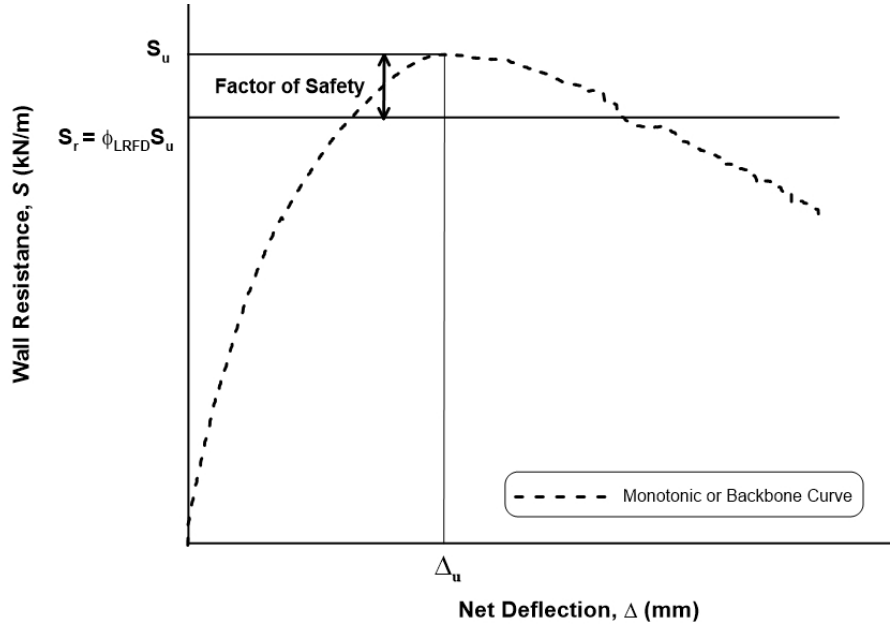

B

Figure 4.7 Factor of safety for LSD (A) and LRFD (B) procedures as the ratio of ultimate over factored shear resistance of double-sheathed shear wall configuration.

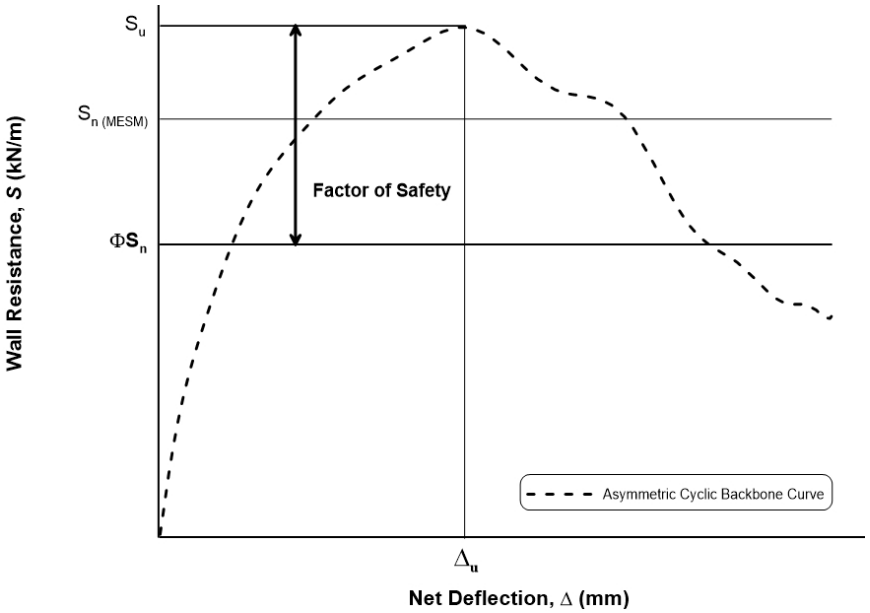

Figure 4.8: Factor of safety as the ratio of ultimate over factored shear resistance of centre-sheathed shear wall configuration.

Tables 4.9 to 4.12 summarize the mean factor of safety for the double-sheathed and centre-sheathed configurations. A mean factor of safety for the monotonic double-sheathed configuration was found to be 1.57 for LSD and 1.25 for LRFD. The double-sheathed configuration cyclic tests resulted in a higher factor of safety for LSD; 1.60, while for LRFD it remained the same; 1.25. These values are lower when compared to the factor of safety of 2.0 (combined monotonic and cyclic) obtained by Balh *(2010)* using the same analysis method (EEEP) for LSD.

The centre-sheathed specimens considered for determining the factors of safety were the ones that showed no frame failure during testing, as was the case for determining the resistance factors in Section 4.4.1. Only one centre-sheathed specimen was tested monotonically, W15-MR3, and therefore no significant factor of safety can be discussed, however the factor of safety for W15-MR3 is shown in Table 4.11 for completeness. The average factors of safety for the centre-sheathed configuration cyclic tests were 1.54 for LSD and 1.35 for LRFD with a coefficient of variation of 8.51%, which is higher than the double-sheathed configuration cyclic tests. The use of a new prediction method to determine the nominal resistance of the centre-sheathed specimens introduced some variability since it needs to be further developed in future research.

Table 4.9: Factor of Safety for Monotonic Specimens – Double Sheathed Shear Walls

Test	S_u [1] (kN/m)	$S_{y\ (EEEP)}$ [2] (kN/m)	$S_{r,\ LSD}$ (ϕ = 0.7) (kN/m)	$S_{r,\ LRFD}$ (ϕ = 0.8) (kN/m)	F.S. (LSD) $S_u/S_{r,\ LSD}$	F.S. (LRFD) $S_u/S_{r,\ LRFD}$
W19-M	39.6	35.5	24.9	31.7	1.59	1.25
W20-M	27.3	25.2	17.6	21.8	1.55	1.25
W21-M	45.9	41.4	29.0	36.7	1.58	1.25
W22-M	28.4	26.8	18.8	22.7	1.51	1.25
W28-M[3]	61.0	54.2	37.9	48.8	1.61	1.25
W29-M[3]	38.2	34.8	24.4	30.6	1.57	1.25
W30-M[3]	65.4	58.8	41.2	52.3	1.59	1.25
W31-M[3]	39.3	36.3	25.4	31.4	1.55	1.25
				Average	1.57	1.25
				STD. DEV.	0.031	0.00
				C.V.	1.99%	0.00%

[1] Monotonic ultimate resistance from Table 3.1
[2] Monotonic nominal resistance from Table 4.1
[3] Tested by Brière *(2017)*

Table 4.10: Factor of Safety for Cyclic Specimens – Double-Sheathed Shear Walls

Test	$S_{u,avg}$ [1] (kN/m)	$S_{y,avg\ (EEEP)}$ [2] (kN/m)	$S_{r,\ LSD}$ (ϕ = 0.7) (kN/m)	$S_{r,\ LRFD}$ (ϕ = 0.8) (kN/m)	F.S. (LSD) $S_{u,avg}/S_{r,\ LSD}$	F.S. (LRFD) $S_{u,avg}/S_{r,\ LRFD}$
W19-C	44.7	40.6	28.4	35.8	1.57	1.25
W20-C	30.1	26.5	18.6	24.1	1.62	1.25
W21-C	46.2	41.8	29.3	37.0	1.58	1.25
W22-C	29.8	26.9	18.8	23.8	1.58	1.25
W28-M[3]	61.8	54.0	37.8	49.4	1.63	1.25
W29-M[3]	40.4	36.1	25.3	32.3	1.60	1.25
W30-M[3]	69.8	62.2	43.5	55.8	1.60	1.25
W31-M[3]	45.1	39.5	27.6	36.0	1.63	1.25
				Average	1.60	1.25
				STD.DEV.	0.024	0.00
				C.V.	1.50%	0.00%

[1] Average cyclic resistance from Tables 3.2 and 3.3
[2] Average cyclic resistance from Tables 4.2 and 4.3
[3] Tested by Brière *(2017)*

Table 4.11: Factor of Safety for Monotonic Specimen – Centre-Sheathed Shear Walls

Test	S_u [1] (kN/m)	$S_{n\ (MESM)}$ [2] (kN/m)	$S_{r,\ LSD}$ (ϕ = 0.7) (kN/m)	$S_{r,\ LRFD}$ (ϕ = 0.8) (kN/m)	*F.S.* (LSD) $S_{u,avg}/S_{r,\ LSD}$	*F.S.* (LRFD) $S_{u,avg}/S_{r,\ LRFD}$
W15-MR3	150	162	113	129	1.32	1.16

[1] Monotonic ultimate resistance from Table 3.1
[2] MESM nominal resistance from Table 4.6

Table 4.12: Factor of Safety for Cyclic Specimens – Centre-Sheathed Shear Walls

Test	$S_{u,avg}$ (kN/m)	$S_{n\ (MESM)}$ [3] (kN/m)	$S_{r,\ LSD}$ (ϕ = 0.7) (kN/m)	$S_{r,\ LRFD}$ (ϕ = 0.8) (kN/m)	*F.S.* (LSD) $S_{u,avg}/S_{r,\ LSD}$	*F.S.* (LRFD) $S_{u,avg}/S_{r,\ LRFD}$
W15-CR3[1]	159	162	113	129	1.40	1.23
W15B-CR3[2]	166	162	113	129	1.47	1.28
W23-CR3[1]	147	150	105	120	1.41	1.23
W23B-CR3[2]	159	150	105	120	1.52	1.33
W24-CR3[1]	135	116	81.1	92.6	1.67	1.46
W25-CR3[2]	117	95.7	67.0	76.5	1.75	1.53
W26-CR3[2]	145	132	92.4	106	1.57	1.37
				Average	1.54	1.35
				STD. DEV.	0.131	0.115
				C.V.	8.51%	8.51%

[1] Average cyclic resistance from Tables 3.2 and 3.3
[2] Asymmetric cyclic test, positive resistance only
[3] MESM nominal resistance from Table 4.6

In design, the factor of safety is applied only when wind loads in the horizontal direction are taken into account and gravity loads are not considered. When seismic loads are considered, a capacity based design procedure is required by AISI S400 *(2015)*, which is presented in Section 4.4.3.

4.4.3 Capacity Based Design – Canada

The AISI S400 Standard *(2015)* requires that, in Canada, for the design of seismic force resisting systems (SFRS) such as shear walls, a capacity based design procedure is followed. In capacity based design, a ductile element within the SFRS is responsible for dissipating energy through inelastic deformations. While the energy dissipating element behaves inelastically, the other elements of the SFRS are designed to behave elastically and resist the probable (or expected) forces experienced by the system.

In CFS sheathed and framed shear walls, the energy dissipating element is the sheathing-to-frame screw connections, where the ductility and energy dissipation come from the bearing deformation of the sheathing at the connections. The other shear wall elements such as the holdowns, chord studs, horizontal framing members, field studs, tracks, fasteners, and anchors, behave elastically during a seismic event.

During a design level earthquake, it is expected that the shear wall will reach its ultimate shear capacity when it is pushed to displacements in the inelastic range. An overstrength factor is used to approximate the probable capacity of the shear wall, and it is used in the design of the structural elements of the shear wall to insure that their behaviour remains elastic.

Similar to determining the resistance factors in Section 4.4.1, two different approaches are followed to obtain the overstrength of the double and centre-sheathed configurations as each uses different methods to determine their nominal resistances; EEEP or Modified Effective Strip Method (MESM).

In the case of the double-sheathed configuration, the overstrength factor (Equation (4-13)) is the ratio of the ultimate resistance reached during the test to the nominal shear resistance taken as the yield resistance calculated using the EEEP analysis, $S_{y\,(EEEP)}$.

The overstrength factor of the centre-sheathed configuration is presented as a range between the ultimate overstrength and the design overstrength. The ultimate resistance of the centre-sheathed specimens was reached at large lateral displacements and therefore its ratio to the centre-sheathed configuration's nominal resistance, $S_{n\,(MESM)}$, provides the ultimate overstrength factor (Equation (4-14)). As discussed in Section 4.4.1.1.2, the shear resistance corresponding to 2.5% lateral drift displacement (61 mm or 2.4"), $S_{2.5\%}$, was chosen as a more realistic design value for mid-rise buildings and therefore its ratio to $S_{n\,(MESM)}$ provides the design overstrength factor (Equation (4-14)). The overstrength factors for both configurations are shown in Figures 4.9 and 4.10.

$$Overstrength_{\,(DOUBLE-SHEATHED)} = {S_u}/{S_{y(EEEP)}} \quad (4\text{-}13)$$

$$Overstrength_{\,(CENTRE-SHEATHED)} = \left[\left({S_{2.5\%}}/{S_{n(MESM)}}\right); \left({S_u}/{S_{n(MESM)}}\right)\right] \quad (4\text{-}14)$$

where,

S_u = Ultimate shear resistance observed during the test (kN/m or lb/ft);

$S_{y\,(EEEP)}$ = Nominal shear yield resistance (kN/m or lb/ft);

$S_{2.5\%}$ = Shear force reached at 2.5% lateral drift (61 mm) during the test (kN/m or lb/ft);

$S_{n\,(MESM)}$ = Modified Effective Strip Method nominal shear resistance (kN/m or lb/ft).

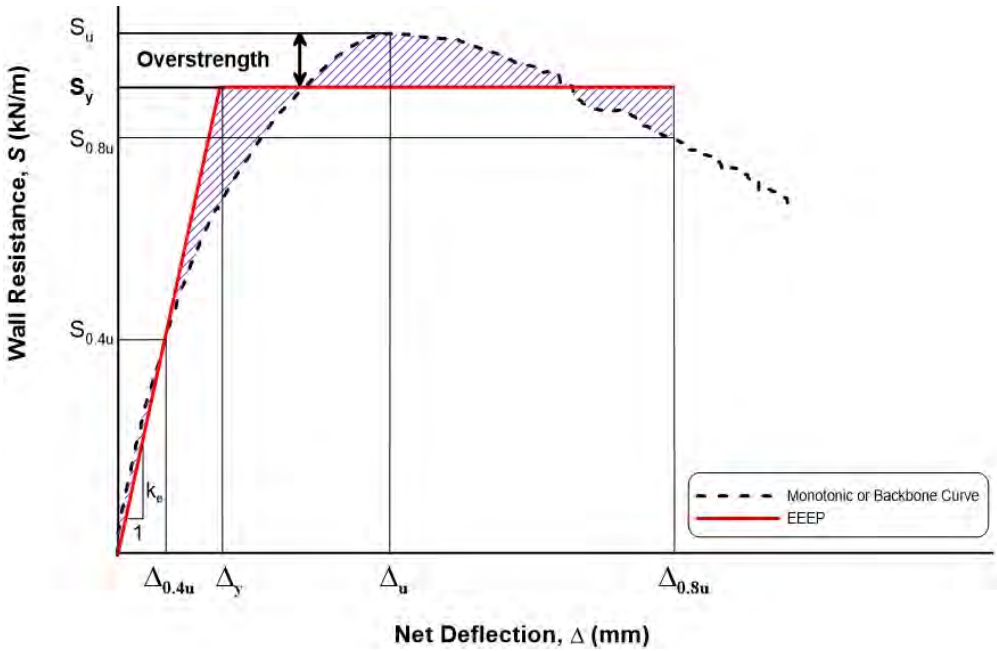

Figure 4.9: Overstrength as the ratio of ultimate over yield shear resistance of a double-sheathed shear wall configuration.

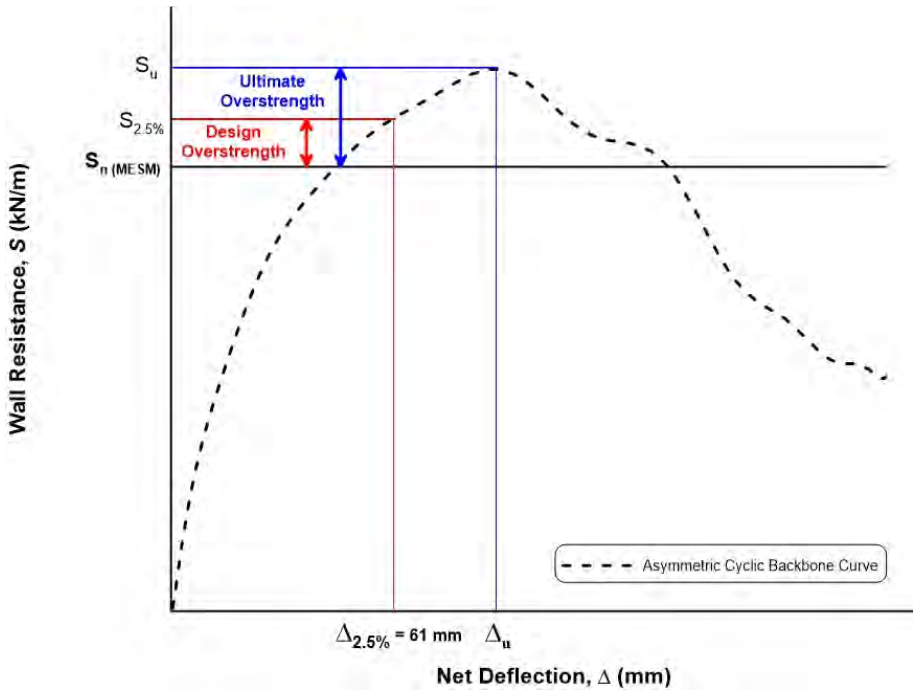

Figure 4.10: Ultimate and design overstrength factors of the centre-sheathed shear wall configuration.

The monotonic and cyclic overstrength factors for each shear wall configuration are presented in Tables 4.13 to 4.16. For the double-sheathed configuration monotonic and cyclic specimens, the average overstrength factors of 1.10 and 1.12 were obtained, respectively, with coefficients of variation of 1.98% and 1.50%. The ultimate overstrength factor for the centre-sheathed cyclic specimens was found to be 1.08 with a coefficient of variation of 8.51%; the design overstrength factor was found to be 0.975 with a coefficient of variation of 11.0%. The overstrength factors for both configurations are lower than the value of 1.4 recommended by Balh *et al. (2014)*. The double-sheathed specimens showed quicker strength degradation due to the detachment of the sheathing from the frame; this resulted in a yield resistance close to the ultimate resistance in order to satisfy the definition of the EEEP method, thus reducing its overstrength. The lower overstrength of the centre-sheathed specimens is attributed to the new prediction method used (see Section 4.3), further tests need to be conducted to improve the prediction method and decide, confidently, what values are most appropriate to calculate the walls' overstrength.

Table 4.13: Overstrength for Monotonic Specimens – Double-Sheathed Shear Walls

Test	S_u [1] (kN/m)	$S_{y\ (EEEP)}$ [2] (kN/m)	*Overstrength* $S_u/S_{y\ (EEEP)}$
W19-M	39.6	35.5	1.12
W20-M	27.3	25.2	1.08
W21-M	45.9	41.4	1.11
W22-M	28.4	26.8	1.06
W28-M	61.0	54.2	1.13
W29-M	38.2	34.8	1.10
W30-M	65.4	58.8	1.11
W31-M	39.3	36.3	1.08
		Average	1.10
		STD. DEV.	0.022
		C.V.	1.98%

Table 4.14: Overstrength for Cyclic Specimens – Double-Sheathed Shear Walls

Test	$S_{u,avg}$ [1] (kN/m)	$S_{y,avg\ (EEEP)}$ [2] (kN/m)	*Overstrength* $S_{u,avg}/S_{y,avg\ (EEEP)}$
W19-C	44.7	40.6	1.10
W20-C	30.1	26.5	1.14
W21-C	46.2	41.8	1.11
W22-C	29.8	26.9	1.11
W28-C	61.8	54.0	1.14
W29-C	40.4	36.1	1.12
W30-C	69.8	62.2	1.12
W31-C	45.1	39.5	1.14
		Average	1.12
		STD. DEV.	0.017
		C.V.	1.50%

Table 4.15: Overstrength for Monotonic Specimen – Centre-Sheathed Shear Walls

Test	S_u (kN/m)	$S_{n\ (MESM)}$ (kN/m)	$S_{2.5\%}$ (kN/m)	*Ultimate Overstrength* $S_u/S_{n\ (MESM)}$	*Design Overstrength* $S_{2.5\%}/S_{n\ (MESM)}$
W15-MR3	150	162	132	0.925	0.814

Table 4.16: Overstrength for Cyclic Specimens – Centre-Sheathed Shear Walls

Test	$S_{u,avg}$ (kN/m)	$S_{n\ (MESM)}$[3] (kN/m)	$S_{2.5\%,avg}$ (kN/m)	*Ultimate Overstrength* $S_{u,avg}/S_{n\ (MESM)}$	*Design Overstrength* $S_{2.5\%,avg}/S_{n\ (MESM)}$
W15-CR3[1]	159	162	135	0.981	0.834
W15B-CR3[2]	166	162	141	1.03	0.873
W23-CR3[1]	147	150	140	0.984	0.935
W23B-CR3[2]	159	150	141	1.06	0.940
W24-CR3[1]	136	116	122	1.13	1.05
W25-CR3[2]	117	95.7	106	1.22	1.11
W26-CR3[2]	145	132	143	1.10	1.09
			Average	1.08	0.975
			STD. DEV.	0.092	0.107
			C.V.	8.51%	11.0%

4.4.4 Seismic Force Resistance Factor Calibration – Canada

In Canada, seismic design may be carried out following the equivalent static force method, defined in Clause 4.1.8.11 of the NBCC (NRC *(2015)),* to calculate the structure's base shear, *V*. The ductility-related force modification factor, R_d, and the overstrength-related force modification factor, R_o, are important factors in calculating the base shear for seismic design using Equation (4-15).

$$V = \frac{S(T_a)M_v I_E W}{R_d R_o} \tag{4-15}$$

where,

V = Lateral earthquake design force at the base of the structure;

$S(T_a)$ = Design spectral acceleration;

I_E = Earthquake importance factor;

M_v = Higher mode effect factor;

W = Weight of the structure;

R_d = Ductility-related force modification factor;

R_o = Overstrength-related force modification factor.

4.4.4.1 Determination of "Test-Based" R_d

The ductility-related force modification factor, R_d, accounts for the structure's ability to dissipate energy through cyclic inelastic behaviour. This energy dissipation occurs through inelastic deformation of the lateral force resisting system within the structure, the CFS framed and sheathed shear walls in this case, dissipate energy through bearing deformation of the sheathing around the connections as discussed in Chapter 3. Newmark and Hall *(1982)* developed relationships, Equations (4-16), (4-17), and (4-18), between ductility, μ (from Tables 4.1, 4.2, and 4.3), and R_d, based on the natural period of the structure, T.

$$R_d = \mu \qquad \text{for } T > 0.5\text{s} \qquad (4\text{-}16)$$

$$R_d = \sqrt{2\mu - 1} \qquad \text{for } 0.1\text{s} < T < 0.5\text{s} \qquad (4\text{-}17)$$

$$R_d = 1 \qquad \text{for } T < 0.03\text{s} \qquad (4\text{-}18)$$

where,

R_d = Ductility-related force modification factor;

μ = Ductility of the shear walls;

T = Natural period of the structure.

It was determined by Boudreault *(2005)* that most light-framed structures have a natural period between 0.03s and 0.5s, and therefore Equation (4-17) was selected to calculate R_d of the specimens tested. Various R_d values were obtained depending on the type of test protocol used, a summary of the results are presented in Tables 4.17 to 4.20. First, R_d values were computed for monotonic tests only (Table 4.17). Next, R_d values were computed for the symmetric reversed cyclic tests, where the average of the ductilities from the positive and negative cycles were

considered; these results are shown in Table 4.18. In Table 4.19, the R_d results for the negative cycles are shown; these involved the specimens tested using the symmetric cyclic protocol only since the asymmetric protocol only displaced the specimens in the positive direction. The R_d values were also calculated considering only the ductility obtained from the positive cycles, which involved all of the specimens (Table 4.20). Lastly, R_d values were found for specimens tested using the asymmetric protocol only (Table 4.21). The asymmetric protocol was introduced in order to observe the full potential of specimens that were not able to reach their ultimate strength or 80% of the ultimate strength post-peak during the symmetric cyclic test. The ductility of these specimens was affected by the limitation of the actuator's stroke during the symmetric cyclic test as no significant strength degradation was observed at the maximum displacement reached.

The cyclic tests of the double-sheathed specimens in Table 4.18 had a lower R_d average than those tested monotonically in Table 4.17. This was a result of the faster strength degradation caused by the sheathing detaching from the frame from the repetitive change in direction during the cyclic tests. Only one centre-sheathed specimen was successfully (with no frame failure) tested monotonically, and therefore a comparison cannot be made.

A comparison can be made between the ductility reached during cyclic tests in the negative displacement range versus the positive displacement range (Tables 4.19 and 4.20). For both shear wall configurations, the average R_d was lower in the negative range compared to the positive range, 14.1% and 12.4% difference for double and centre-sheathed configurations respectively. This is simply due to the nature of the cyclic protocol, as the shear wall cycled in the negative direction it had already sustained damage from the previous positive cycle, thus resulting in a less ductile behaviour in the negative range.

From Table 4.20, the average R_d for the centre-sheathed configuration was lower, 2.82, than the double-sheathed configuration, 2.99. This is a counterintuitive result because it has been observed that the centre-sheathed shear walls can sustain plastic deformations at much greater lateral displacements and shear forces, without strength degradation, than the double-sheathed walls. This result is due to the fact that the behaviour of the centre-sheathed specimens tested with the symmetric cyclic protocol (W15-CR3, W23-CR3, and W24-CR3) was hindered by the stroke

limit of the actuator, yielding a result that does not reflect their true behaviour. Table 4.21 shows an average R_d of 3.01 for the centre-sheathed specimens tested with the asymmetric cyclic protocol (positive cycles only), where they were not restricted by the displacement limit of the actuator. This value is now comparable to the double-sheathed configuration R_d of 2.99, therefore verifying the previous statement.

All R_d values calculated for both configurations, are higher than the R_d = 2.0 listed in Table 1.2-1 of the AISI S400 Standard *(2015)* for steel sheet sheathed shear walls.

Table 4.17: R_d for Monotonic Specimens

Test	Ductility [2] μ	Ductility-Related Force Modification Factor, R_d
Double-Sheathed Configuration		
W19-M	5.46	3.15
W20-M	9.07	4.14
W21-M	5.55	3.18
W22-M	9.13	4.15
W28-M[1]	5.15	3.05
W29-M[1]	10.7	4.52
W30-M[1]	4.26	2.74
W31-M[1]	10.3	4.43
	Average	3.67
	STD. DEV.	0.708
	C.V.	19.3%
Centre-Sheathed Configuration		
W15-MR3	3.87	2.60

[1]Tested by Brière *(2017)*
[2]Values from Table 4.1

Table 4.18: R_d for Specimens Tested with Symmetric Cyclic Protocol
(Average of positive and negative cycles)

Test	Ductility [2] μ_{avg}	Ductility-Related Force Modification Factor, R_d
Double-Sheathed Configuration		
W19-C	4.00	2.64
W20-C	5.83	3.26
W21-C	3.92	2.62
W22-C	5.43	3.14
W28-C[1]	3.56	2.47
W29-C[1]	4.29	2.75
W30-C[1]	3.49	2.44
W31-C[1]	5.47	3.15
	Average	2.81
	STD. DEV.	0.327
	C.V.	11.7%
Centre-Sheathed Configuration		
W15-CR3	3.38	2.40
W23-CR3[1,3]	3.88	2.60
W24-CR3[1]	4.01	2.65
	Average	2.55
	STD. DEV.	0.133
	C.V.	5.20%

[1]Tested by Brière *(2017)*
[2]Average of values from Tables 4.2 and 4.3
[3]Imcomplete negative cycles, only positive value considered

Table 4.19: R_d for Negatives Cycles of Specimens Tested with Symmetric Cyclic Protocol

Test	Ductility [2] μ^-	Ductility-Related Force Modification Factor, R_d
Double-Sheathed Configuration		
W19-C	3.79	2.57
W20-C	4.84	2.95
W21-C	3.72	2.54
W22-C	4.80	2.93
W28-C[1]	2.88	2.18
W29-C[1]	3.39	2.40
W30-C[1]	3.09	2.28
W31-C[1]	5.26	3.09
	Average	2.62
	STD. DEV.	0.335
	C.V.	12.8%
Centre-Sheathed Configuration		
W15 CR3	3.23	2.34
W24-CR3[1]	4.12	2.69
	Average	2.51
	STD. DEV.	0.250
	C.V.	9.96%

[1]Tested by Brière *(2017)*
[2]Values from Table 4.3

Table 4.20: R_d for Positive Cycles of Specimens Tested with Symmetric and Asymmetric Cyclic Protocols

Test	Ductility [3] μ^+	Ductility-Related Force Modification Factor, R_d
Double-Sheathed Configuration		
W19-C	4.20	2.72
W20-C	6.82	3.56
W21-C	4.12	2.69
W22-C	6.05	3.33
W28-C[1]	4.23	2.73
W29-C[1]	5.19	3.06
W30-C[1]	3.88	2.60
W31-C[1]	5.68	3.22
	Average	2.99
	STD. DEV.	0.354
	C.V.	11.8%
Centre-Sheathed Configuration		
W15 CR3	3.52	2.46
W15B-CR3[2]	7.62	3.77
W23-CR3[1]	3.88	2.60
W23B-CR3[1,2]	5.00	3.00
W24-CR3[1]	3.89	2.60
W25-CR3[2]	5.12	3.04
W26-CR3[1,2]	2.99	2.23
	Average	2.82
	STD. DEV.	0.510
	C.V.	18.1%

[1]Tested by Brière *(2017)*
[2]Asymmetric cyclic tests
[3]Values from Table 4.2

Table 4.21: R_d for Specimens Tested with Asymmetric Cyclic Protocols Only

Test	Ductility [2] μ	Ductility-Related Force Modification Factor, R_d
Centre-Sheathed Configuration		
W15B-CR3	7.62	3.77
W23B-CR3[1]	5.00	3.00
W25-CR3	5.12	3.04
W26-CR3[1]	2.99	2.23
	Average	3.01
	STD. DEV.	0.630
	C.V.	20.9%

[1]Tested by Brière *(2017)*
[2]Values from Table 4.2

In order to make a clearer comparison in terms of ductility between the double-sheathed and centre-sheathed configurations, their yield displacements, Δ_y, were compared since ductility is inversely proportional to yield displacement (Equation (4-4)), and both configurations have similar stiffnesses (Tables 4.1 to 4.3). Table 4.22 shows that on average, the double-sheathed specimens experienced yielding at 10.4 mm (0.409") lateral displacement and the centre-sheathed specimens experienced yielding at 29.7 mm (1.17"). Overall, the centre-sheathed specimens started to yield at a lateral displacement 2.85 times larger than the double-sheathed specimens. In order for the centre-sheathed walls to have a comparable ductility to the double-sheathed walls, they need to deform inelastically within a lateral displacement interval 2.85 times larger than the double-sheathed walls.

Table 4.22: Summary of Yield Displacement, Δy, and Elastic Stiffness, k_e

Test	k_e [2] ((kN/m)/mm)	Δ_y [2] (mm)
Double-Sheathed Configuration		
W19-C	3.40	12.4
W20-C	3.58	7.41
W21-C	3.52	12.3
W22-C	3.75	7.18
W28-C[1]	4.48	11.9
W29-C[1]	4.69	7.79
W30-C[1]	4.15	15.4
W31-C[1]	4.73	8.52
Average	4.04	10.4
STD. DEV.	0.545	3.04
C.V.	13.5	29.3%
Centre-Sheathed Configuration		
W15 CR3	4.22	32.4
W15B-CR3	4.80	28.4
W23-CR3[1]	4.29	32.3
W23B-CR3[1]	4.54	30.4
W24-CR3[1]	4.01	29.5
W25-CR3	3.84	26.8
W26-CR3[1]	4.52	27.9
Average	4.32	29.7
STD. DEV.	0.331	2.16
C.V.	7.66	7.27%

[1]Tested by Brière *(2017)*
[2]Values from Table 4.2

Although the test-based R_d values were all higher than the 2.0 recommended in the AISI S400 Standard *(2015)* for steel-sheathed shear walls in Canada, they do not represent the shear walls' superior behaviour in terms of ductility, especially the behaviour of the centre-sheathed configuration. In order to recommend design R_d values that are representative of the centre-sheathed configuration's ability to undergo extensive inelastic deformations at large lateral displacements, further research needs to be conducted. Dynamic analysis using models that incorporate the complete force vs. deformation hysteretic response, under different ground motions, of mid-rise building models incorporating the shear wall configurations presented in this report, would help expand the knowledge on the behaviour of these new CFS shear walls.

4.4.4.2 Determination of "Test-Based" R_o

In seismic design, the overstrength-related force modification factor, R_o, accounts for the dependable portion of reserve strength of the energy dissipating elements in a structure. As previously discussed, the NBCC (NRC *(2015)*) limit states design requires that the factored resistance be larger than the factored applied loads based on the most critical load combination (Equation (4-6)). The factored applied loads are usually overestimated to produce conservative design values, however in capacity based design this overestimation is avoided by using the overstrength factor, R_o, to allow the energy dissipating elements to reach their inelastic range. Proposed by Mitchell *et al. (2003)*, R_o is calculated using Equation (4-19).

$$R_o = R_{size} R_{\emptyset} R_{yield} R_{sh} R_{mech} \tag{4-19}$$

where,

R_{size} = Overstrength due to restricted choices for size of components;

R_{ϕ} = $1/\phi$, ($\phi_{(LSD)}$ = 0.8 for double-sheathed and $\phi_{(LSD)}$ = 0.7 for centre-sheathed);

R_{yield} = Ratio of test yield strength to minimum specified yield strength;

R_{sh} = Overstrength due to the development of strain hardening;

R_{mech} = Overstrength due to the collapse mechanism.

R_{size} accounts for the limitation of component sizes available from manufacturers; it was taken as 1.05. R_{ϕ} reverts the factored loads used in limit states design to nominal loads in capacity

based design; it is taken as the inverse of the resistance factor for LSD (0.8 for double-sheathed walls and 0.7 for centre-sheathed walls, refer to Table 4.8). For the double-sheathed configuration specimens, R_{yield} was taken as 1.11, the average of overstrength factors for monotonic and cyclic tests in Tables 4.13 and 4.14.

For the centre-sheathed configuration, the specimens were considered to have no overstrength based on the design overstrength factor average from Table 4.16, 0.975, and therefore R_{yield} was taken as 1.0. Furthermore, the centre-sheathed configuration overstrength was not calculated using the yield strength, but the strength at 2.5% lateral drift instead. Additionally, only the cyclic tests were considered since only one centre-sheathed wall was tested monotonically.

The strain hardening overstrength, R_{sh}, was chosen as 1.0 because shear walls are not affected by strain hardening of steel.

Lastly, the overstrength related to the collapse mechanism, R_{mech}, was also chosen as 1.0 because a collapse mechanism for steel-sheathed shear walls has not yet been established.

Table 4.23 summarizes the five overstrength factors used to calculate R_o for the double-sheathed and centre-sheathed shear wall configurations. R_o values of 1.46 and 1.50 were obtained for the double-sheathed and centre-sheathed configurations, respectively. The value recommended in the AISI S400 Standard *(2015)* for steel sheet sheathed shear walls is 1.3, which is lower than the values obtained, however these are new shear wall configurations and further research needs to be done in order for a R_o value to be recommended.

Table 4.23: Overstrength Factors to Calculate R_o

Configuration	R_{size}	R_{ϕ}	R_{yield}	R_{sh}	R_{mech}	R_o
Double-Sheathed	1.05	1.25	1.11	1.00	1.00	1.46
Centre-Sheathed	1.05	1.43	1.00	1.00	1.00	1.50

4.4.5 Recommendation of R_d and R_o Values in the Future

The seismic performance factors used in Canada, R_d and R_o, were presented in Section 4.4.4. The factors were determined for the double-sheathed and centre-sheathed configurations and were based on the experimental data obtained during the research program. The higher shear strength and improved ductile behaviour of the centre-sheathed shear walls, compared to the double-sheathed shear walls, were not accurately represented by the *test-based* R-values, as these values were similar for both configurations.

The use of the *test-based* R_d and R_o for the centre-sheathed shear walls in seismic design would result in an overestimation of the design base shear (Equation (4-15)). Consequentially, with an overestimated base shear, the structure's seismic force-resisting systems (SFRS) would be overdesigned since R_d and R_o do not reflect the shear wall's ability to reach a higher shear strength and ductility. A greater number of SFRSs within the structure would be needed to resist the overestimated base shear, as well as larger SFRS members and connections to transfer the overestimated lateral loads. The use of the *test-based* R-values in design would not allow the designer to explore the advantages of the centre-sheathed shear walls, resulting in a comparable design to what is currently available in the CFS standards.

The Federal Emergency Management Agency (FEMA) outlines a methodology to determine seismic performance factors; the Component Equivalency Methodology in FEMA P795 *(2011)*. This methodology was derived from an earlier publication, FEMA P695 *(2009)* Quantification of Building Seismic Performance Factors, which provides a methodology for the evaluation of complete SFRSs and their implementation into building codes. The Component Equivalency Methodology in FEMA P795 *(2011)* allows for the evaluation of individual SFRS components, structural elements and connections for example, which are proposed as substitutes for equivalent components of an already established SFRS, in this case steel-sheathed shear walls.

Using the FEMA P795 *(2011)* methodology, chosen components of the centre-sheathed shear wall configuration would serve as substitutes for defined equivalent reference components of a well-established SFRS such as steel-sheathed shear walls with a single sheet on one side. The

definition of the reference component would be the same as described by Rizk *(2017)*, based on the single-sheathed CFS shear walls tested in past research programs.

The seismic performance factors following the FEMA P795 methodology were not obtained for the test program presented in this report. The number of test specimens for analysis did not meet the methodology's requirement. In addition, had the methodology been completed, the centre-sheathed configuration would have been defined as a substitute for the reference component, leading to the disregard of its superior behaviour.

In order to properly evaluate and confidently recommend representative design R-values for the centre-sheathed shear wall configuration more extensive experimental programs, with larger sample sizes, need to be completed. With the future expansion of the experimental data, the Modified Effective Strip Method (MESM) as a shear strength prediction method should be further refined, in particular the influence of location of the sheathing fasteners. Finally, for the complete evaluation of the centre-sheathed shear wall configuration, future research should also focus on the numerical non-linear dynamic analysis of representative buildings under different representative ground motions, with the implementation of the shear walls being studied, similar to the methodology described in FEMA P695 *(2009)*. It is predicted that a thorough and successful numerical analysis of the centre-sheathed configuration would result in higher R_d and R_o values for use in design, representing of the shear wall's true ductile behaviour and shear capacity, resulting in a more efficient design.

CHAPTER 5 – CONCLUSIONS AND FUTURE RESEARCH

5.1 Conclusions

The innovative cold-formed steel (CFS) shear wall configurations tested in this research program were developed as potential solutions to overcome the force limitations associated with the shear wall configuration currently recommended by the AISI S400 Standard *(2015)*. The CFS framed and sheathed shear walls currently used in design are built with sheathing on one side only and with steel members with shear resistances not typically suitable for mid-rise buildings. The use of thicker framing and sheathing with the standard shear wall configuration has been shown to cause chord stud damage from the out-of-plane twisting of the wall, caused by torsional forces arising from the eccentricity of the sheathing placement, even when frame blocking was present in some cases.

The main goals of the new CFS shear wall configurations, the double-sheathed configuration and the centre-sheathed configuration, were to achieve higher shear resistance and ductility for the purpose of mid-rise construction. To achieve this, thicker framing and sheathing were used to construct the walls while having a concentric sheathing placement to avoid twisting of the chord studs.

The development of these new shear wall configurations involved an experimental phase, where a total of 31 – 1.22 m × 2.44 m (4’ × 8’) specimens with different parameter combinations were tested (16 double-sheathed and 15 centre-sheathed). The wall parameter combinations involved varying the fastener spacing, frame thickness, sheathing thickness, and fastener size. The test data of each specimen was then analyzed and the analysis results were used in the development of design procedures used in Canada, the USA, and Mexico. In this research program, the author was responsible for 16 test specimens, while Brière *(2017)* reported on the remaining 15 test specimens.

5.1.1 Double-Sheathed Configuration

Following the observations made by Rizk *(2017)*, the double-sheathed configuration was designed with revised construction details. It was built by fastening two sheathing panels, one on

each side of the wall, to face-to-face built-up chords (box shaped). The chord studs were designed to resist the combination of high bending moments and axial forces previously experienced by CFS shear walls built following the standard configuration. Additionally, the box shape of the chord stud provided higher resistance against possible twisting compared to the back-to-back chord studs used in standard shear wall design.

Each unique double-sheathed shear wall, of a specific wall parameters combination, was tested using a monotonic loading protocol and the CUREE reversed cyclic loading protocol. The parameter combinations involved fastener spacing from 100 mm (4”) to 50 mm (2”), two different sheathing thicknesses, 0.36 mm (0.014”) and 0.47 mm (0.019”), as well as two framing thicknesses, 1.73 mm (0.068”) and 2.46 mm (0.097”), and screw sizes varying from No. 10 to No. 12. The shear resistance of the specimens varied according to the wall parameters, with the specimens built using smaller fastener spacing, thicker framing and sheathing, and larger screws reaching the highest resistance.

The behaviour among the double-sheathed specimens was consistent, no significant frame damage occurred, while damage primarily developed in the form of bearing at the sheathing-to-frame connections. The strongest double-sheathed shear wall reached a shear resistance two times higher than what is currently available for design in the AISI S400 Standard *(2015)*. Although a higher shear resistance was achieved, the ductility was not improved. The ductility of the double-sheathed walls was limited by the detachment of the sheathing from the frame; the sheathing was able to pull through the head of the screws when enough bearing deformation was sustained (a slot hole formed around the connection). This was more pronounced during the cyclic tests due to the repetitive back and forth displacement of the wall and the out-of-plane forces applied to the sheathing due to its shear buckling.

To be consistent with past CFS shear wall research, the Equivalent Energy Elastic Plastic (EEEP) method was used to analyze the double-sheathed shear wall test data. It represented the nonlinear behaviour of the shear walls as an equivalent bilinear curve. The EEEP method provided key design parameters such as the yield resistance and its corresponding displacement, elastic stiffness, ductility, and energy dissipated. These design parameters were used to develop the Limit

States Design (LSD) procedure, used in Canada. The Load and Resistance Factor Design (LRFD) procedure, used in the USA and Mexico, was established using design values corresponding to the ultimate shear strength reached during testing.

The double-sheathed configuration load resistance factors, $\phi = 0.71$ and $\phi = 0.86$, were obtained for LSD and LRFD, respectively. Factors of safety for lateral design considering wind loading were computed as the ratio of the ultimate to factored shear resistance.

For seismic design, capacity based design parameters were calculated. The average overstrength values were found to be 1.10 and 1.12 for the monotonic and cyclic tests, respectively. The overstrength of the double-sheathed walls was lower than the 1.4 value recommended previously by Balh *et al. (2014)*. This result was attributed to the quick loss of strength once ultimate resistance was reached, which resulted in an EEEP yield resistance close to the ultimate resistance. Lastly, the "test-based" seismic force modification factors for use in Canada, R_d and R_o, were computed. R_d was found to have an average value of 3.67 for the monotonic tests and 2.81 for the cyclic tests, both larger than the recommended value of 2.0 by the AISI S400 Standard *(2015)*. A R_o of 1.46 for the double-sheathed configuration was calculated, which again, was larger than the recommended AISI S400 Standard *(2015)* value of 1.3 for steel sheet sheathed shear walls.

To address the shortcomings of the double-sheathed configuration, a new shear wall configuration was designed, the centre-sheathed configuration. The behaviour of the centre-sheathed walls showed further increase in shear resistances in addition to improved ductility.

5.1.2 Centre-Sheathed Configuration

The centre-sheathed walls were built with a single sheathing panel fastened between the back-to-back chord studs and horizontal framing members, keeping the placement of the sheathing concentric. The confinement of the sheathing did not allow it to detach from the frame at large lateral displacements, as was observed for the double-sheathed configuration.

The centre-sheathed configuration went through a design evolution throughout the testing program. Initially, the specimens were designed based on the Effective Strip Method recommended by Yanagi and Yu *(2014)* and found in the AISI S400 Standard *(2015)*; however, this method underestimated the shear forces experienced during the tests. The unexpected higher shear forces reached during the tests caused the compression chord stud to fail due to bending and high axial forces. The underestimate of the shear resistance of the centre-sheathed configuration by the Effective Strip Method was attributed to the fact that it was developed based on research done with shear walls built using sheathing on one side only and single shear (2-ply) sheathing-to-frame connections (i.e. standard configuration). The observed tension field width of the centre-sheathed specimens was larger than that calculated by the Effective Strip Method; therefore, the design of the subsequent specimens was based on the observed tension field width contributing to the shear resistance. An iterative process was followed and a final centre-sheathed configuration, which saw no frame damage, was designed based on the contribution of all sheathing connections participating in the shear resistance of the wall, meaning that the tension field width was observed to be along the entire height of the wall. Additionally, the 3-ply sheathing-to-frame connection of the centre-sheathed configuration was represented in the design by calculating its bearing resistance using the bolt double shear connection equation from the AISI S100 Standard *(2016)* and CSA S136 Standard *(2016)*, since such an equation has not been developed for screw connections.

The final centre-sheathed configuration involved attaching a box shaped reinforcement to the chord studs to avoid frame failure and adding a second holdown at the bottom of the wall to resist the high uplift forces. With this final configuration, various specimens were tested using different wall parameter combinations. Specimens were tested with fastener spacing of 50 mm (2”), 100 mm (4”), and 150 mm (6”), sheathing thicknesses of 0.84 mm (0.033”) and 1.09 mm (0.043”), and No. 10 and No. 12 screws. Like the double-sheathed configuration, the shear resistance was higher for specimens built with thicker sheathing, smaller fastener spacing, and larger screws. However, for this configuration, limits on the fastener spacing were observed. If the fastener spacing was too small, the shear forces experienced by the wall were too great, causing frame failure or force degradation was not observed within the actuator’s stroke limit. If the

spacing was too large, the shear buckling of the sheathing caused the back-to-back chord studs to separate and no longer work as a built-up member, resulting in loss of strength.

The specimens were first tested using the CUREE reversed cyclic loading protocol. However, force degradation was not reached by some specimens within the actuator's stroke limit due to their high shear resistance and ductility. Because of this, some specimens were tested using an asymmetric cyclic protocol to observe the specimens' full inelastic behaviour. The asymmetric cyclic protocol allowed for specimens to cycle mainly in the positive direction, giving a lateral displacement limit of 225 mm (8.86").

The asymmetric cyclic protocol allowed the specimens to reach very high shear resistances at large lateral drifts (7%), with the strongest centre-sheathed specimen reaching a shear capacity four times higher than what is currently listed for design in the AISI S400 Standard *(2015)*. This superior shear strength and ductile behaviour over the standard and the double-sheathed shear wall configurations was attributed to the confinement of the sheathing between the frame members. Confining the sheathing between the chord studs and the horizontal framing members allowed the bearing deformations at the sheathing connection to fully develop, resulting in an increase in the wall's shear resistance and ductility.

Because of their high shear resistance and ductility, most centre-sheathed specimens did not reach a post-peak shear force equivalent to 80% of the ultimate force during the tests given the limited actuator stroke. Therefore, it was concluded that using the EEEP analysis results for the development of a design procedure for this configuration would not produce design parameters representative of the true behaviour of the specimens. Instead, a new shear resistance prediction method, the Modified Effective Strip Method (MESM), was developed based on the observations made throughout the design evolution of the centre-sheathed configuration. Currently, still in its initial development stages, the MESM is a modification of the Effective Strip Method, which better represents the construction details and behaviour of the centre-sheathed shear wall configuration.

In the computation of the LSD and LRFD parameters, the ratio of test-to-predicted shear resistance was computed using the test force corresponding to the 2.5% lateral drift limit from the NBCC (NRC *(2015)*). The centre-sheathed specimens reached their ultimate resistance at very large lateral displacements, unrealistic for design, hence the 2.5% drift limit was chosen. The resistance factors corresponding to the LSD and LRFD were found to be $\phi = 0.64$ and $\phi = 0.79$ respectively. From previous research, a LSD resistance factor of 0.7 has been recommended for CFS framed and sheathed shear walls. The lower value obtained for the centre-sheathed configuration is attributed to the fact that the force prediction method, MESM, needs further improvements in terms of calculating the connection resistance for screws instead of using the equation for bolts. In addition, the MESM would be improved by incorporating the extent to which the sheathing fasteners at different locations contribute to the shear resistance of the wall, for example, the influence of fasteners at the corners versus the fasteners at the mid-height or mid-width of the wall since not all connection undergo the same extent of bearing deformation. It is expected that these improvements will lead to a lower coefficient of variation of the professional factor, resulting in a higher resistance factor. For this reason, resistance factor ranges were used; 0.7 to 0.75 for LSD and 0.8 to 0.9 for LRFD.

For capacity based design, the overstrength was calculated, however due to the current uncertainty of what is the ideal test value to consider (ultimate resistance or resistance at 2.5% lateral drift) and the need for further refinement of the prediction method, the centre-sheathed configuration was considered to have no overstrength. The centre-sheathed configuration yielded R_d values comparable to the double-sheathed configuration, even though the specimens were able to sustain inelastic deformations at very large lateral displacements under larger shear forces. In order to better understand the ductile behaviour of the centre-sheathed configuration and recommend representative R_d and R_o values, numerical modelling of the centre-sheathed shear walls following the Federal Emergency Management Agency (FEMA) P695 *(2009)* methodology should be carried out.

5.2 Recommendations for Future Research

Two new shear wall configurations were tested during this research program; however, the centre-sheathed configuration showed true potential in terms of implementation in CFS mid-rise

construction as it reached higher shear resistances and ductility. Although the centre-sheathed configuration was considered to have performed well, its behaviour is still not fully understood and further research is necessary.

The validation of the R_d and R_o values using the Quantification of Building Seismic Performance Factors as per FEMA P695 *(2009)* is recommended to further investigate the centre-sheathed shear wall configuration. This methodology allows for the evaluation new SFRSs by developing a representative building model which incorporates the test data of the SFRSs and subjecting it to nonlinear analyses under different ground motions.

In the development of the new shear force prediction method for the centre-sheathed walls, it became obvious that two main aspects need to be further researched in order to improve the outcome of the predictions. First, parameters that influence the extent of the sheathing screw's contribution to the wall's shear resistance need to be identified and incorporated in the MESM equation. From the test observations, it was clear that the location of the screws along the perimeter of the sheathing influenced the extent of bearing damage; screws at the corners sustained more extensive bearing damages than the screws at mid-height or mid-width of the sheathing, thus a more in depth study into about this behaviour needs to be conducted. The second aspect is the absence, in the CFS standards, of a bearing resistance equation for cold-formed steel double shear screw connections. The establishment of such an equation would more closely reflect the type of sheathing connection of the centre-sheathed configuration and result in a more accurate shear resistance prediction.

The shear resistances reached by the centre-sheathed shear walls were beyond the forces a mid-rise building would experience during a design level earthquake. Realistically, mid-rise buildings would experience shear forces between 30 kN/m (2055 lb/ft) and 75 kN/m (5138 lb/ft) during a design level seismic event, therefore optimizing the design of the centre-sheathed configuration with resistances within this range is desirable, while maintaining its ductile behaviour. Testing centre-sheathed shear walls with thinner framing and smaller screw sizes than what has been tested in this research program would be a step towards this goal. The use of larger

screw spacing and thinner sheathing to achieve lower shear resistance would likely negatively impact the performance of the shear walls in terms of frame integrity and ductility respectively.

Improvements can be made in the future design iterations of the centre-sheathed configuration in terms of constructability. The high uplift forces experienced by the centre-sheathed walls led to the installation of a second holdown at each corner at the bottom of the walls. Although no failure occurred, holdown damage was still observed, therefore a new anchorage system to sustain these levels of uplift forces would perhaps be worth investigating.

In a more global scale, the load transfer mechanisms that transfer the lateral loads between different systems within the structure also need to be studied since higher forces are being transferred with the integration of these new highly resistant cold-formed steel shear walls.

REFERENCES

AISI (American Iron and Steel Institute) S100 (2016). *North American Specification for the Design of Cold-Formed Steel Structural Members. Washington, DC: AISI.*

AISI (American Iron and Steel Institute) S213 (2004). *North American Standard for Cold-Formed Steel Framing – Lateral Design. Washington, DC: AISI.*

AISI (American Iron and Steel Institute) S213 (2007). *North American Standard for Cold-Formed Steel Framing – Lateral Design. Washington, DC: AISI.*

AISI (American Iron and Steel Institute) S240 (2015). *North American Standard for Cold-Formed Steel Structural Framing. Washington, DC: AISI.*

AISI (American Iron and Steel Institute) S400 (2015). *North American Standard for Seismic Design of Cold-Formed Steel Structural Systems. Washington, DC: AISI.*

ASCE (2016). *Minimum Design Loads and Associated Criteria for Buildings and Other Structures. ASCE/SEI 7-16,* ASCE (American Society of Civil Engineers, Reston, VA.

ASTM (American Society for Testing and Materials) A193 (2016). *Standard Specification for Alloy-Steel and Stainless Steel Bolting for High Temperature or High Pressure Service and Other Special Purpose Applications.* West Conshohocken, PA: ASTM International.

ASTM (American Society for Testing and Materials) A653 (2015). *Standard Specification for Steel Sheet, Zinc-Coated (Galvanized) or Zinc-Iron Alloy-Coated (Galvannealed) by the Hot-dip Process*. West Conshohocken, PA: ASTM International.

ASTM (American Society for Testing and Materials) A370 (2017). *Standard Test Methods and Definitions for Mechanical Testing of Steel Products.* West Conshohocken, PA: ASTM International.

ASTM (American Society for Testing and Materials) E2126 (2011). *Standard Test Methods for Cyclic (Reversed) Load Test for Shear Resistance of Vertical Elements of the Lateral Force Resisting Systems for Buildings*. West Conshohocken, PA: ASTM International.

Balh, N. (2010). *Development of Sesimic Design Provisions for Steel Sheathed Shear Walls.* M.Eng. Thesis. Montreal, QC: Department of Civil Engineering and Applied Mechanics, McGill University.

Balh, N., DaBreo, J., Ong-Tone, C., El-Saloussy, K., Yu, C. and Rogers, C. (2014). Design of steel sheathed cold-formed steel framed shear walls. *Thin-Walled Structures, 75*, 76-86.

Boudreault, F.A. (2005). *Seismic Analysis of Steel Frame / Wood Panel Shear Walls*. M.Eng. Thesis. Montreal, QC: Department of Civil Engineering and Applied Mechanics, McGill University.

Branston, A. (2004). *Development of a Design Methodology for Steel Frame / Wood Panel Shear Walls.* M.Eng. Thesis. Montreal, QC: Department of Civil Engineering and Applied Mechanics, McGill University.

Branston, A., Boudreault, F., Chen, C. and Rogers, C. (2006). Light-gauge steel-frame - wood structural panel shear wall design method. *Canadian Journal of Civil Engineering*, *33*(7), 872-889.

Brière, V. (2017). *Higher Capacity Cold-Formed Steel Sheathed and Framed Shear Walls for Mid-Rise Buildings: Part 2*. M.Eng. Thesis. Montreal, QC: Department of Civil Engineering and Applied Mechanics, McGill University.

CSA (Canadian Standards Association) S136 (2012). *North American Specification for the Design of Cold-Formed Steel Structural Members. Mississauga, ON: CSA Group.*

CSA (Canadian Standards Association) S136 (2016). *North American Specification for the Design of Cold-Formed Steel Structural Members. Mississauga, ON: CSA Group.*

DaBreo, J. (2012). *Impact of Gravity Loads on the Lateral Performance of Cold-Formed Steel Frame/Steel Sheathed Shear Walls*. M.Eng. Thesis. Montreal, QC: Department of Civil Engineering and Applied Mechanics, McGill University.

DaBreo, J., Balh, N., Ong-Tone, C. and Rogers, C. (2014). Steel sheathed cold-formed steel framed shear walls subjected to lateral and gravity loading. *Thin-Walled Structures*, *74*, 232-245.

FEMA (Federal Emergency Management Agency) P695 (2009). *Quantification of Building Seismic Performance Factors*. Redwood City, CA: Applied Technology Council.

FEMA (Federal Emergency Management Agency) P795 (2011). *Quantification of Building Seismic Performance Factors: Component Equivalency Methodology*. Redwood City, CA: Applied Technology Council.

Foliente, G. C. (1996). Issues in seismic performance testing and evaluation of timber structural systems. *International Wood Engineering Conference*, New Orleans, USA.

Hawaii Steel Alliance (2017). Benefits of steel framing. Retrieved from http://www.hawaiisteel.com/benefits-of-steel-framing

Hikita, K. E. (2006). *Impact of Gravity Loads on the Lateral Performance of Light Gauge Steel Frame / Wood Panel Shear Walls*, M.Eng. Thesis. Montreal, QC: Department of Civil Engineering and Applied Mechanics, McGill University.

Krawinkler, H., Parisi, F., Ibarra, L., Ayoub, A. and Medina, R. (2001). *Development of a Testing Protocol for Woodframe Structures*. CUREE-Caltech Woodframe Project. Richmond, CA: Consortium of Universities for Research in Earthquake Engineering (CUREE) Publication No. W-02.

Mitchell, D., Tremblay, R., Karacabeyli, E., Paultre, P., Saatcioglu, M., and Anderson, D. L. (2003). Seismic force modification factors for the proposed 2005 edition of the national building code of Canada. *Canadian Journal of Civil Engineering*, *30*(2), 308-327.

NRC (National Research Council of Canada), (2015). *National Building Code of Canada (NBCC) Volume 1, Part 4*. Ottawa, ON.

Newmark, N. M. and Hall, W. J. (1982). Earthquake spectra and design. *Engineering Monograph*, Earthquake Research Institute Berkeley, California, USA.

Ong-Tone, C. (2009). *Tests and Evaluation of Cold-Formed Steel Frame/Steel Sheathed Shear Wall.* Project Report. Montreal, QC: Department of Civil Engineering and Applied Mechanics, McGill University.

Park, R. (1989). Evaluation of ductility of structures and structural assemblages from laboratory testing. *Bulletin of the New Zealand National Society for Earthquake Engineering, 22*(3), 155-166.

Rizk, R. (2017). *Cold-Formed Steel Frame – Steel Sheathed Shear Walls: Improved Range of Shear Strength Values Accounting for Effect of Full Frame Blocking and Thick Sheathing/Framing Members*. M.Eng. Thesis. Montreal, QC: Department of Civil Engineering and Applied Mechanics, McGill University.

Serrette, R., Nguyen, H., and Hall, G. (1996). *Shear Wall Values for Light Weight Steel Framing.* Report No. LGSRG-3-96. Santa Clara, CA: Department of Civil Engineering, Santa Clara University.

Serrette, R., Encalada, J., Hall, G., Matchen, B., Nguyen, H., and Williams, A. (1997). *Additional Shear Wall Values for Light Weight Steel Framing.* Report No. LGSRG-1-97. Santa Clara, CA: Department of Civil Engineering, Santa Clara University.

Shamim, I. (2012). Seismic Design of Lateral Force Resisting Cold-Formed Steel Framed (CFS) Structures. M.Eng. Thesis. Montreal, QC: Department of Civil Engineering and Applied Mechanics, McGill University.

Shamim, I., and Rogers, C. (2013). Steel sheathed/CFS framed shear walls under dynamic loading: numerical modelling and calibration. *Thin-Walled Structures, 71*, 57-71.

Shamim, I., and Rogers, C. (2015). Numerical evaluation: AISI S400 steel-sheathed CFS framed shear wall seismic design method. *Thin-Walled Structures, 95*, 48-59.

Steel Framing Industry Association (2017). The history of cold-formed steel. Retrieved from https://sfia.memberclicks.net/history

Yanagi, N. and Yu, C. (2014). Effective strip method for the design of cold-formed steel framed shear wall with steel sheet sheathing. *Journal of Structural Engineering, 140*(4), 1-8.

Yu, C. (2010). Shear resistance of cold-formed steel framed shear walls with 0.686-mm, 0.762-mm, and 0.838-mm steel sheet sheathing. *Journal of Structural Engineering, 32*(6), 1522-1529.

Yu, C., and Chen, Y. (2009). *Steel Sheet Sheathing Options for Cold-Formed Steel Framed Shear Wall Assemblies Providing Shear Resistance - Phase 2*. Report No. UNT-G70752. Denton, TX: Department of Engineering Technology, University of North Texas.

Yu, C., and Chen, Y. (2011). Detailing recommendations for 1.83 m wide cold-formed steel shear walls with steel sheathing. *Journal of Constructional Steel Research, 67*(1), 93-101.

Yu, C., Vora, H., Dainard, T., Tucker, J., and Veetvkuri, P. (2007). *Steel Sheet Sheathing Options for Cold-Formed Steel Framed Shear Wall Assemblies Providing Shear Resistance*. Report No. UNT-G76234. Denton, TX: Department of Engineering Technology, University of North Texas.

Zhao, Y. (2002). *Cyclic Performance of Cold-Formed Steel Stud Shear Walls*. M.Eng. Thesis. Montreal, QC: Department of Civil Engineering and Applied Mechanics, McGill University.

APPENDIX A:

SPECIFICATIONS OF SHEAR WALL TEST SPECIMENS

DOUBLE-SHEATHED CONFIGURATIONS

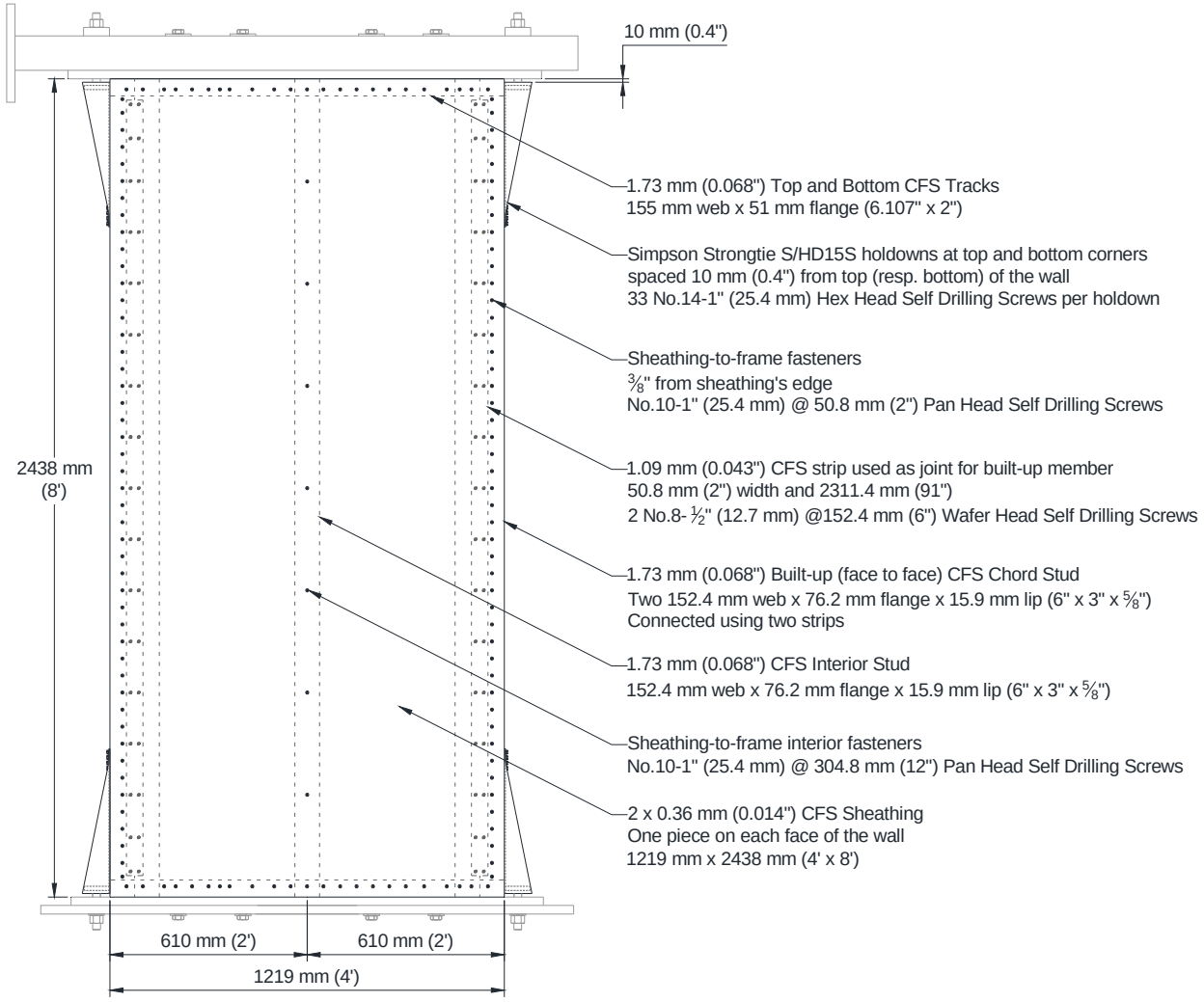

Figure A1: Nominal dimensions and specifications of specimen W19 (M and C).

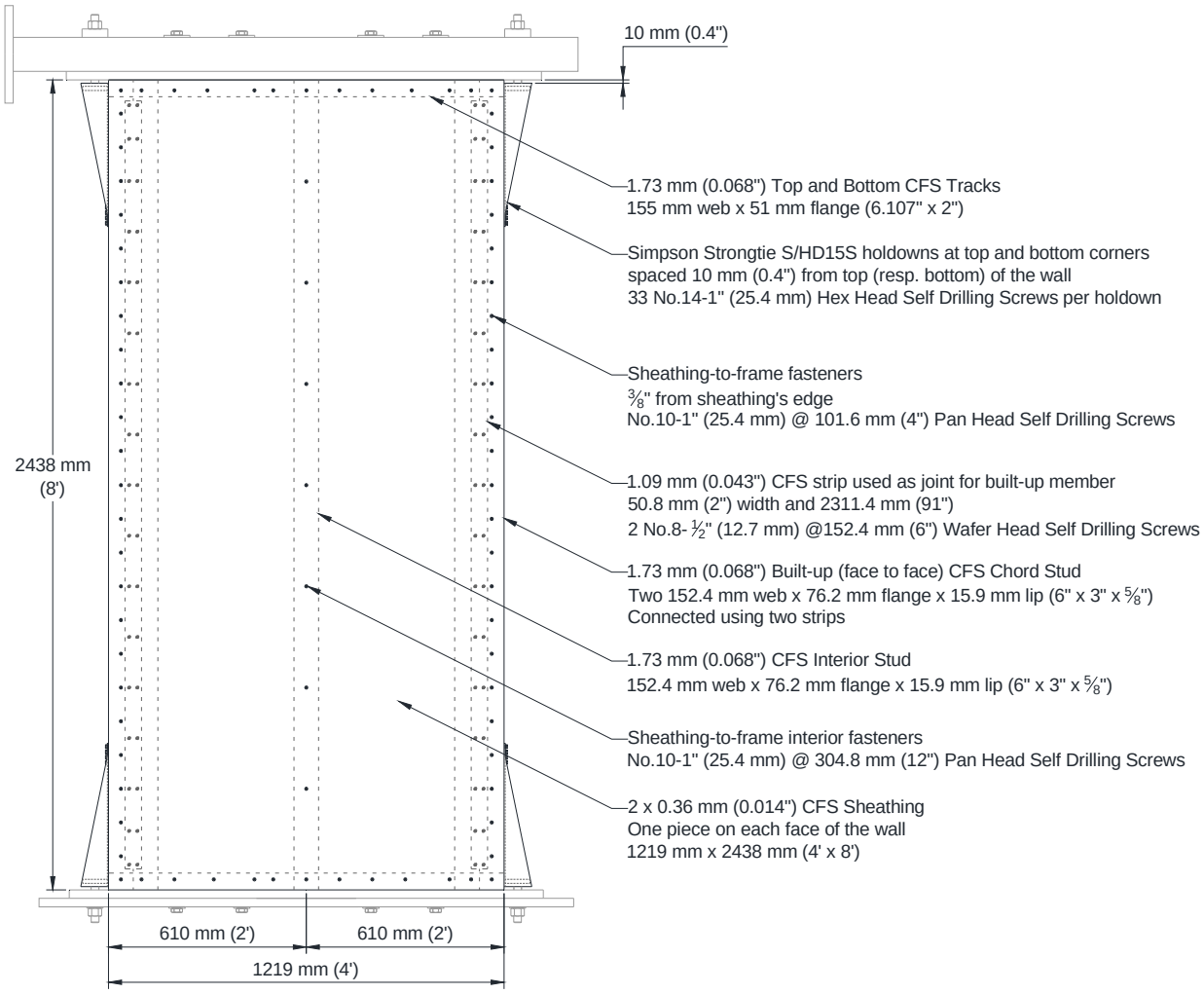

Figure A2: Nominal dimensions and specifications of specimen W20 (M and C).

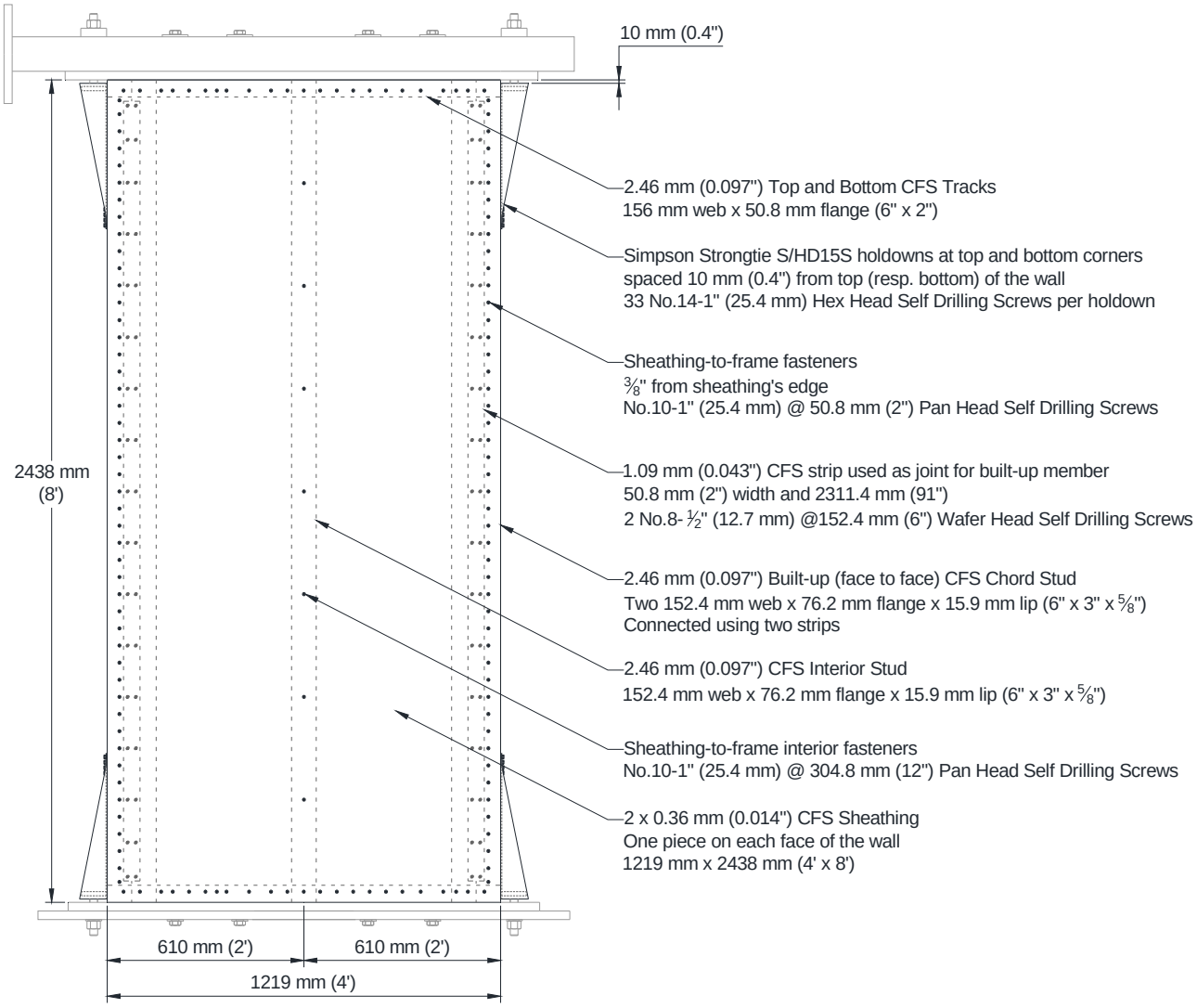

Figure A3: Nominal dimensions and specifications of specimen W21 (M and C).

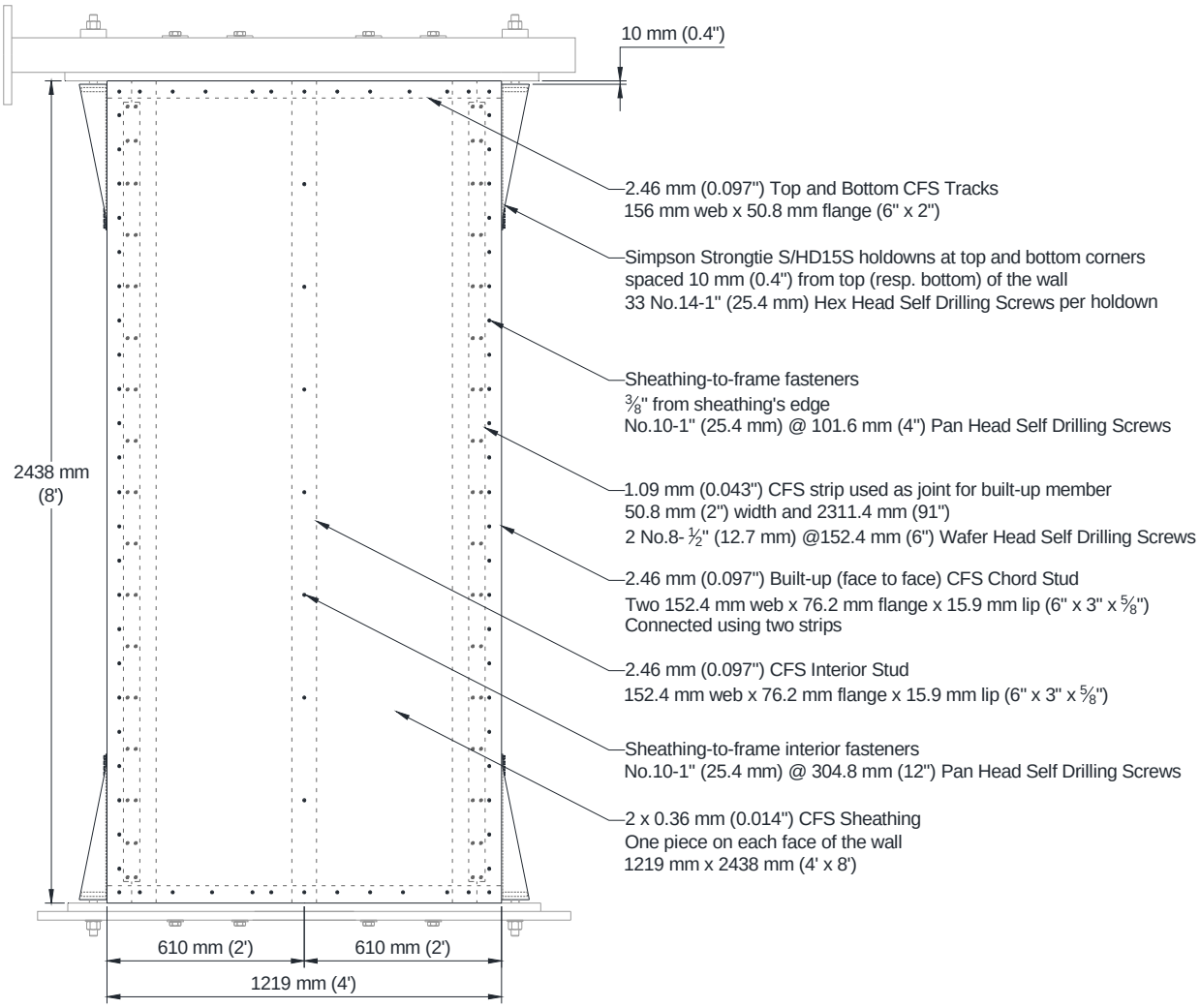

Figure A4: Nominal dimensions and specifications of specimen W22 (M and C).

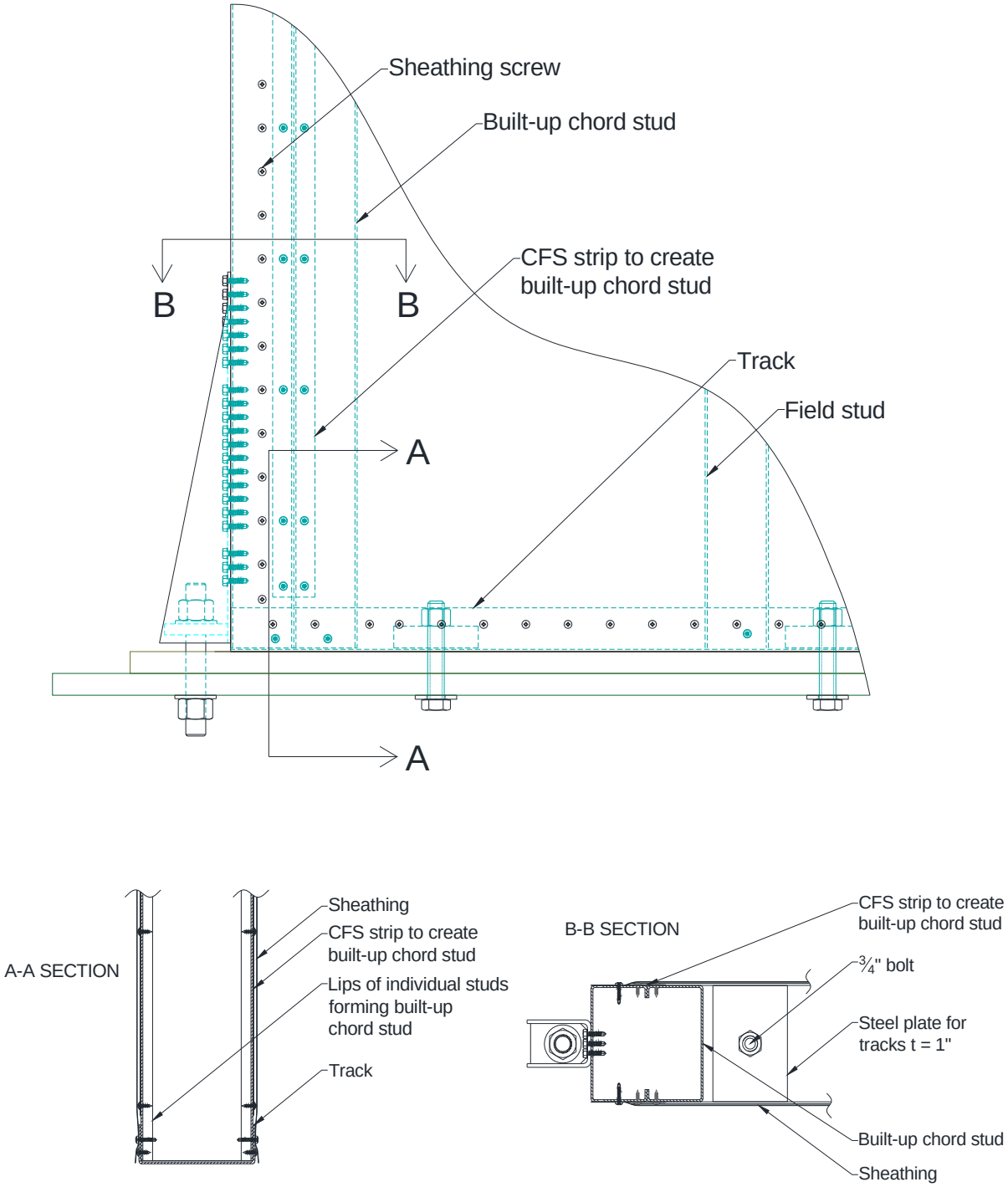

Figure A5: Double-sheathed configuration cross-section details.

CENTRE-SHEATHED CONFIGURATIONS

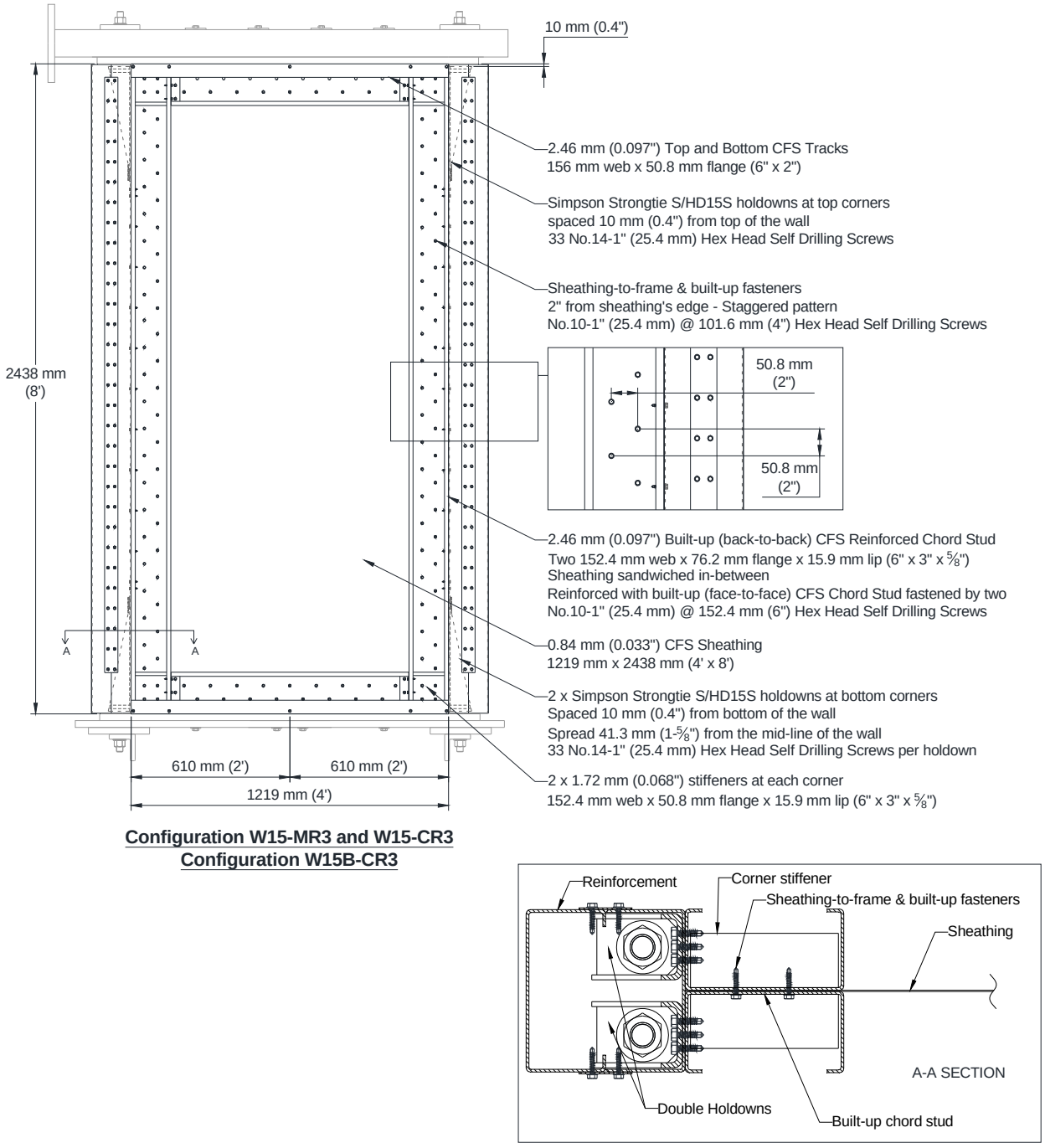

Configuration W15-MR3 and W15-CR3
Configuration W15B-CR3

Figure A6: Nominal dimensions and specifications of specimens W15-MR3, W15-CR3, and W15B-CR3.

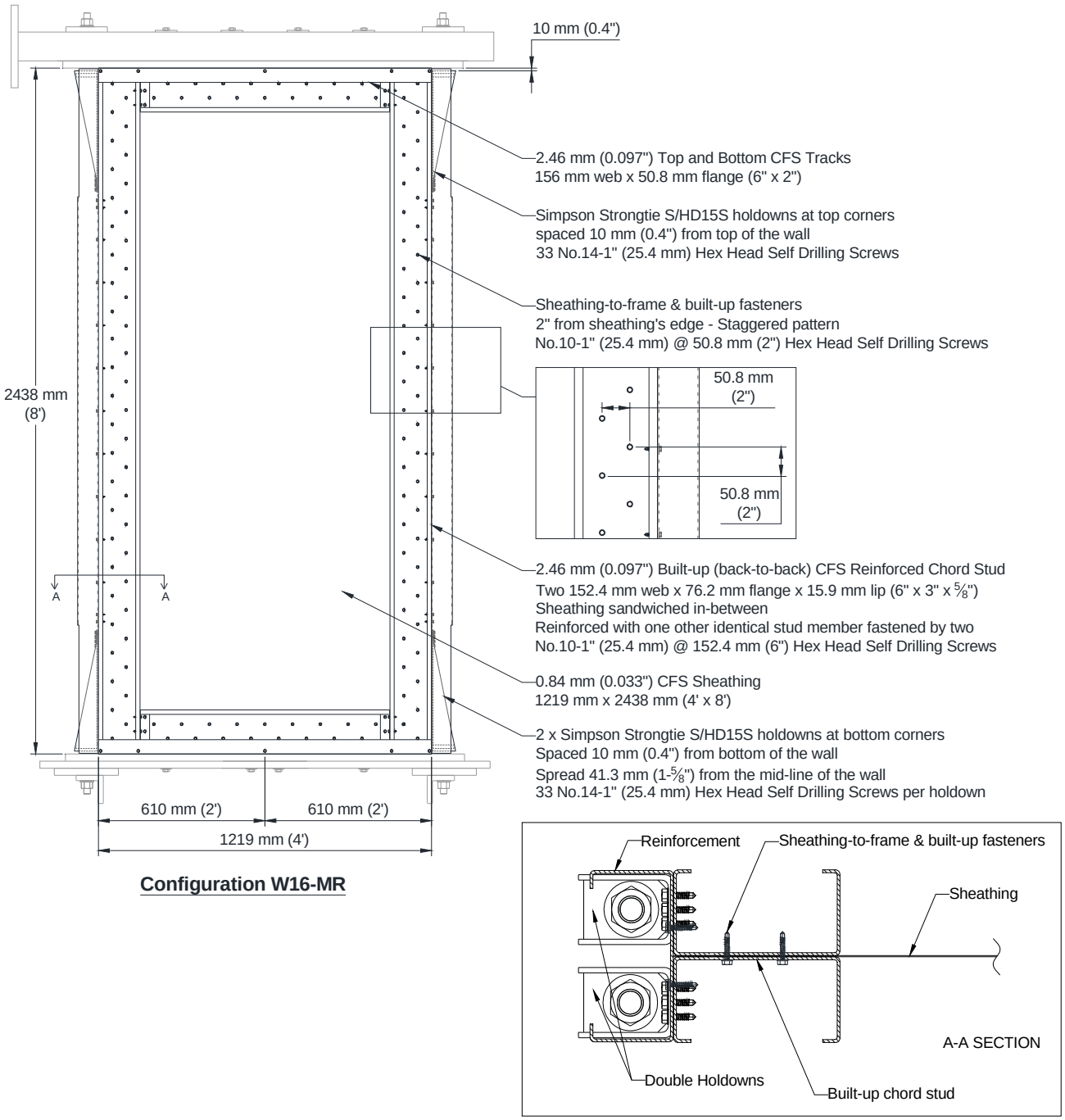

Figure A7: Nominal dimensions and specifications of specimen W16-MR.

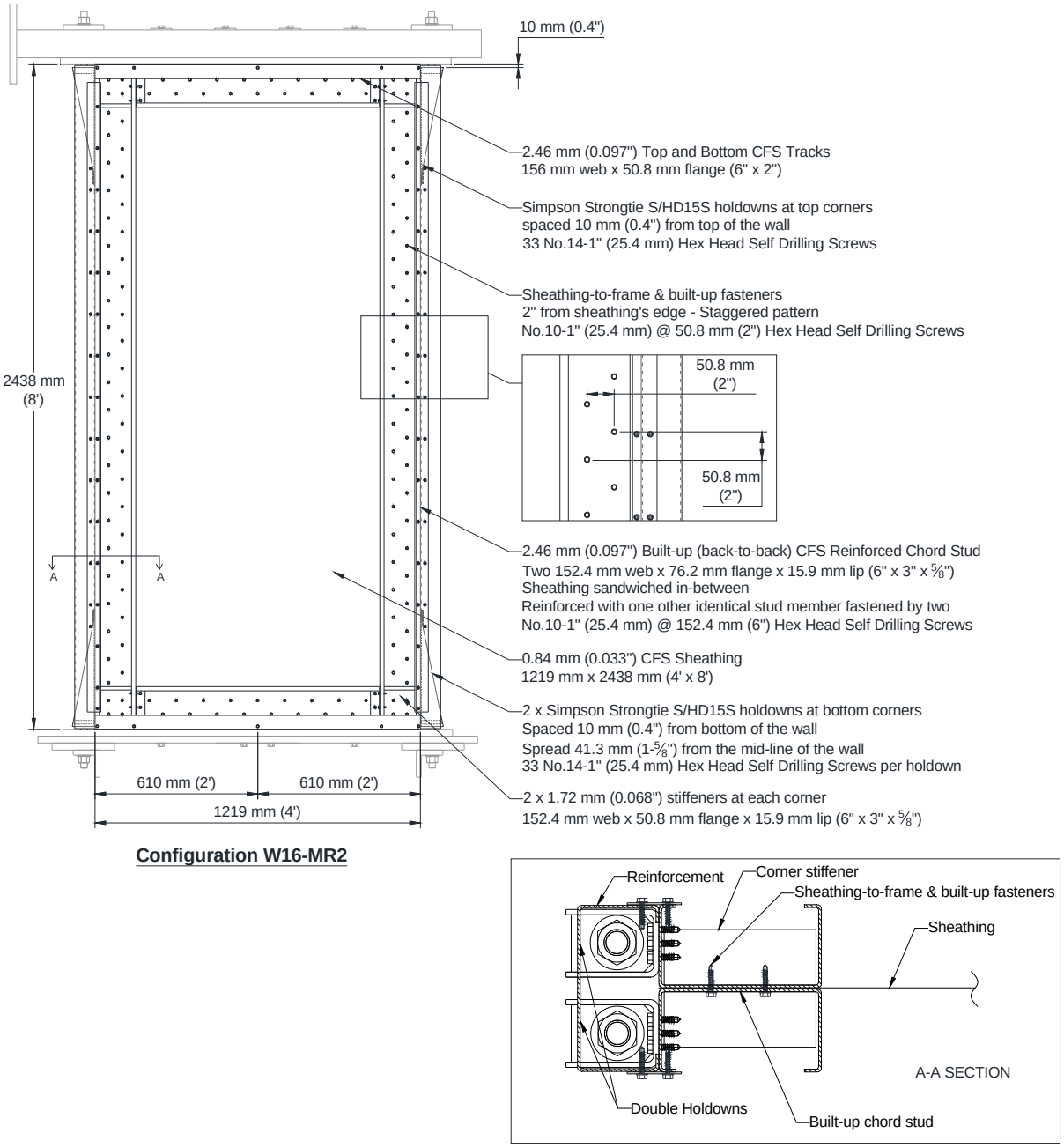

Figure A8: Nominal dimensions and specifications of specimen W16-MR2.

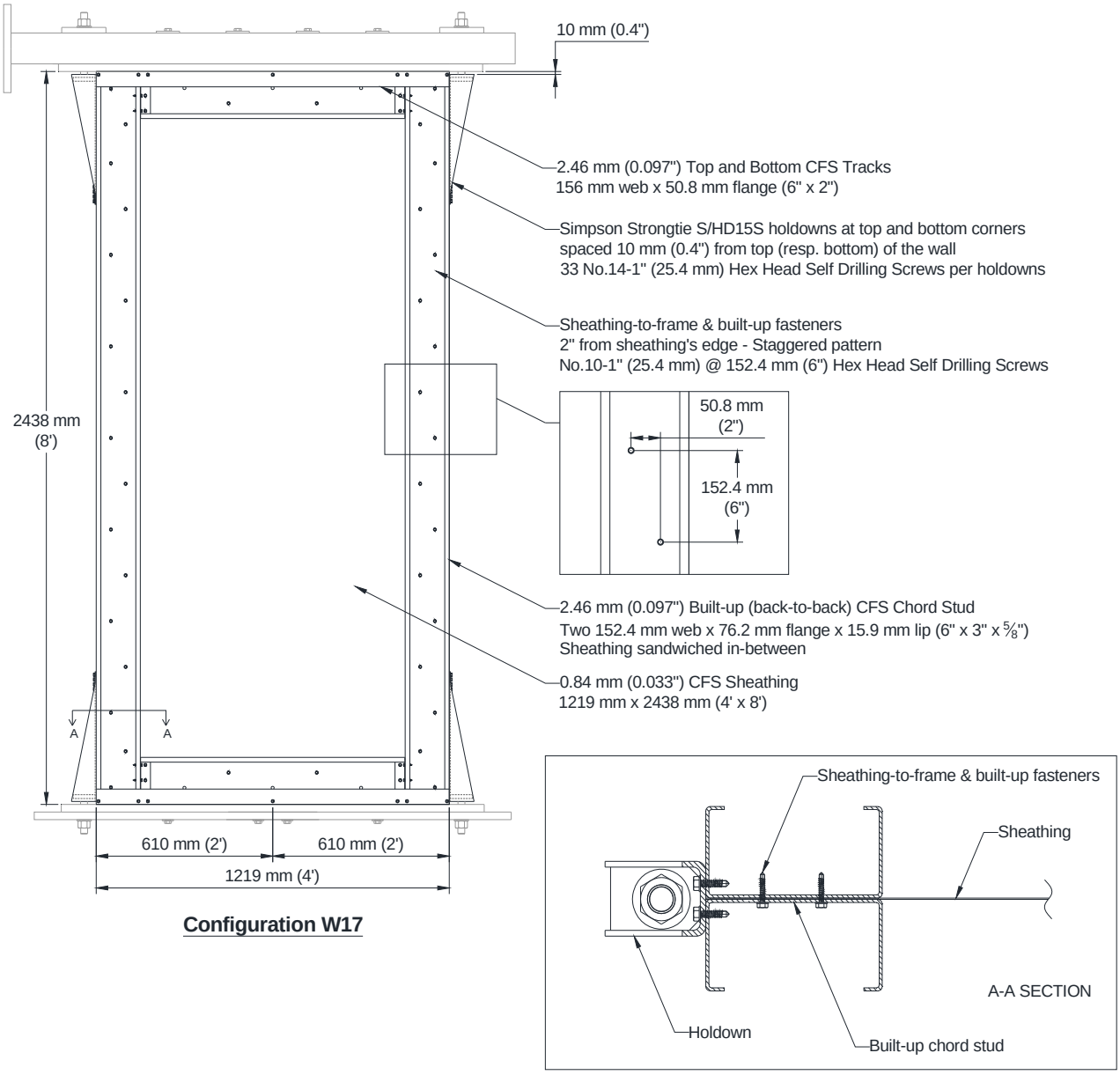

Figure A9: Nominal dimensions and specifications of specimen W17 (M and C).

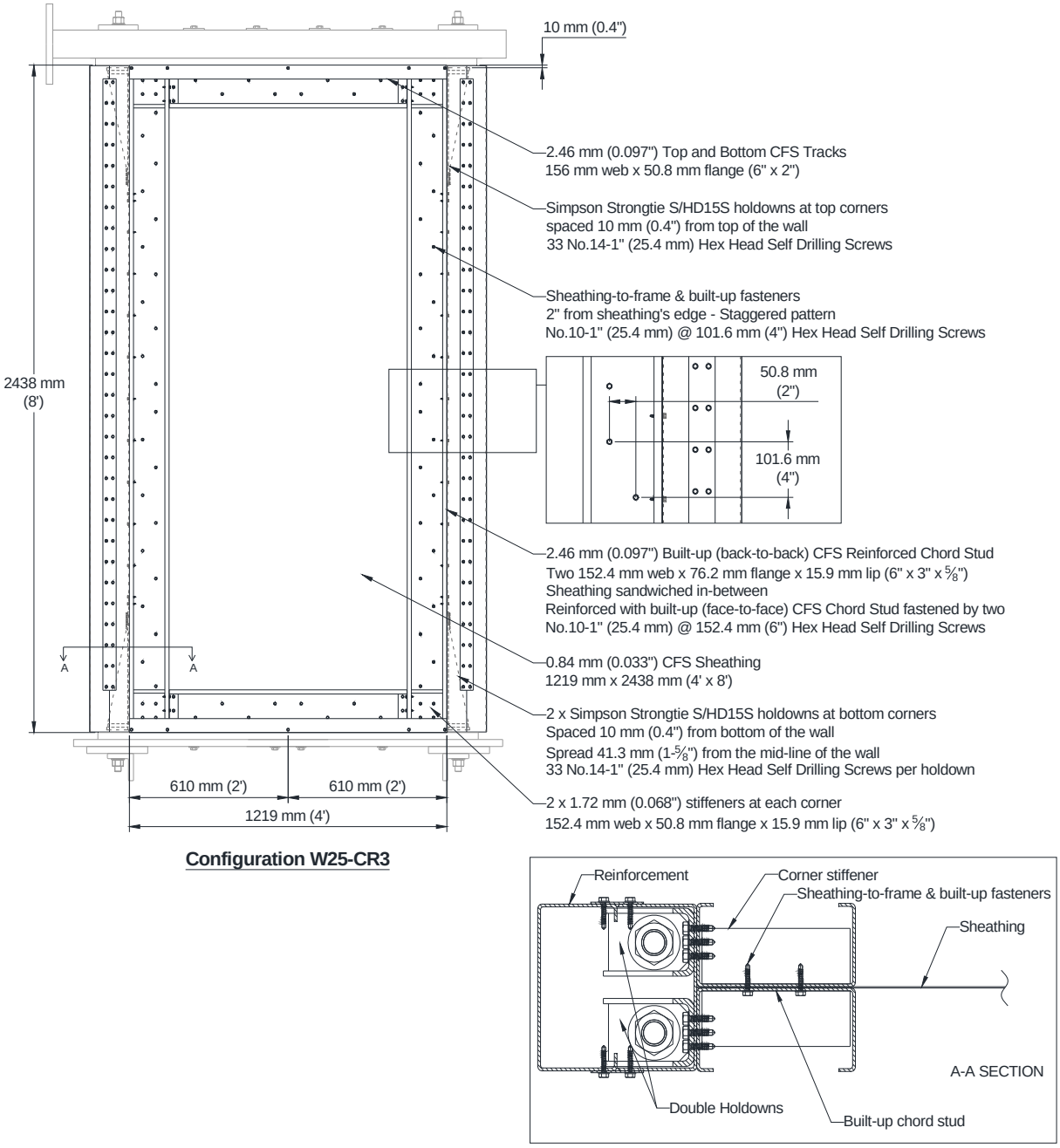

Figure A10: Nominal dimensions and specifications of specimen W25-CR3.

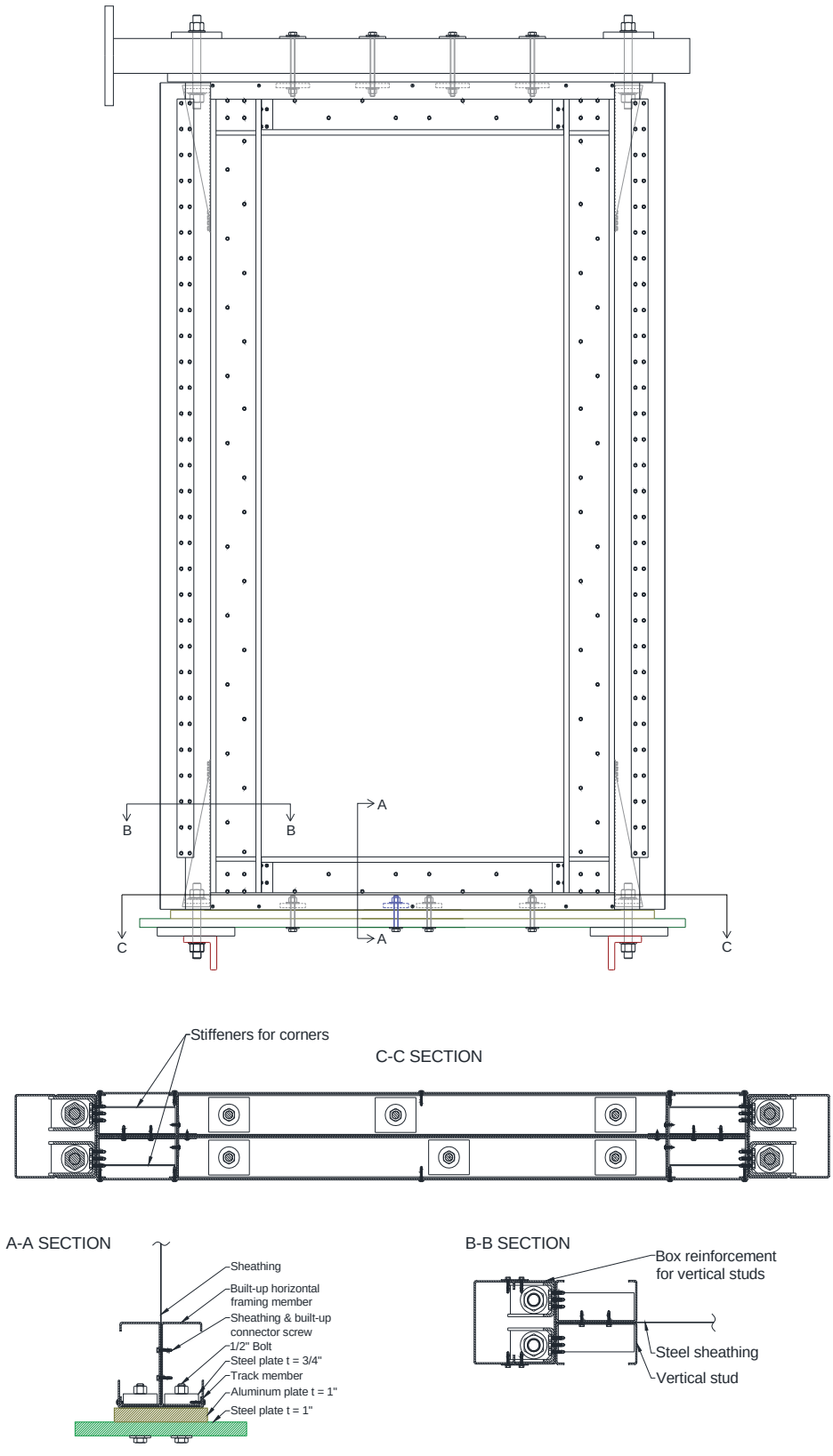

Figure A11: Centre-sheathed configuration cross-section details.

APPENDIX B:

SHEAR WALL SHEAR STRENGTH PREDICTION

USING EFFECTIVE STRIP METHOD

Step-by-step procedure to choose the wall's chord stud section sizes by predicting the wall's nominal shear strength V_n, using the Effective Strip Method, modelling the wall configurations in SAP2000© for analysis, and checking the design of the chord stud members following the AISI S100 Standard *(2012)* / CSA S136 Standard *(2012)* in the CFS 9.0 Software©.

The prediction of the specimens' shear strength and choosing the appropriate chord stud design was an iterative process where modifications to the Effective Strip Method were made and various chord stud sections (including reinforcements) were selected and tested. The steps outlined in this Appendix were repeated several times in order to select the adequate chord stud sections and configurations. A numerical example of the procedure presented is shown at the end of the Appendix.

Step 1) Prediction of the wall's nominal shear strength, V_n, using the Effective Strip Method

V_n was calculated using the Effective Strip Method developed by Yanagi and Yu *(2014)*. Below are the Effective Strip Method equations.

Effective Strip Width

$$W_e = \begin{cases} W_{max,} & if\ \lambda \leq 0.0819 \\ \rho W_{max,} & if\ \lambda > 0.0819 \end{cases} \qquad \text{(Figure B1)}$$

$$W_{max} = W/sin\alpha$$

$$\alpha = tan^{-1}(a)$$

$$\rho = \frac{1 - 0.55(\lambda - 0.08)^{0.12}}{\lambda^{0.12}}$$

$$\lambda = 1.736\frac{\alpha_1\alpha_2}{\beta_1\beta_2\beta_3^2 a}$$

$$\alpha_1 = \frac{F_{e,ush}}{310.3\ MPa}, \qquad \alpha_2 = \frac{F_{e,uf}}{310.3\ MPa}$$

$$F_{e,ush} = R_t F_{ush}, \qquad F_{e,uf} = R_t F_{uf}$$

$$\beta_1 = \frac{t_{sh}}{0.457}, \qquad \beta_2 = \frac{t_f}{0.457}, \qquad \beta_3 = \frac{s}{152.4}$$

where,

W_e = effective strip width (mm);

W_{max} = maximum width of effective strip (mm);

a = shear wall's aspect ratio (height/width);

$F_{e,ush}$ = expected tensile strength of steel sheet sheathing (MPa);

$F_{e,uf}$ = expected controlling tensile strength of framing materials (smaller of track and stud, MPa);

R_t = ratio of expected tensile strength and specified minimum tensile strength (Table A3.2-1 in AISI S400 *(2015)*;

F_{ush} = tensile strength of steel sheet sheathing (MPa);

F_{uf} = controlling tensile strength of framing materials (smaller of track and stud, MPa);

t_{sh} = thickness of sheathing (mm);

t_f = smaller of thickness of track and stud (mm);

s = fastener spacing on the sheathing panel edges (spacing on track and stud are assumed to be equivalent, mm).

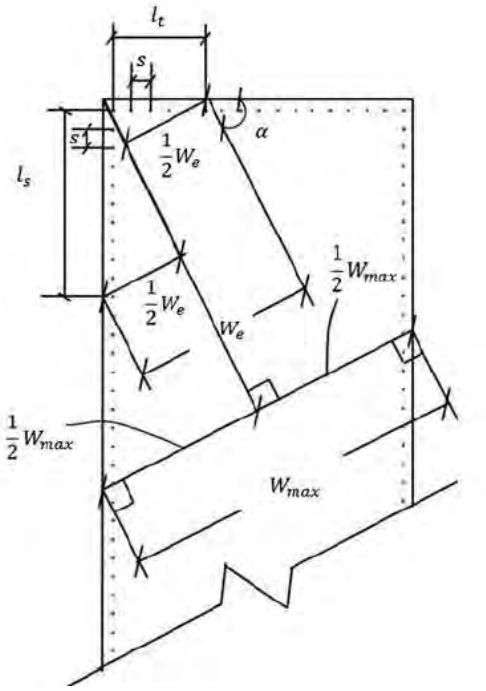

Figure B1: Illustration of effective strip width and maximum effective strip width on a typical sheathing-to-frame fastener connection layout (Yanagi and Yu *(2014))*.

Nominal Capacity of Individual Fasteners

$$P_{ns} = \min(P_{ns,a}, P_{ns,b}, P_{ns,c})$$

$$for\ {}^{t_2}/_{t_1} \leq 1.0 \qquad P_{ns,a} = min\begin{cases} 4.2(t_2^3 d)^{1/2} F_{e,u2} \\ 2.7 t_1 d F_{e,u1} \\ 2.7 t_2 d F_{e,u2} \end{cases}$$

$$for\ {}^{t_2}/_{t_1} \geq 2.5 \qquad P_{ns,a} = min\begin{cases} 2.7 t_1 d F_{e,u1} \\ 2.7 t_2 d F_{e,u2} \end{cases}$$

$$* \textit{Use linear interpolation between the previous cases if } \ 1.0 < {}^{t_2}/_{t_1} \geq 2.5$$

$$F_{e,u1} = R_t F_{u1}, \qquad F_{e,u2} = R_t F_{u2}$$

$$P_{ns,b} = te F_{e,ush}$$

$$e = \frac{w_f}{2cos\alpha} \qquad \text{(Figure B2)}$$

$$P_{ns\,c} = \textit{fastener shear strength provided by manufacturer}$$

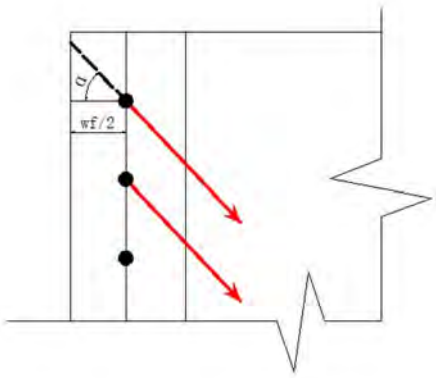

Figure B2: Illustration of the geometry to calculate distance *e*.

where,

t_1 = thickness of member with contact with screw head or washer (mm);

t_2 = thickness of member not in contact with screw head or washer (mm);

d = nominal screw diameter (mm);

F_{u1} = tensile strength of member in contact with screw head or washer (MPa);

F_{u2} = tensile strength of member not in contact with screw head or washer (MPa);

$F_{e,u1}$ = expected tensile strength of member in contact with screw head or washer (MPa);

$F_{e,u2}$ = expected tensile strength of member not in contact with screw head or washer (MPa);

P_{ns} = nominal capacity of individual fasteners (kN);

$P_{ns,a}$ = connection capacity based on tilting and bearing (kN);

$P_{ns,b}$ = connection capacity based on end distance shear (kN);

$P_{ns,c}$ = connection capacity based on manufacturer's shear strength (kN);

t = thickness of part in which the end distance is measured (mm);

e = distance measured in line of force from centre of a standard hole to nearest end of connection (mm);

w_f = width of stud flange (mm).

Nominal Shear Strength of the Shear Wall

$$V_n = min\left\{\left[\left(\frac{W_e}{2s\ sin\alpha}P_{ns,t} + \frac{W_e}{2s\ cos\alpha}\ P_{ns,s} + P_{ns,s\&t}\right)cos\alpha\right], W_e t_{sh} F_{e,ysh}\ cos\alpha\right. \qquad \text{(Figure B3)}$$

$$F_{e,ysh} = R_y F_{ysh}$$

where,

V_n = nominal shear strength of the shear wall (kN);

$P_{ns,s}$ = nominal capacity of individual fasteners in sheathing to stud connection (kN);

$P_{ns,t}$ = nominal capacity of individual fasteners in track connection (kN);

$P_{ns,s\&t}$ = nominal capacity of individual fasteners in stud to track connection (kN);

F_{ysh} = nominal yield stress of sheathing (MPa);

R_y = Ratio of expected yield stress to specified minimum yield stress (Table A3.2-1 in AISI S400 *(2015)*);

$F_{e,ysh}$ = expected yield stress of sheathing (MPa);

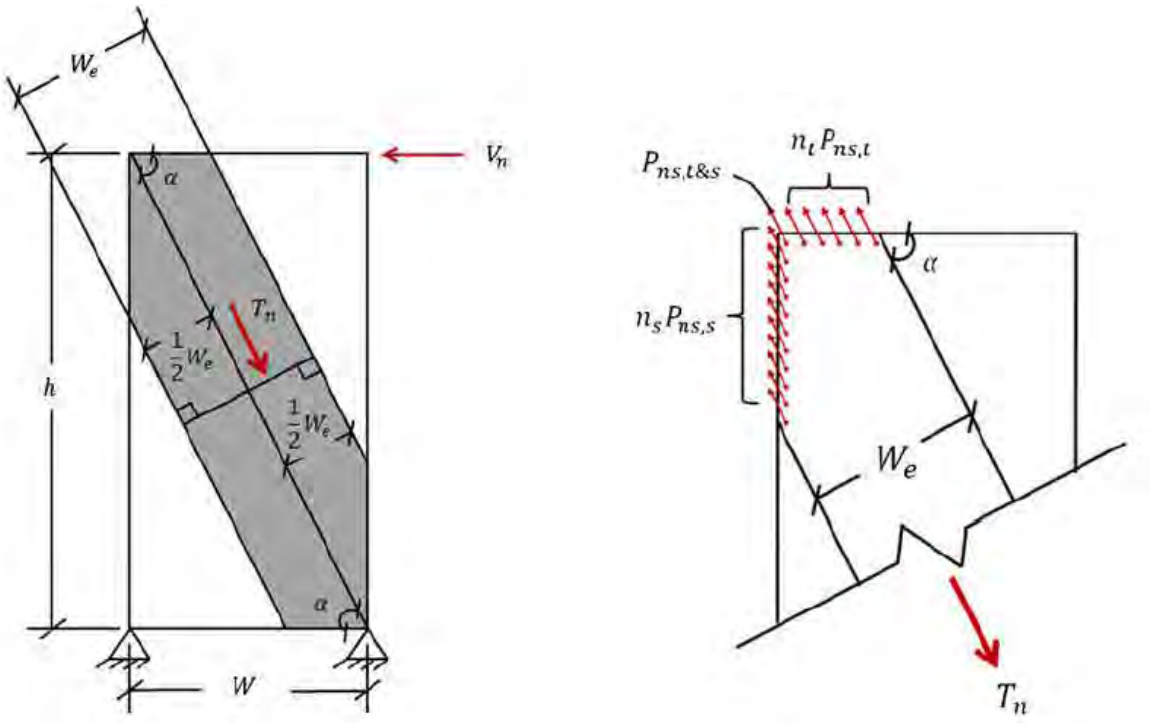

Figure B3: Tension field force in sheathing in equilibrium with sum of shear capacity of connection (Yanagi and Yu *(2014)*).

The Effective Strip Method equations were implemented into a MATLAB code for computational efficiency.

Step 2) Analysis in SAP2000©

SAP2000© models were created for each type of wall configurations (varying frame and sheathing thicknesses and chord stud members) to perform structural analysis to obtain the compression chord stud member forces: axial, *P*, bending moment, *M*, and shear, *V*.

Modelling of Equivalent Effective Strip Elements

In the models, the effective width of the sheathing, W_e, was represented by equivalent strip elements pin-connected to the studs and tracks at the appropriate fastener spacing. The strip elements' dimensions and section properties were calculated based on the geometry of the wall and of the diagonal tension field as shown by the following equations.

$$n = \frac{W_e}{2s\,cos\alpha}$$

$$s_t = \frac{s}{a}$$

$$w_s = \frac{W_e}{2n+1}$$

$$A_s = w_s t_{sh}$$

$$I_x = \frac{t_{sh} w_s^3}{12} \; and \; I_y = \frac{w_s t_{sh}^3}{12}$$

$$S_x = \frac{t_{sh} w_s^2}{6} \; and \; S_y = \frac{w_s t_{sh}^2}{6}$$

where,

n = number of screws along the chord studs and tracks within the effective width, W_e;

s = fasteners spacing along the chord studs (mm);

α = angle between the track and the effective width W_e;

s_t = theoretical track fastener spacing in order connect the same number of strip elements along the tracks and chord studs in the model (mm);

a = wall's aspect ratio;

w_s = width of one strip element, where the sum of the widths of all elements is equal to W_e (mm);

A_s = cross-sectional area of one strip element (mm^2);

t_{sh} = thickness of one strip element taken as the thickness of the sheathing (mm);

I_x and I_y = moment of inertias of one strip element (mm^4);

S_x and S_y = elastic section moduli of one strip element (mm^3);

The plastic section moduli, Z_x and Z_y, were assumed to be the same as the elastic section moduli because local buckling and overall buckling of the section were assumed to occur before plastic deformation was observed.

The section properties of the strip elements were computed in MATLAB and then defined as frame sections in SAP2000© (Figure B4). Frame sections were also created for the tracks and chord studs using SAP2000©'s cold-formed steel sections. In the cases where the section shape was not available in SAP2000© (i.e. chord stud built-up members), a channel section was chosen and Property Modifiers were input to represent the properties of the actual section. Once all materials and frame sections were defined, they were assigned to the model as shown in Figure B5.

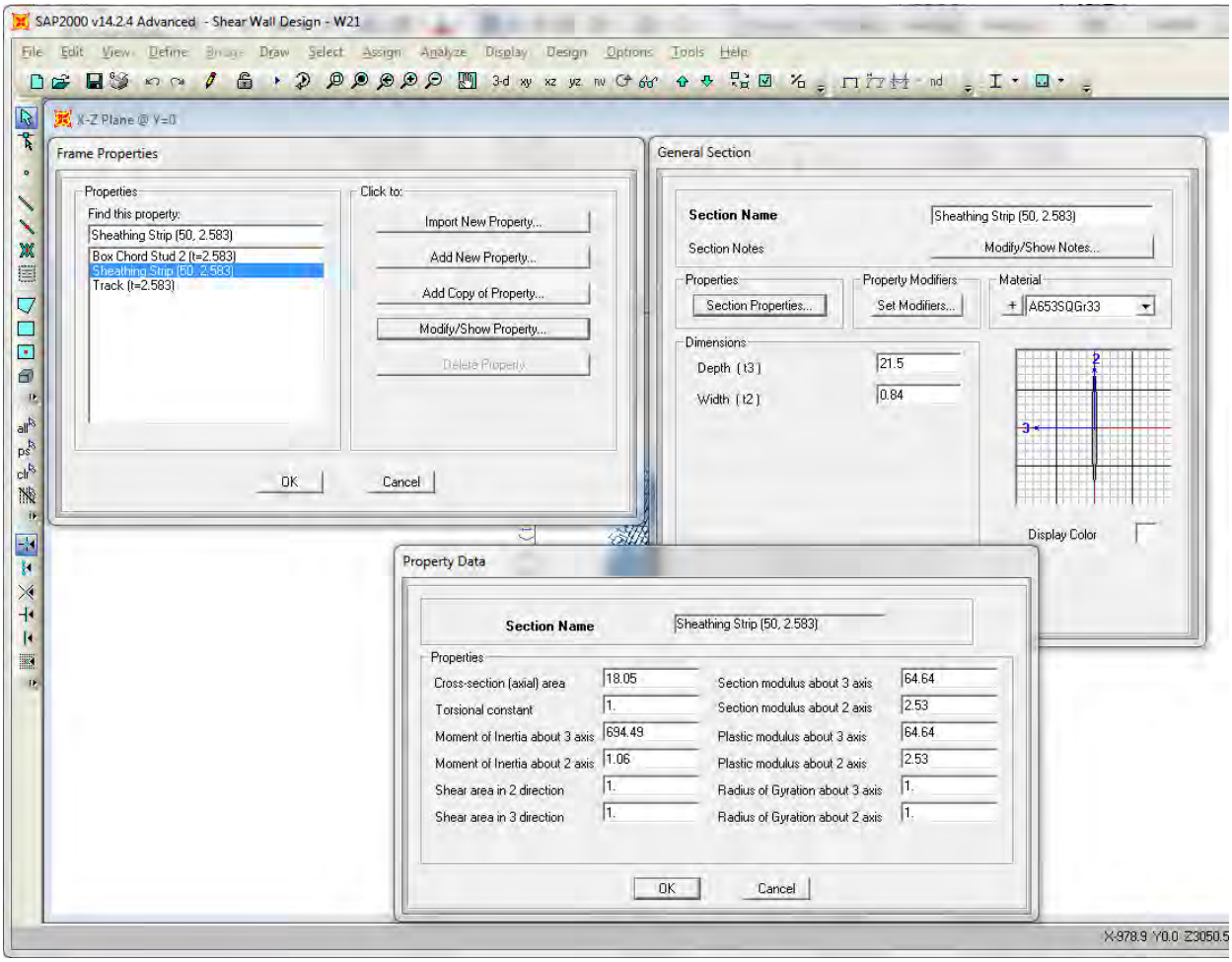

Figure B4: Strip element defined as frame section in SAP2000© model.

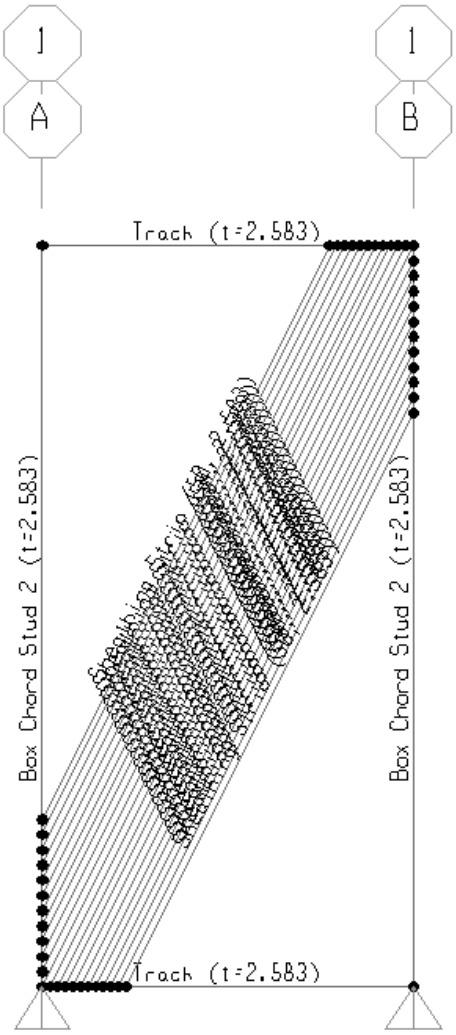

Figure B5: SAP2000© model of shear wall W21 with assigned frame sections.

Load Assignment and Analysis

A Load Pattern was defined as SHEAR since the load to be applied at the top of the wall was a shear load. The nominal shear strength, V_n, calculated previously was assigned, under Frame Loads, as a uniformly distributed shear load in the global x-direction in *kN/mm* along the top track of the wall as seen in Figure B6.

Before running the analysis, the model was viewed in Extruded view and rotated in 3-D (Figure B7) to verify that all members were oriented correctly.

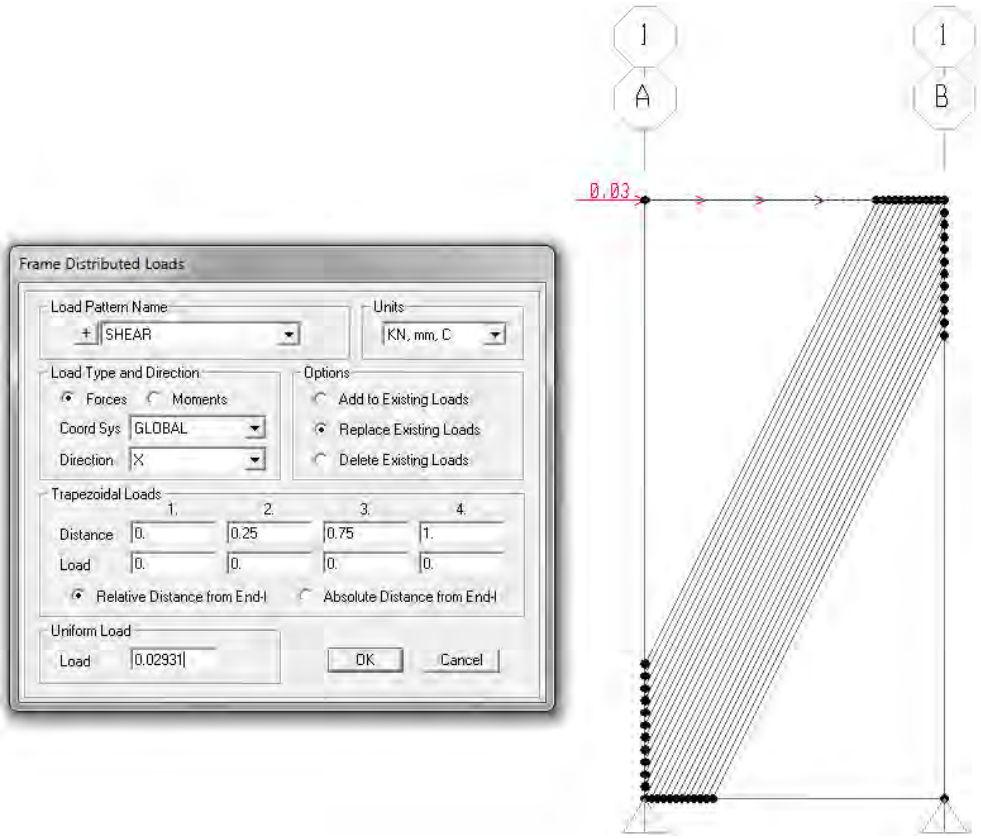

Figure B6: Uniformly distributed shear load assignment in SAP2000©.

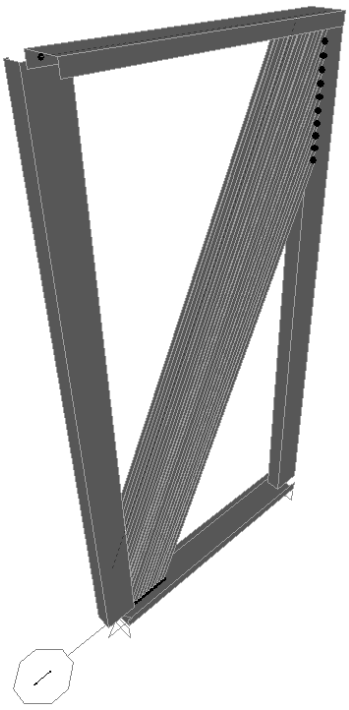

Figure B7: SAP2000© shear wall model in Extruded view.

Run Analysis was selected and the maximum compression chord stud member forces (*P*, *M*, and *V*) were recorded, shown in Figure B8.

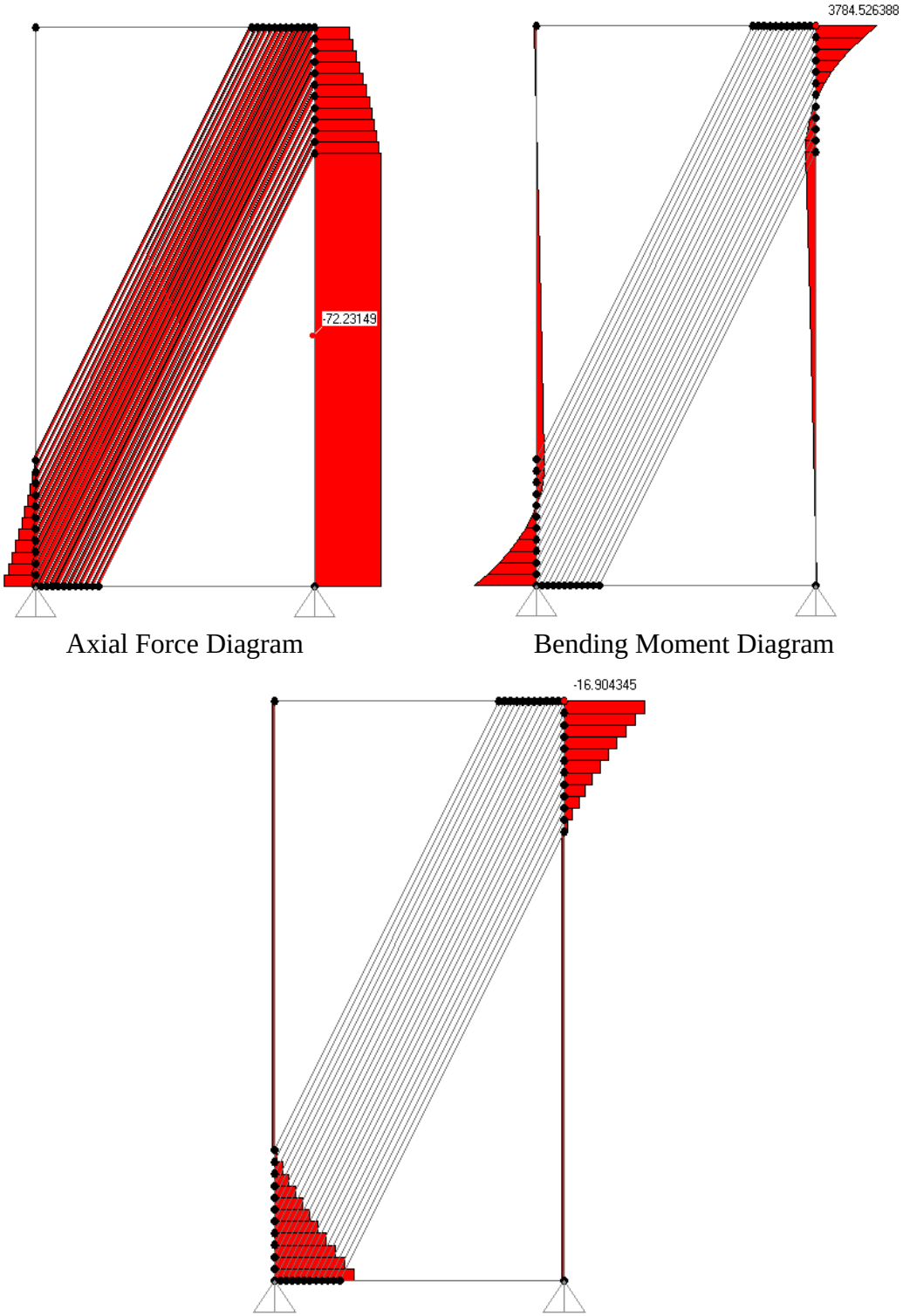

Axial Force Diagram

Bending Moment Diagram

Shear Force Diagram

Figure B8: Analysis force diagrams of specimen W21 in SAP2000©

Step 3) Design check of chord studs

The design of the compression chord studs under the forces resulting from the shear force at the top of the wall was checked to insure that the frame would not fail during the tests. This design check was done using AISI S100 Standard *(2012)* / CSA S136 Standard *(2012)* and verified using the CFS 9.0 Software© where the most recent specification available, 2012 NAS – Canada (LSD), was selected.

AISI S100 / CSA S136 Interaction Equations

The design of the compression chord studs was determined adequate if the shear-moment and axial compression-moment interaction equations were satisfied.

$$\sqrt{\left(\frac{M_f}{\phi_b M_{nxo}}\right)^2 + \left(\frac{V_f}{\phi_v V_n}\right)^2} \leq 1.0$$

$$\frac{P_f}{\phi_c P_n} + \frac{C_{mx} M_{fx}}{\phi_b M_{nx} \propto_x} \leq 1.0$$

$$\frac{P_f}{\phi_c P_{no}} + \frac{M_{fx}}{\phi_b M_{nx}} \leq 1.0$$

where,

M_f = required flexural strength;

V_f = required shear strength;

P_f = required compressive axial strength;

M_{nxo} = nominal flexural strength about centroidal x-axis;

V_n = nominal shear strength when shear alone is considered;

P_{no} = nominal axial strength;

P_n = nominal axial strength when $F_n = F_y$;

$Ø_b$ = resistance factor for bending, 0.90;

$Ø_v$ = resistance factor for shear, 0.80;

$Ø_c$ = resistance factor for compressive load, 0.80;

C_{mx} = end moment coefficient, 1.0;

α_x = magnification factor, Eq. C5.2.2-4 in CSA S136 Standard *(2012)*.

Creating Chord Stud Sections and Member Check in CFS 9.0 Software©

To verify the chord stud design in CFS 9.0 Software©, first, the chord stud cross-section was created and the appropriate material properties entered in the Section Inputs window. A Member Check was then computed in order to check the design of the chord stud. In the Member Parameters window (Figure B9) the unbraced lengths, L_x, L_y, and L_t, were taken as the height of the wall and the maximum internal forces obtained from the SAP2000© analysis were entered (P, M_x, and V_x).

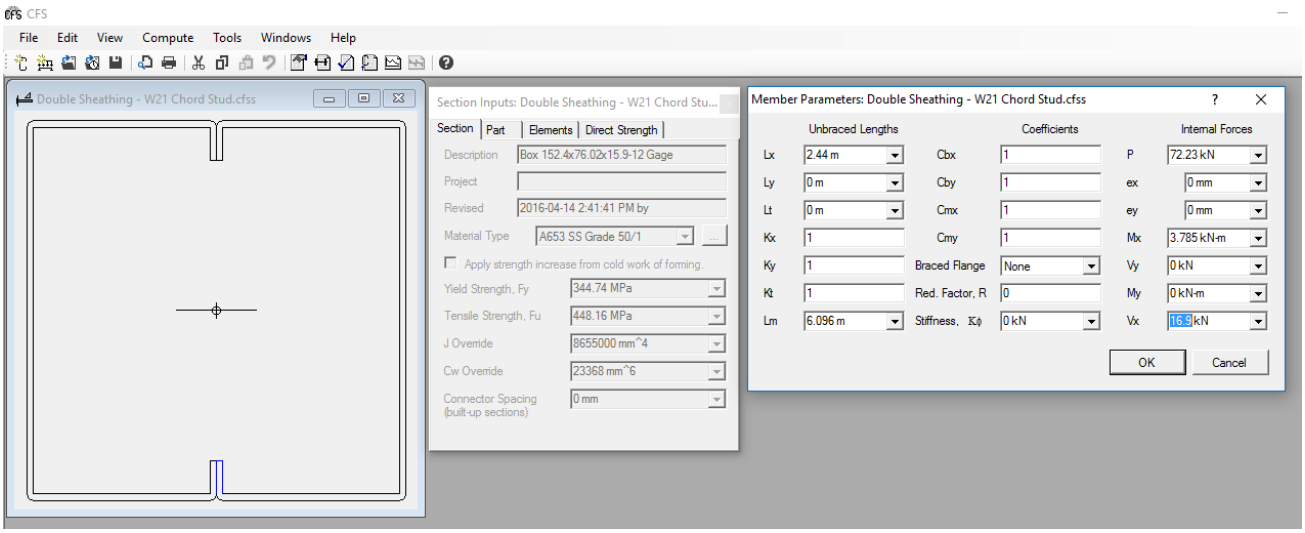

Figure B9: CFS 9.0 Software© Member Parameters window inputs.

The cold-formed steel beam-column and moment-shear interaction equations from the AISI S100 Standard *(2012)* / CSA S136 Standard *(2012)* were computed in CFS 9.0 Software© as a result of the Member Check. An example of the final Member Check report is shown in Figure B10. The chord stud was considered adequate if the interaction equations were satisfied.

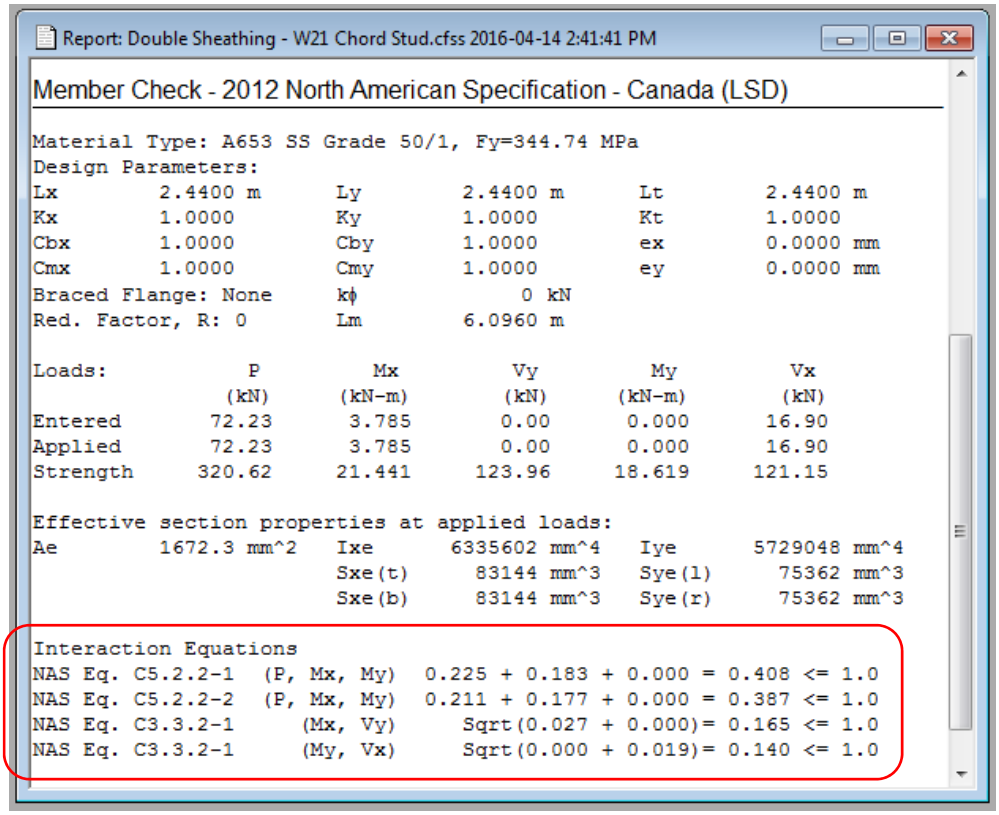

Report: Double Sheathing - W21 Chord Stud.cfss 2016-04-14 2:41:41 PM

Member Check - 2012 North American Specification - Canada (LSD)

```
Material Type: A653 SS Grade 50/1, Fy=344.74 MPa
Design Parameters:
Lx         2.4400 m      Ly         2.4400 m      Lt         2.4400 m
Kx         1.0000        Ky         1.0000        Kt         1.0000
Cbx        1.0000        Cby        1.0000        ex         0.0000 mm
Cmx        1.0000        Cmy        1.0000        ey         0.0000 mm
Braced Flange: None      kϕ               0 kN
Red. Factor, R: 0        Lm         6.0960 m

Loads:             P          Mx          Vy          My          Vx
                  (kN)       (kN-m)      (kN)        (kN-m)      (kN)
Entered          72.23       3.785       0.00        0.000       16.90
Applied          72.23       3.785       0.00        0.000       16.90
Strength        320.62      21.441     123.96       18.619      121.15

Effective section properties at applied loads:
Ae         1672.3 mm^2   Ixe       6335602 mm^4   Iye       5729048 mm^4
                         Sxe(t)      83144 mm^3   Sye(l)      75362 mm^3
                         Sxe(b)      83144 mm^3   Sye(r)      75362 mm^3

Interaction Equations
NAS Eq. C5.2.2-1   (P, Mx, My)   0.225 + 0.183 + 0.000 = 0.408 <= 1.0
NAS Eq. C5.2.2-2   (P, Mx, My)   0.211 + 0.177 + 0.000 = 0.387 <= 1.0
NAS Eq. C3.3.2-1      (Mx, Vy)      Sqrt(0.027 + 0.000)= 0.165 <= 1.0
NAS Eq. C3.3.2-1      (My, Vx)      Sqrt(0.000 + 0.019)= 0.140 <= 1.0
```

Figure B10: CFS 9.0 Software© Member Check report.

Effective Strip Method Modifications

The Effective Strip Method developed by Yanagi and Yu *(2014)* was based on research done on lower strength shear walls. These shear walls were built using a single-sided sheathing placement, currently recommended in the standards, with thinner sheathing and framing members than those tested in the research presented in this report.

After testing the first shear walls, it was observed that the shear strength, V_n, calculated using the Effective Strip Method was lower than the forces reached during the tests and the tension field width was wider than the calculated effective strip width, W_e. Therefore modifications to this method were made to improve the wall's shear strength prediction and to select chord stud sections for the subsequent specimens.

Observed Effective Width, W_e

To predict the shear strength of the next specimens, the effective tension field width was not calculated using the strip method equation, but instead determined based on observations from previous tests. The width was determined by looking at the damaged sheathing and counting the sheathing screw connections with bearing damage. Using this wider effective width a higher V_n was predicted which required stronger chord studs.

To strengthen the chord studs, reinforcing members were attached to the chord studs. Different reinforcement configurations were tested until it was observed that all screws connections around the sheathing were deforming in bearing and the entire height of the wall contributed to the tension field. Finally, to predict V_n of the specimens, W_e was taken as the full height of the wall, H.

3-Ply Tilting and Bearing Connection Capacity

The Effective Strip Method uses the 2-ply (single shear) screw tilting and bearing connection capacity to calculate P_{ns}. However, the centre-sheathed design used a 3-ply (double shear) connection between the frame and the sheathing and therefore using the Effective Strip Method led to under predicting the tilting and bearing capacity of the connection.

Currently, there does not exist an equation to predict the double shear tilting and bearing capacity of screw connections, instead the cold-formed steel bolt bearing strength for an inside sheet of double shear connection equation from AISI S100 *(2016)* / CSA S136 *(2016)* was used to calculate the fastener's nominal tilting and bearing capacity, $P_{ns,a}$.

$$P_{ns,a} = Cm_f dt_{sh} F_{ush}$$

where,

C = bearing factor, 3.0 for $d/t_{sh} < 10$

d = diameter of fastener (mm);

t_{sh} = thickness of the sheathing (mm);

F_{ush} = tensile strength of the sheathing (MPa);

SHEAR STRENGTH PREDICTION AND DESIGN CHECK EXAMPLE
SPECIMEN W21

1) Strip Method MATLAB Code Results

```
SHEAR WALL PROPERTIES:
h = 2440.00 mm
w = 1220.00 mm
a = 2.00(wall aspect ratio)
tsh = 0.84 mm (sheathing thickness)
tf = 2.58 mm (framing thickness)
s = 50.00 mm, s = 100.00 mm, and s = 150.00 mm (fastener spacing tested)
d = 4.826 mm (fastener's nominal diameter - No 10 screws)
Fye,sh = 345.00 MPa (expected nominal yield strength of sheathing)
Fye,f = 385.00 MPa (expected nominal yield strength of framing)
Fue,sh = 372.00 MPa (expected ultimate tensile strength of sheathing)
Fue,f = 495.00 MPa (expected ultimate yield strength of sheathing)
alpha = 63.43 (tension force angle)
wf = 76.02 mm (flange width of stud)

Using s = 50.00 mm

EFFECTIVE STRIP WIDTH OF THE SHEATHING:
We = 555.62 mm

NOMINAL SHEAR CAPACITY OF FASTENERS:

Sheathing to Stud Connection
Pns,s(bearing) = 4.07 kN
Pns,s(end distance) = 26.56 kN
Pns,s(manufacturer) = 6.23 kN

Pns,s = 4.07 kN

Sheathing to Track Connection
Pns,t = 4.07 kN

Sheathing to Stud and Track Connection
Pns,st = 4.07 kN

NOMINAL SHEAR CAPACITY OF THE SHEAR WALL:
Vn = 35.76 kN (shear force)
vn = 29.31 kN/m (shear flow)

PARAMETERS FOR SAP2000 MODEL:
n,s = 12.42 (number of screws on stud's effective length)
s,t = 25.00 mm (spacing of screws on track)
ws = 21.50 mm (width of one strip)
Ix,strip = 695.26 mm^4
Iy,strip = 1.06 mm^4
Sx,strip = 64.69 mm^3
Sy,strip = 2.53 mm^3
A,strip = 18.06 mm^2
```

2) SAP2000 Model Analysis Results

Member forces along height of compression chord stud (values exported from SAP2000©). Maximum M3, V2, and P selected.

TABLE: Element Forces - Frames				
Station	**OutputCase**	**P**	**V2**	**M3**
mm	Text	KN	KN	KN-mm
0	SHEAR	-72.23149017	0.388237152	99.68667432
1220	SHEAR	-72.23149017	0.388237152	-373.9626516
1890	SHEAR	-72.23149017	0.388237152	-634.0815438
1890	SHEAR	-70.14597936	-0.654518256	-634.0815438
1940	SHEAR	-70.14597936	-0.654518256	-601.3556309
1940	SHEAR	-67.85147319	-1.801771341	-601.3556309
1990	SHEAR	-67.85147319	-1.801771341	-511.2670639
1990	SHEAR	-65.33745488	-3.058780493	-511.2670639
2040	SHEAR	-65.33745488	-3.058780493	-358.3280393
2040	SHEAR	-62.59622395	-4.429395961	-358.3280393
2090	SHEAR	-62.59622395	-4.429395961	-136.8582412
2090	SHEAR	-59.62431949	-5.91534819	-136.8582412
2140	SHEAR	-59.62431949	-5.91534819	158.9091683
2140	SHEAR	-56.42393759	-7.515539138	158.9091683
2190	SHEAR	-56.42393759	-7.515539138	534.6861252
2190	SHEAR	-53.00434888	-9.225333495	534.6861252
2240	SHEAR	-53.00434888	-9.225333495	995.9528
2240	SHEAR	-49.38331783	-11.03584902	995.9528
2290	SHEAR	-49.38331783	-11.03584902	1547.745251
2290	SHEAR	-45.58852081	-12.93324753	1547.745251
2340	SHEAR	-45.58852081	-12.93324753	2194.407627
2340	SHEAR	-41.65895509	-14.89803039	2194.407627
2390	SHEAR	-41.65895509	-14.89803039	2939.309147
2390	SHEAR	-37.6463262	-16.90434483	2939.309147
2440	SHEAR	-37.6463262	-16.90434483	3784.526388

3) CFS 9.0© Design Check Results

CFS Version 9.0.4
Section: Double Sheathing - W21 Chord Stud.cfss
Box 152.4x76.02x15.9-12 Gage

Rev. Date: 2016-04-14

Printed: 2017-05-24

Full Section Properties

Area	1672.3 mm^2	Wt.	0.12862 kN/m	Width	647.38 mm
Ix	6335602 mm^4	rx	61.551 mm	Ixy	-1 mm^4
Sx(t)	83144 mm^3	y(t)	76.200 mm	α	0.000 deg
Sx(b)	83144 mm^3	y(b)	76.200 mm		
		Height	152.400 mm		
Iy	5729048 mm^4	ry	58.531 mm	Xo	0.000 mm
Sy(l)	75362 mm^3	x(l)	76.020 mm	Yo	0.000 mm
Sy(r)	75362 mm^3	x(r)	76.020 mm	jx	0.000 mm
		Width	152.040 mm	jy	0.000 mm
I1	6335602 mm^4	r1	61.551 mm		
I2	5729048 mm^4	r2	58.531 mm		
Ic	12064650 mm^4	rc	84.938 mm	Cw	2.3368e04 mm^6
Io	12064650 mm^4	ro	84.938 mm	J	8655036 mm^4

Member Check - 2012 North American Specification - Canada (LSD)

Material Type: A653 SS Grade 50/1, Fy=344.74 MPa
Design Parameters:

Lx	2.4400 m	Ly	2.4400 m	Lt	2.4400 m
Kx	1.0000	Ky	1.0000	Kt	1.0000
Cbx	1.0000	Cby	1.0000	ex	0.0000 mm
Cmx	1.0000	Cmy	1.0000	ey	0.0000 mm
Braced Flange: None		kϕ	0 kN		
Red. Factor, R: 0		Lm	6.0960 m		

Loads:	P (kN)	Mx (kN-m)	Vy (kN)	My (kN-m)	Vx (kN)
Entered	72.23	3.785	0.00	0.000	16.90
Applied	72.23	3.785	0.00	0.000	16.90
Strength	320.62	21.441	123.96	18.619	121.15

Effective section properties at applied loads:

Ae	1672.3 mm^2	Ixe	6335602 mm^4	Iye	5729048 mm^4
		Sxe(t)	83144 mm^3	Sye(l)	75362 mm^3
		Sxe(b)	83144 mm^3	Sye(r)	75362 mm^3

Interaction Equations

NAS Eq. C5.2.2-1	(P, Mx, My)	0.225 + 0.183 + 0.000 = 0.408 <= 1.0
NAS Eq. C5.2.2-2	(P, Mx, My)	0.211 + 0.177 + 0.000 = 0.387 <= 1.0
NAS Eq. C3.3.2-1	(Mx, Vy)	Sqrt(0.027 + 0.000)= 0.165 <= 1.0
NAS Eq. C3.3.2-1	(My, Vx)	Sqrt(0.000 + 0.019)= 0.140 <= 1.0

APPENDIX C:

CYCLIC TESTING PROTOCOLS

DOUBLE-SHEATHED CONFIGURATIONS

Table C1: W19-C CUREE Protocol

F_u = 48.262 kN (10850 lb)	Frame: 1.73 mm (0.068”)
$\Delta_{0.8Fu}$ = 57.048 mm (2.25”)	Sheathing: 2 x 0.36 mm (0.014”)
Δ = 0.60 $\Delta_{0.8Fu}$ = 34.229 mm (1.35”)	Screw Pattern: 50 mm (2”)

Displacement	Actuator Input (mm)	No. of Cycles	Cycle Type
0.050 Δ	1.729	6	Initiation
0.075 Δ	2.593	1	Primary
0.056 Δ	1.936	6	Trailing
0.10 Δ	3.458	1	Primary
0.075 Δ	2.593	6	Trailing
0.20 Δ	6.916	1	Primary
0.15 Δ	5.187	3	Trailing
0.30 Δ	10.373	1	Primary
0.225 Δ	7.780	3	Trailing
0.40 Δ	13.831	1	Primary
0.30 Δ	10.373	2	Trailing
0.70 Δ	24.205	1	Primary
0.525 Δ	18.153	2	Trailing
1.00 Δ	34.578	1	Primary
0.75 Δ	25.933	2	Trailing
1.5 Δ	51.867	1	Primary
1.125 Δ	38.900	2	Trailing
2.00 Δ	69.156	1	Primary
1.5 Δ	51.867	2	Trailing
2.5 Δ	86.445	1	Primary
1.875 Δ	64.834	2	Trailing
3.00 Δ	103.734	1	Primary
2.25 Δ	77.800	2	Trailing
3.50 Δ	121.023	1	Primary
2.625 Δ	90.767	2	Trailing

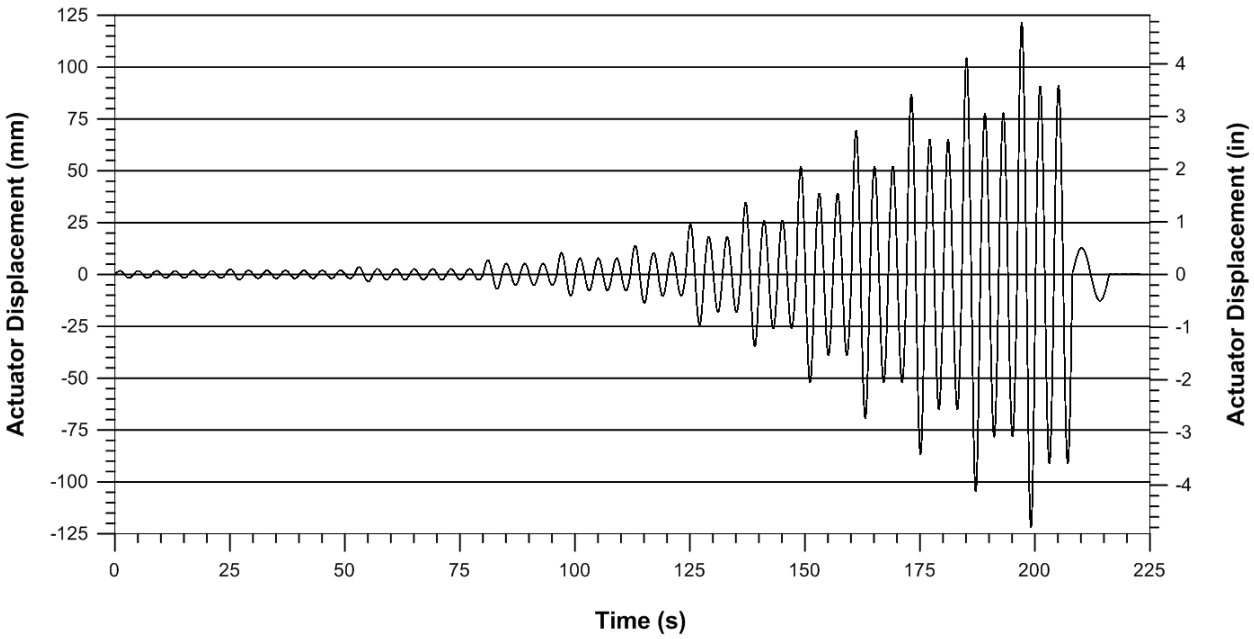

Figure C1: W19-C CUREE Displacement Time-History. Frequency of 0.25 Hz.

Table C2: W20-C CUREE Protocol

F_u = 33.283 kN (7482.3 lb)	Frame: 1.73 mm (0.068”)
$\Delta_{0.8Fu}$ = 67.401 mm (2.65”)	Sheathing: 2 x 0.36 mm (0.014”)
Δ = 0.60 $\Delta_{0.8Fu}$ = 40.44 mm (1.59”)	Screw Pattern: 100 mm (4”)

Displacement	Actuator Input (mm)	No. of Cycles	Cycle Type
0.050 Δ	2.0220	6	Initiation
0.075 Δ	3.0330	1	Primary
0.056 Δ	2.2647	6	Trailing
0.10 Δ	4.0440	1	Primary
0.075 Δ	3.0330	6	Trailing
0.20 Δ	8.0881	1	Primary
0.15 Δ	6.0661	3	Trailing
0.30 Δ	12.1321	1	Primary
0.225 Δ	9.0991	3	Trailing
0.40 Δ	16.1761	1	Primary
0.30 Δ	12.1321	2	Trailing
0.70 Δ	28.3082	1	Primary
0.525 Δ	21.2312	2	Trailing
1.00 Δ	40.4403	1	Primary
0.75 Δ	30.3303	2	Trailing
1.5 Δ	60.6605	1	Primary
1.125 Δ	45.4954	2	Trailing
2.00 Δ	80.8807	1	Primary
1.5 Δ	60.6605	2	Trailing
2.5 Δ	101.1009	1	Primary
1.875 Δ	75.8257	2	Trailing
3.00 Δ	121.3210	1	Primary
2.25 Δ	90.9908	2	Trailing

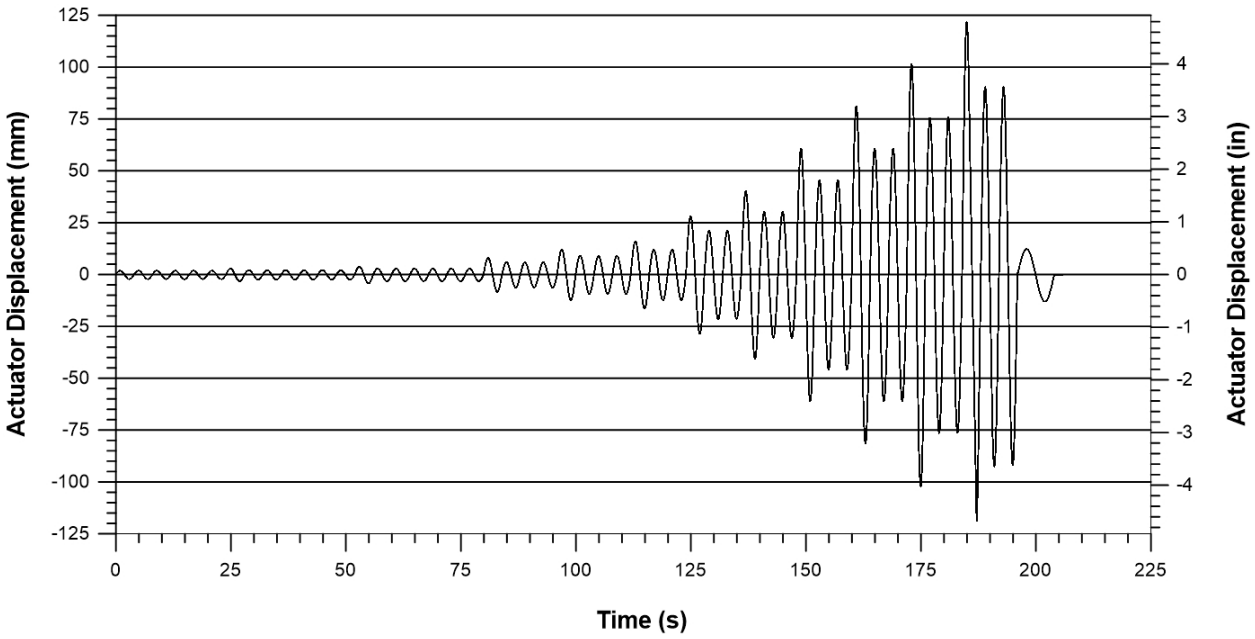

Figure C2: W20-C CUREE Displacement Time-History. Frequency of 0.25 Hz.

Table C3: W21-C CUREE Protocol

F_u = 55.961 kN (12580 lb)	Frame: 2.46 mm (0.097”)
$\Delta_{0.8Fu}$ = 56.202 mm (2.21”)	Sheathing: 2 x 0.36 mm (0.014”)
Δ = 0.60 $\Delta_{0.8Fu}$ = 33.721 mm (1.33”)	Screw Pattern: 50 mm (2”)

Displacement	Actuator Input (mm)	No. of Cycles	Cycle Type
0.050 Δ	1.7032	6	Initiation
0.075 Δ	2.5548	1	Primary
0.056 Δ	1.9076	6	Trailing
0.10 Δ	3.4063	1	Primary
0.075 Δ	2.5548	6	Trailing
0.20 Δ	6.8127	1	Primary
0.15 Δ	5.1095	3	Trailing
0.30 Δ	10.2190	1	Primary
0.225 Δ	7.6643	3	Trailing
0.40 Δ	13.6254	1	Primary
0.30 Δ	10.2190	2	Trailing
0.70 Δ	23.8444	1	Primary
0.525 Δ	17.8833	2	Trailing
1.00 Δ	34.0635	1	Primary
0.75 Δ	25.5476	2	Trailing
1.5 Δ	51.0952	1	Primary
1.125 Δ	38.3214	2	Trailing
2.00 Δ	68.1269	1	Primary
1.5 Δ	51.0952	2	Trailing
2.5 Δ	85.1587	1	Primary
1.875 Δ	63.8690	2	Trailing
3.00 Δ	102.1904	1	Primary
2.25 Δ	76.6428	2	Trailing
3.50 Δ	119.2221	1	Primary
2.625 Δ	89.4166	2	Trailing

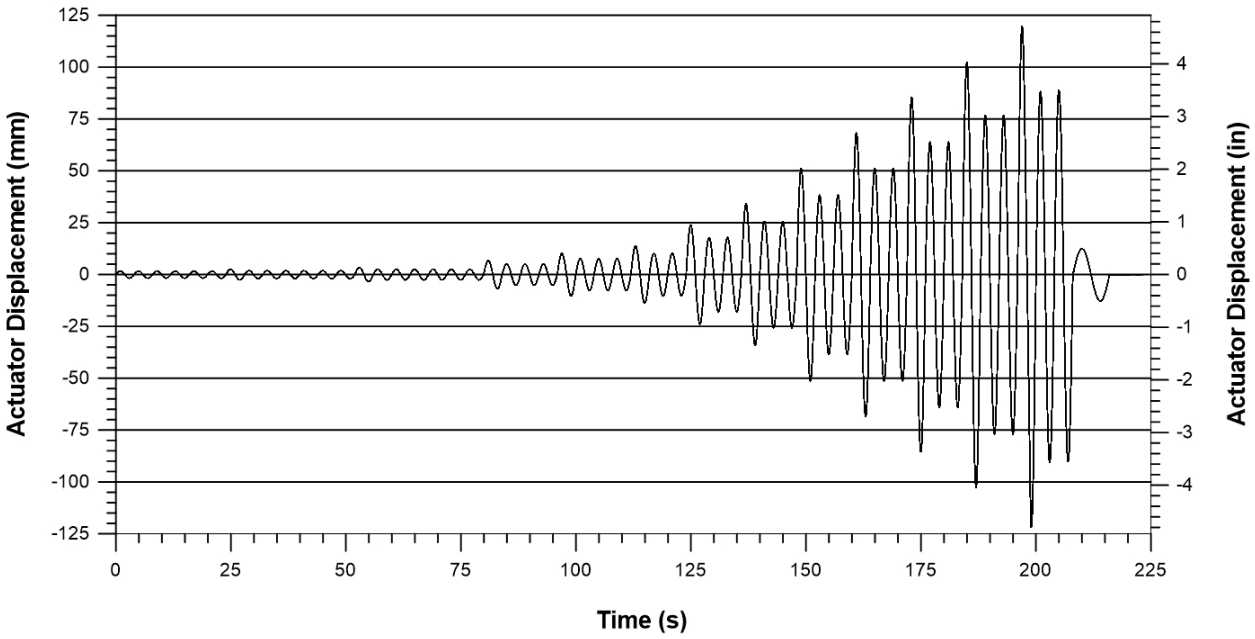

Figure C3: W21-C CUREE Displacement Time-History. Frequency of 0.25 Hz.

Table C4: W22-C CUREE Protocol

F_u = 34.604 kN (7779 lb)	Frame: 2.46 mm (0.097”)
$\Delta_{0.8Fu}$ = 74.472 mm (2.93”)	Sheathing: 2 x 0.36 mm (0.014”)
Δ = 0.60 $\Delta_{0.8Fu}$ = 44.683 mm (1.76”)	Screw Pattern: 100 mm (4”)

Displacement	Actuator Input (mm)	No. of Cycles	Cycle Type
0.050 Δ	2.257	6	Initiation
0.075 Δ	3.385	1	Primary
0.056 Δ	2.528	6	Trailing
0.10 Δ	4.514	1	Primary
0.075 Δ	3.385	6	Trailing
0.20 Δ	9.027	1	Primary
0.15 Δ	6.771	3	Trailing
0.30 Δ	13.541	1	Primary
0.225 Δ	10.156	3	Trailing
0.40 Δ	18.055	1	Primary
0.30 Δ	13.541	2	Trailing
0.70 Δ	31.596	1	Primary
0.525 Δ	23.697	2	Trailing
1.00 Δ	45.137	1	Primary
0.75 Δ	33.853	2	Trailing
1.5 Δ	67.705	1	Primary
1.125 Δ	50.779	2	Trailing
2.00 Δ	90.273	1	Primary
1.5 Δ	67.705	2	Trailing
2.5 Δ	112.842	1	Primary
1.875 Δ	84.631	2	Trailing

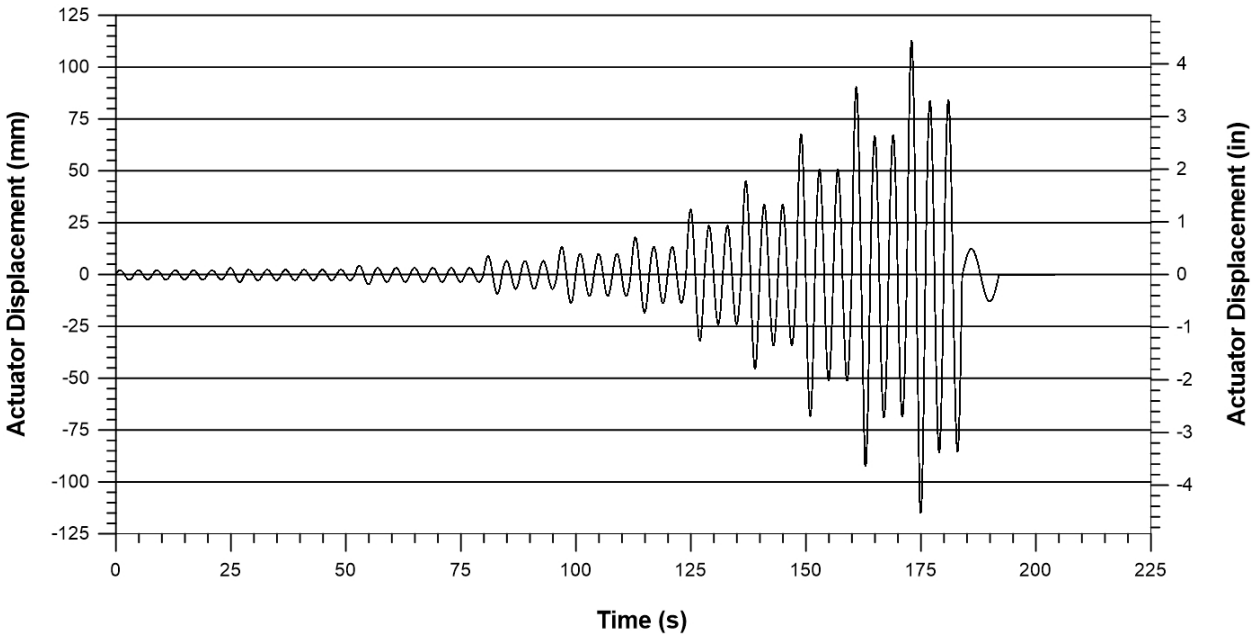

Figure C4: W22-C CUREE Displacement Time-History. Frequency of 0.25 Hz.

CENTRE-SHEATHED CONFIGURATIONS

Table C5: CUREE Protocol for All Centre-Sheathed Symmetric Tests

$\Delta_{0.8Fu}$ = Not Reached
Δ = 60 mm (2.36”)

Displacement	Actuator Input (mm)	No. of Cycles	Cycle Type
0.050 Δ	3.0307	6	Initiation
0.075 Δ	4.5461	1	Primary
0.056 Δ	3.3944	6	Trailing
0.10 Δ	6.0614	1	Primary
0.075 Δ	4.5461	6	Trailing
0.20 Δ	12.1229	1	Primary
0.15 Δ	9.0922	3	Trailing
0.30 Δ	18.1843	1	Primary
0.225 Δ	13.6382	3	Trailing
0.40 Δ	24.2458	1	Primary
0.30 Δ	18.1843	2	Trailing
0.70 Δ	42.4301	1	Primary
0.525 Δ	31.8226	2	Trailing
1.00 Δ	60.6144	1	Primary
0.75 Δ	45.4608	2	Trailing
1.5 Δ	90.9216	1	Primary
1.125 Δ	68.1912	2	Trailing
2.00 Δ	121.2288	1	Primary
1.5 Δ	90.9216	2	Trailing

Table C6: CUREE Protocol for All Centre-Sheathed Asymmetric Tests

$\Delta_{0.8Fu}$ = Not Reached
Δ = 60 mm (2.36”)

Displacement	Actuator Input (mm)	No. of Cycles	Cycle Type
0.050 Δ	3.0307	6	Initiation
0.075 Δ	4.5461	1	Primary
0.056 Δ	3.3944	6	Trailing
0.10 Δ	6.0614	1	Primary
0.075 Δ	4.5461	6	Trailing
0.20 Δ	12.1229	1	Primary
0.15 Δ	9.0922	3	Trailing
0.30 Δ	18.1843	1	Primary
0.225 Δ	13.6382	3	Trailing
0.40 Δ	24.2458	1	Primary
0.30 Δ	18.1843	2	Trailing
0.70 Δ	42.4301	1	Primary
0.525 Δ	31.8226	2	Trailing
1.00 Δ	60.6144	1	Primary
0.75 Δ	45.4608	2	Trailing
1.5 Δ	90.9216	1	Primary
1.125 Δ	68.1912	2	Trailing
2.00 Δ	121.2288	1	Primary
1.5 Δ	90.9216	2	Trailing
2.5 Δ	151.5360	1	Primary
1.875 Δ	113.6520	2	Trailing
3.00 Δ	181.8432	1	Primary
2.25 Δ	136.3824	2	Trailing
3.50 Δ	212.1504	1	Primary
2.625 Δ	159.1128	2	Trailing

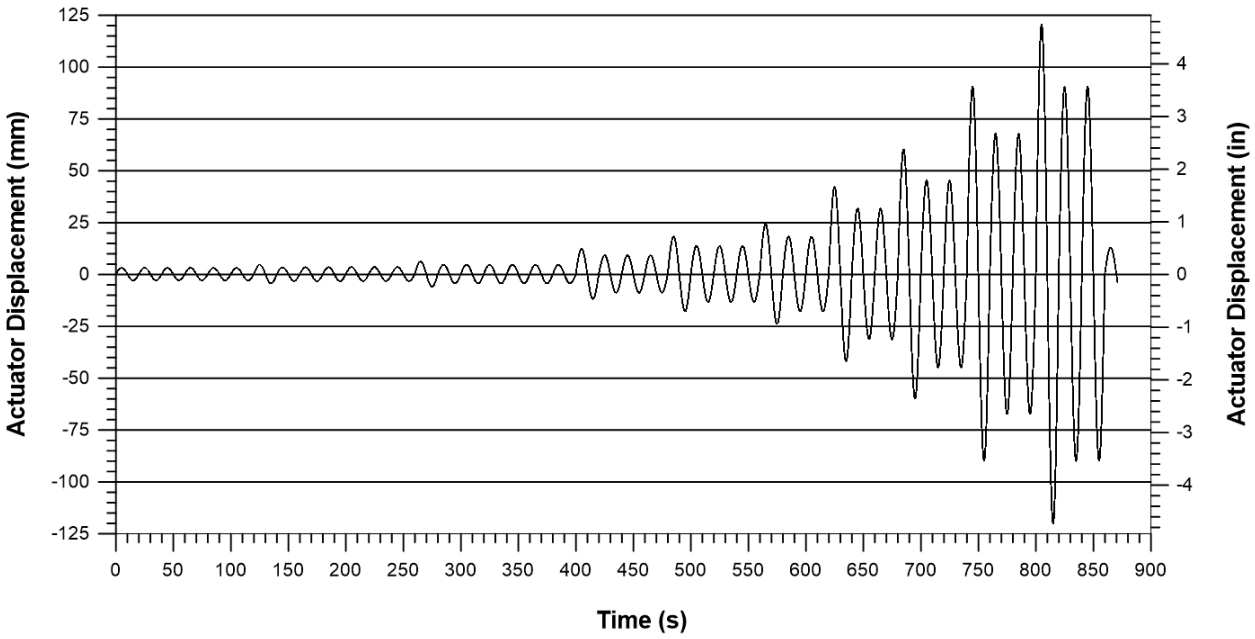

Figure C5: W15-CR3 CUREE Displacement Time-History. Frequency of 0.05 Hz.

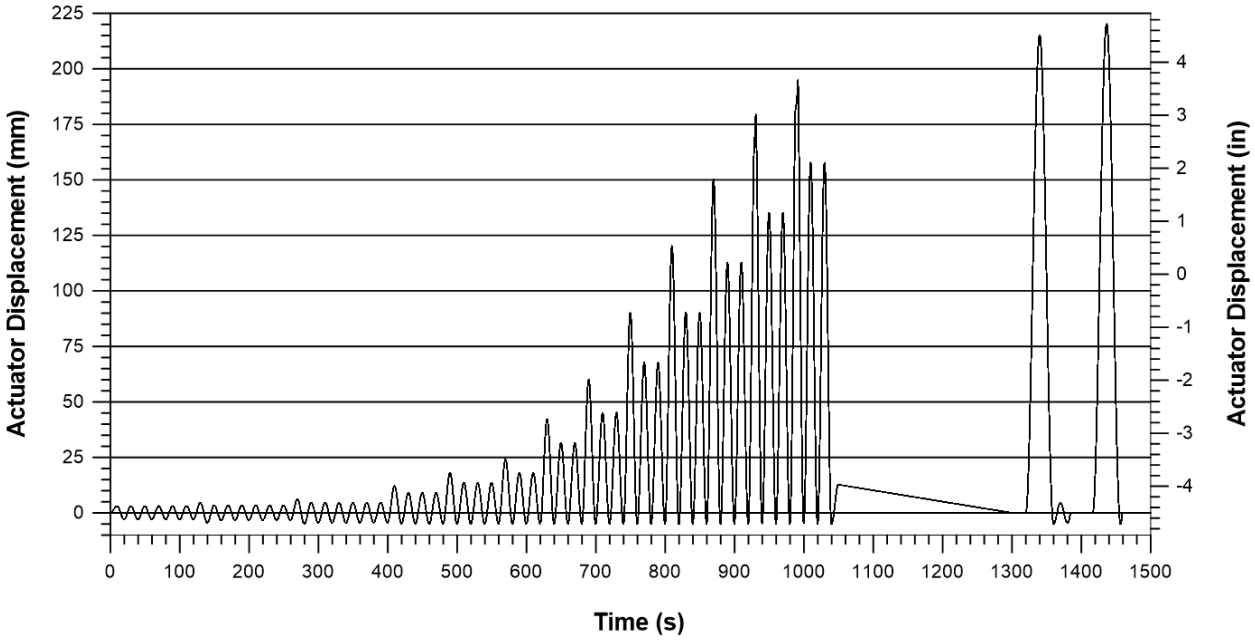

Figure C6: W15B-CR3 CUREE Asymmetric Displacement Time-History. Frequency of 0.05 Hz for the first 11 primary cycles and 0.025 Hz for the last 2 primary cycles which were controlled manually to 215 mm and 220 mm displacements as a safety precaution.

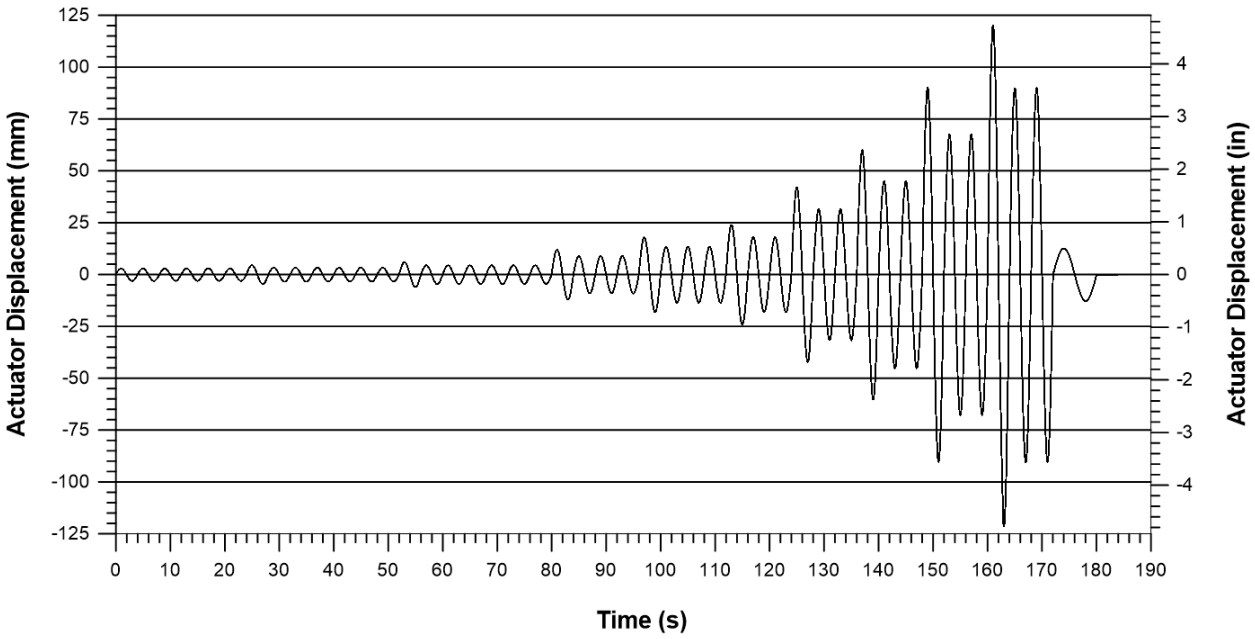

Figure C7: W17-C CUREE Displacement Time-History. Frequency of 0.25 Hz.

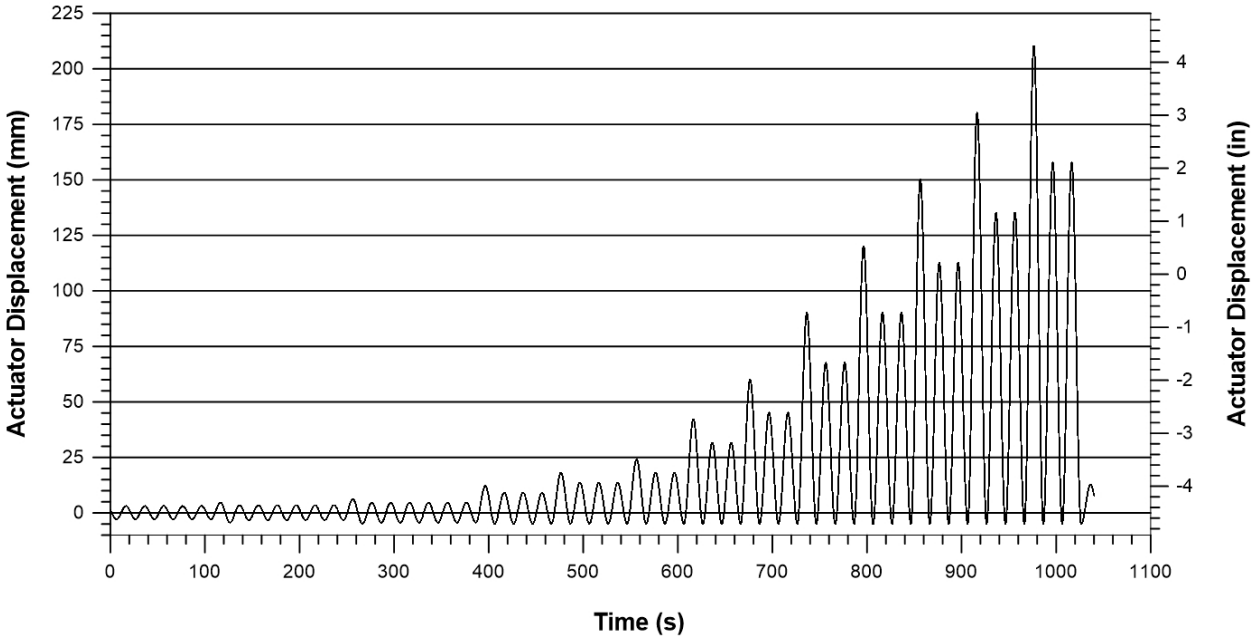

Figure C8: W25-CR3 CUREE Asymmetric Displacement Time-History. Frequency of 0.05 Hz.

APPENDIX D:

TEST OBSERVATION SHEETS

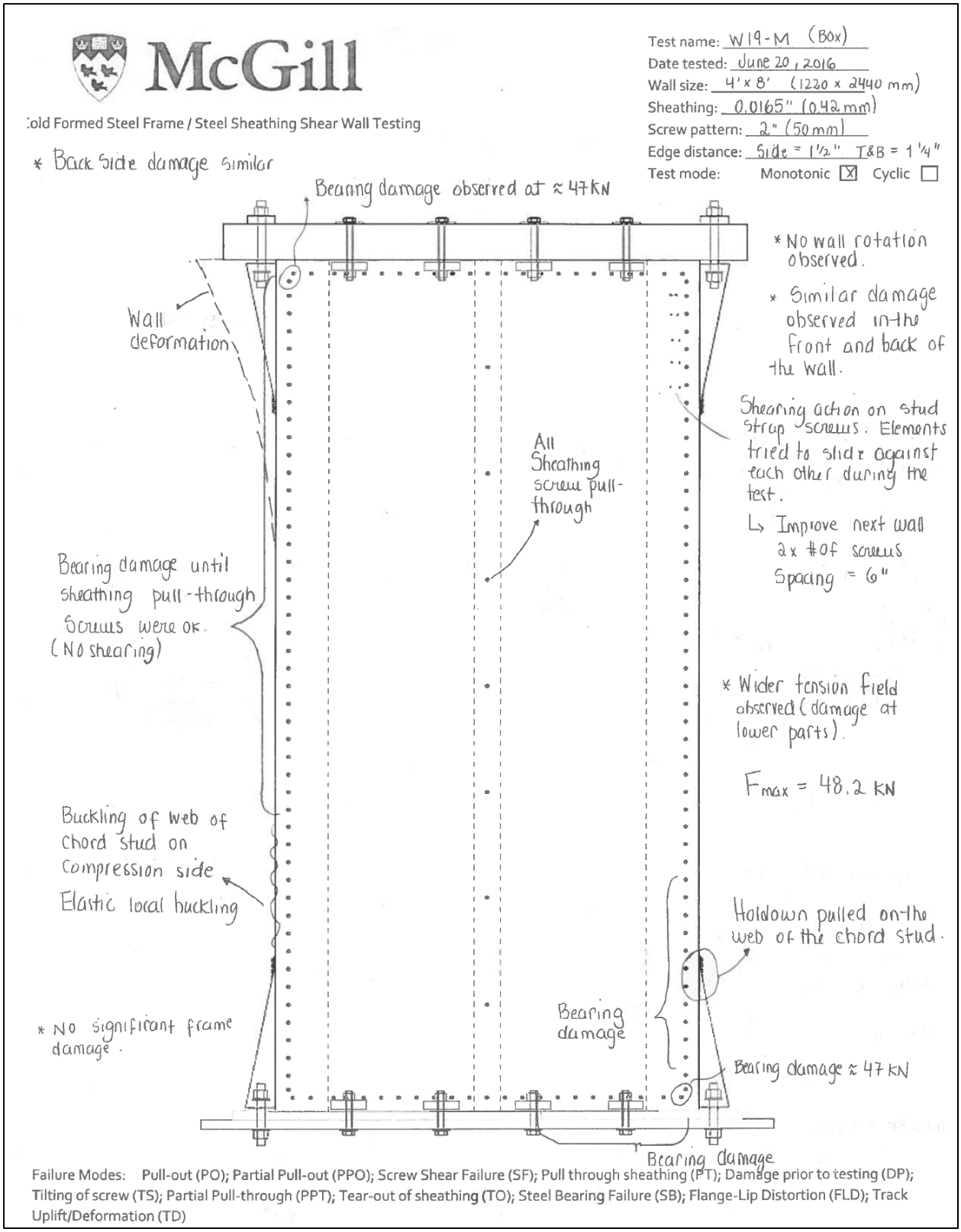

Figure D1: Test observations of double-sheathed specimen W19-M.

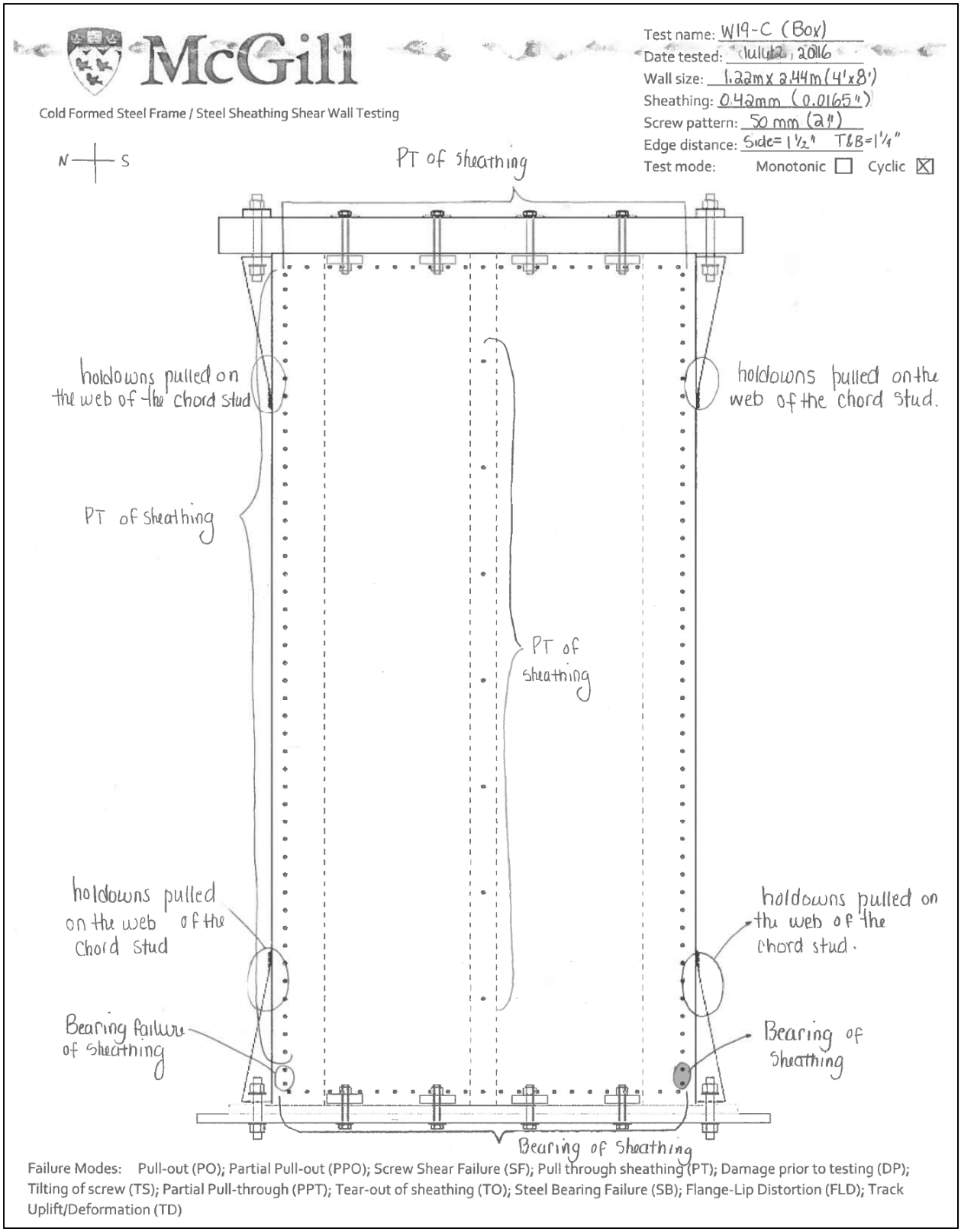

Figure D2: Test observations of double-sheathed specimen W19-C.

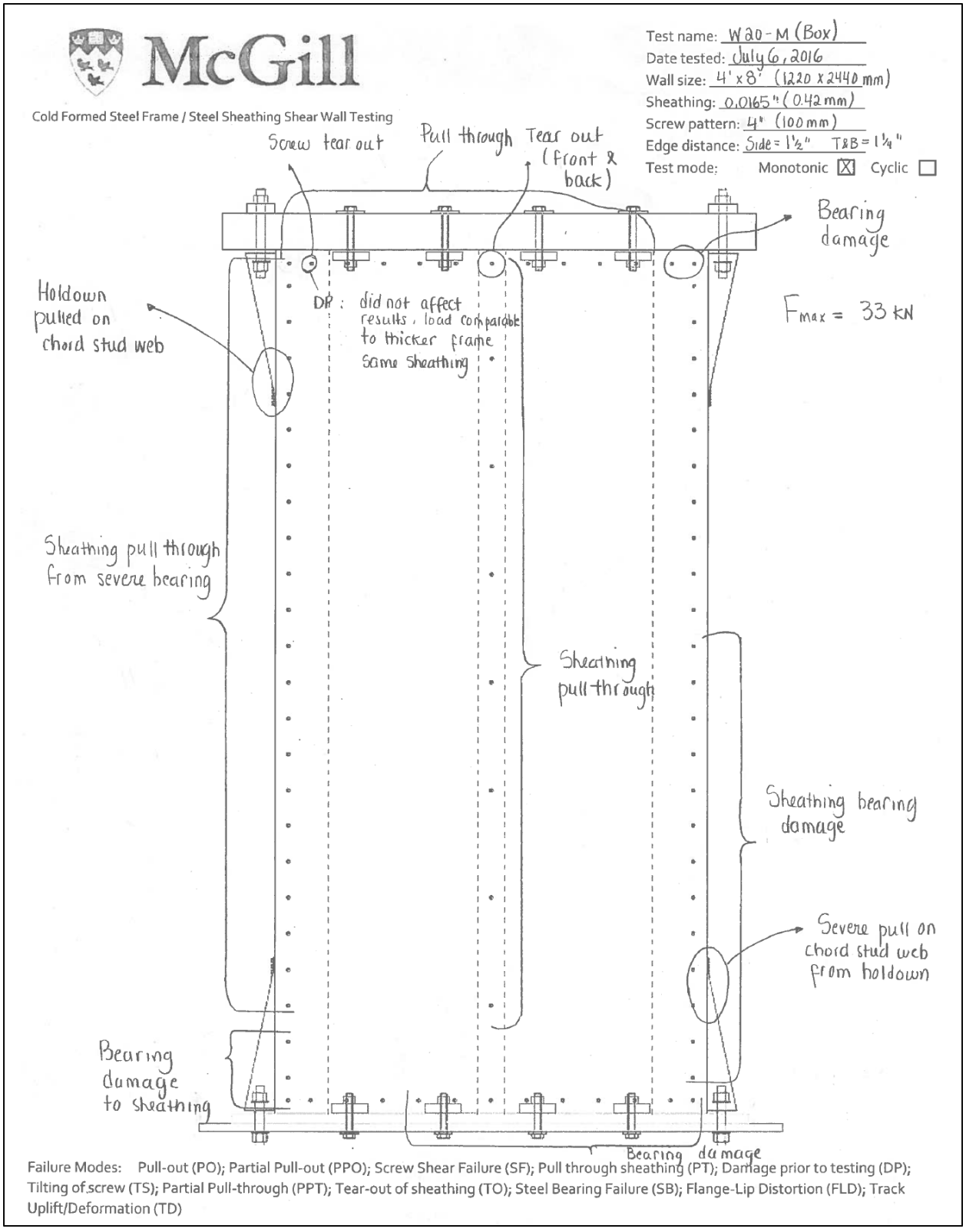

Figure D3: Test observations of double-sheathed specimen W20-M.

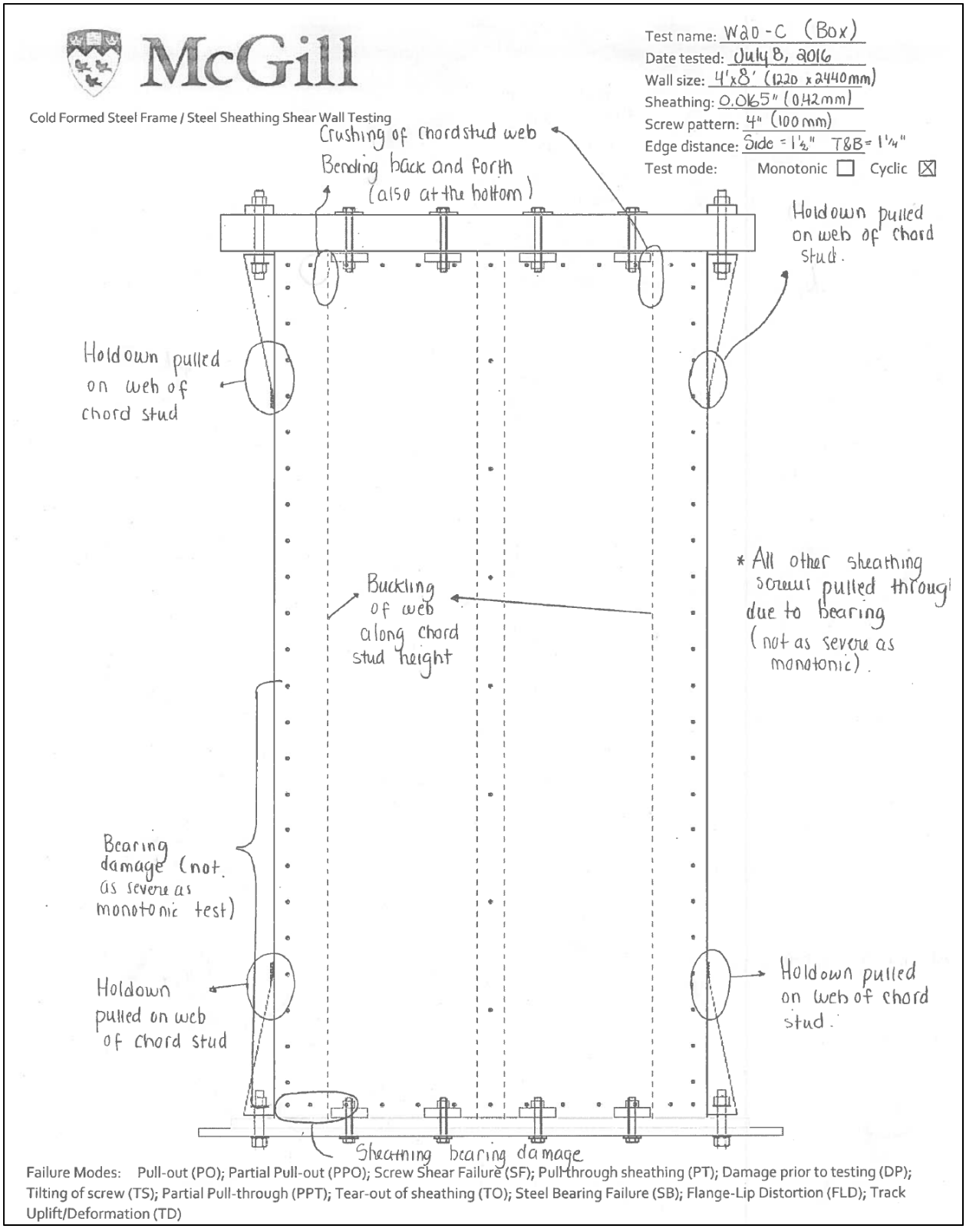

Figure D4: Test observations of double-sheathed specimen W20-C.

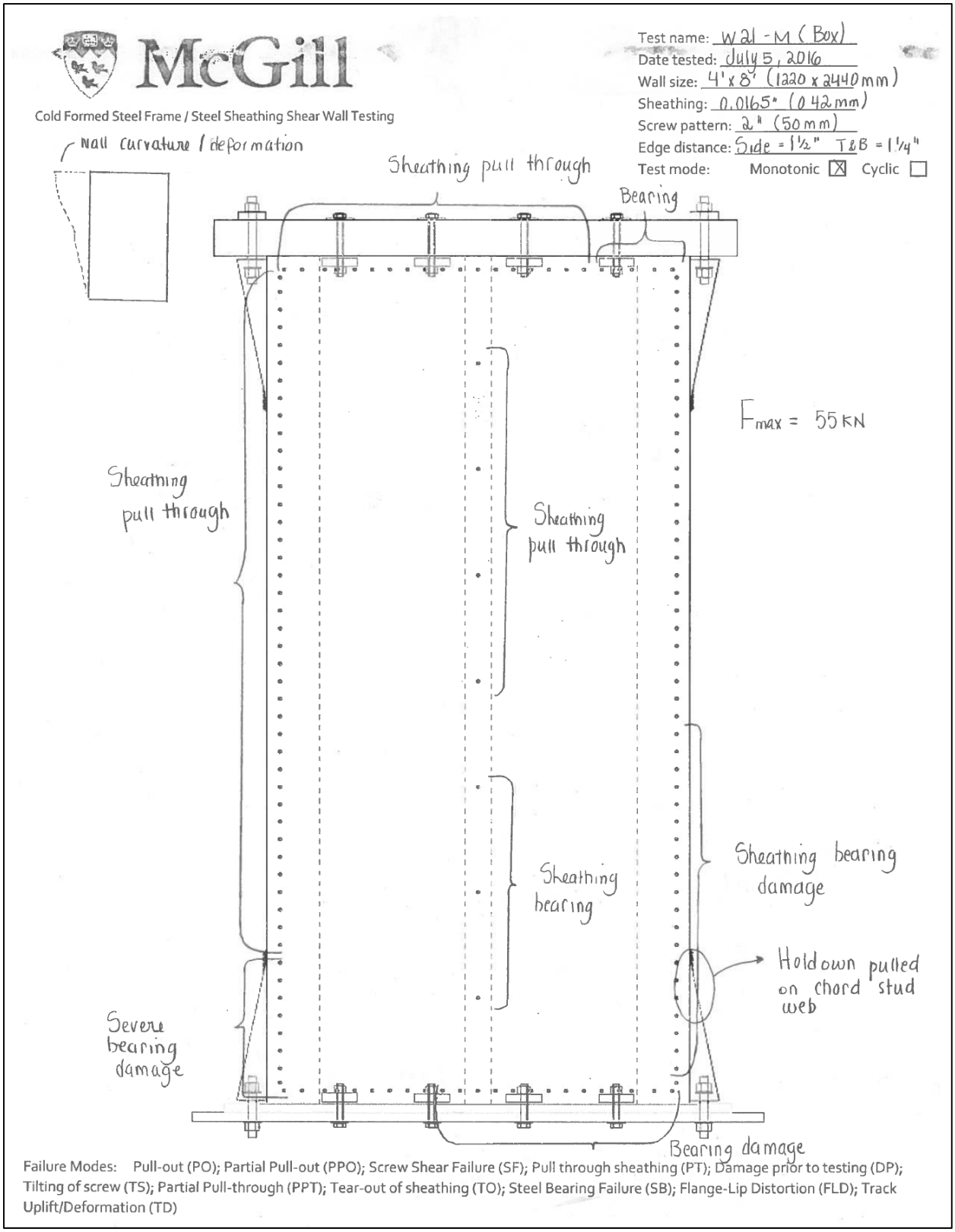

Figure D5: Test observations of double-sheathed specimen W21-M.

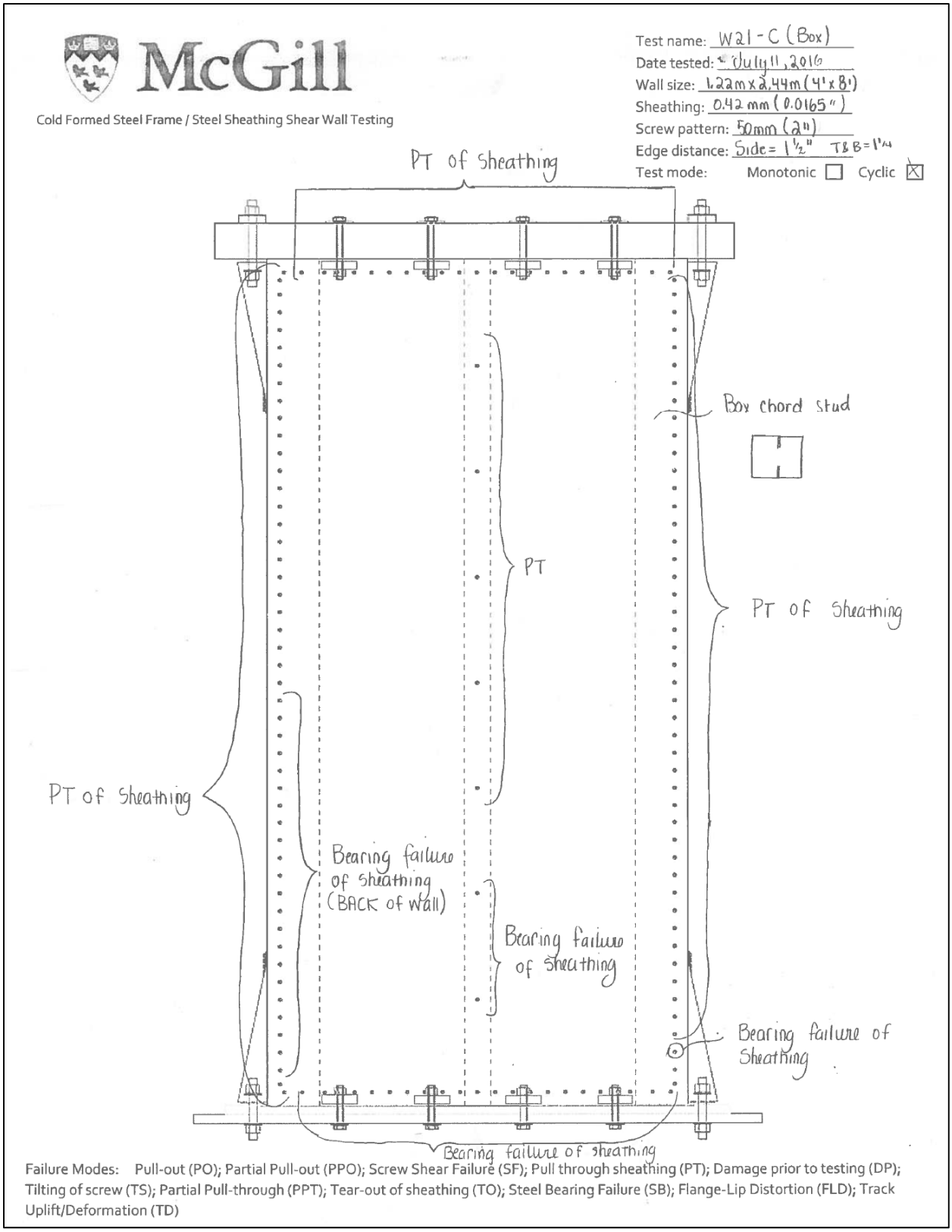

Figure D6: Test observations of double-sheathed specimen W21-C.

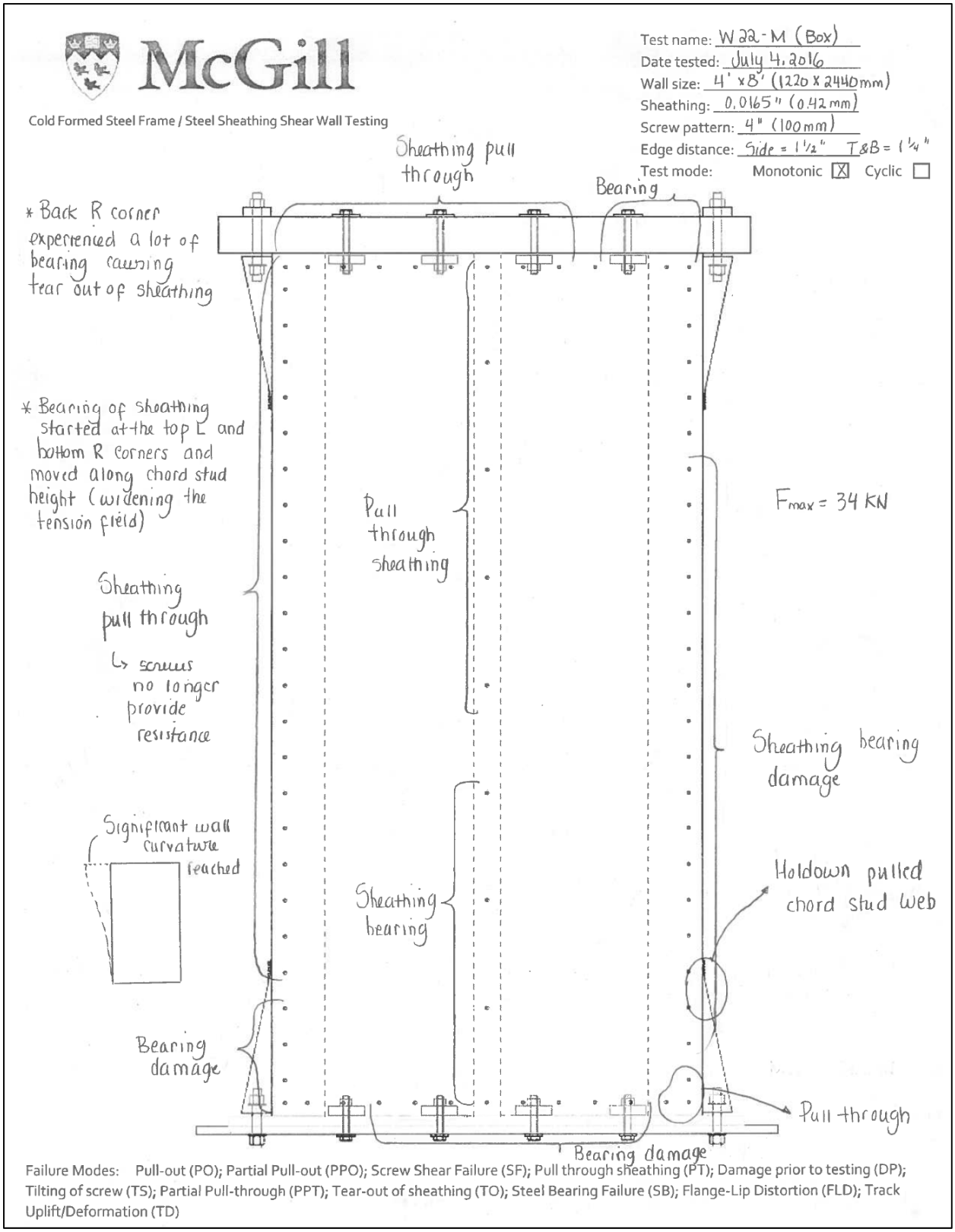

Figure D7: Test observations of double-sheathed specimen W22-M.

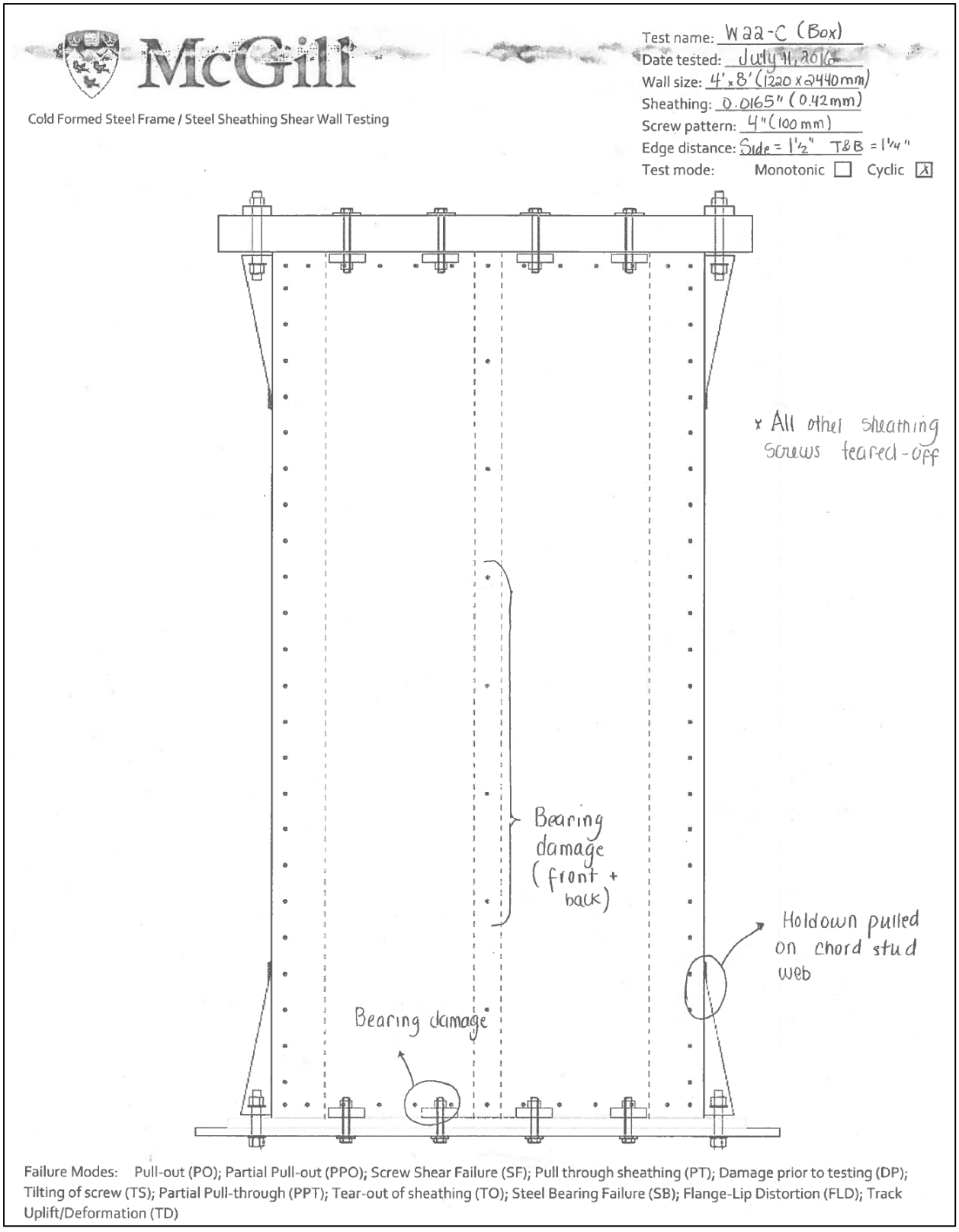

Figure D8: Test observations of double-sheathed specimen W22-C.

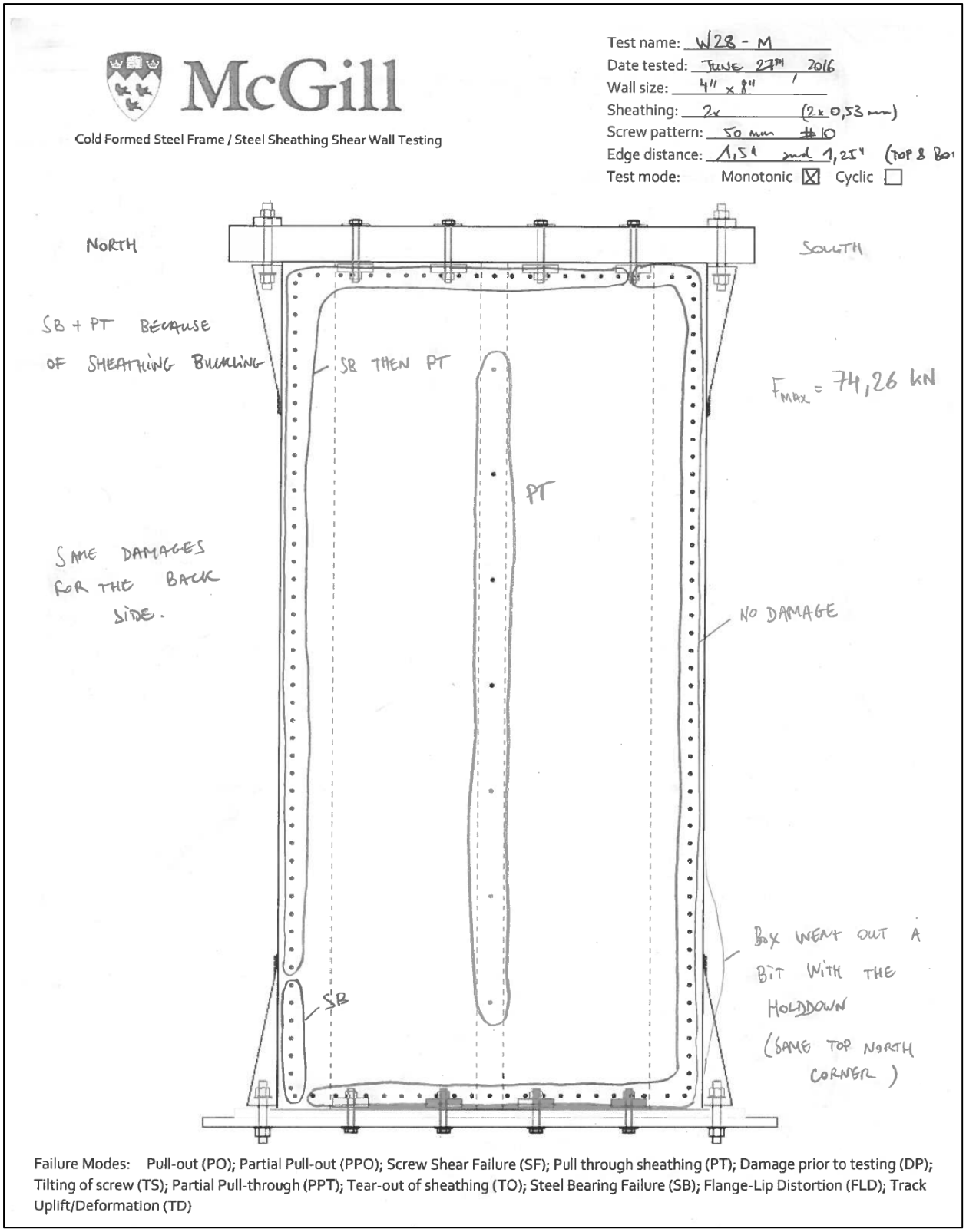

Figure D9: Test observations of double-sheathed specimen W28-M.

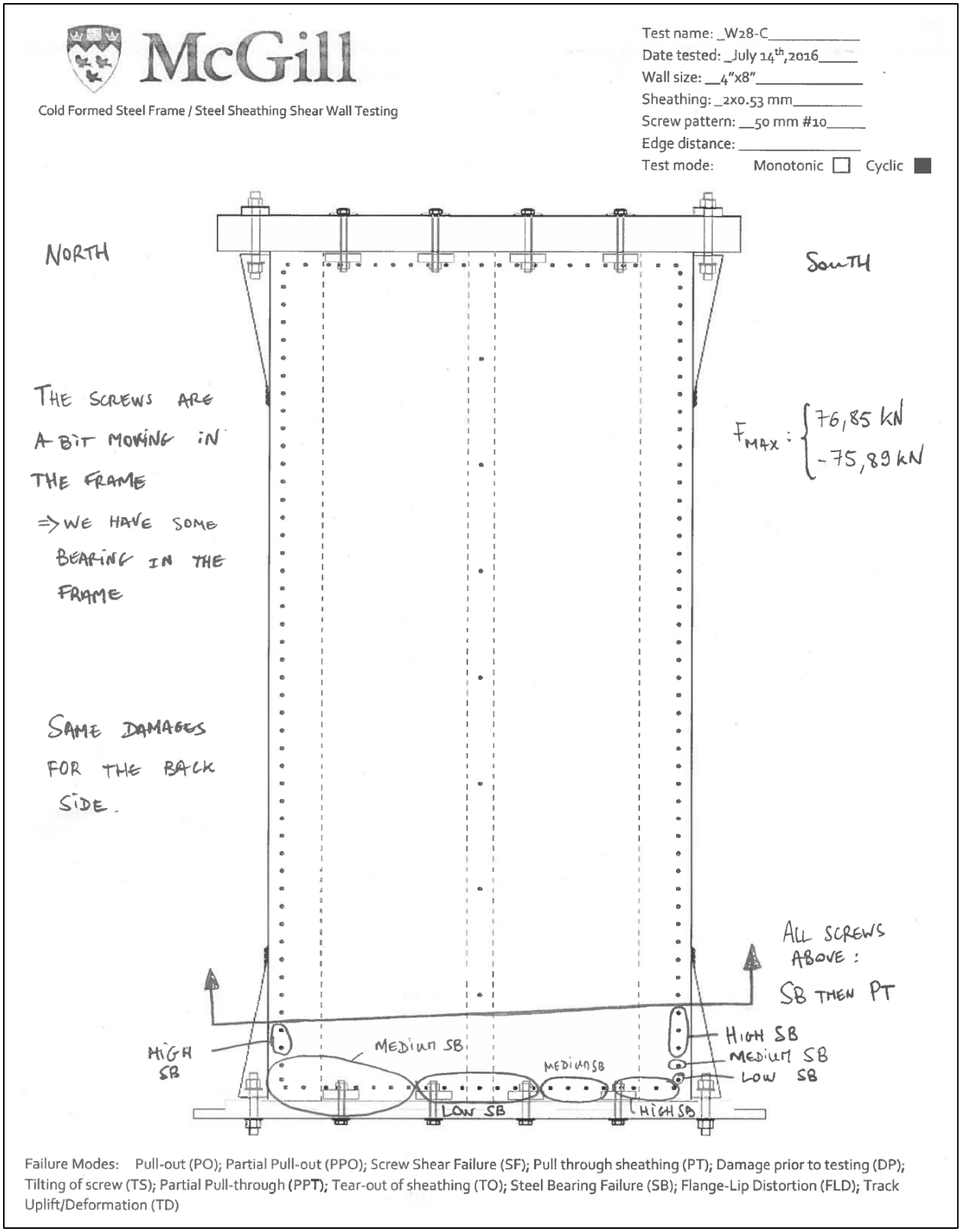

Figure D10: Test observations of double-sheathed specimen W28-C.

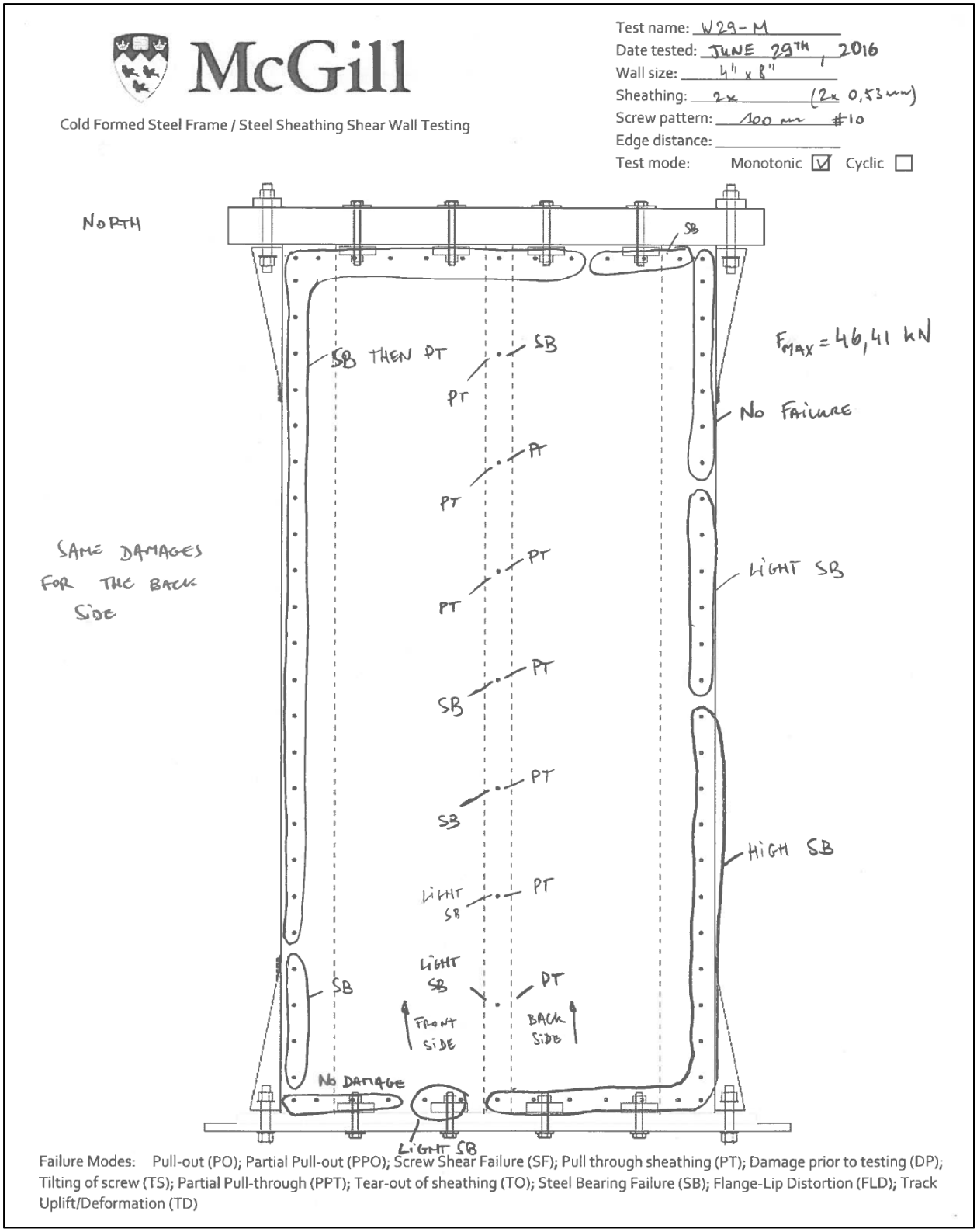

Figure D11: Test observations of double-sheathed specimen W29-M.

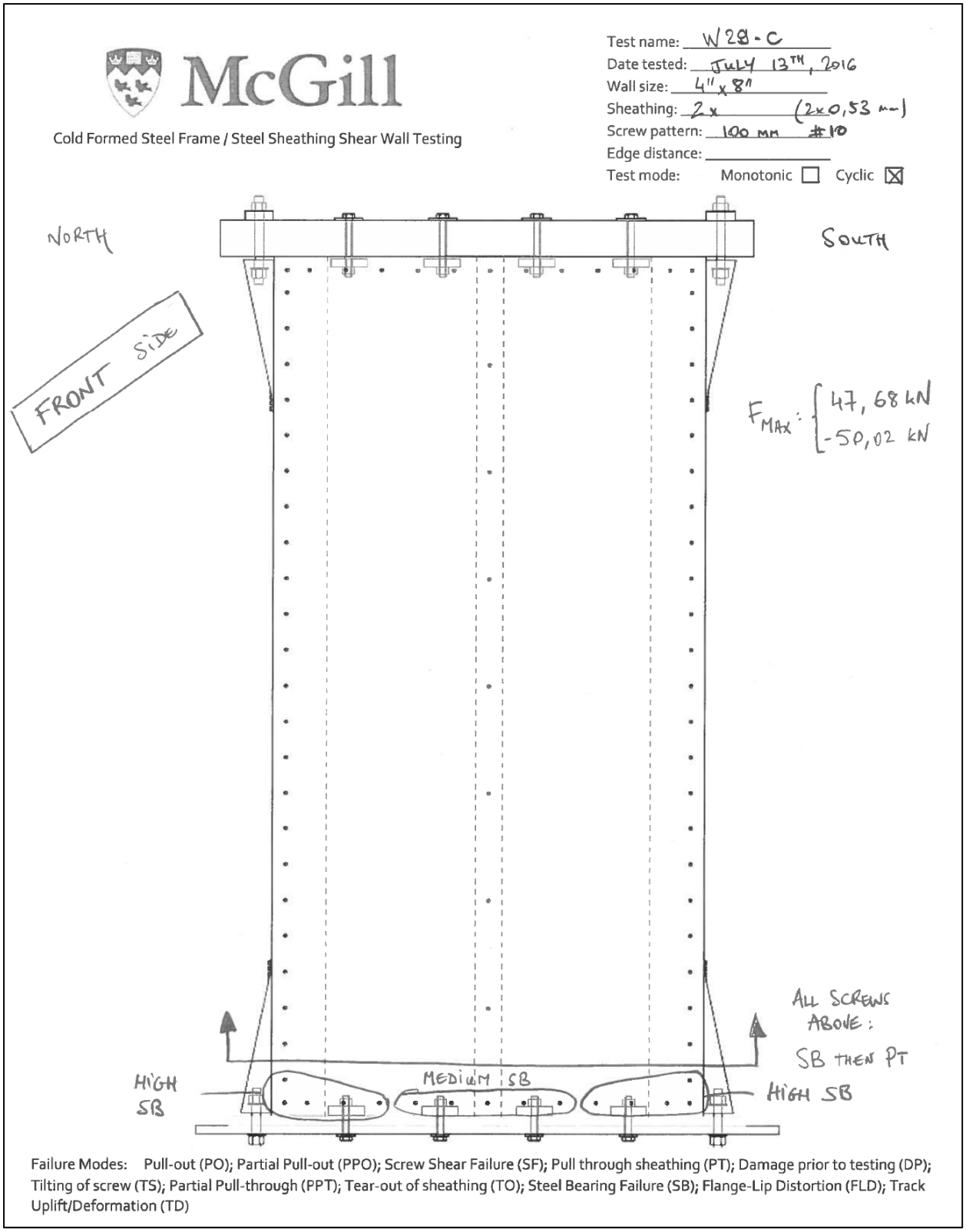

Figure D12: Test observations of double-sheathed specimen W29-C (front).

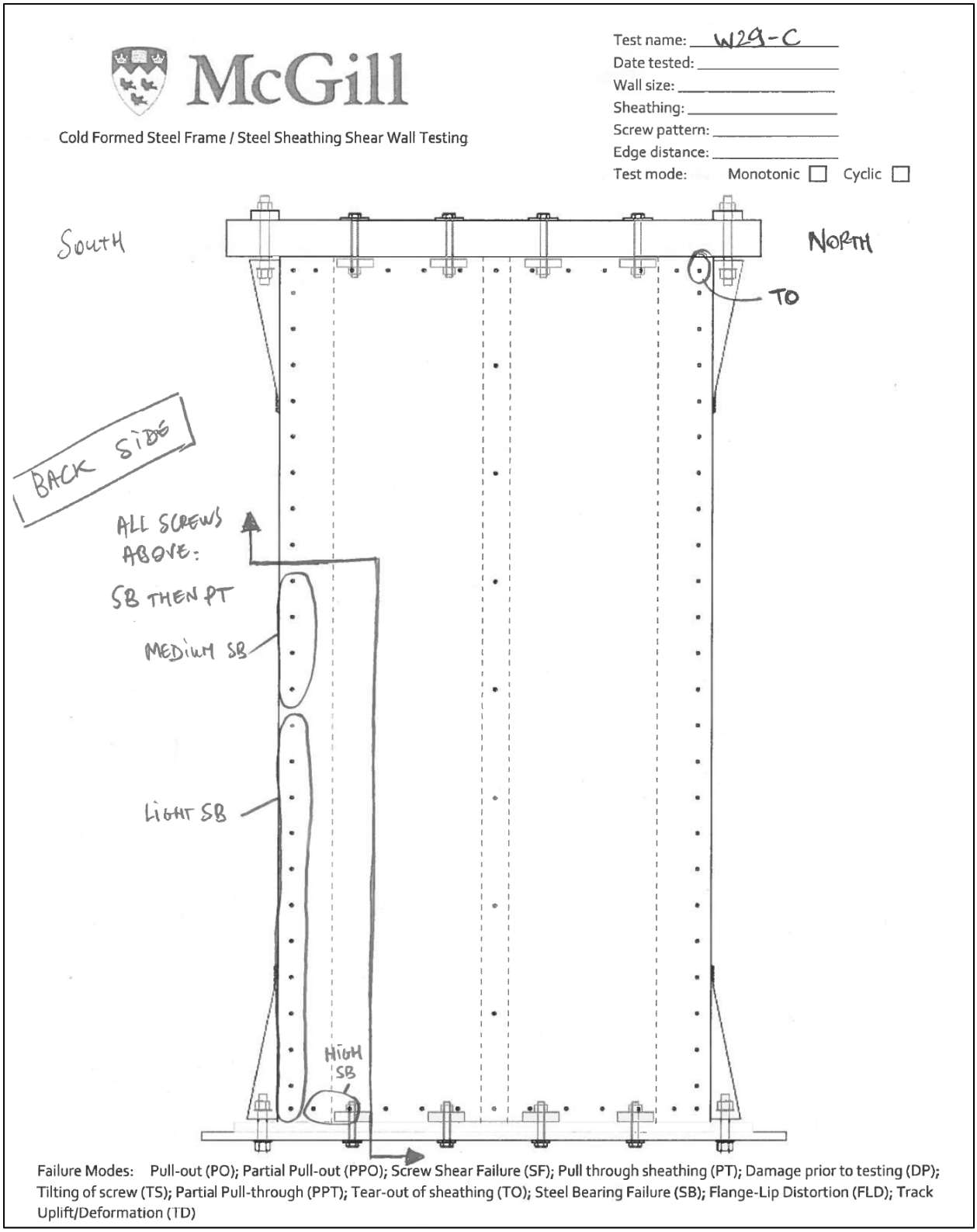

Figure D13: Test observations of double-sheathed specimen W29-C (back).

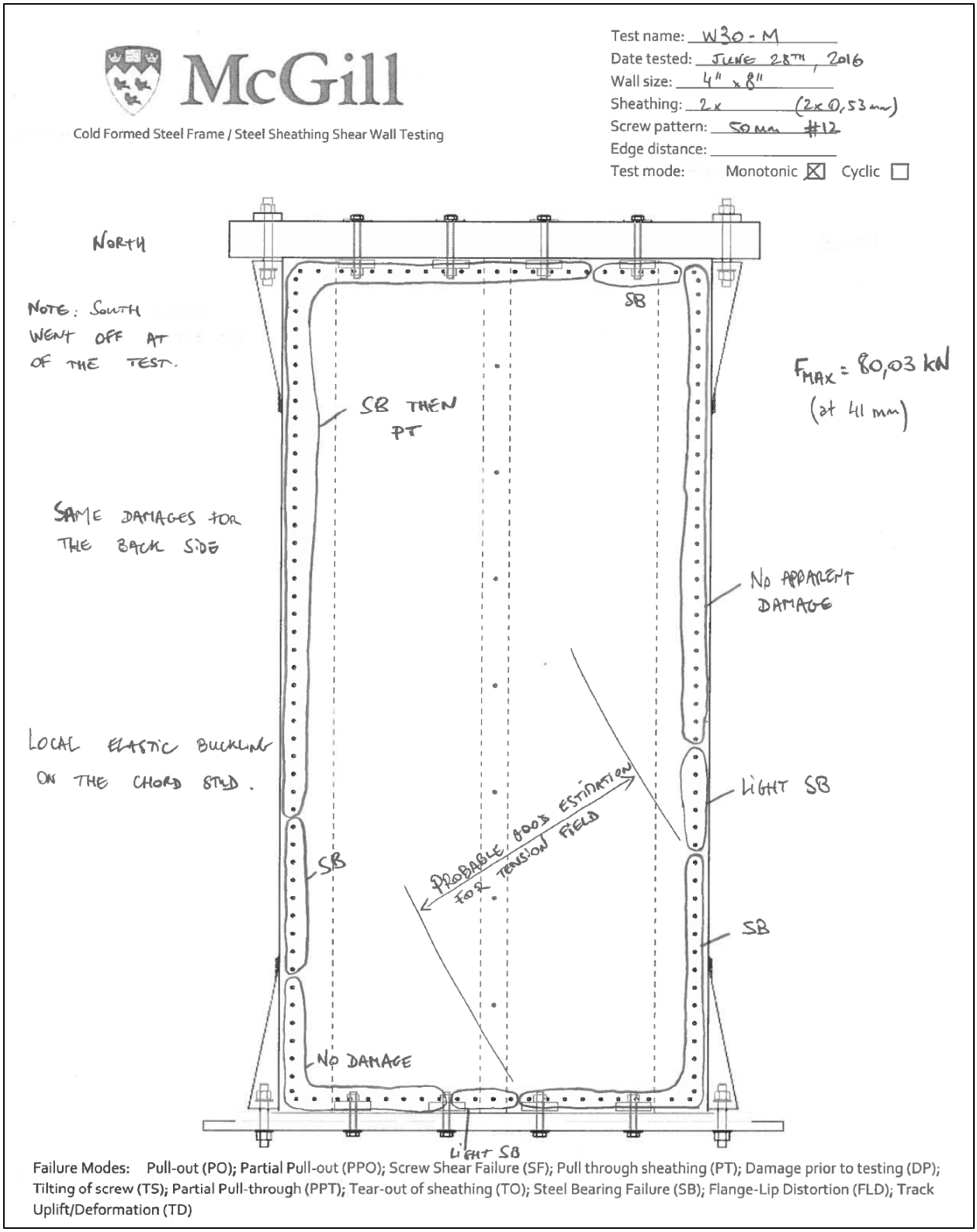

Figure D14: Test observations of double-sheathed specimen W30-M.

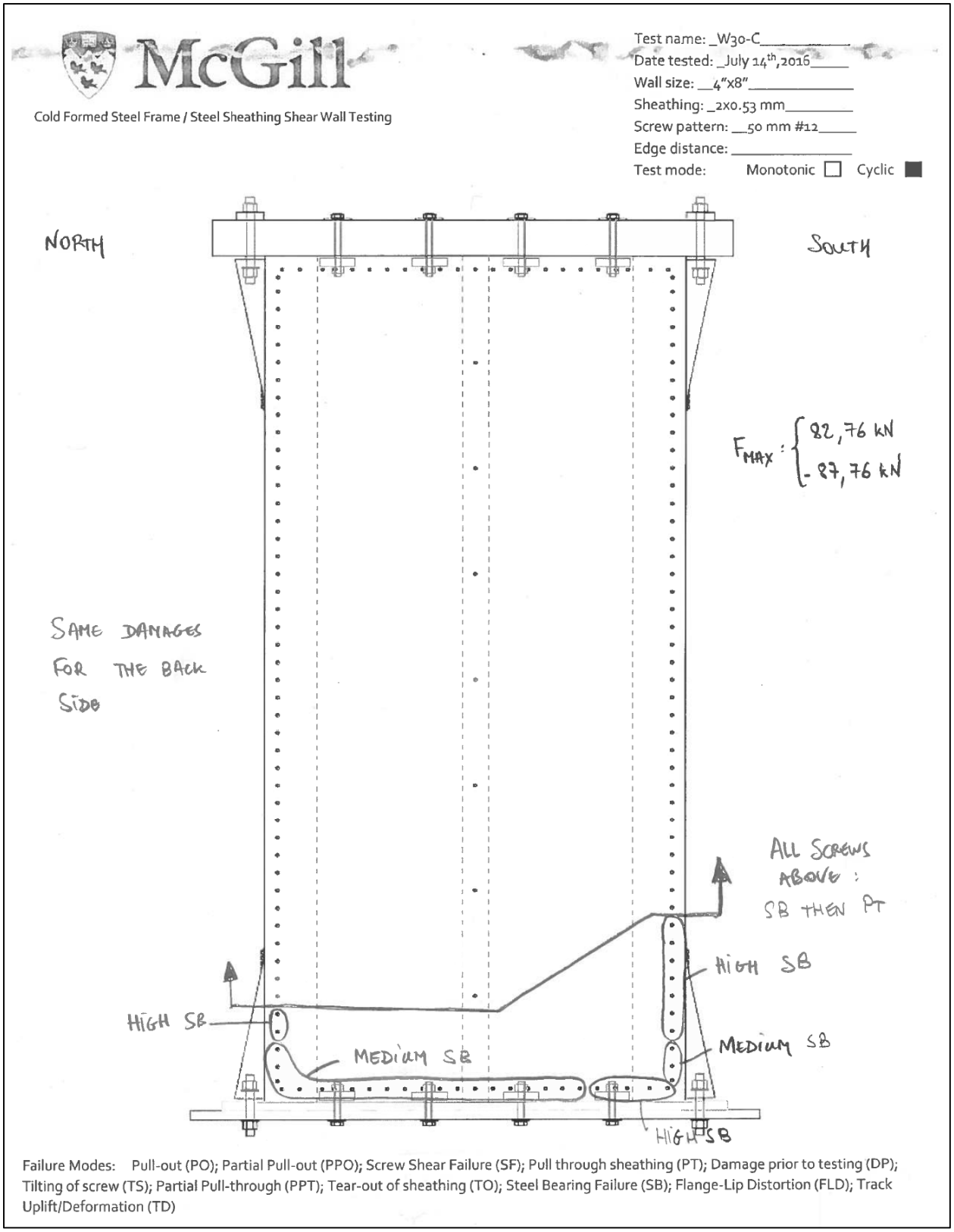

Figure D15: Test observations of double-sheathed specimen W30-C.

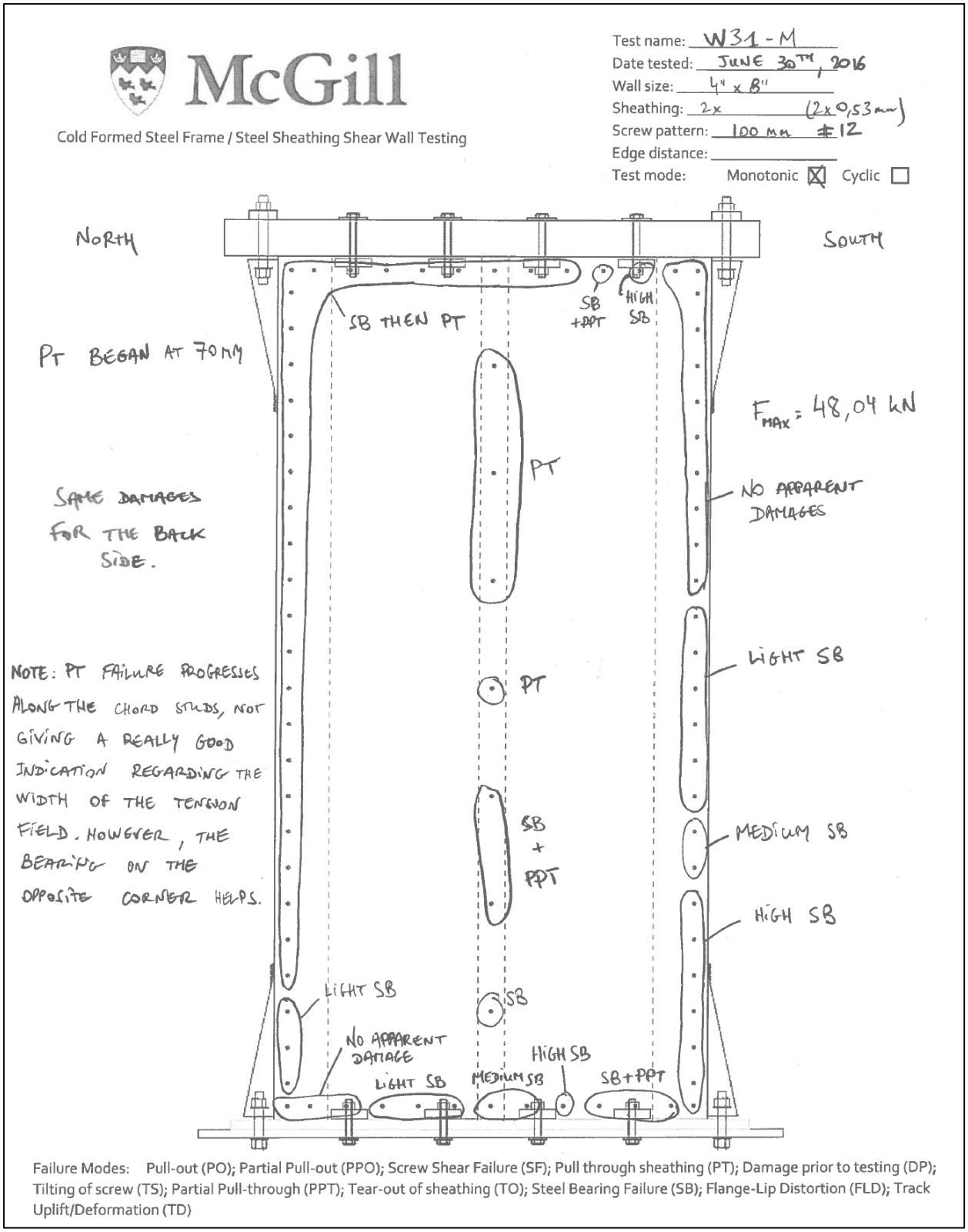

Figure D16: Test observations of double-sheathed specimen W31-M.

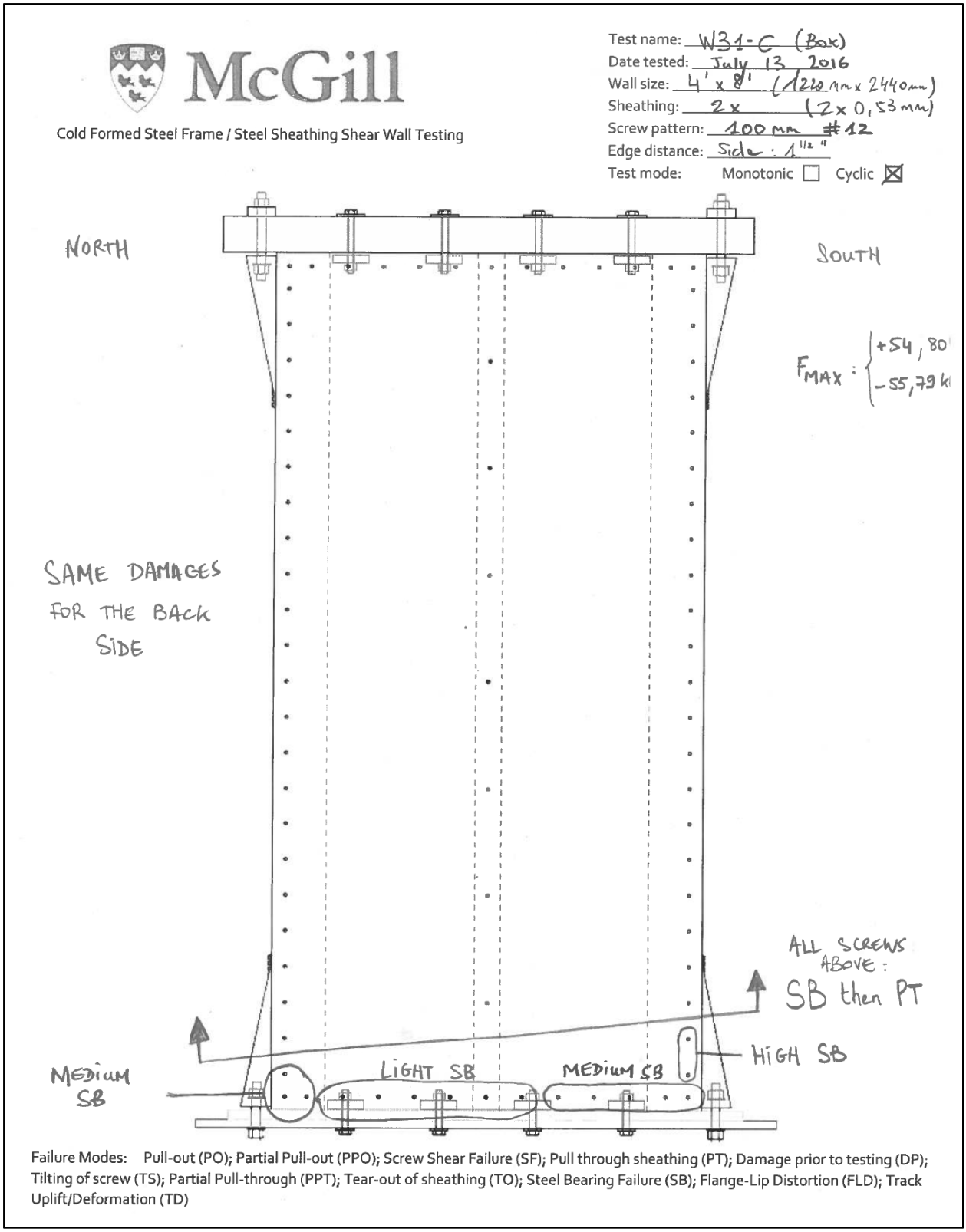

Figure D17: Test observations of double-sheathed specimen W31-C.

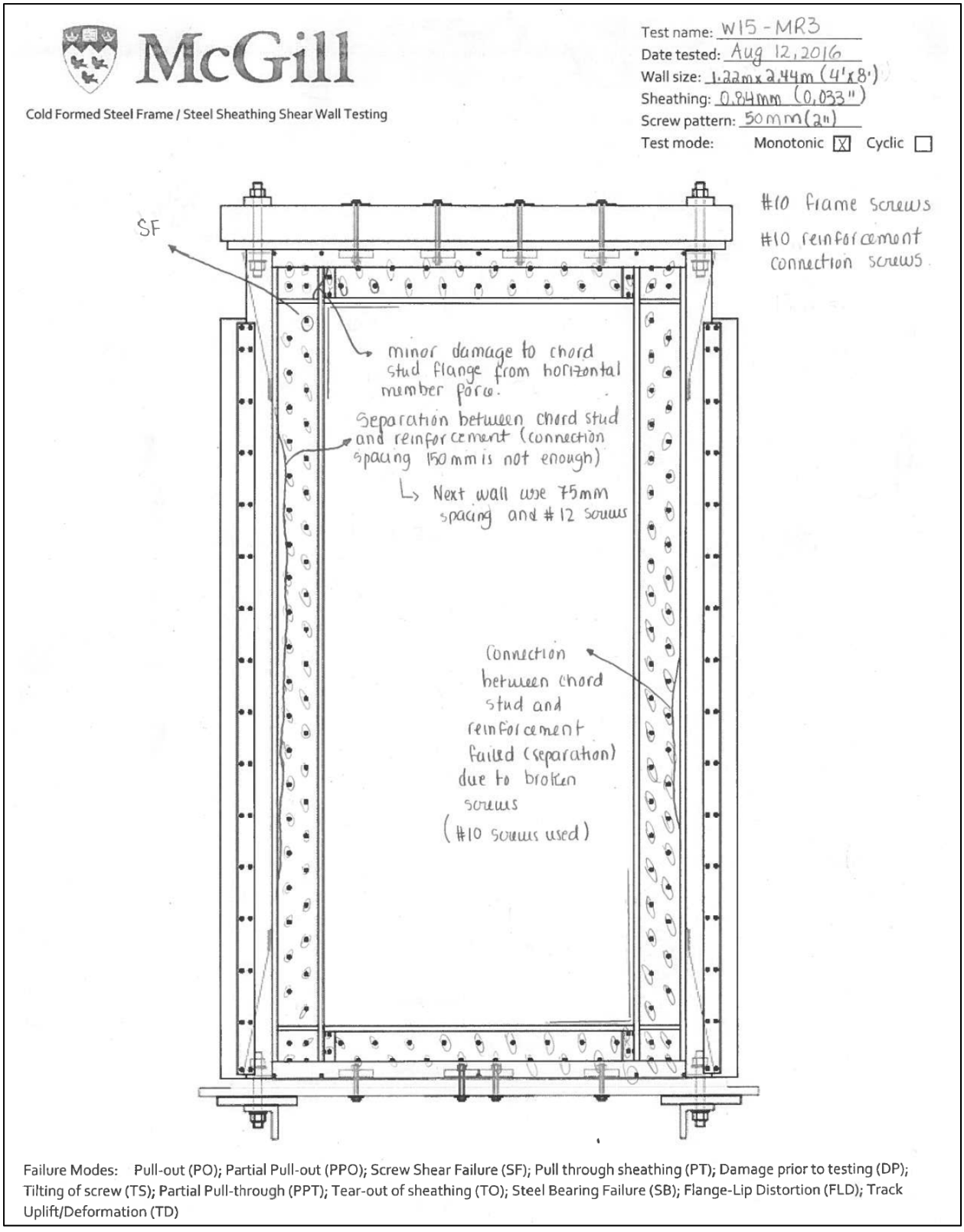

Figure D18: Test observations of centred-sheathed specimen W15-MR3.

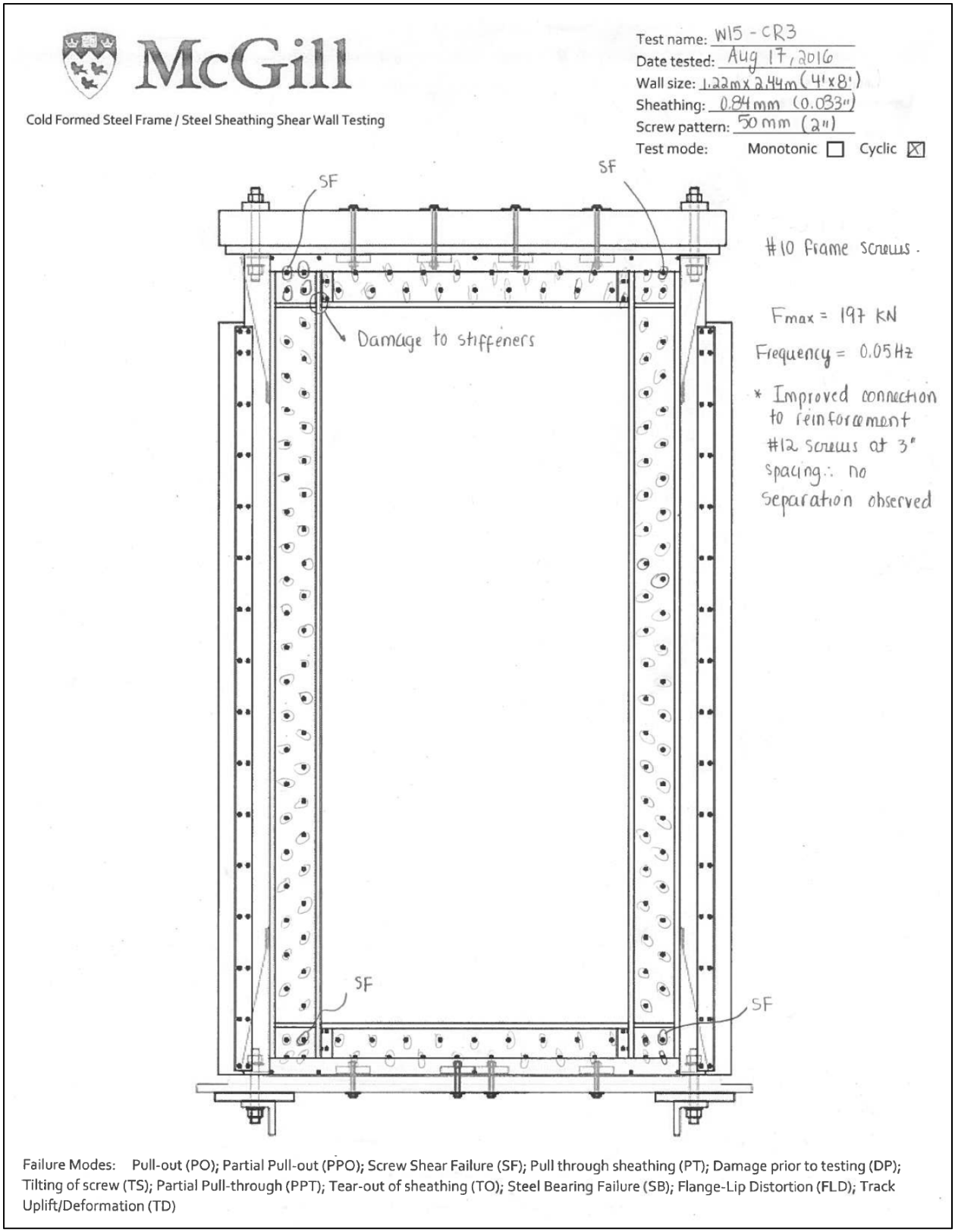

Figure D19: Test observations of centred-sheathed specimen W15-CR3.

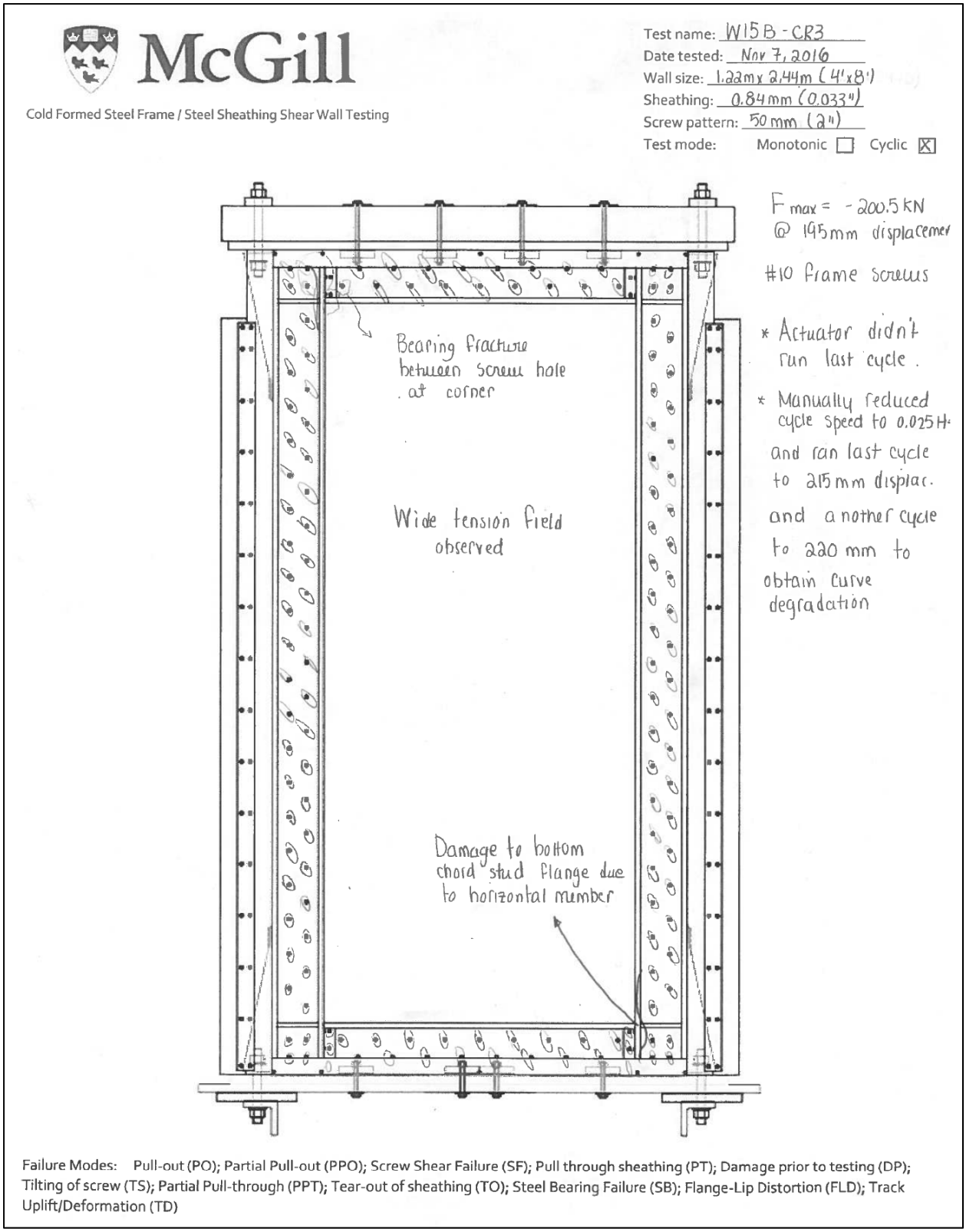

Figure D20: Test observations of centred-sheathed specimen W15B-CR3.

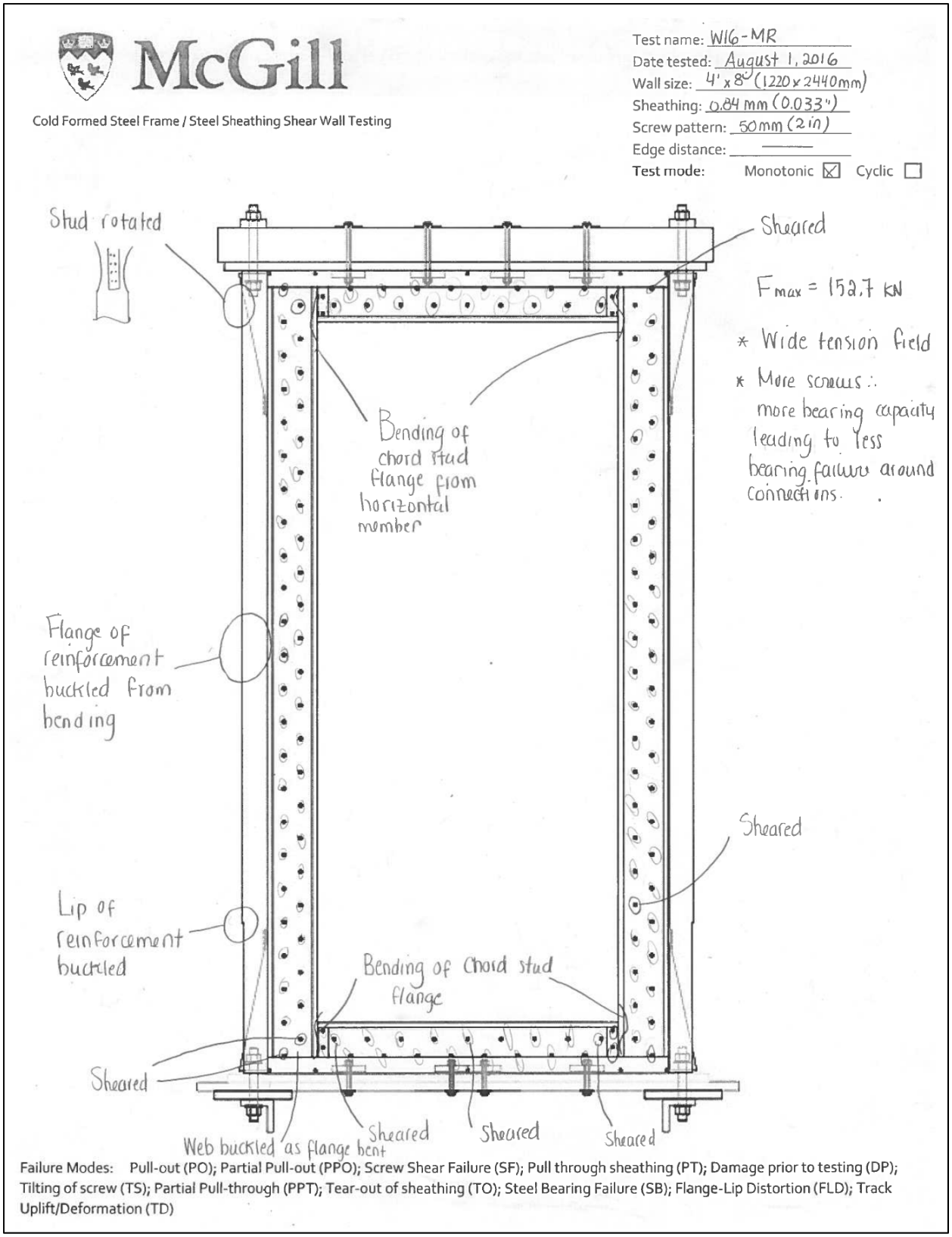

Figure D21: Test observations of centred-sheathed specimen W16-MR.

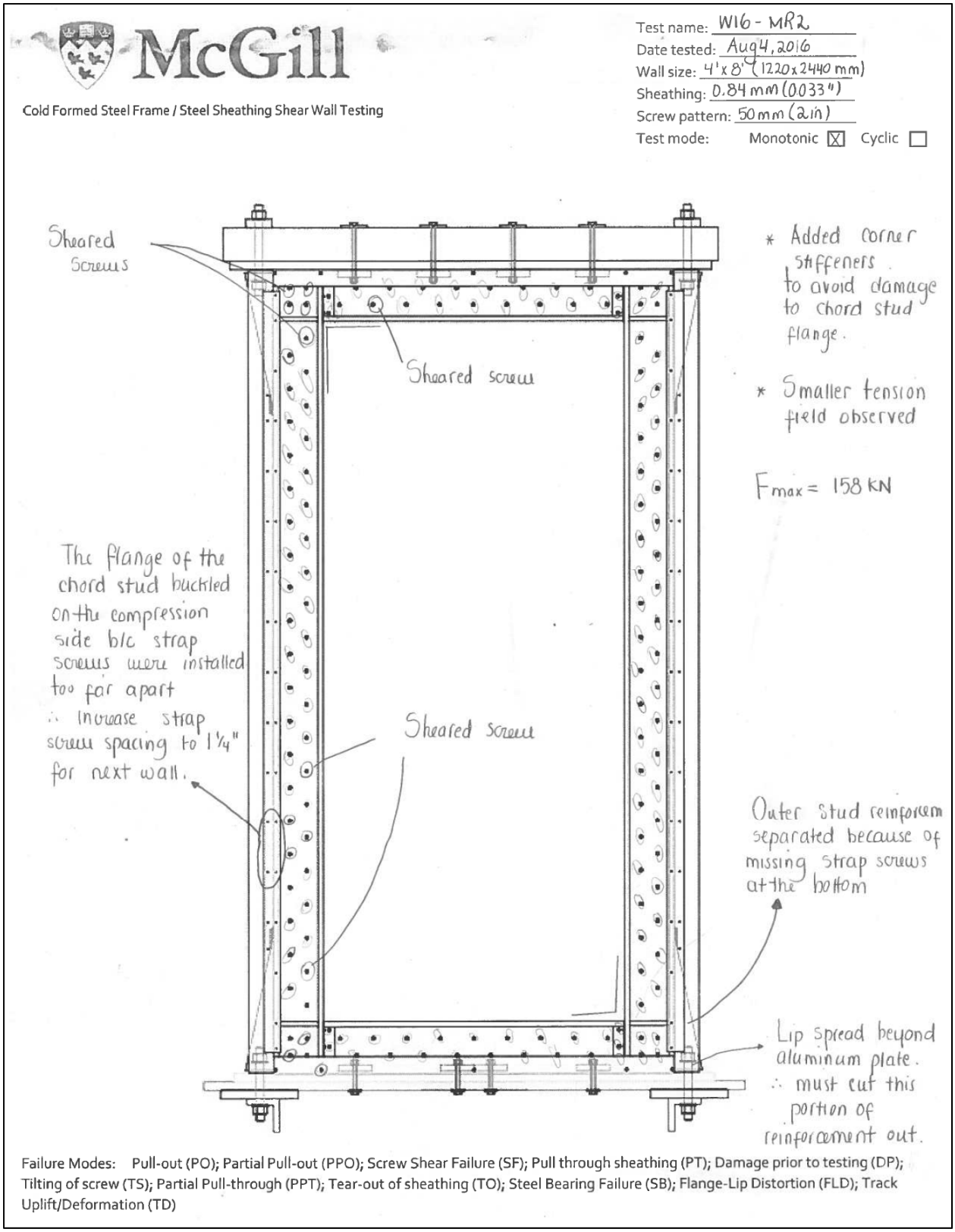

Figure D22: Test observations of centred-sheathed specimen W16-MR2.

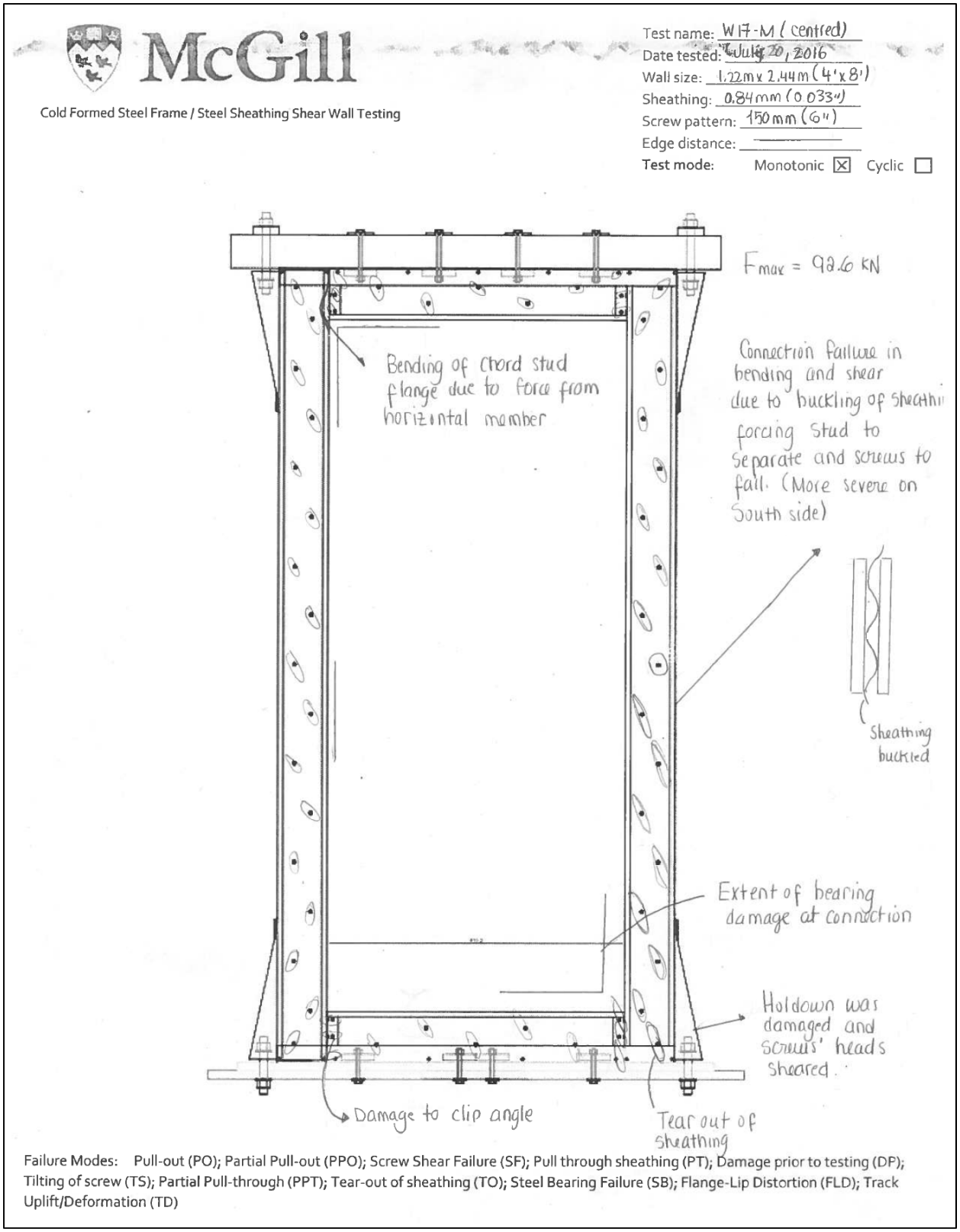

Figure D23: Test observations of centred-sheathed specimen W17-M.

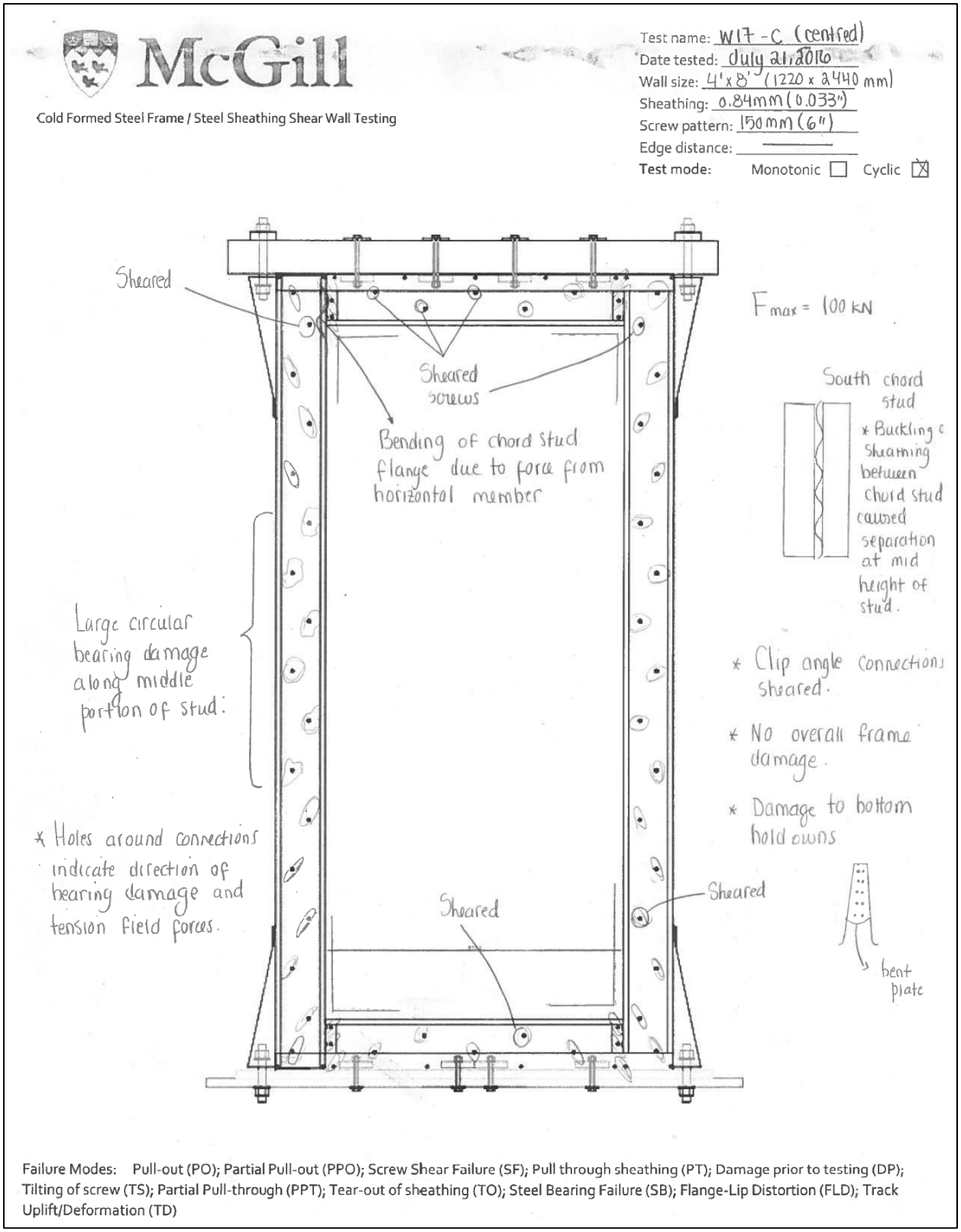

Figure D24: Test observations of centred-sheathed specimen W17-C.

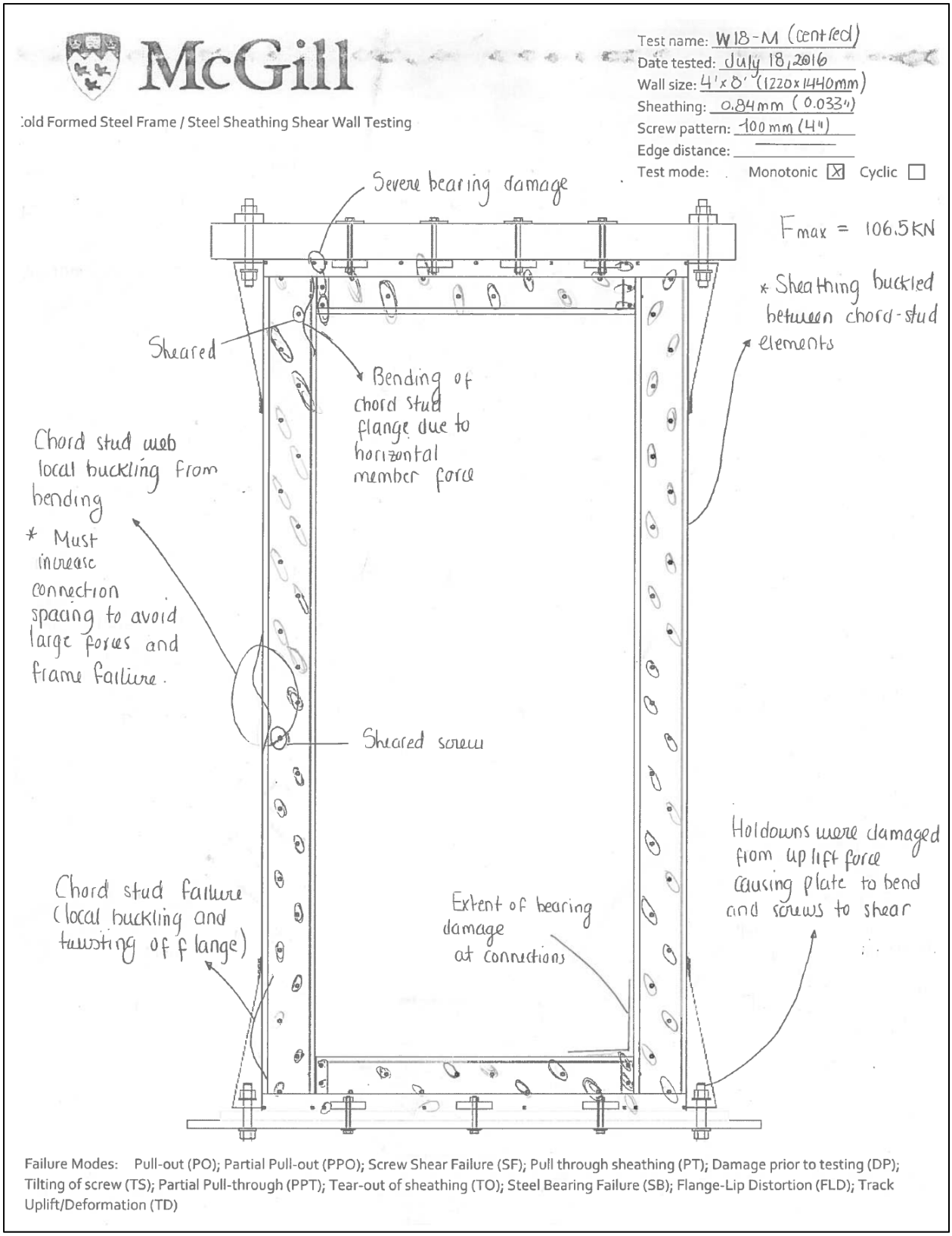

Figure D25: Test observations of centred-sheathed specimen W18-M.

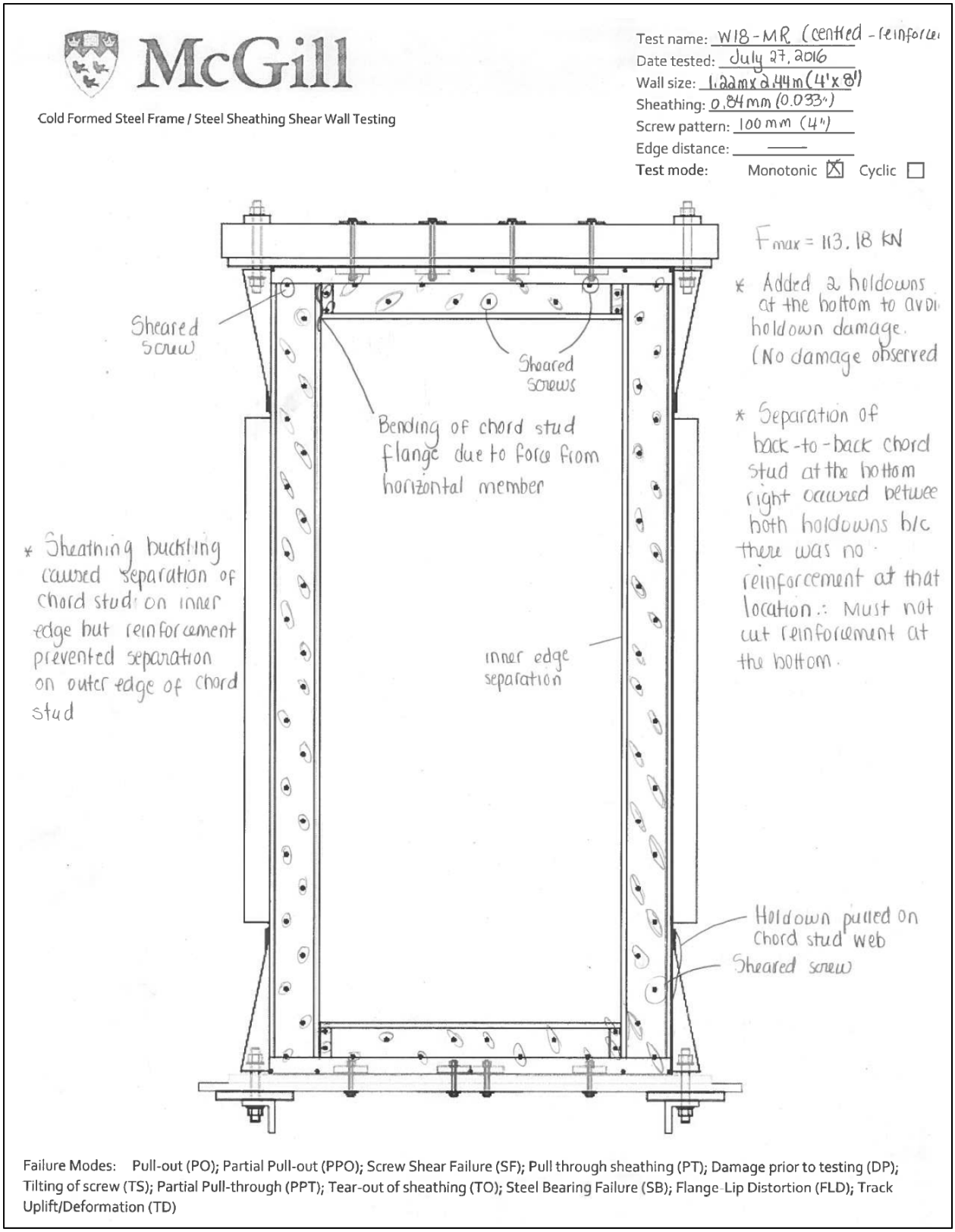

Figure D26: Test observations of centred-sheathed specimen W18-MR.

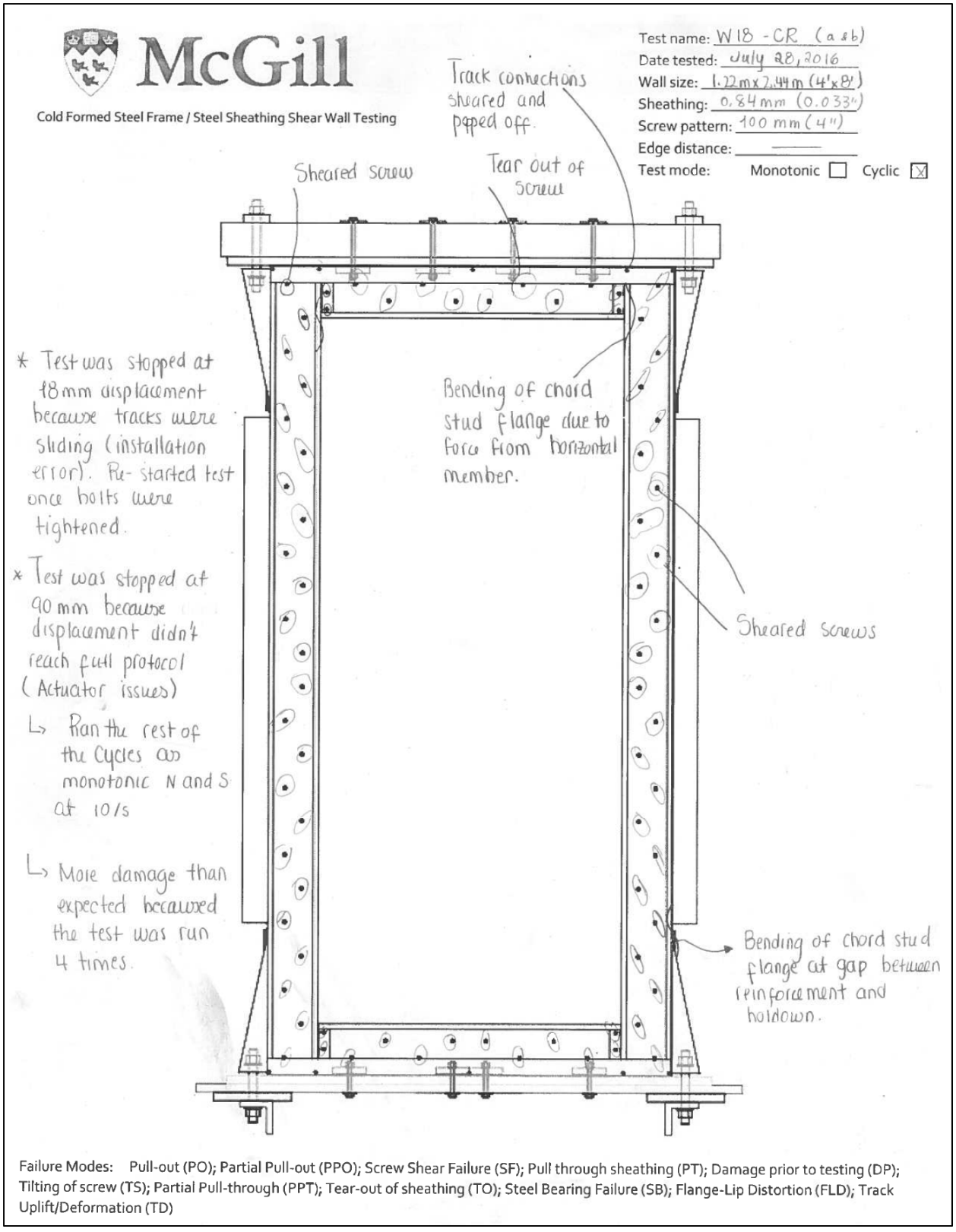

Figure D27: Test observations of centred-sheathed specimen W18-CR.

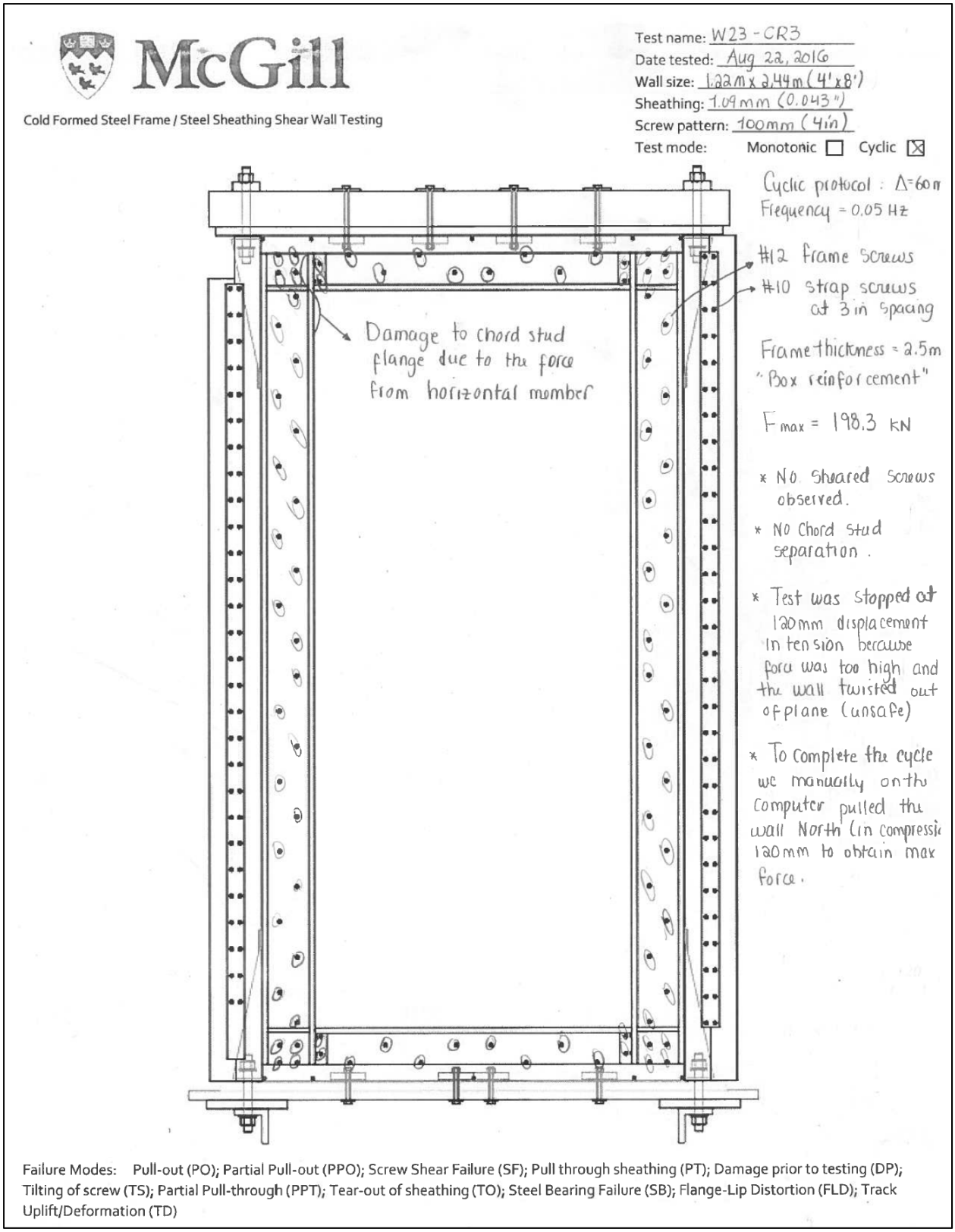

Figure D28: Test observations of centred-sheathed specimen W23-CR3.

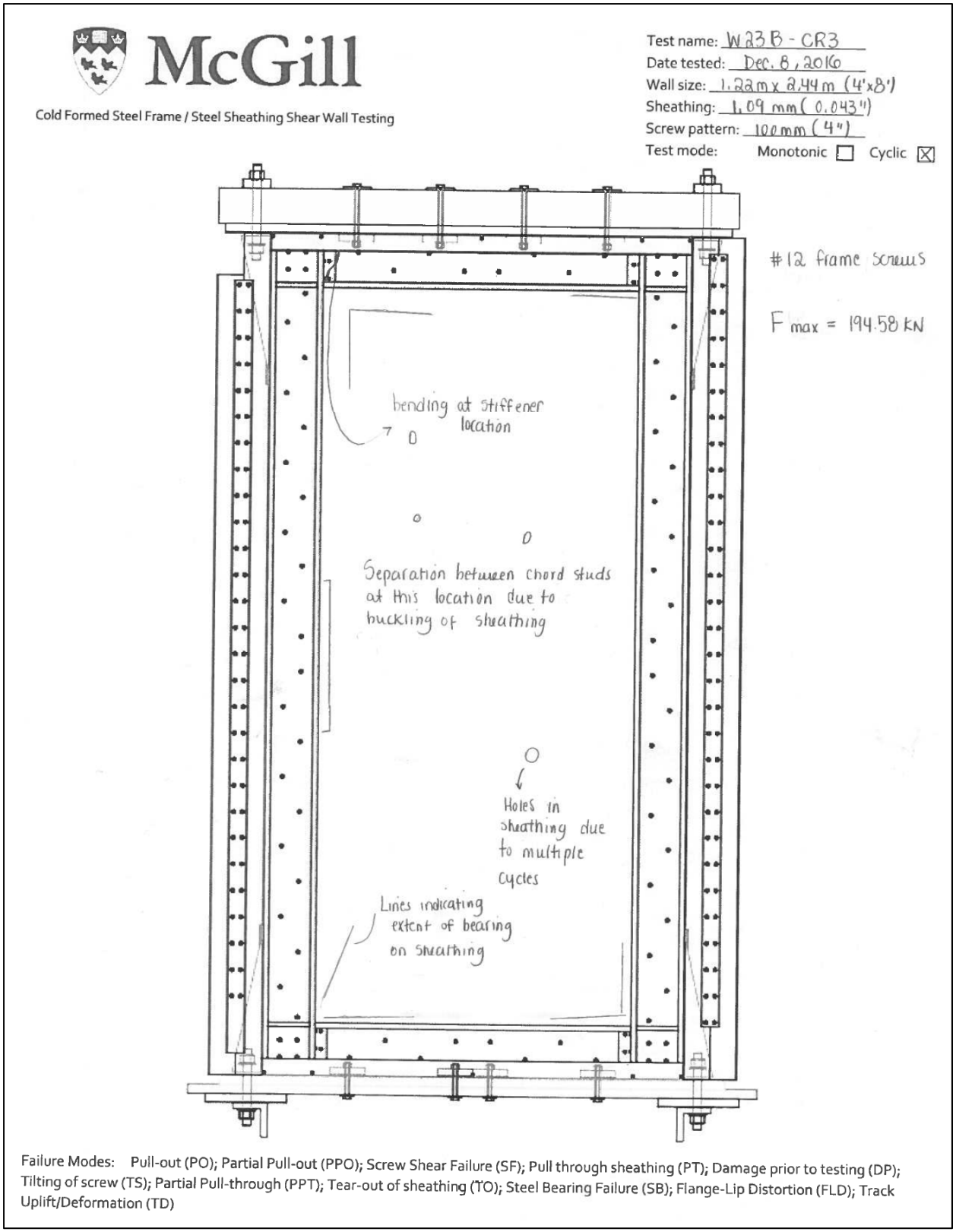

Figure D29: Test observations of centred-sheathed specimen W23B-CR3.

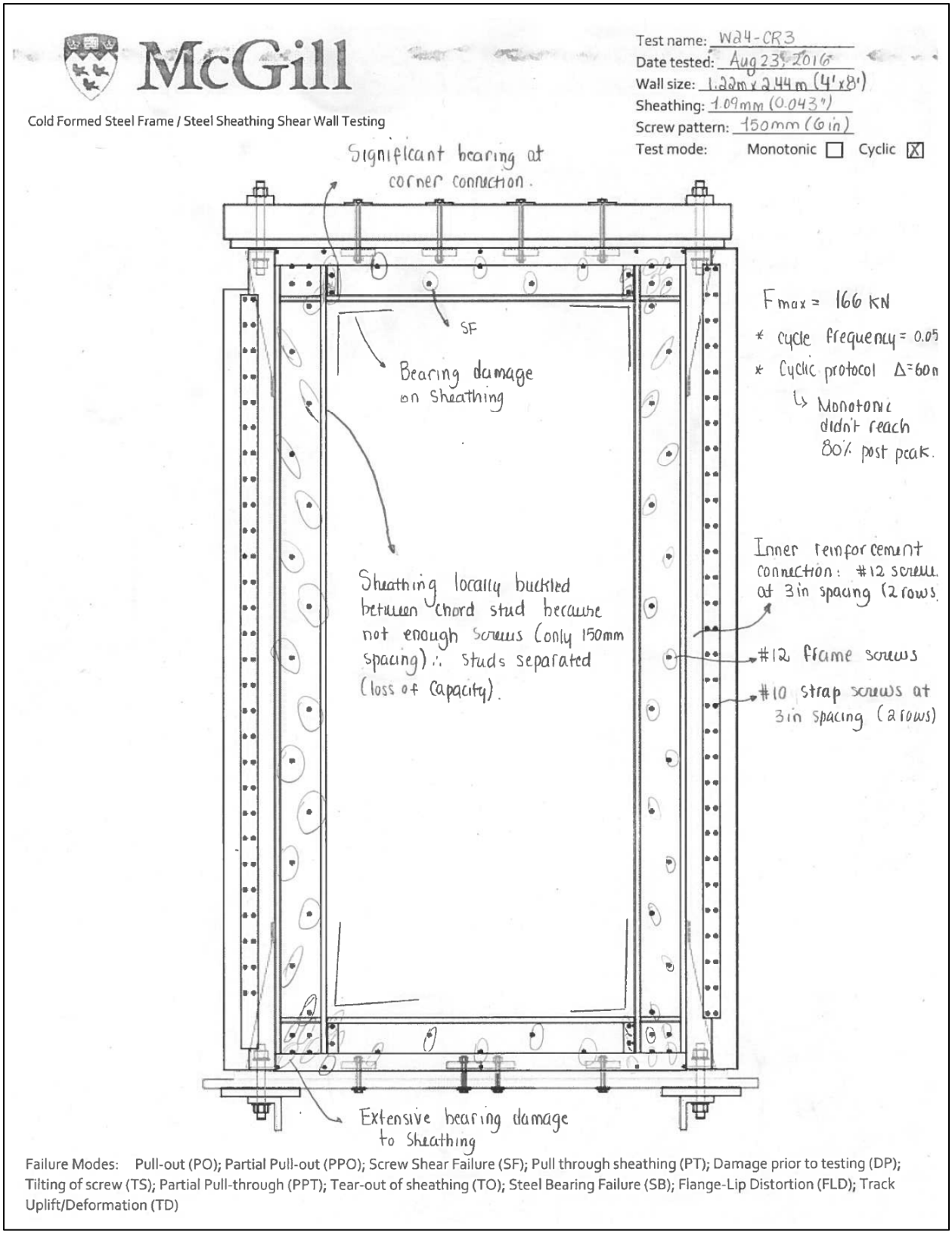

Figure D30: Test observations of centred-sheathed specimen W24-CR3.

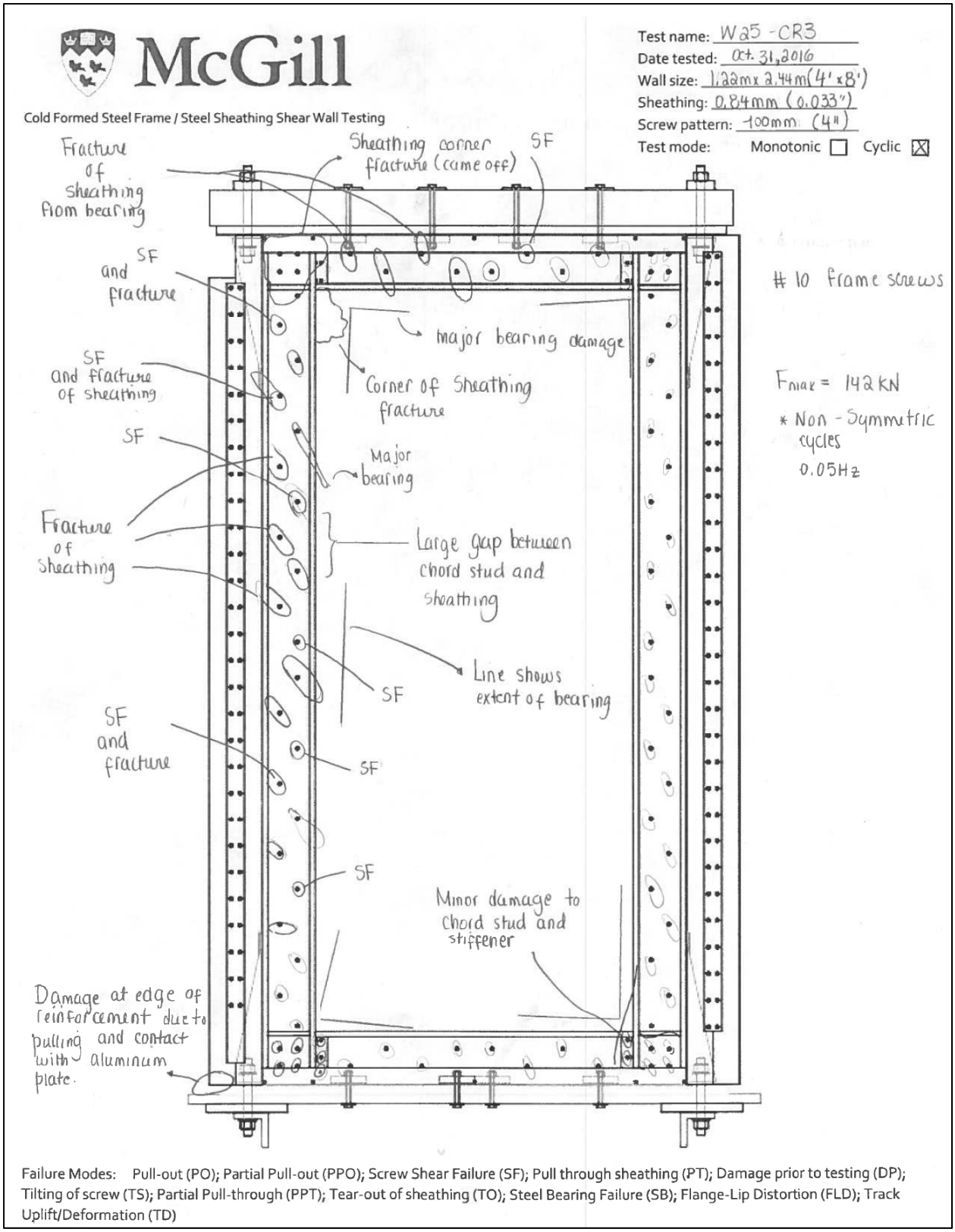

Figure D31: Test observations of centred-sheathed specimen W25-CR3.

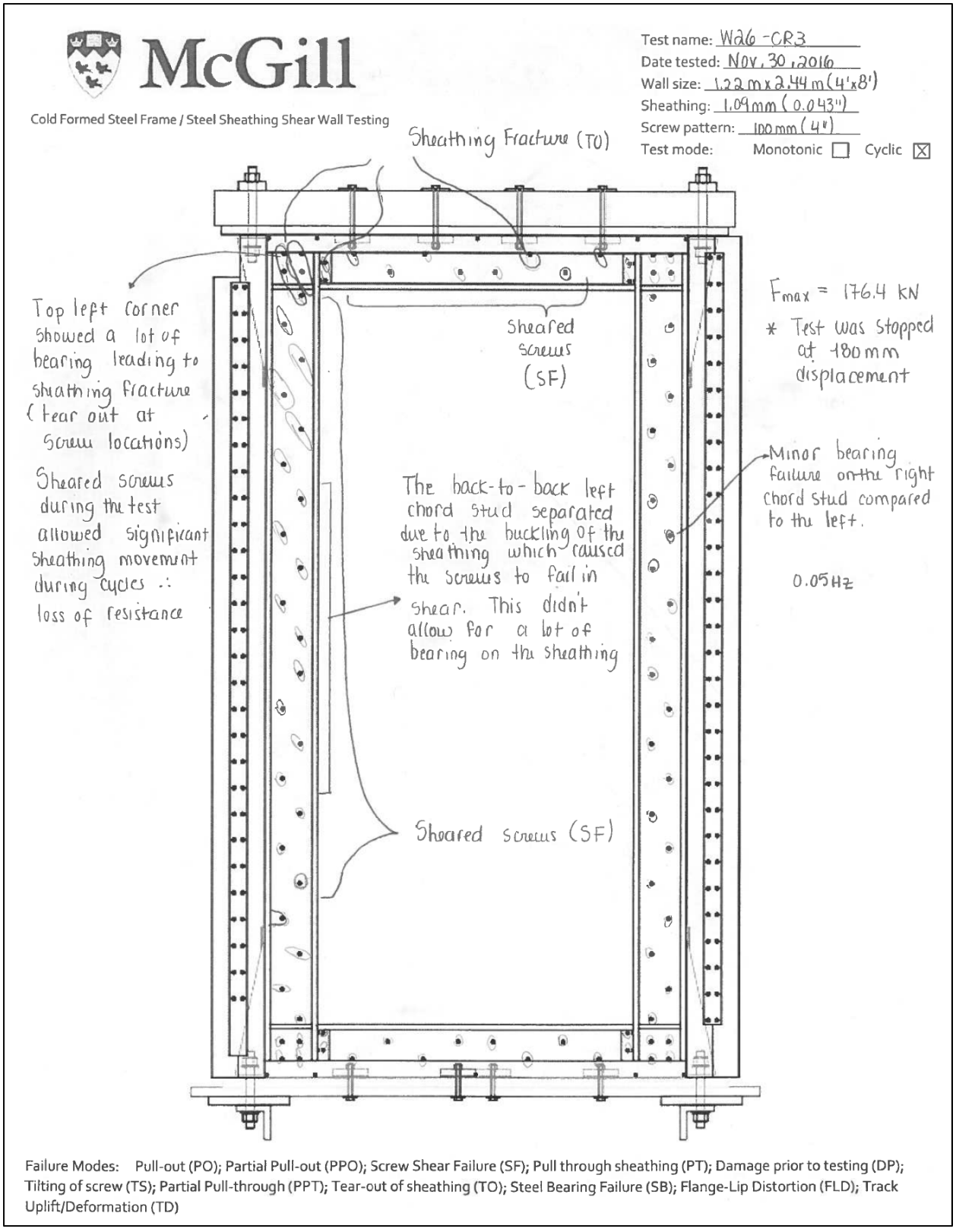

Figure D32: Test observations of centred-sheathed specimen W26-CR3.

APPENDIX E:

REDUCED TEST DATA

Table E1: Summary of Monotonic Shear Wall Test Results – Metric

Test	S_u (kN/m)	$S_{0.4u}$ (kN/m)	Δ_u (mm)	$\Delta_{0.4u}$ (mm)	$\Delta_{0.8u}$[1] (mm)	θ_u (radx10^{-3})	$\theta_{0.4u}$ (radx10^{-3})	$\theta_{0.8u}$[1] (radx10^{-3})	E_{total} (J)
Double-Sheathed Configuration									
W19-M	39.6	15.8	28.1	4.65	57.1	11.5	1.91	23.4	4230
W20-M	27.3	10.9	39.3	3.18	66.7	16.1	1.31	27.4	3158
W21-M	45.9	18.3	27.0	4.47	56.1	11.1	1.83	23.0	4980
W22-M	28.4	11.3	41.2	3.45	74.5	16.9	1.41	30.5	3606
W28-M[2]	61.0	24.4	31.7	5.41	61.8	13.0	2.22	25.4	6463
W29-M[2]	38.2	15.3	34.3	3.51	85.0	14.1	1.44	34.9	4674
W30-M[2]	65.4	26.2	39.0	7.16	68.7	16.0	2.94	28.2	7248
W31-M[2]	39.3	15.7	29.9	3.21	76.2	12.3	1.32	31.2	4783
Centre-Sheathed Configuration									
W15-MR3	150	59.9	120	14.7	100	49.2	6.03	41.0	16788
W16-MR	125	49.89	67.5	12.3	100	27.7	5.06	41.0	14479
W16-MR2	130	51.8	106	15.1	100	43.3	6.21	41.0	15207
W17-M	75.7	30.3	99.4	10.9	100	40.8	4.45	41.0	9221
W18-M[2]	87.2	34.9	68.2	10.8	100	28.0	4.43	41.0	10481
W18-MR[2]	92.6	37.1	87.3	10.8	100	35.8	4.44	41.0	11211

[1] Calculated based on the 4% lateral drift (approximately 100 mm) value.
[2] Test results computed by Brière *(2017)*.

Table E2: Summary of Monotonic Shear Wall Test Results – Imperial

Test	S_u (lb/ft)	$S_{0.4u}$ (lb/ft)	Δ_u (in)	$\Delta_{0.4u}$ (in)	$\Delta_{0.8u}$[1] (in)	θ_u (radx10^{-3})	$\theta_{0.4u}$ (radx10^{-3})	$\theta_{0.8u}$[1] (radx10^{-3})	E_{total} (ft·lb)
Double-Sheathed Configuration									
W19-M	2711	1082	1.11	0.183	2.25	11.5	1.91	23.4	3120
W20-M	1869	747	1.55	0.125	2.63	16.1	1.31	27.4	2329
W21-M	3143	1253	1.06	0.176	2.21	11.1	1.83	23.0	3673
W22-M	1943	776	1.62	0.136	2.93	16.9	1.41	30.5	2660
W28-M[2]	4179	1672	1.25	0.213	2.43	13.0	2.22	25.4	4767
W29-M[2]	2619	1048	1.35	0.138	3.35	14.1	1.44	34.9	3447
W30-M[2]	4483	1793	1.54	0.282	2.71	16.0	2.94	28.2	5346
W31-M[2]	2692	1077	1.18	0.126	3.00	12.3	1.32	31.2	3528
Centre-Sheathed Configuration									
W15-MR3	10265	4107	4.72	0.579	3.94	49.2	6.03	41.0	12382
W16-MR	8538	3418	2.66	0.485	3.94	27.7	5.06	41.0	10679
W16-MR2	8880	3551	4.15	0.596	3.94	43.3	6.21	41.0	11216
W17-M	5188	2073	3.91	0.428	3.94	40.8	4.45	41.0	6801
W18-M[2]	5976	2390	2.69	0.426	3.94	28.0	4.43	41.0	7730
W18-MR[2]	6349	2540	3.44	0.426	3.94	35.8	4.44	41.0	8269

[1] Calculated based on the 4% lateral drift (approximately 4") value.
[2] Test results computed by Brière *(2017).*

Table E3-a: Summary of Positive Cyclic Shear Wall Test Results – Metric

Test	S_u^+ (kN/m)	$S_{0.4u}^+$ (kN/m)	Δ_u^+ (mm)	$\Delta_{0.4u}^+$ (mm)	$\Delta_{0.8u}^{+\,1}$ (mm)	θ_u^+ (radx10^{-3})	$\theta_{0.4u}^+$ (radx10^{-3})	$\theta_{0.8u}^{+\,1}$ (radx10^{-3})	E_{BB}^+ (J)	E_{total} (J)
Double-Sheathed Configuration										
W19-C	46.5	21.6	34.0	6.36	52.0	13.9	2.61	21.3	4224	15062
W20-C	29.9	12.6	28.0	3.51	50.5	11.5	1.44	20.7	2892	10508
W21-C	47.6	21.3	29.1	6.04	50.6	11.9	2.48	20.7	4158	13970
W22-C	29.8	11.9	26.2	3.17	43.4	10.7	1.30	17.8	2770	9493
W28-C[2]	61.4	24.6	29.5	5.48	50.5	12.1	2.25	20.7	5415	18482
W29-C[2]	40.8	16.3	25.7	3.48	40.4	10.6	1.43	16.6	3569	12611
W30-C[2]	71.0	28.4	38.2	6.84	59.8	15.7	2.81	24.5	7109	24628
W31-C[2]	45.7	18.3	31.9	3.86	48.4	13.1	1.58	19.9	3987	14282

[1] Calculated based on the 4% lateral drift (approximately 100 mm) value.
[2] Test results computed by Brière *(2017)*.

Table E3-b: Summary of Positive Cyclic Shear Wall Test Results – Metric

Test	S_u^+ (kN/m)	$S_{0.4u}^+$ (kN/m)	Δ_u^+ (mm)	$\Delta_{0.4u}^+$ (mm)	$\Delta_{0.8u}^{+\,1}$ (mm)	θ_u^+ (radx10^{-3})	$\theta_{0.4u}^+$ (radx10^{-3})	$\theta_{0.8u}^{+\,1}$ (radx10^{-3})	E_{BB}^+ (J)	E_{total} (J)
Centre-Sheathed Configuration										
W15-CR3	162	63.3	112	15.0	100	45.9	6.15	41.0	16695	75743
W15B-CR3[2]	166	63.9	160	13.3	100	65.6	5.46	41.2	37285	109013
W17-C	81.8	32.5	74.3	12.4	101	30.5	5.09	41.3	7908	56432
W18-CR[3]	94.8	37.9	89.0	13.0	100	36.5	5.34	41.0	11079	64012
W23-CR3[3]	163	65.0	121	15.1	100	49.4	6.21	41.0	18288	48419
W23B-CR3[2,3]	159	63.4	122	14.0	100	49.9	5.74	41.0	30306	98377
W24-CR3[3]	135	54.1	81.2	13.5	100	33.3	5.54	41.0	14510	76112
W25-CR3[2]	117	48.6	86.0	12.7	100	35.3	5.20	41.0	20117	70483
W26-CR3[2,3]	145	58.1	65.7	12.9	83.5	27.0	5.28	34.3	19176	61059

[1] Calculated based on the 4% lateral drift (approximately 100 mm) value.
[2] Asymmetric cyclic test, only positive parameters obtained.
[3] Test results computed by Brière *(2017)*.

Table E4-a: Summary of Positive Cyclic Shear Wall Test Results – Imperial

Test	S_u^+ (lb/ft)	$S_{0.4u}^+$ (lb/ft)	Δ_u^+ (in)	$\Delta_{0.4u}^+$ (in)	$\Delta_{0.8u}^{+\,1}$ (in)	θ_u^+ (radx10^{-3})	$\theta_{0.4u}^+$ (radx10^{-3})	$\theta_{0.8u}^{+\,1}$ (radx10^{-3})	E_{BB}^+ (ft·lb)	E_{total} (ft·lb)
Double-Sheathed Configuration										
W19-C	3188	1482	1.34	0.250	2.05	13.9	2.61	21.3	3115	11109
W20-C	2045	861	1.10	0.138	1.99	11.5	1.44	20.7	2133	7750
W21-C	3260	1456	1.14	0.238	1.99	11.9	2.48	20.7	3067	10304
W22-C	2042	814	1.03	0.125	1.71	10.7	1.30	17.8	2043	7002
W28-C[2]	4207	1683	1.16	0.216	1.99	12.1	2.25	20.7	3994	13632
W29-C[2]	2796	1118	1.01	0.137	1.59	10.6	1.43	16.6	2632	9302
W30-C[2]	4862	1945	1.50	0.269	2.36	15.7	2.81	24.5	5243	18165
W31-C[2]	3128	1251	1.25	0.152	1.91	13.1	1.58	19.9	2941	10534

[1] Calculated based on the 4% lateral drift (approximately 4") value.
[2] Test results computed by Brière *(2017).*

Table E4-b: Summary of Positive Cyclic Shear Wall Test Results – Imperial

Test	S_u^+ (lb/ft)	$S_{0.4u}^+$ (lb/ft)	Δ_u^+ (in)	$\Delta_{0.4u}^+$ (in)	$\Delta_{0.8u}^{+\,1}$ (in)	θ_u^+ (radx10^{-3})	$\theta_{0.4u}^+$ (radx10^{-3})	$\theta_{0.8u}^{+\,1}$ (radx10^{-3})	E_{BB}^+ (ft·lb)	E_{total} (ft·lb)
Centre-Sheathed Configuration										
W15-CR3	11101	4337	4.41	0.591	3.94	45.9	6.15	41.0	12314	55865
W15B-CR3[2]	11354	4380	6.30	0.524	3.95	65.6	5.46	41.2	27500	80404
W17-C	5602	2230	2.92	0.488	3.96	30.5	5.09	41.3	5833	41622
W18-CR[3]	6492	2597	3.51	0.513	3.94	36.5	5.34	41.0	8171	47213
W23-CR3[3]	11135	4454	4.74	0.596	3.94	49.4	6.21	41.0	13489	35712
W23B-CR3[2,3]	10868	4347	4.79	0.551	3.94	49.9	5.74	41.0	22353	72560
W24-CR3[3]	9271	3708	3.20	0.532	3.94	33.3	5.54	41.0	10702	56138
W25-CR3[2]	7997	3332	3.39	0.499	3.94	35.3	5.20	41.0	14838	51986
W26-CR3[2,3]	9956	3982	2.59	0.507	3.29	27.0	5.28	34.3	14143	45035

[1] Calculated based on the 4% lateral drift (approximately 4") value.
[2] Asymmetric cyclic test, only positive parameters obtained.
[3] Test results computed by Brière *(2017).*

Table E5-a: Summary of Negative Cyclic Shear Wall Test Results – Metric

Test	S_u^- (kN/m)	$S_{0.4u}^-$ (kN/m)	Δ_u^- (mm)	$\Delta_{0.4u}^-$ (mm)	$\Delta_{0.8u}^{-\,1}$ (mm)	θ_u^- (radx10^{-3})	$\theta_{0.4u}^-$ (radx10^{-3})	$\theta_{0.8u}^{-\,1}$ (radx10^{-3})	E_{BB}^- (J)	E_{total} (J)
Double-Sheathed Configuration										
W19-C	-42.9	-21.0	-25.0	-6.43	-45.5	-10.3	-2.64	-18.7	3771	15062
W20-C	-30.3	-13.2	-24.5	-3.69	-36.0	-10.0	-1.51	-14.8	2476	10508
W21-C	-44.8	-17.6	-21.5	-4.80	-41.0	-8.83	-1.97	-16.8	3675	13970
W22-C	-29.8	-11.2	-24.0	-3.41	-39.3	-9.83	-1.40	-16.1	2644	9493
W28-C[2]	-62.1	-24.9	-26.4	-6.03	-38.1	-10.8	-2.47	-15.6	4833	18482
W29-C[2]	-39.9	-15.9	-24.3	-4.90	-37.2	-9.97	-2.01	-15.3	3239	12611
W30-C[2]	-68.6	-27.4	-31.2	-6.45	-44.0	-12.8	-2.65	-18.0	6204	24628
W31-C[2]	-44.4	-17.8	-26.5	-3.86	-44.2	-10.9	-1.58	-18.1	3750	14282

[1] Calculated based on the 4% lateral drift (approximately 100 mm) value.
[2] Test results computed by Brière *(2017)*.

Table E5-b: Summary of Negative Cyclic Shear Wall Test Results – Metric

Test	S_u^- (kN/m)	$S_{0.4u}^-$ (kN/m)	Δ_u^- (mm)	$\Delta_{0.4u}^-$ (mm)	$\Delta_{0.8u}^{-\,1}$ (mm)	θ_u^- (radx10^{-3})	$\theta_{0.4u}^-$ (radx10^{-3})	$\theta_{0.8u}^{-\,1}$ (radx10^{-3})	E_{BB}^- (J)	E_{total} (J)
Centre-Sheathed Configuration										
W15-CR3	-156	-63.5	-103	-15.5	-100	-42.3	-6.35	-41.0	14219	75743
W15B-CR3[2]	-	-	-	-	-	-	-	-	-	-
W17-C	-79.8	-32.9	-78.89	-10.9	-99.6	-32.4	-4.47	-40.9	7831	56432
W18-CR[3]	-89.9	-36.0	-70.7	-12.7	-100	-29.0	-5.22	-41.0	9775	9775
W23-CR3[3]	-132	-52.7	-50.3	-11.1	-50.3	-20.6	-4.56	-20.6	5074	5074
W23B-CR3[2,3]	-	-	-	-	-	-	-	-	-	-
W24-CR3[3]	-128	-51.0	-78.0	-11.9	-100	-32.0	-4.88	-41.0	13367	13367
W25-CR3[2]	-	-	-	-	-	-	-	-	-	-
W26-CR3[2,3]	-	-	-	-	-	-	-	-	-	-

[1] Calculated based on the 4% lateral drift (approximately 100 mm) value.
[2] Asymmetric cyclic test, only positive parameters obtained.
[3] Test results computed by Brière *(2017)*.

Table E6-a: Summary of Negative Cyclic Shear Wall Test Results – Imperial

Test	S_u^- (lb/ft)	$S_{0.4u}^-$ (lb/ft)	Δ_u^- (in)	$\Delta_{0.4u}^-$ (in)	$\Delta_{0.8u}^{-\,1}$ (in)	θ_u^- (radx10^{-3})	$\theta_{0.4u}^-$ (radx10^{-3})	$\theta_{0.8u}^{-\,1}$ (radx10^{-3})	E_{BB}^- (ft·lb)	E_{total} (ft·lb)
Double-Sheathed Configuration										
W19-C	-2938	-1436	-0.984	-0.253	-1.79	-10.3	-2.64	-18.7	2781	11109
W20-C	-2077	-902	-0.964	-0.145	-1.42	-10.0	-1.51	-14.8	1826	7750
W21-C	-3068	-1207	-0.848	-0.189	-1.61	-8.83	-1.97	-16.8	2711	10304
W22-C	-2043	-769	-0.944	-0.134	-1.55	-9.83	-1.40	-16.1	1950	7002
W28-C[2]	-4258	-1703	-1.04	-0.237	-1.50	-10.8	-2.47	-15.6	3565	13632
W29-C[2]	-2731	-1092	-0.957	-0.193	-1.46	-9.97	-2.01	-15.3	2389	9302
W30-C[2]	-4700	-1880	-1.23	-0.254	-1.73	-12.8	-2.65	-18.0	4576	18165
W31-C[2]	-3044	-1218	-1.04	-0.152	-1.74	-10.9	-1.58	-18.1	2766	10534

[1] Calculated based on the 4% lateral drift (approximately 4") value.
[2] Test results computed by Brière *(2017)*.

Table E6-b: Summary of Negative Cyclic Shear Wall Test Results – Imperial

Test	S_u^- (lb/ft)	$S_{0.4u}^-$ (lb/ft)	Δ_u^- (in)	$\Delta_{0.4u}^-$ (in)	$\Delta_{0.8u}^{-\,1}$ (in)	θ_u^- (radx10^{-3})	$\theta_{0.4u}^-$ (radx10^{-3})	$\theta_{0.8u}^{-\,1}$ (radx10^{-3})	E_{BB}^- (ft·lb)	E_{total} (ft·lb)
Centre-Sheathed Configuration										
W15-CR3	-10669	-4349	-4.06	-0.609	-3.94	-42.3	-6.35	-41.0	10487	55865
W15B-CR3[2]	-	-	-	-	-	-	-	-	-	-
W17-C	-5465	-2255	-3.11	-0.429	-3.92	-32.4	-4.47	-40.9	5776	41622
W18-CR[3]	-6161	-2464	-2.78	-0.501	-3.94	-29.0	-5.22	-41.0	7210	47213
W23-CR3[3]	-9031	-3612	-1.98	-0.438	-1.98	-20.6	-4.56	-20.6	3742	35712
W23B-CR3[2,3]	-	-	-	-	-	-	-	-	-	-
W24-CR3[3]	-8737	-3495	-3.07	-0.469	-3.94	-32.0	-4.88	-41.0	9859	56138
W25-CR3[2]	-	-	-	-	-	-	-	-	-	-
W26-CR3[2,3]	-	-	-	-	-	-	-	-	-	-

[1] Calculated based on the 4% lateral drift (approximately 4") value.
[2] Asymmetric cyclic test, only positive parameters obtained.
[3] Test results computed by Brière *(2017)*.

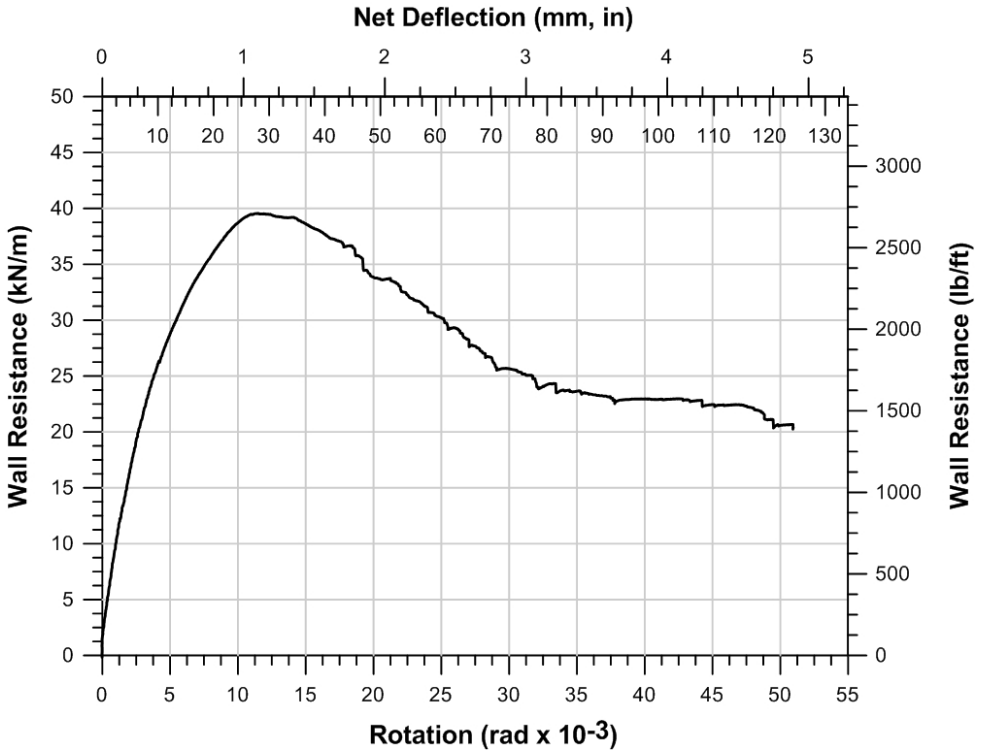

Figure E1: Monotonic test data of double-sheathed specimen W19-M.

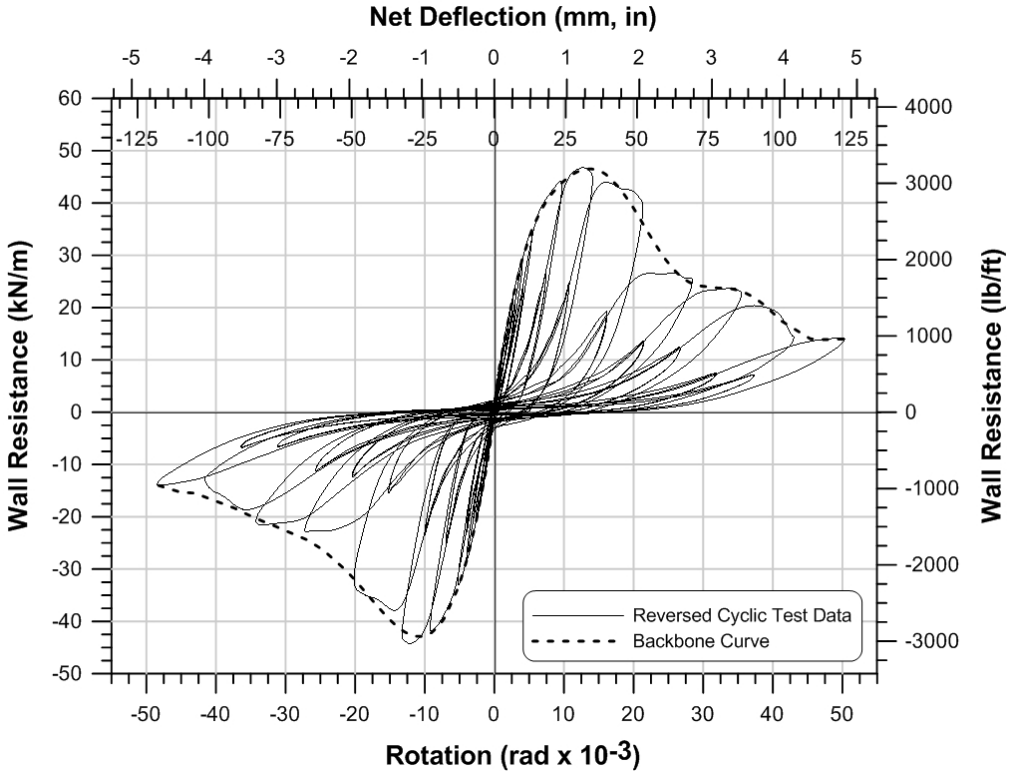

Figure E2: Reversed cyclic test data and backbone curve of double-sheathed specimen W19-C.

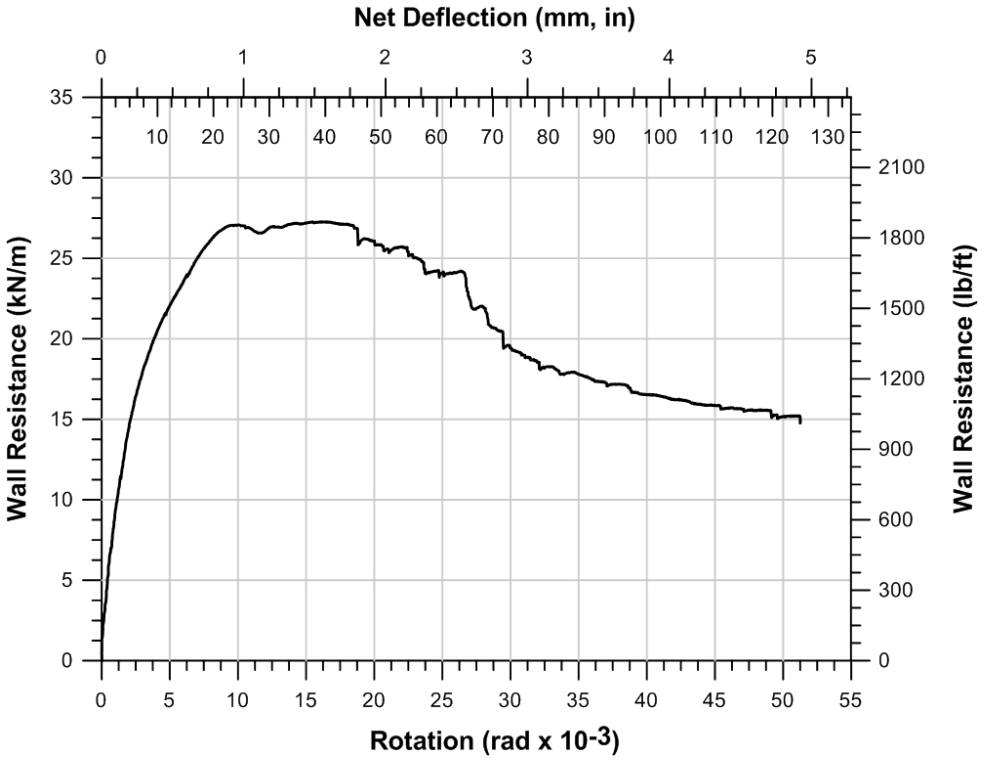

Figure E3: Monotonic test data of double-sheathed specimen W20-M.

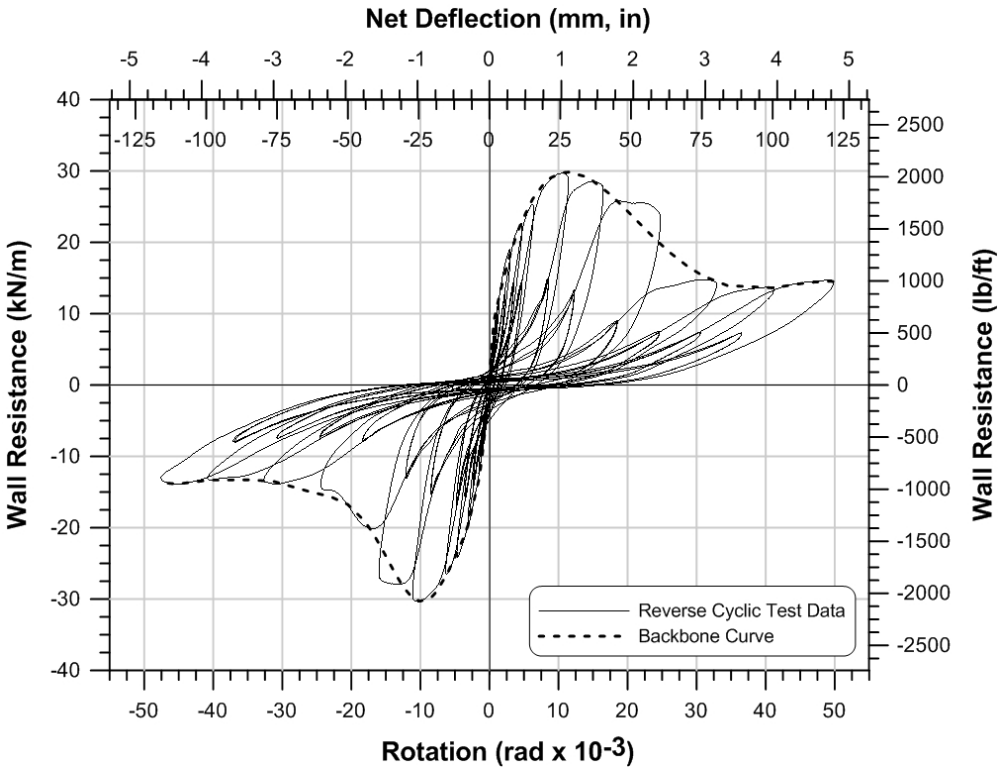

Figure E4: Reversed cyclic test data and backbone curve of double-sheathed specimen W20-C.

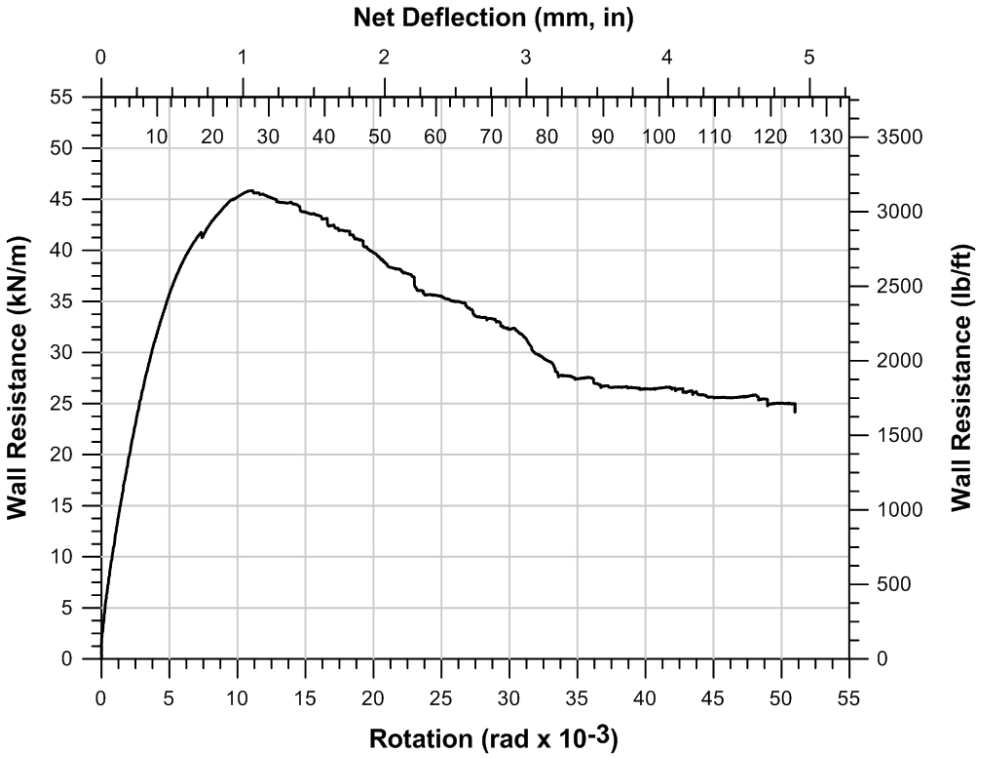

Figure E5: Monotonic test data of double-sheathed specimen W21-M.

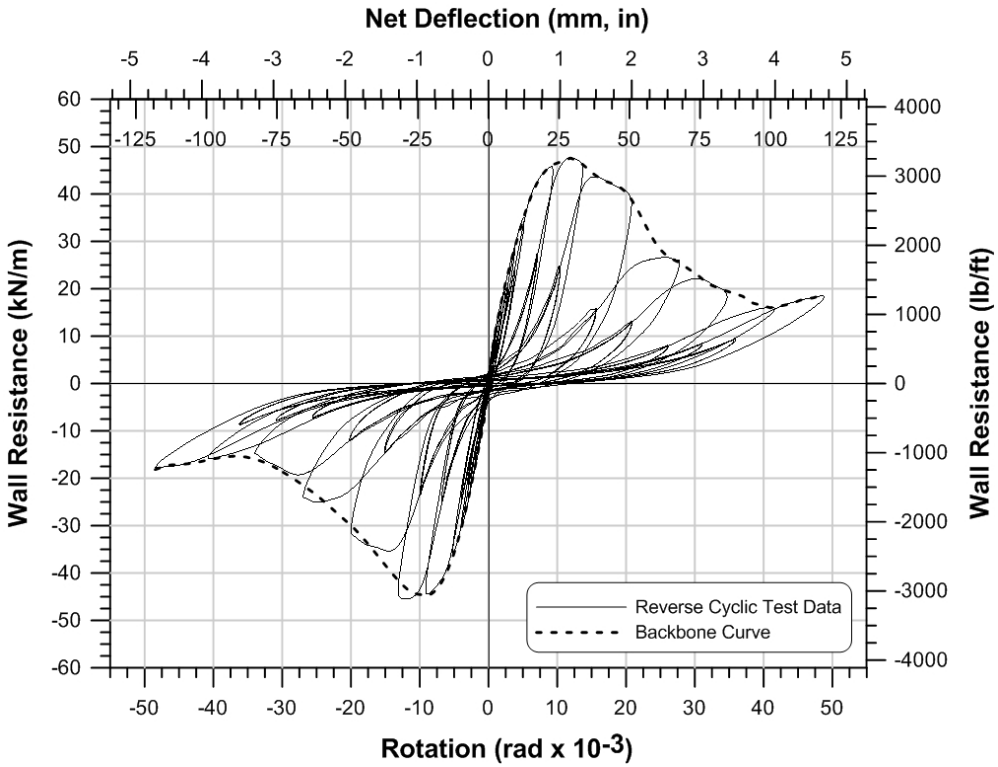

Figure E6: Reversed cyclic test data and backbone curve of double-sheathed specimen W21-C.

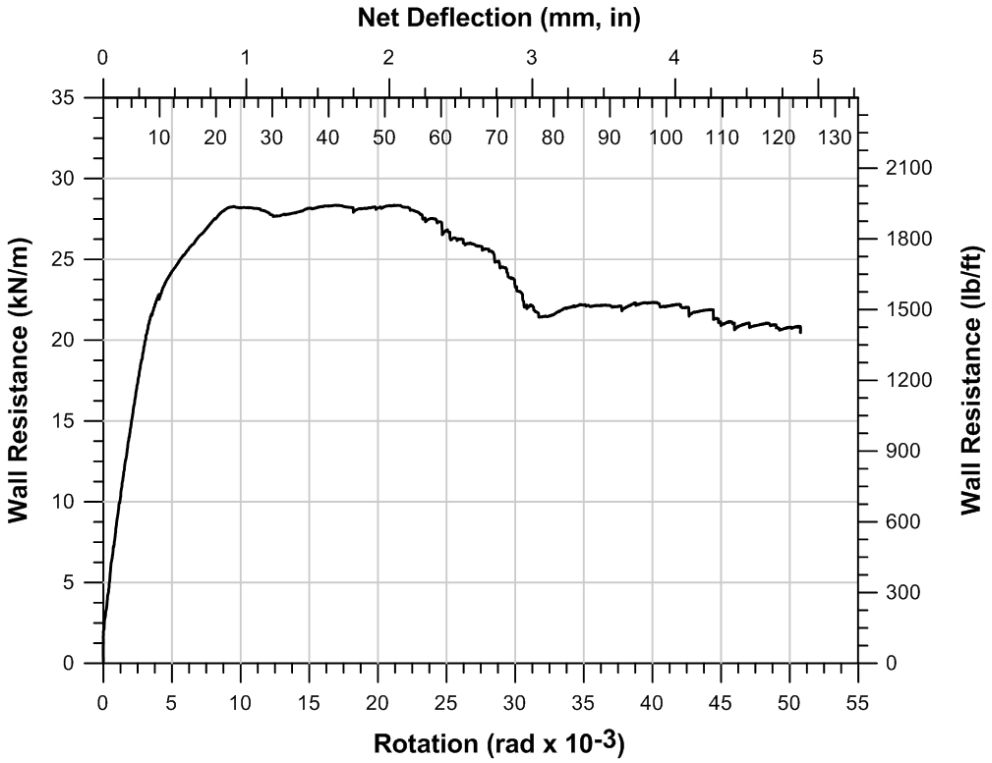

Figure E7: Monotonic test data of double-sheathed specimen W22-M.

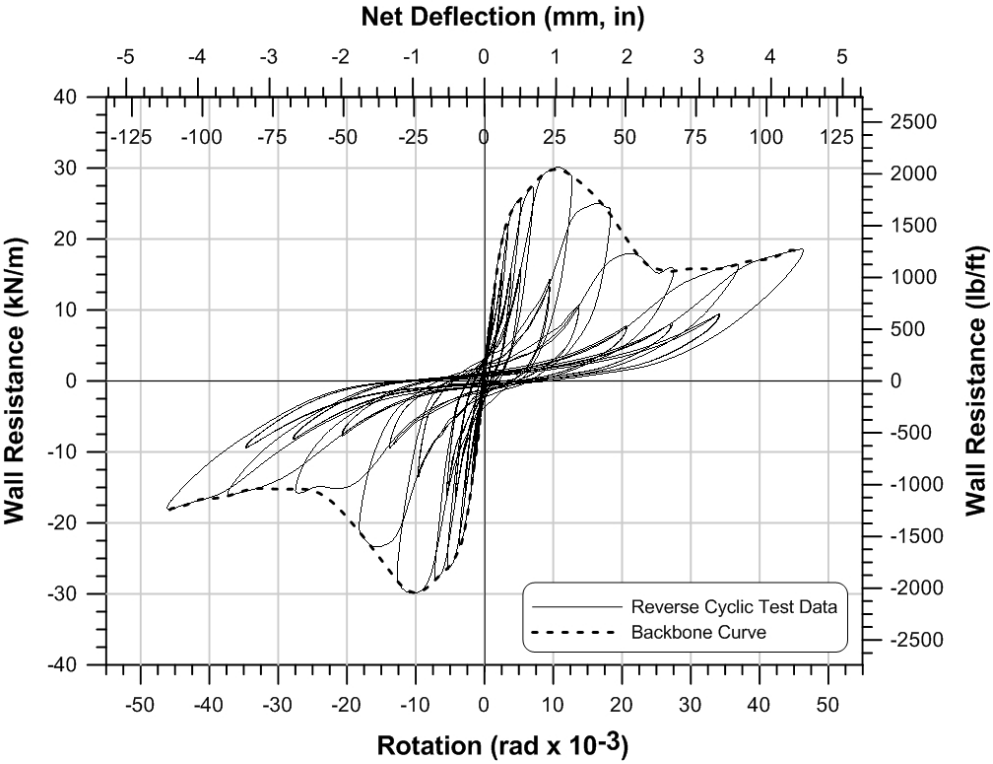

Figure E8: Reversed cyclic test data and backbone curve of double-sheathed specimen W22-C.

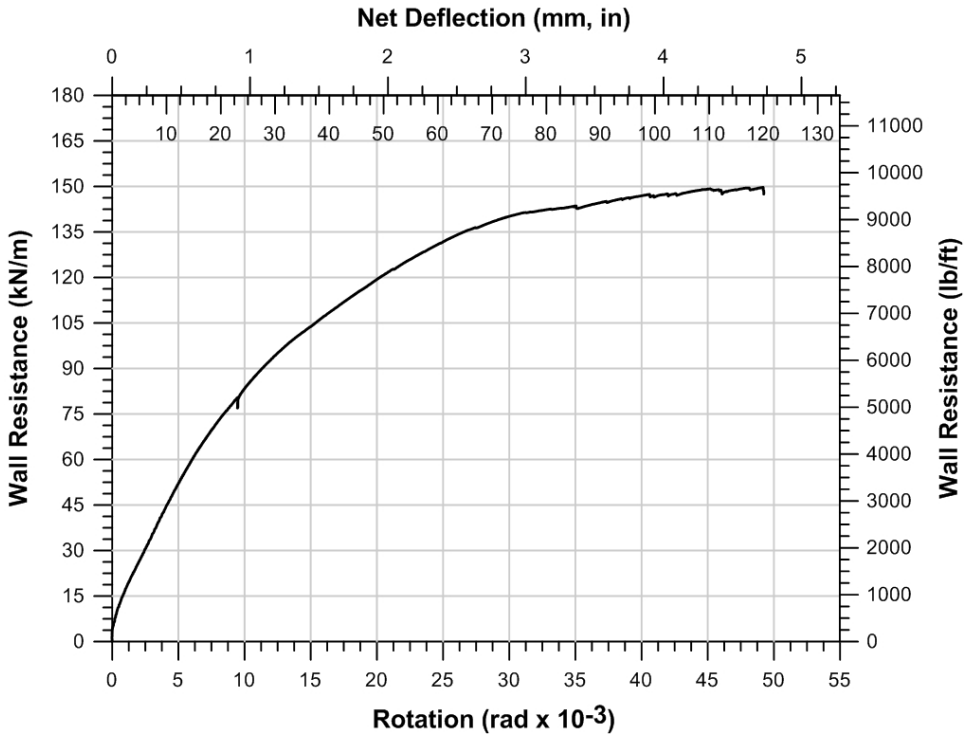

Figure E9: Monotonic test data of centre-sheathed specimen W15-MR3.

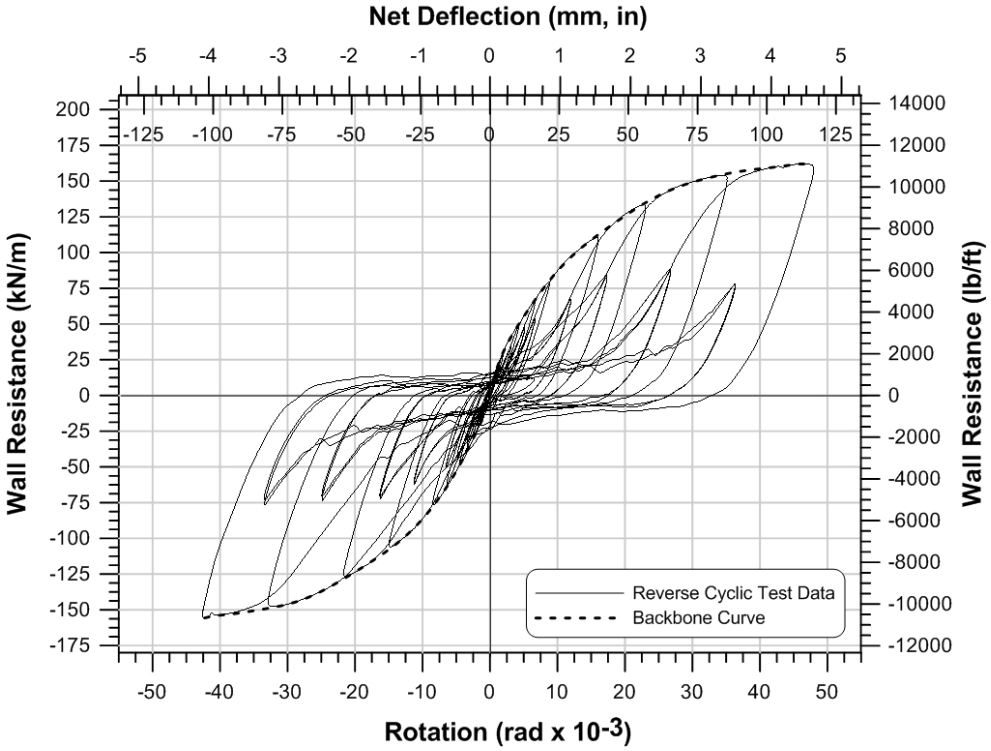

Figure E10: Reversed cyclic test data and backbone curve of centre-sheathed specimen W15-CR3.

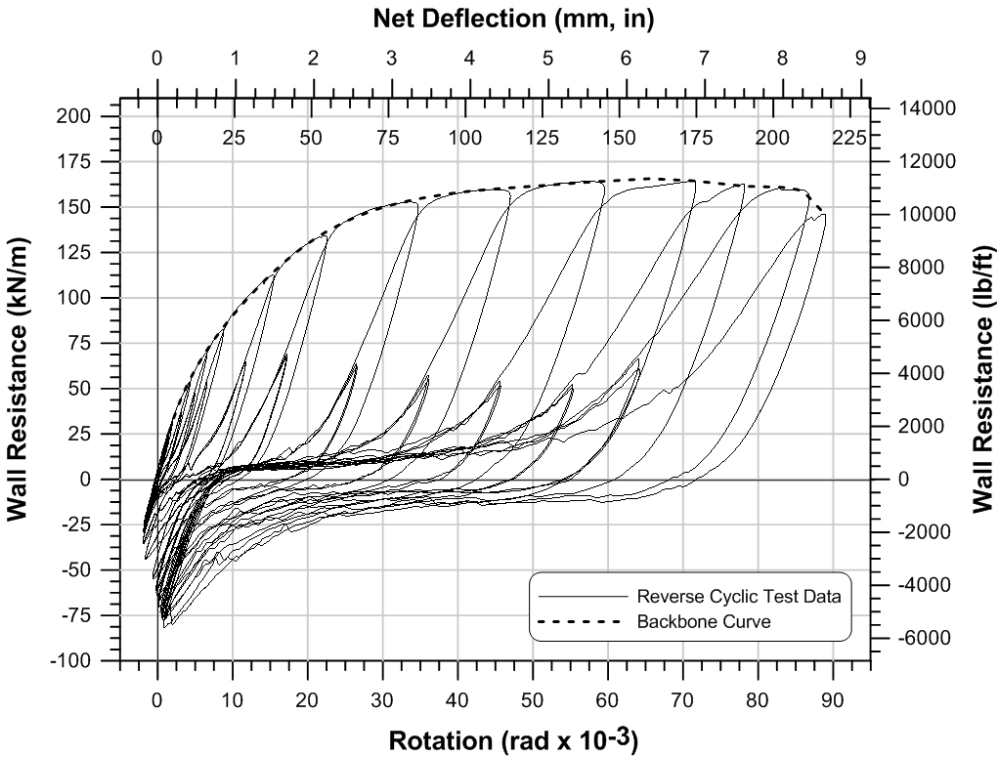

Figure E11: Asymmetric cyclic test data and backbone curve of centre-sheathed specimen W15B-CR3.

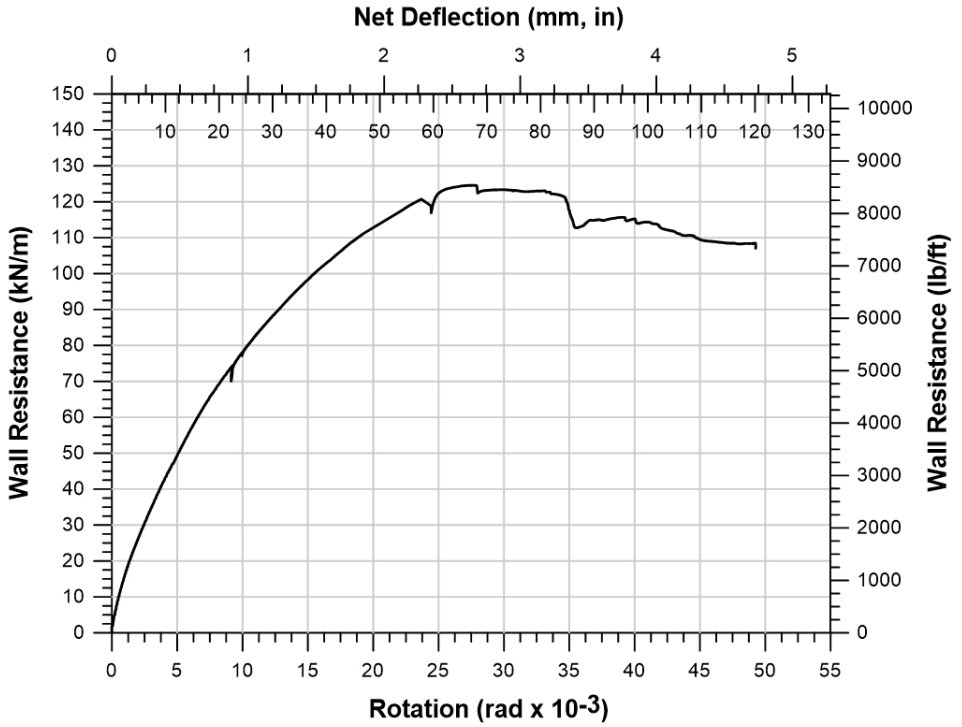

Figure E12: Monotonic test data of centre-sheathed specimen W16-MR.

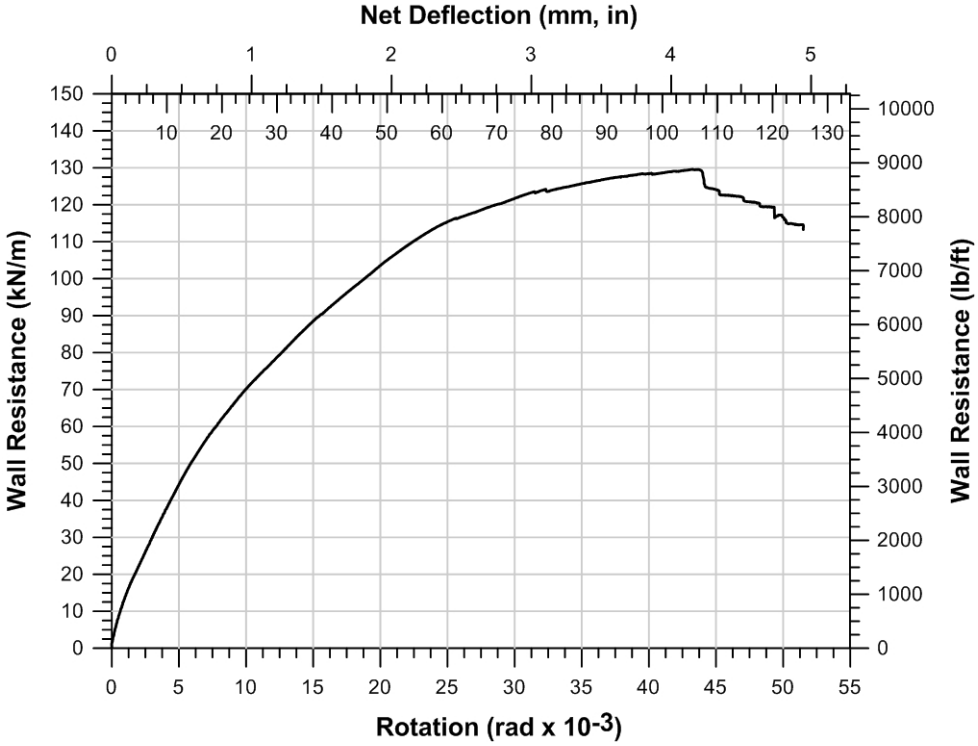

Figure E13: Monotonic test data of centre-sheathed specimen W16-MR2.

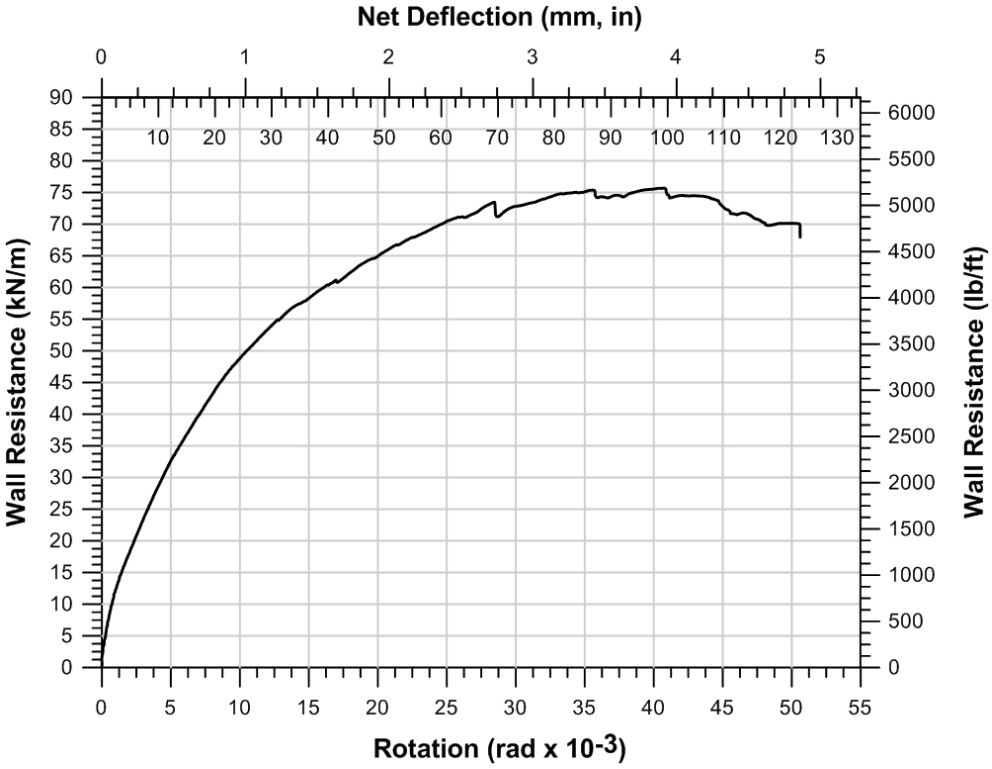

Figure E14: Monotonic test data of centre-sheathed specimen W17-M.

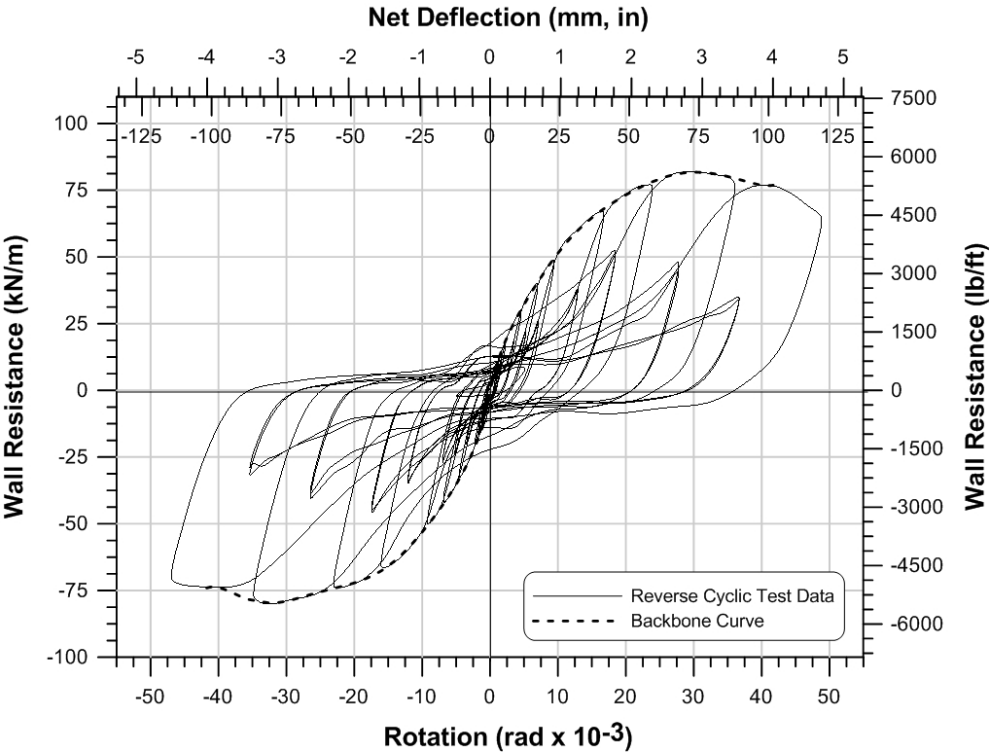

Figure E15: Reversed cyclic test data and backbone curve of centre-sheathed specimen W17-C.

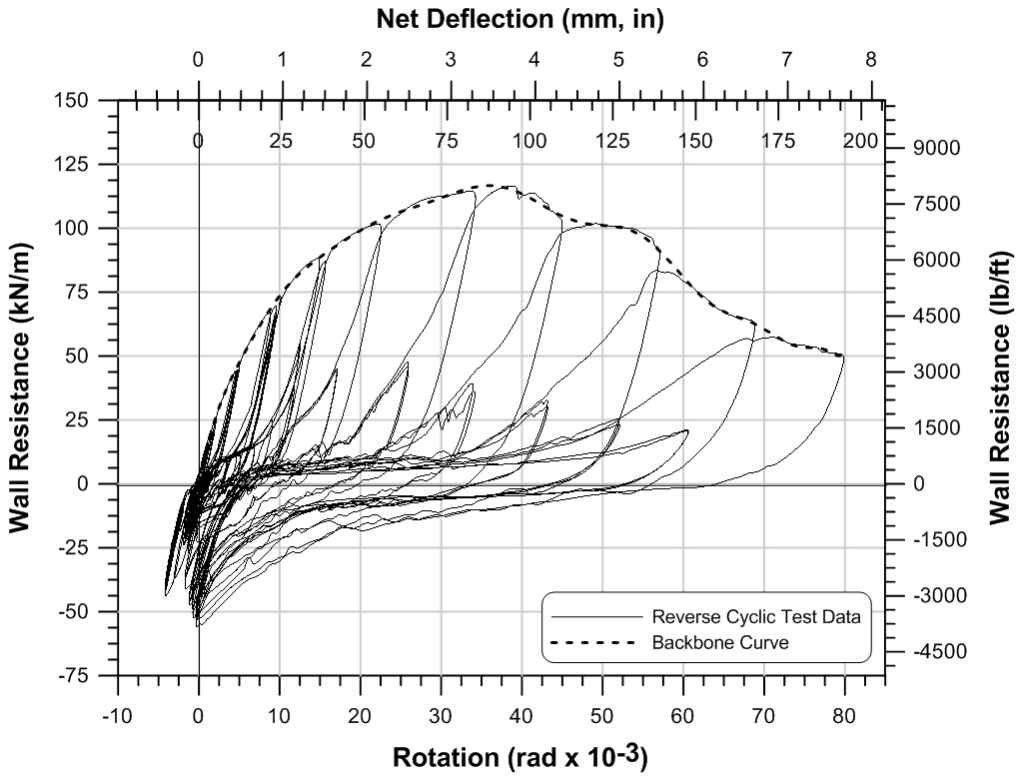

Figure E16: Asymmetric cyclic test data and backbone curve of centre-sheathed specimen W25-CR3.

APPENDIX F:

COUPON TEST RESULTS

For each type and thickness of material, 3 or 2 coupon samples were tested.

Table F1: Summary of Coupon Test Measurements and Results

Coupon	**Member**	***Nominal Thickness*** **mm (in)**	***Base Metal Thickness*** **mm (in)**	F_y **MPa (ksi)**	F_u **MPa (ksi)**	$\frac{F_u}{F_y}$	***Elongation*** **(%)**
A Transversal dir.	Sheathing	0.84 (0.033)	0.88 (0.035)	302 (43.8)	352 (51.1)	1.17	40
A Longitudinal dir.	Sheathing	0.84 (0.033)	0.87 (0.034)	276 (40.1)	358 (51.9)	1.30	39
B Transverse dir.	Sheathing	0.48[1] (0.019)	0.48 (0.019)	318 (46.1)	361 (52.3)	1.14	37.5
B Longitudinal dir.	Sheathing	0.47[1] (0.019)	0.47 (0.019)	340 (49.3)	368 (53.3)	1.08	39
C Transverse dir.	Sheathing	0.36[1] (0.014)	0.36 (0.014)	344 (50.0)	370 (53.7)	1.07	29
C Longitudinal dir.	Sheathing	0.36[1] (0.014)	0.36 (0.014)	305 (44.2)	358 (52.0)	1.18	26
D	Sheathing	1.09 (0.043)	1.12 (0.044)	316 (45.9)	380 (55.1)	1.20	-
Strap	Steel Strap	1.09 (0.043)	1.11 (0.044)	366 (53.1)	447 (64.8)	1.22	30
Stud A / Track A	Stud/Track	1.73 (0.068)	1.77 (0.070)	386 (56.0)	466 (67.6)	1.21	34
Track B	Track	2.46 (0.097)	2.54 (0.100)	380 (55.1)	451 (65.4)	1.19	35
Stud B	Stud	2.46 (0.097)	2.54 (0.100)	389 (56.4)	461 (66.9)	1.19	34

[1]Non-standard thicknesses, no nominal value.
Note: Sheathing samples were cut and tested in the transverse and longitudinal directions of the sheathing.

Table F2: Summary of Rt and R_y Values

Coupon	Member	*Thickness* mm (in)	R_t	R_y
A Transversal dir.	Sheathing	0.84 (0.033)	1.1	1.3
A Longitudinal dir.	Sheathing	0.84 (0.033)	1.2	1.2
B Transverse dir.	Sheathing	0.48 (0.019)	1.2	1.4
B Longitudinal dir.	Sheathing	0.47 (0.019)	1.2	1.5
C Transverse dir.	Sheathing	0.36 (0.014)	1.2	1.5
C Longitudinal dir.	Sheathing	0.36 (0.014)	1.2	1.3
D	Sheathing	1.09 (0.043)	1.2	1.4
Strap	Steel Strap	1.09 (0.043)	1.0	1.1
Stud A / Track A	Stud/Track	1.73 (0.068)	1.0	1.1
Track B	Track	2.46 (0.097)	1.0	1.1
Stud B	Stud	2.46 (0.097)	1.0	1.1

Note: Sheathing samples were cut and tested in the transverse and longitudinal directions of the sheathing.

APPENDIX G:

TEST DATA ANALYSIS RESULTS

Table G1: Monotonic Shear Wall EEEP Design Values – Metric

Test	S_y (kN/m)	Δ_y (mm)	$\Delta_{0.4u}$ (mm)	θ_y (radx10^{-3})	$\theta_{0.4u}$ (radx10^{-3})	k_e ((kN/m)/mm)	μ	E_{EEEP}[2] (J)
Double-Sheathed Configuration								
W19-M	35.5	10.5	4.65	4.29	1.91	3.39	5.46	2242
W20-M	25.2	7.36	3.18	3.02	1.31	3.42	9.07	1937
W21-M	41.4	10.1	4.47	4.15	1.83	4.10	5.55	2581
W22-M	26.8	8.15	3.45	3.34	1.41	3.29	9.13	2301
W28-M[1]	54.2	12.0	5.41	4.93	2.22	4.52	5.15	3691
W29-M[1]	34.8	7.97	3.51	3.27	1.44	4.37	10.7	3441
W30-M[1]	58.8	16.1	7.16	6.61	2.94	3.65	4.26	4349
W31-M[1]	36.3	7.43	3.21	3.05	1.32	4.88	10.3	3207
Centre-Sheathed Configuration								
W15-MR3	128	31.0	14.3	12.7	5.85	4.12	3.87	13158
W16-MR	112	27.7	12.3	11.4	5.06	4.05	4.34	11774
W16-MR2	111	32.3	15.0	13.3	6.13	3.44	3.88	11377
W17-M	66.6	23.9	10.9	9.80	4.45	2.79	5.16	7154
W18-M[1]	78.3	24.3	10.8	9.96	4.43	3.23	5.06	8397
W18-MR[1]	81.5	23.8	10.8	9.75	4.44	3.43	5.15	8754

[1] Test results computed by Brière *(2017)*.
[2] Total energy dissipated under the monotonic EEEP curve.

Table G2: Monotonic Shear Wall EEEP Design Values – Imperial

Test	S_y (lb/ft)	Δ_y (in)	$\Delta_{0.4u}$ (in)	θ_y (radx10^{-3})	$\theta_{0.4u}$ (radx10^{-3})	k_e ((lb/ft)/in)	μ	E_{EEEP}[2] (ft·lb)
Double-Sheathed Configuration								
W19-M	2430	0.411	0.183	4.29	1.91	5907	5.46	1654
W20-M	1725	0.290	0.125	3.02	1.31	5956	9.07	1429
W21-M	2839	0.398	0.176	4.15	1.83	7129	5.55	1904
W22-M	1836	0.321	0.136	3.34	1.41	5719	9.13	1697
W28-M[1]	3715	0.473	0.213	4.93	2.22	7866	5.15	2723
W29-M[1]	2385	0.314	0.138	3.27	1.44	7603	10.7	2538
W30-M[1]	4028	0.635	0.282	6.61	2.94	6351	4.26	3208
W31-M[1]	2486	0.292	0.126	3.05	1.32	8506	10.3	2365
Centre-Sheathed Configuration								
W15-MR3	8743	1.22	0.561	12.7	5.85	7162	3.87	9705
W16-MR	7674	1.09	0.485	11.4	5.06	7044	4.34	8684
W16-MR2	7620	1.27	0.589	13.3	6.13	5987	3.88	8391
W17-M	4565	0.941	0.428	9.80	4.45	4851	5.16	5277
W18-M[1]	5367	0.956	0.426	9.96	4.43	5619	5.06	6194
W18-MR[1]	5581	0.956	0.426	9.75	4.44	5966	5.15	6457

[1] Test results computed by Brière *(2017)*.
[2] Total energy dissipated under the EEEP curve.

Table G3: Positive Cyclic Shear Wall EEEP Design Values – Metric

Test	S_y^+ (kN/m)	Δ_y^+ (mm)	$\Delta_{0.4u}^+$ (mm)	θ_y^+ (radx10^{-3})	$\theta_{0.4u}^+$ (radx10^{-3})	k_e^+ ((kN/m)/mm)	μ^+	E_{EEEP}^{+3} (J)
Double-Sheathed Configuration								
W19-C	42.1	12.4	6.36	5.07	2.61	3.40	4.20	2352
W20-C	26.5	7.41	3.51	3.04	1.44	3.58	6.82	1515
W21-C	43.2	12.3	6.04	5.03	2.48	3.52	4.12	2339
W22-C	26.9	7.18	3.17	2.95	1.30	3.75	6.05	1307
W28-C[2]	53.5	11.9	5.48	4.90	2.25	4.48	4.23	2909
W29-C[2]	36.5	7.79	3.48	3.19	1.43	4.69	5.19	1627
W30-C[2]	63.9	15.4	6.84	6.32	2.81	4.15	3.88	4063
W31-C[2]	40.3	8.52	3.86	3.50	1.58	4.73	5.68	2173
Centre-Sheathed Configuration								
W15-CR3	137	32.4	15.0	13.3	6.15	4.22	3.52	13970
W15B-CR3[1]	136	28.4	13.3	11.7	5.46	4.80	7.62	14347
W17-C	74.0	28.2	12.4	11.6	5.09	2.62	3.61	7812
W18-CR[2]	86.0	29.6	13.0	12.1	5.34	2.91	4.02	8943
W23-CR3[2]	139	32.3	15.1	13.3	6.21	4.29	3.88	14203
W23B-CR3[1,2]	138	30.4	14.0	12.5	5.74	4.54	5.00	14281
W24-CR3[2]	118	29.5	13.5	12.1	5.54	4.01	3.89	12295
W25-CR3[1]	103	26.8	12.7	11.0	5.20	3.84	5.12	10866
W26-CR3[1,2]	126	27.9	12.9	11.4	5.28	4.52	2.99	10693

[1] Asymmetric cyclic test, only positive parameters obtained.
[2] Test results computed by Brière *(2017)*.
[3] Total energy dissipated under the positive EEEP curve.

Table G4: Positive Cyclic Shear Wall EEEP Design Values – Imperial

Test	S_y^+ (lb/ft)	Δ_y^+ (in)	$\Delta_{0.4u}^+$ (in)	θ_y^+ (radx10^{-3})	$\theta_{0.4u}^+$ (radx10^{-3})	k_e^+ ((lb/ft)/in)	μ^+	E_{EEEP}^{+3} (ft·lb)
Double-Sheathed Configuration								
W19-C	2886	0.487	0.250	5.07	2.61	5925	4.20	1735
W20-C	1818	0.292	0.138	3.04	1.44	6233	6.82	1117
W21-C	2957	0.483	0.238	5.03	2.48	6119	4.12	1725
W22-C	1843	0.283	0.125	2.95	1.30	6520	6.05	964
W28-C[2]	3669	0.470	0.216	4.90	2.25	7806	4.23	2145
W29-C[2]	2501	0.307	0.137	3.19	1.43	8160	5.19	1200
W30-C[2]	4379	0.606	0.269	6.32	2.81	7226	3.88	2997
W31-C[2]	2765	0.336	0.152	3.50	1.58	8243	5.68	1602
Centre-Sheathed Configuration								
W15-CR3	9360	1.27	0.591	13.3	6.15	7345	3.52	10304
W15B-CR3[1]	9346	1.12	0.524	11.7	5.46	8352	7.62	10582
W17-C	5070	1.11	0.488	11.6	5.09	4567	3.61	5762
W18-CR[2]	5894	1.16	0.513	12.1	5.34	5068	4.02	6596
W23-CR3[2]	9516	1.27	0.596	13.3	6.21	7478	3.88	10476
W23B-CR3[1,2]	9462	1.20	0.551	12.5	5.74	7898	5.00	10533
W24-CR3[2]	8100	1.16	0.532	12.1	5.54	6979	3.89	9068
W25-CR3[1]	7044	1.06	0.499	11.0	5.20	6678	5.12	8014
W26-CR3[1,2]	8631	1.10	0.506	11.4	5.28	7866	2.99	7887

[1] Asymmetric cyclic test, only positive parameters obtained.
[2] Test results computed by Brière *(2017)*.
[3] Total energy dissipated under the positive EEEP curve.

Table G5: Negative Cyclic Shear Wall EEEP Design Values – Metric

Test	S_y^- (kN/m)	Δ_y^- (mm)	$\Delta_{0.4u}^-$ (mm)	θ_y^- (radx10^{-3})	$\theta_{0.4u}^-$ (radx10^{-3})	k_e^- ((kN/m)/mm)	μ^-	E_{EEEP}^{-3} (J)
Double-Sheathed Configuration								
W19-C	-39.1	-12.0	-6.43	-4.92	-2.64	3.26	3.79	1882
W20-C	-26.5	-7.43	-3.69	-3.05	-1.52	3.56	4.84	1043
W21-C	-40.4	-11.0	-4.80	-4.52	-1.97	3.67	3.72	1748
W22-C	-26.9	-8.17	-3.41	-3.35	-1.40	3.29	4.80	1154
W28-C[2]	-54.5	-13.2	-6.03	-5.42	-2.47	4.12	2.88	2091
W29-C[2]	-35.7	-11.0	-4.90	-4.50	-2.01	3.25	3.39	1381
W30-C[2]	-60.4	-14.2	-6.45	-5.83	-2.65	4.25	3.09	2717
W31-C[2]	-38.6	-8.40	-3.86	-3.44	-1.58	4.60	5.26	1885
Centre-Sheathed Configuration								
W15-CR3	-133	-31.9	-14.5	-13.1	-5.95	4.17	3.23	13629
W15B-CR3[1]	-	-	-	-	-	-	-	-
W17-C	-71.3	-23.6	-10.9	-9.68	-4.47	3.02	4.31	7638
W18-CR[2]	-79.0	-28.0	-12.7	-11.5	-5.22	2.83	3.58	8300
W23-CR3[2]	-106	-22.4	-11.1	-9.20	-4.56	4.74	2.11	5074
W23B-CR3[1,2]	-	-	-	-	-	-	-	-
W24-CR3[2]	-113	-26.5	-11.9	-10.9	-4.88	4.28	4.12	12006
W25-CR3[1]	-	-	-	-	-	-	-	-
W26-CR3[1,2]	-	-	-	-	-	-	-	-

[1] Asymmetric cyclic test, only positive parameters obtained.
[2] Test results computed by Brière *(2017)*.
[3] Total energy dissipated under the positive EEEP curve.

Table G6: Negative Cyclic Shear Wall EEEP Design Values – Imperial

Test	S_y^- (lb/ft)	Δ_y^- (in)	$\Delta_{0.4u}^-$ (in)	θ_y^- (radx10^{-3})	$\theta_{0.4u}^-$ (radx10^{-3})	k_e^- ((lb/ft)/in)	μ^-	E_{EEEP}^{-3} (ft·lb)
Double-Sheathed Configuration								
W19-C	-2677	-0.472	-0.253	-4.92	-2.64	5670	3.79	1388
W20-C	-1814	-0.293	-0.145	-3.05	-1.52	6198	4.84	769
W21-C	-2770	-0.434	-0.189	-4.52	-1.97	6386	3.72	1289
W22-C	-1843	-0.322	-0.134	-3.35	-1.40	5728	4.80	851
W28-C[2]	-3734	-0.520	-0.237	-5.42	-2.47	7183	2.88	1542
W29-C[2]	-2446	-0.432	-0.193	-4.50	-2.01	5667	3.39	1018
W30-C[2]	-4138	-0.559	-0.254	-5.83	-2.65	7402	3.09	2004
W31-C[2]	-2648	-0.331	-0.152	-3.44	-1.58	8014	5.26	1390
Centre-Sheathed Configuration								
W15-CR3	-9107	-1.26	-0.571	-13.1	-5.95	7254	3.23	10052
W15B-CR3[1]	-	-	-	-	-	-	-	-
W17-C	-4884	-0.929	-0.429	-9.68	-4.47	5256	4.31	5633
W18-CR[2]	-5416	-1.10	-0.501	-11.5	-5.22	4925	3.58	6122
W23-CR3[2]	-7289	-0.88	-0.438	-9.20	-4.56	8256	2.11	3743
W23B-CR3[1,2]	-	-	-	-	-	-	-	-
W24-CR3[2]	-7772	-1.04	-0.469	-10.9	-4.88	7457	4.12	8855
W25-CR3[1]	-	-	-	-	-	-	-	-
W26-CR3[1,2]	-	-	-	-	-	-	-	-

[1] Asymmetric cyclic test, only positive parameters obtained.
[2] Test results computed by Brière *(2017)*.
[3] Total energy dissipated under the positive EEEP curve.

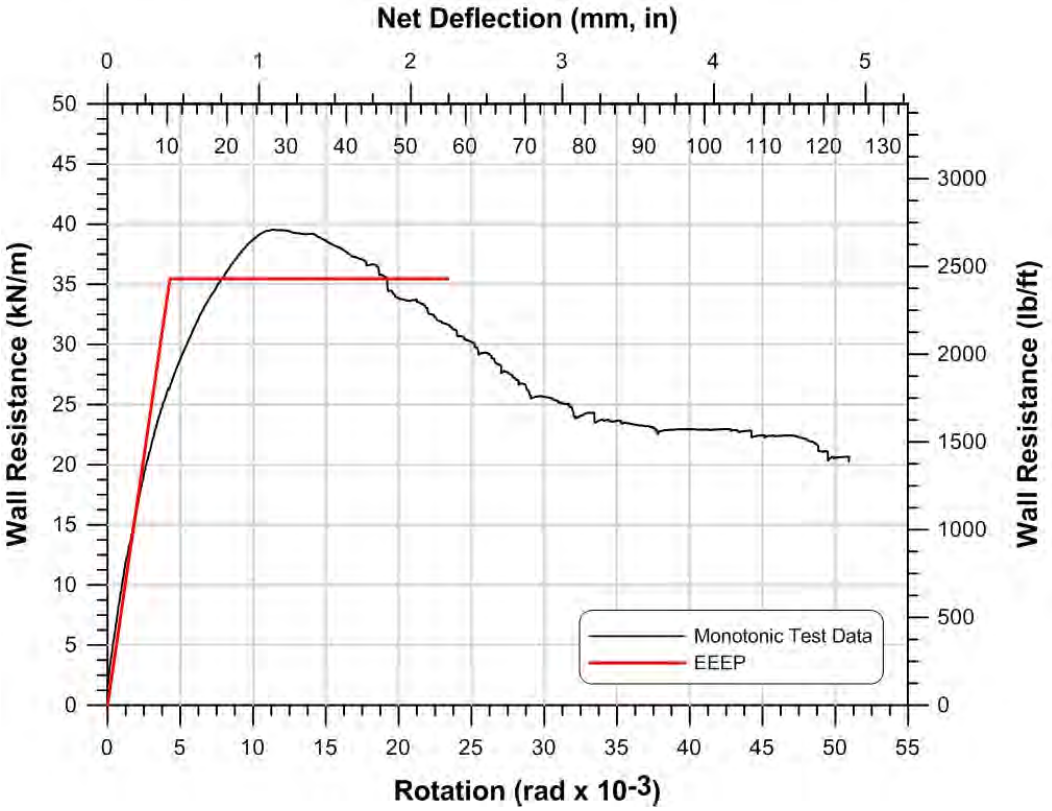

Figure G1: EEEP plot and monotonic test data of double-sheathed specimen W19-M.

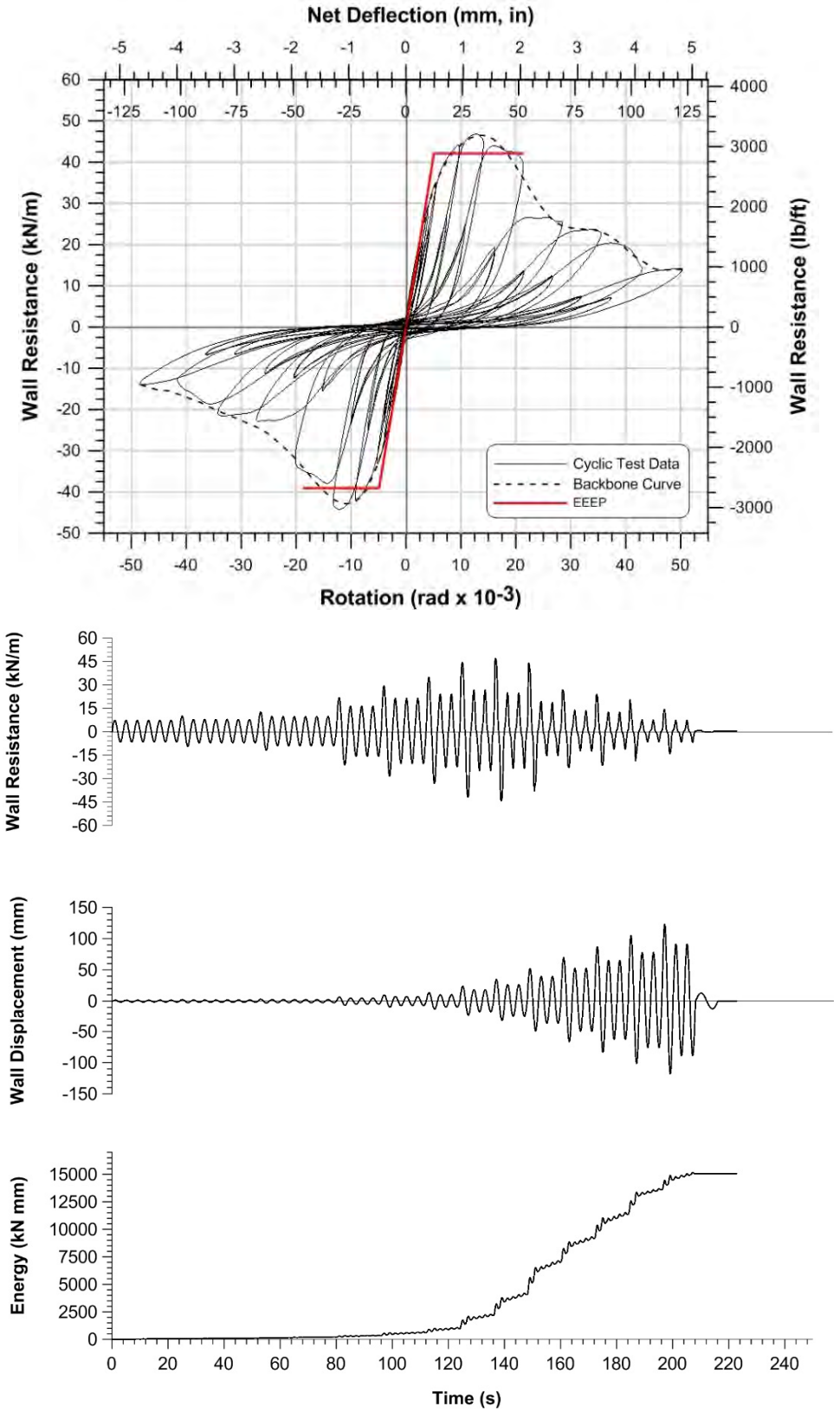

Figure G2: EEEP plot, cyclic test data, and time-history of double-sheathed specimen W19-C.

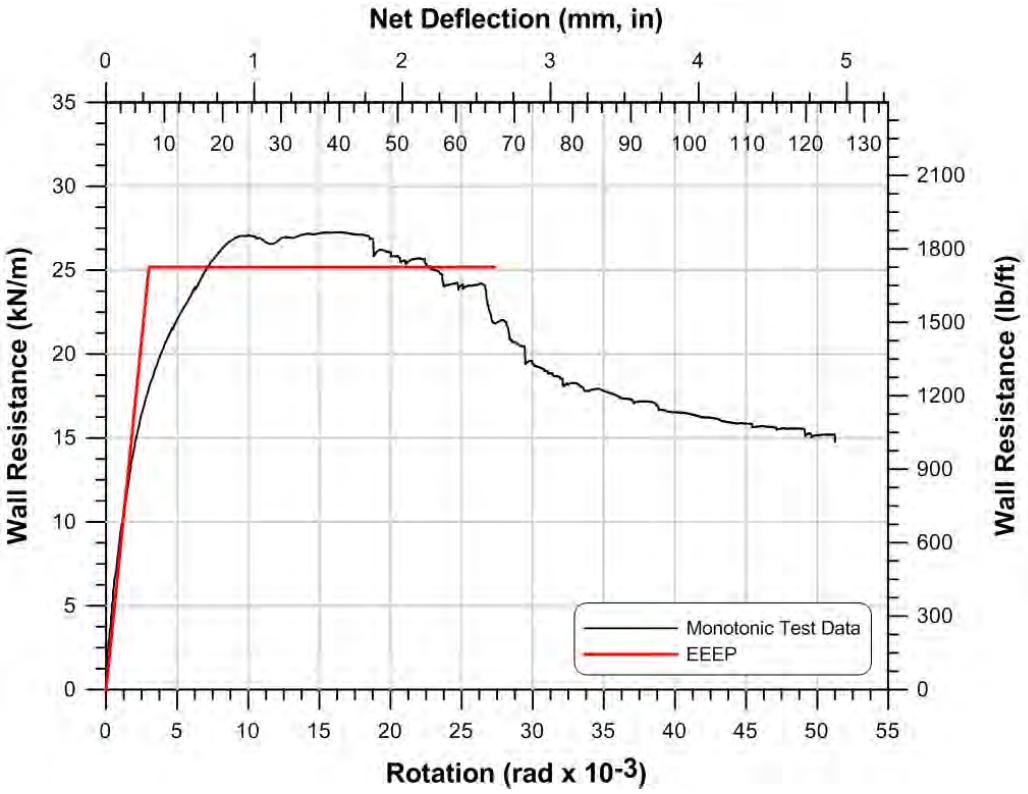

Figure G3: EEEP plot and monotonic test data of double-sheathed specimen W20-M.

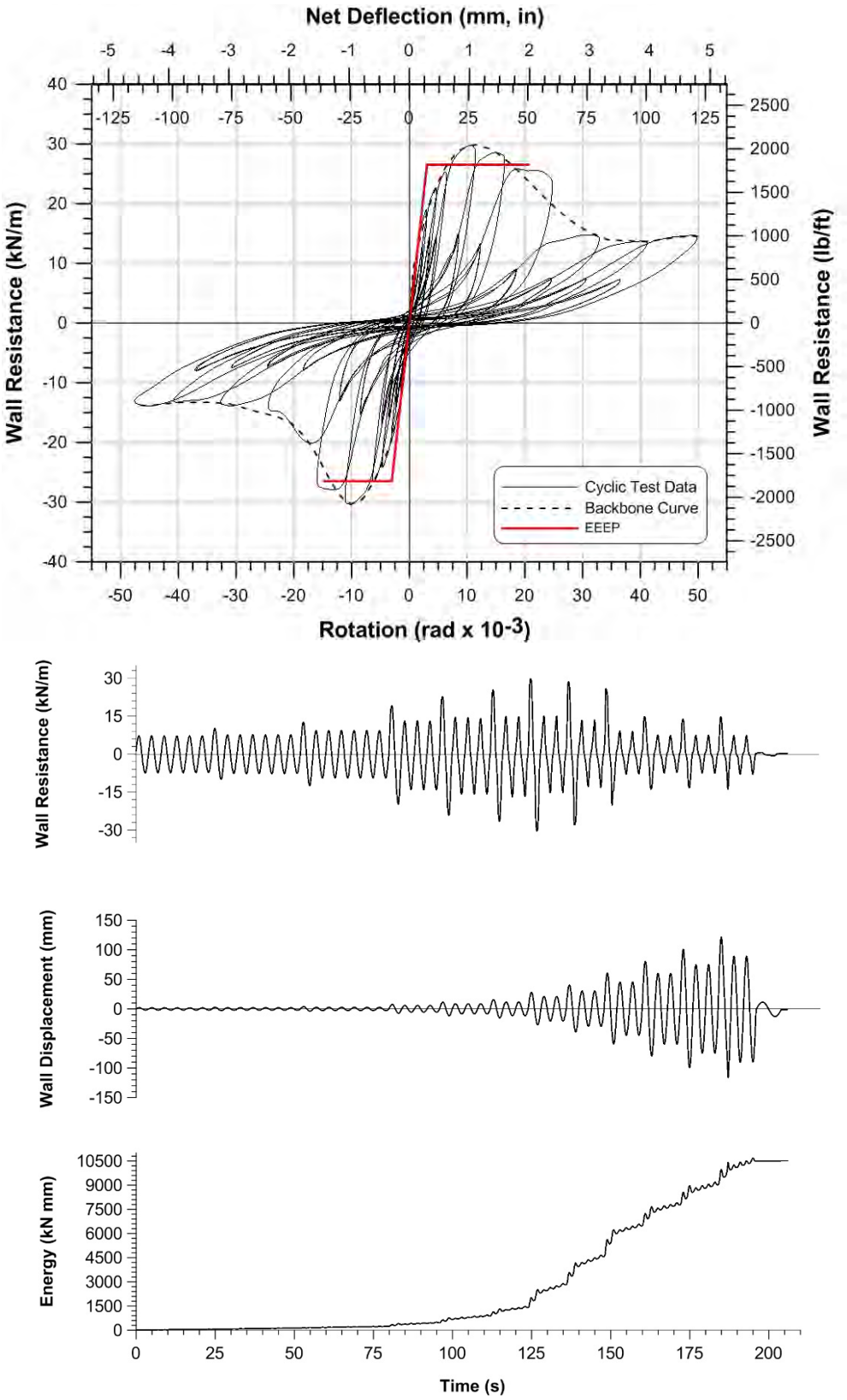

Figure G4: EEEP plot, cyclic test data, and time-history of double-sheathed specimen W20-C.

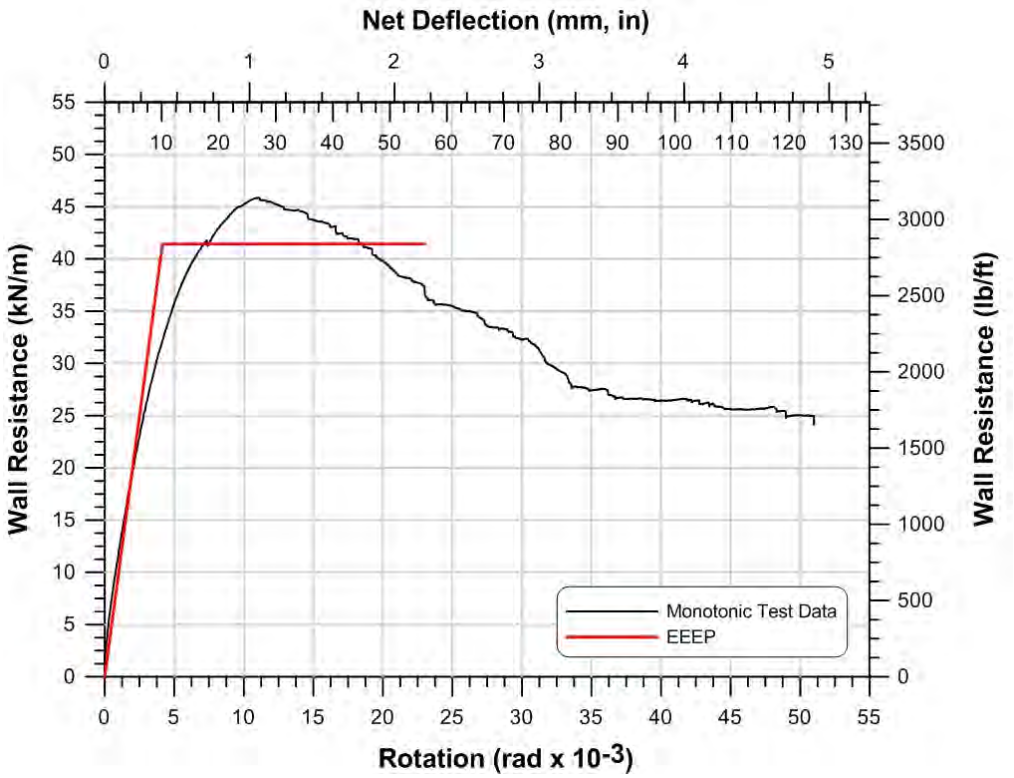

Figure G5: EEEP plot and monotonic test data of double-sheathed specimen W21-M.

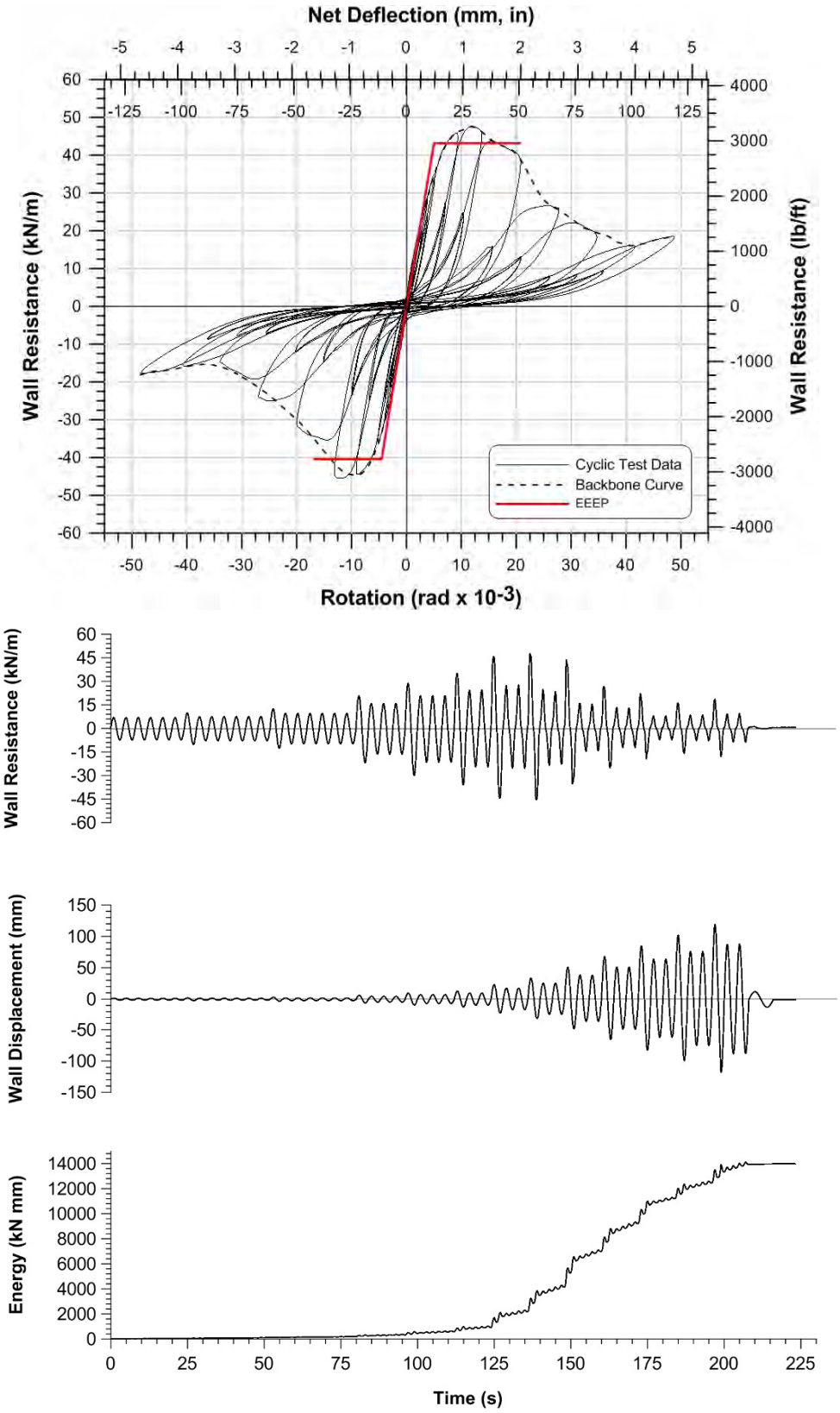

Figure G6: EEEP plot, cyclic test data, and time-history of double-sheathed specimen W21-C.

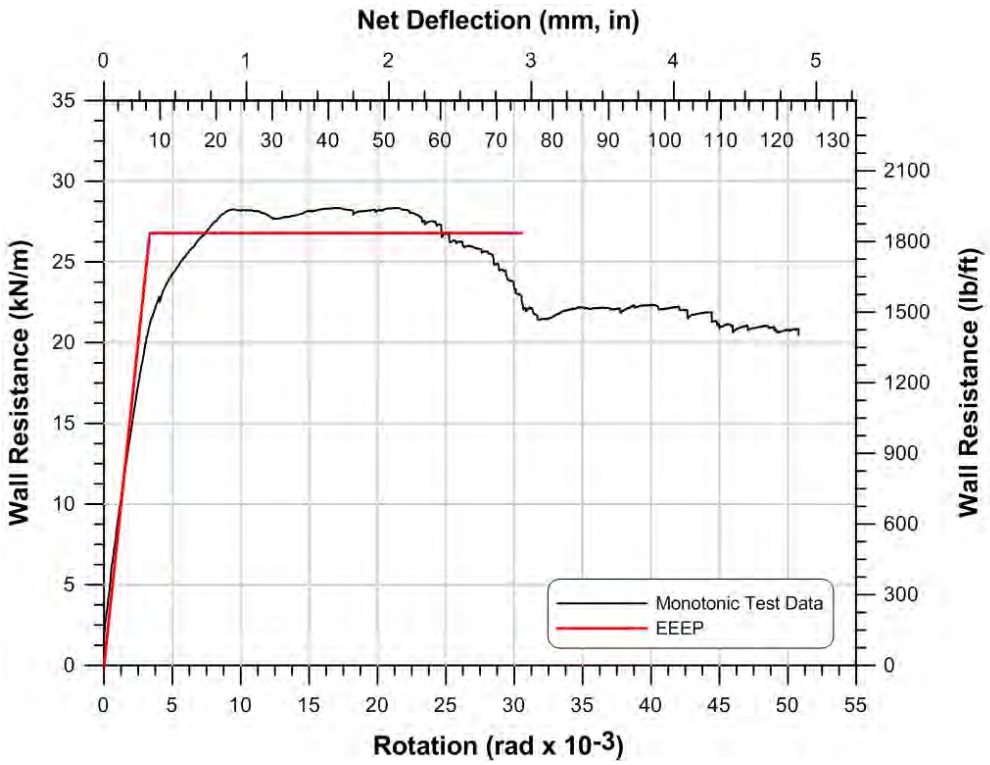

Figure G7: EEEP plot and monotonic test data of double-sheathed specimen W22-M.

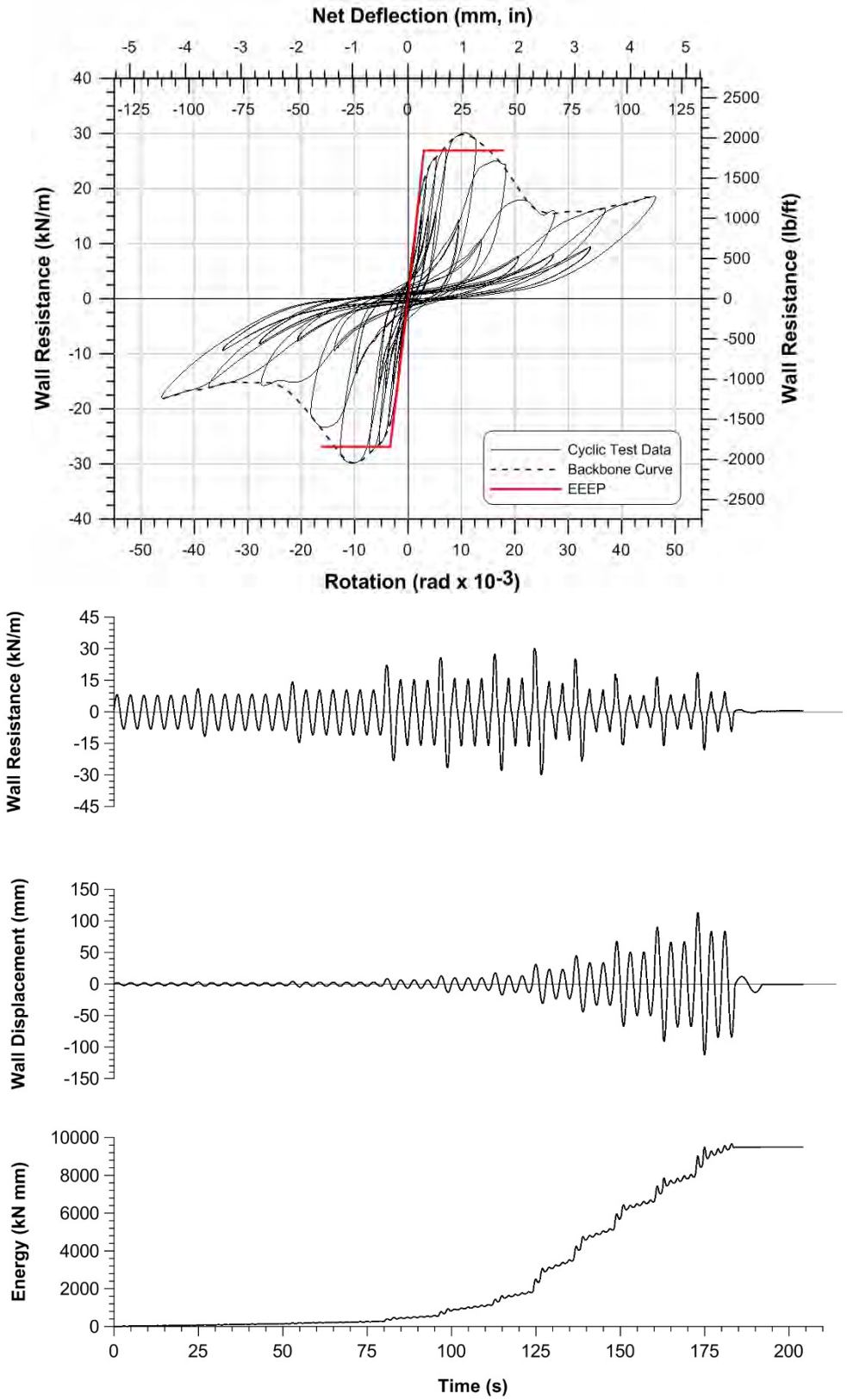

Figure G8: EEEP plot, cyclic test data, and time-history of double-sheathed specimen W22-C.

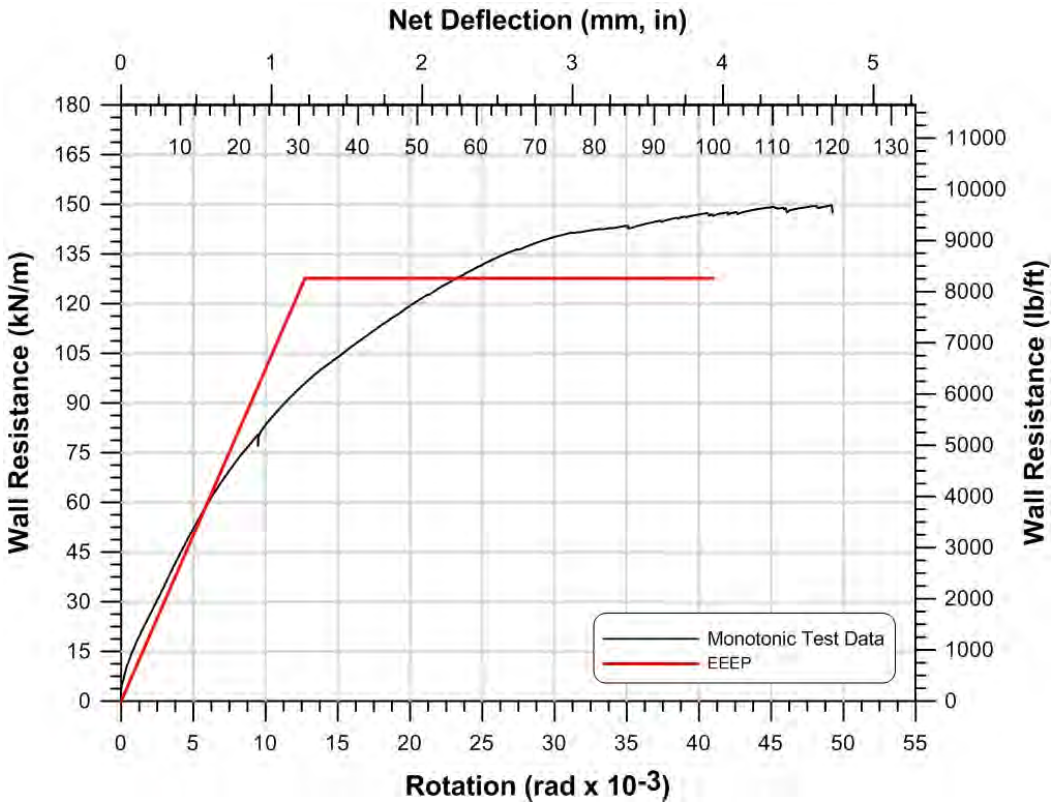

Figure G9: EEEP plot and monotonic test data of centre-sheathed specimen W15-MR3.

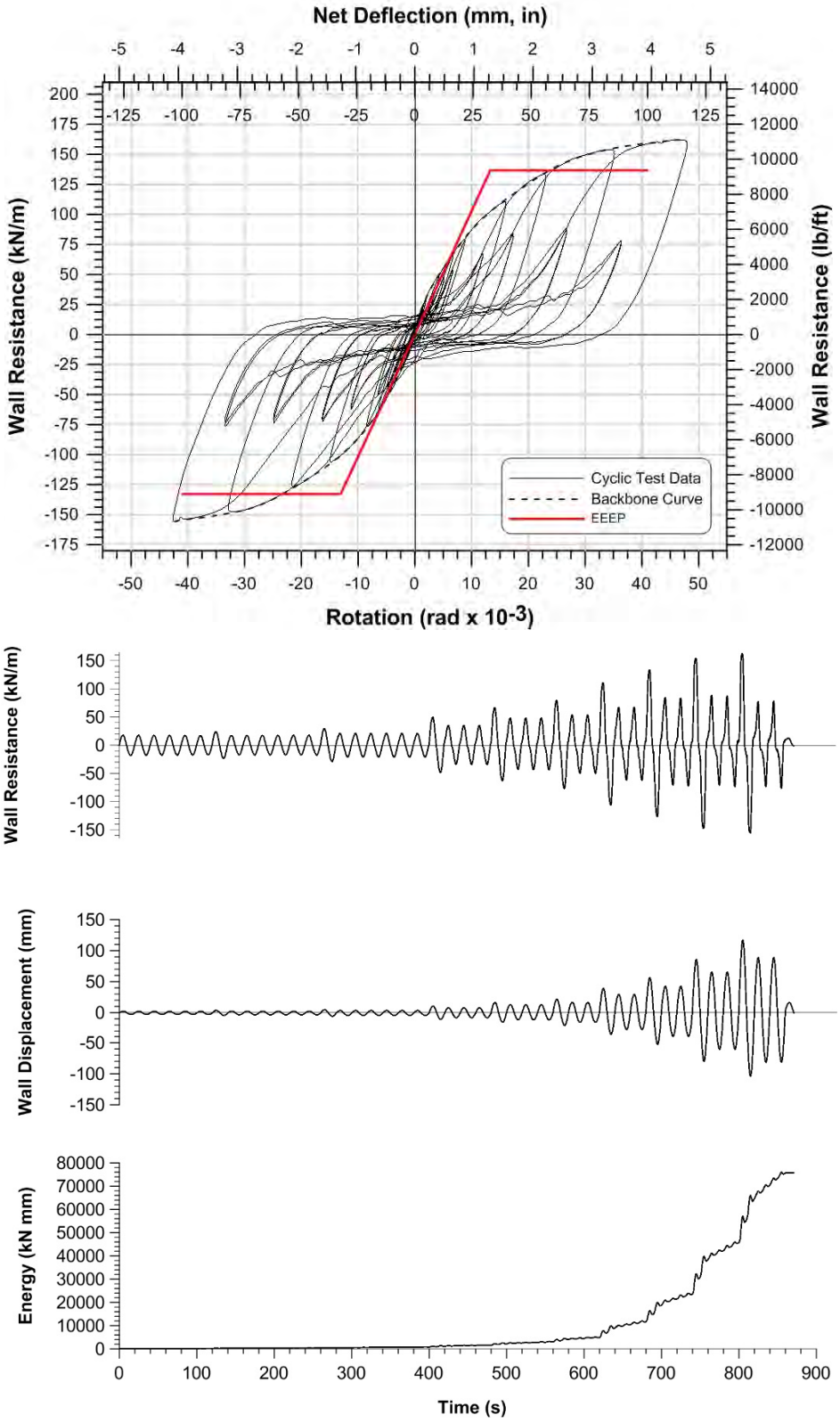

Figure G10: EEEP plot, cyclic test data, and time-history of double-sheathed specimen W15-CR3.

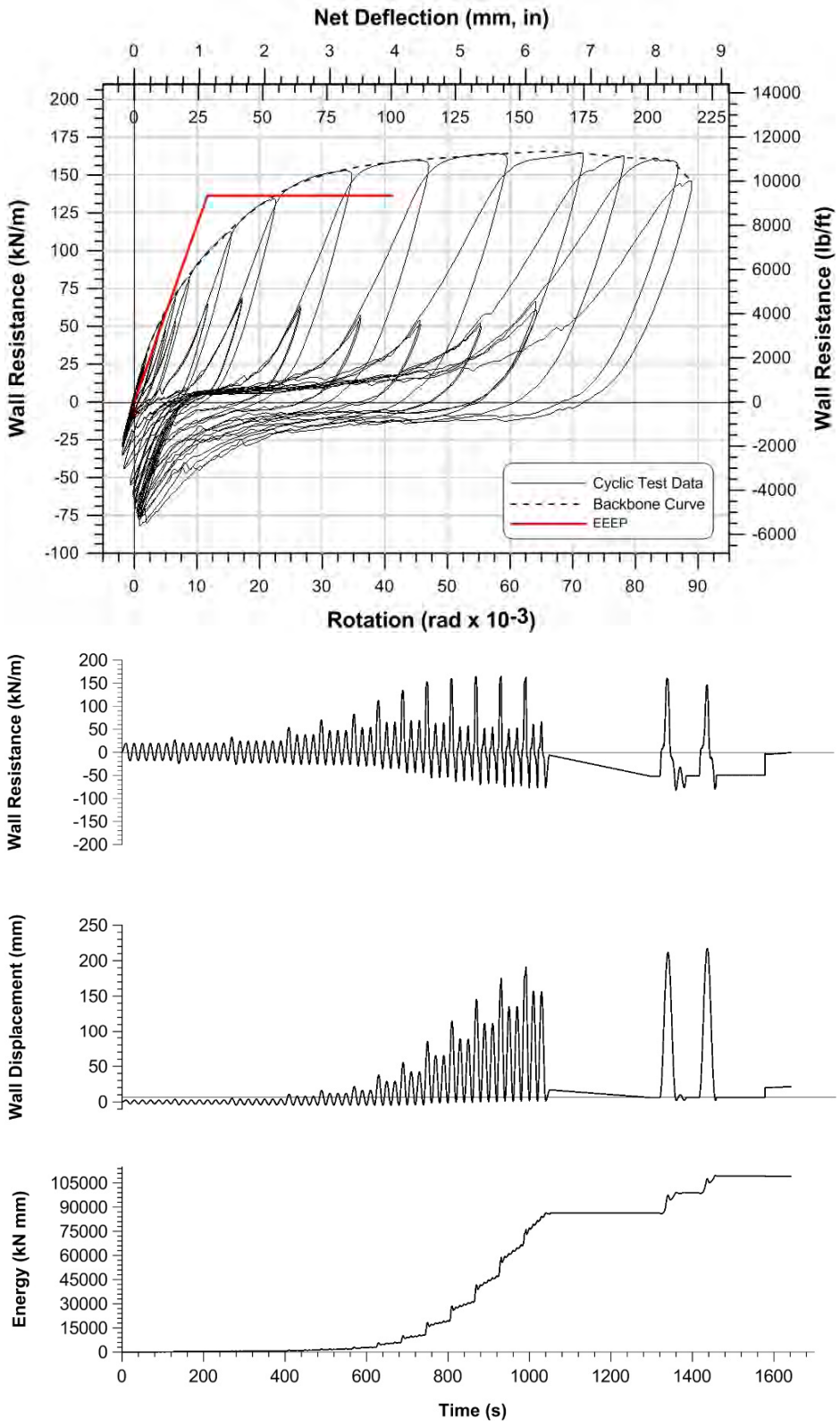

Figure G11: EEEP plot, asymmetric cyclic test data, and time-history of double-sheathed specimen W15B-CR3.

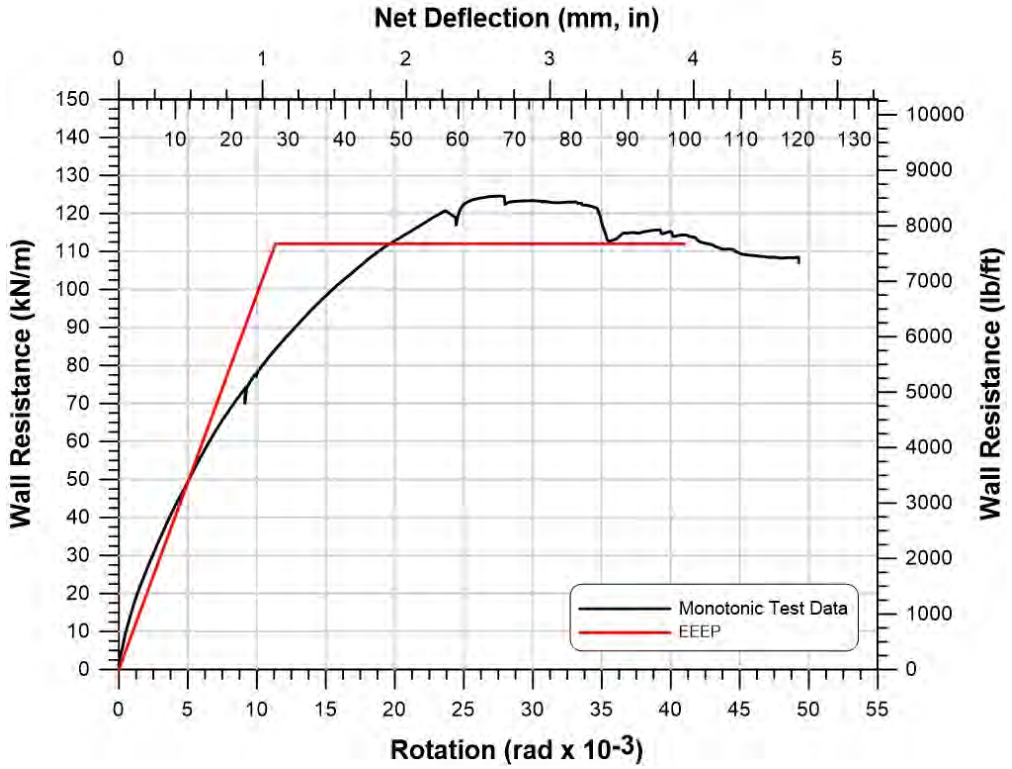

Figure G12: EEEP plot and monotonic test data of centre-sheathed specimen W16-MR.

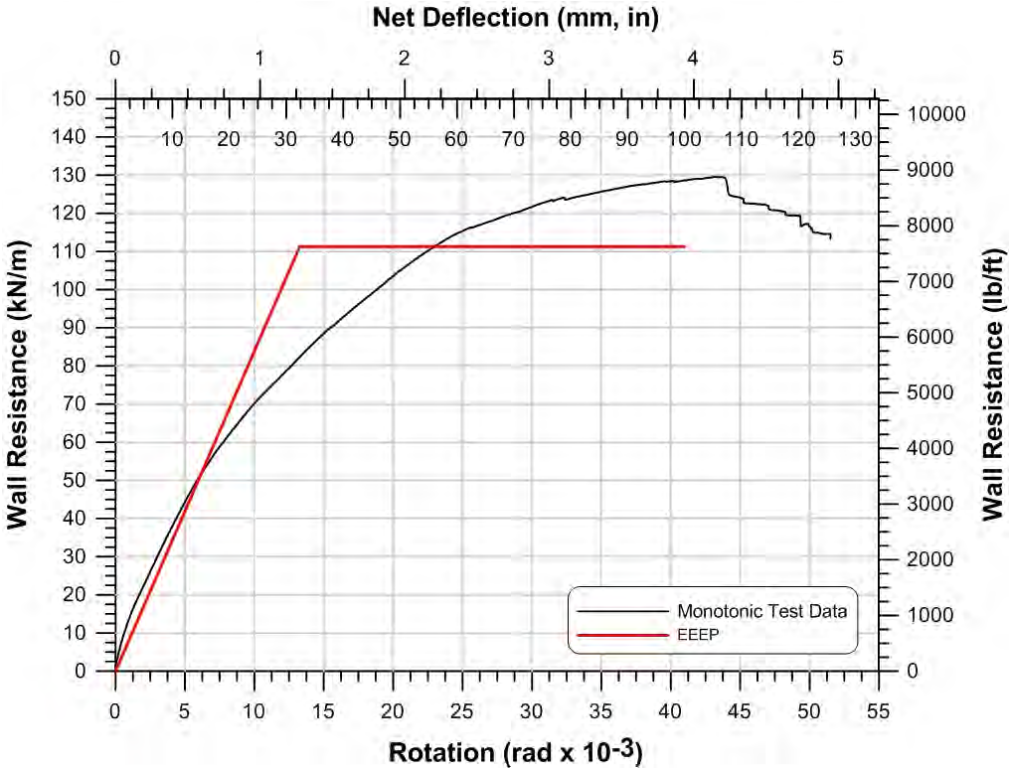

Figure G13: EEEP plot and monotonic test data of centre-sheathed specimen W16-MR2.

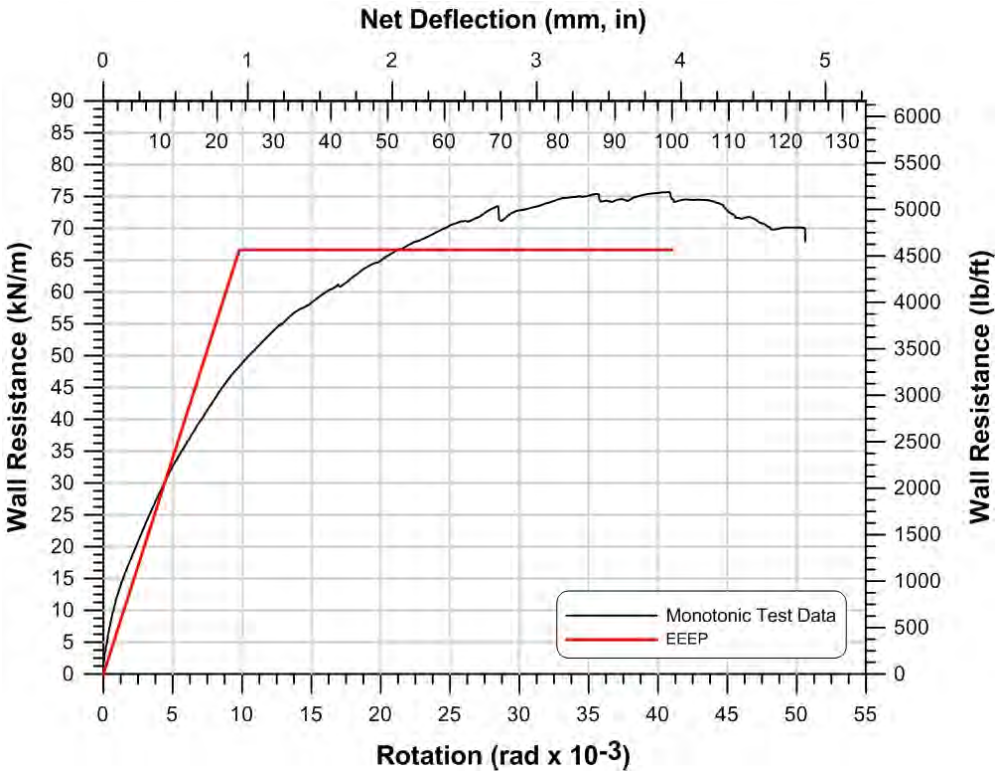

Figure G14: EEEP plot and monotonic test data of centre-sheathed specimen W17-M.

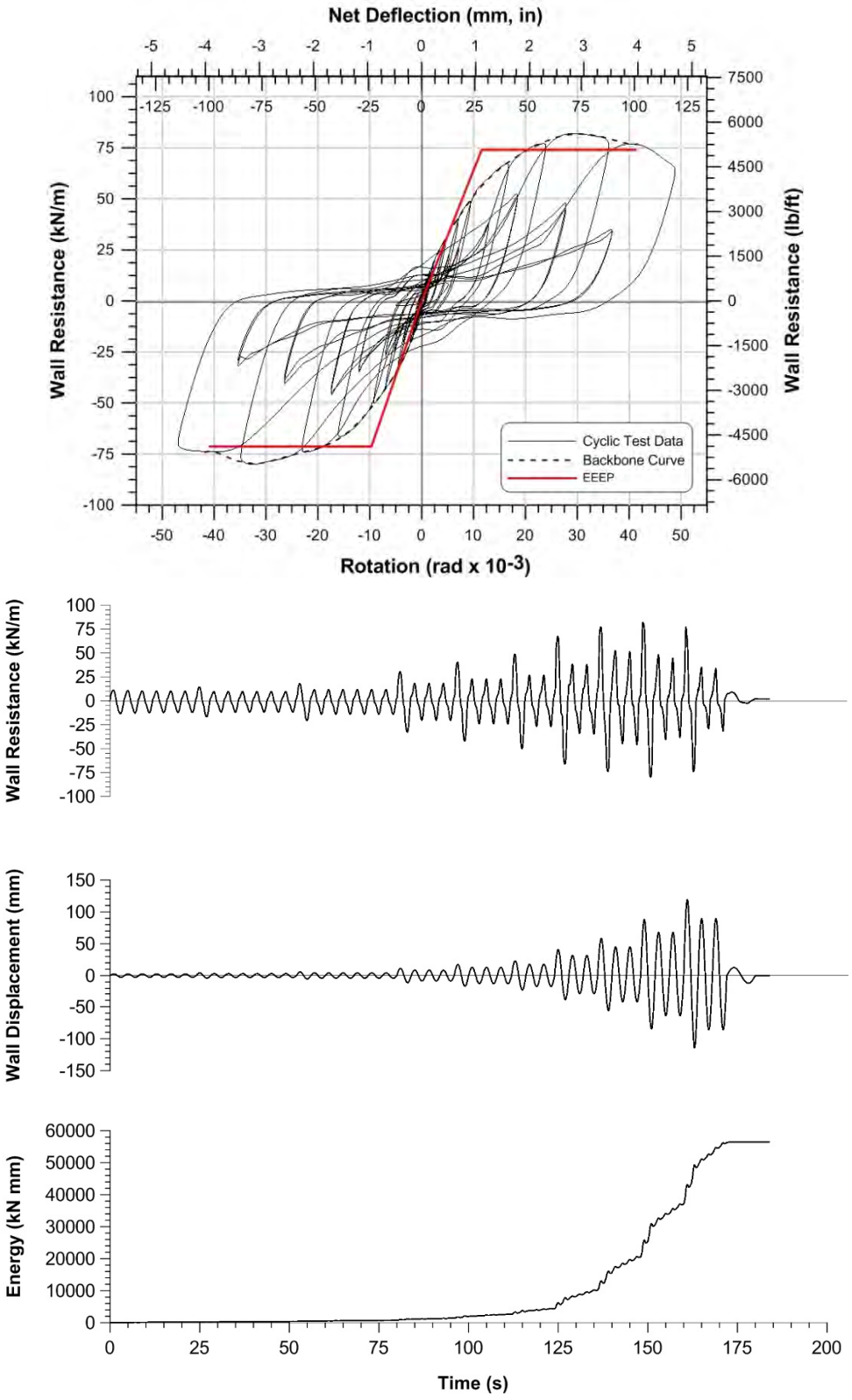

Figure G15: EEEP plot, cyclic test data, and time-history of double-sheathed specimen W17-C.

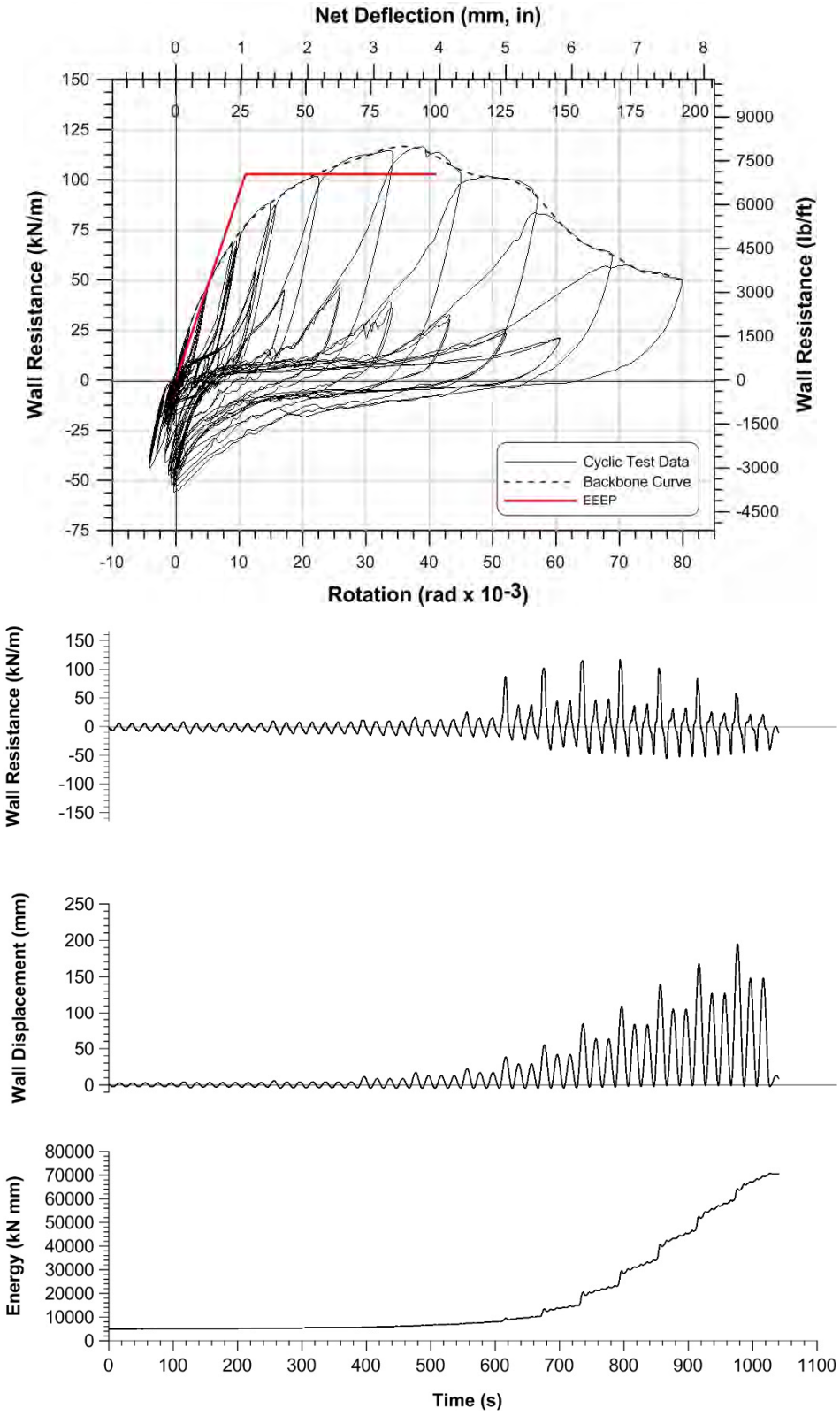

Figure G16: EEEP plot, asymmetric cyclic test data, and time-history of double-sheathed specimen W25-CR3.

American Iron and Steel Institute

25 Massachusetts Avenue, NW
Suite 800
Washington, DC 20001

www.steel.org

Research Report RP-17-5